NASA TECHNICAL MEMORANDUM

NASA TM X-3310

NASA TM X-3310

EXPERIMENTAL AERODYNAMIC CHARACTERISTICS FOR SLENDER BODIES WITH THIN WINGS AND TAIL AT ANGLES OF ATTACK FROM 0° TO 58° AND MACH NUMBERS FROM 0.6 TO 2.0

Leland H. Jorgensen and Edgar R. Nelson

Ames Research Center

Moffett Field, Calif. 94035

NATIONAL AERONAUTICS AND SPACE ADMINISTRATION • WASHINGTON, D. C. • MARCH 1976

1. Report No.	2. Government Accession No.	3. Recipier 's Catalog No.
TM X-3310		

4. Title and Subtitle	5. Report Date
EXPERIMENTAL AERODYNAMIC CHARACTERISTICS FOR SLENDER BODIES WITH THIN WINGS AND TAIL AT ANGLES OF ATTACK FROM 0° TO 58° AND MACH NUMBERS FROM 0.6 TO 2.0	February 1976
	6. Performing Organization Code

7. Author(s)	8. Performing Organization Report No.
Leland H. Jorgensen and Edgar R. Nelson	A-6248
	10. Work Unit No.
9. Performing Organization Name and Address	505-06-81
Ames Research Center Moffett Field, Calif. 94035	11. Contract or Grant No.
	13. Type of Report and Period Covered
12. Sponsoring Agency Name and Address	Technical Memorandum
National Aeronautics and Space Administration Washington, D. C. 20546	14. Sponsoring Agency Code

15. Supplementary Notes

16. Abstract

An experimental investigation was conducted in the Ames 6- by 6-Foot Wind Tunnel to measure the static aerodynamic characteristics for bodies of circular and elliptic cross section with various thin flat-plate wings and a thin tail consisting of horizontal and vertical parts. Three wings had aspect ratios of 4 and taper ratios of about 0, 0.25, and 0.5. Two additional wings, which had taper ratios near 0.25 and aspect ratios of about 3 and 5, were also tested in combination with the bodies and tail. All wings had about the same planform area. The exposed area of the horizontal portion of the tail was about 33 to 36 percent of the exposed area of the wings. The exposed area of the vertical tail fin was about 22 to 24 percent of the exposed area of the wings. The elliptic body, with an a/b = 2 cross section, had the same length and axial distribution of cross sectional area as the circular body. The circular body had a cylindrical aftersection of fineness ratio 7, and it was tested with the wings and tail in combination with tangent ogive noses that had fineness ratios of 2.5, 3.0, 3.5, and 5.0. In addition, an ogive nose with a rounded tip and an ogive nose with two different nose strake arrangements were used.

Nineteen configuration combinations were tested at Mach numbers of 0.6, 0.9, 1.5, and 2.0 at angles of attack from 0° to 58°. The Reynolds numbers, based on body base diameter, were about 4.3×10^5.

17. Key Words (Suggested by Author(s))	18. Distribution Statement
High angle of attack aerodynamics Body-wing-tail aerodynamics	Unlimited STAR Category – 02

19. Security Classif. (of this report)	20. Security Classif. (of this page)	21. No. of Pages	22. Price*
Unclassified	Unclassified	159	$6.25

* For sale by the National Technical Information Service, Springfield, Virginia 22161

NOMENCLATURE

All forces and moments except C_L and C_D are referred to the body axis coordinate system.

Symbol	Definition
A_r	reference area = body base area = 34.26 cm^2 (5.31 $in.^2$)
A_w	exposed wing planform area (2 panels)
AR	aspect ratio for wing extended into center of body B_1
AR_e	aspect ratio for two exposed wing panels joined together
a, b	semimajor and semiminor axes of elliptic cross section
C_A	axial-force coefficient, $C_{A_{bal}} - C_{A_{base}}$
$C_{A_{bal}}$	balance axial-force coefficient, $\frac{F_A}{qA_r}$
$C_{A_{base}}$	base-pressure force coefficient, $\frac{(p - p_{base})}{q}$
C_D	drag coefficient, $\frac{drag}{qA_r}$
C_L	lift coefficient, $\frac{lift}{qA_r}$
C_m	pitching-moment coefficient about balance center 4d from body base, $\frac{\text{pitching moment}}{qA_rX}$
C_N	normal-force coefficient, $\frac{F_N}{qA_r}$
C_n	yawing-moment coefficient about balance center, 4d from body base, $\frac{\text{yawing moment}}{qA_rX}$
C_Y	side-force coefficient, $\frac{F_Y}{qA_r}$
c_r, c_t	wing root and tip chords

d	body base diameter = 6.60 cm (2.60 in.)
F_A, F_N, F_Y	axial, normal, and side force, respectively
L/D	lift-to-drag ratio
ℓ	body length
ℓ_N	nose length
M	free-stream Mach number
p	free-stream static pressure
p_{base}	base pressure
q	free-stream dynamic pressure
r	body base radius = 3.30 cm (1.30 in.)
Re	Reynolds number based on d
s	wing semispan from body centerline
X	reference length = d = 6.60 cm (2.60 in.)
$\frac{x_{ac_N}}{d}$	distance (in diameters) from body base to aerodynamic force center in normal-force plane, $\left(\frac{C_m}{C_N} + \frac{x_m}{X}\right)$
x_m	distance from body base to balance moment reference = 4d = 26.42 cm (10.40 in.)
α	angle of attack, deg
ϵ	wing semiapex angle, deg
ϕ	angle of bank about body longitudinal axis, deg

Configuration Code

Because the data are computer plotted, both the conventional symbol and the plot symbol are given.

Symbol	Plot Symbol	Component
B_1	B1	basic circular body (tangent ogive nose of fineness ratio 3 with cylinder aftersection of fineness ratio 7)
B_2	B2	body with elliptic cross section of constant $\frac{a}{b} = 2$
ϕ=0°	PHI=0	body banked 0° about longitudinal axis (see fig. 1(a))
ϕ=90°	PHI=90	body banked 90° about longitudinal axis (see fig. 1(a))

			Fineness Ratio
C_1	C1	circular cylinder	7
N_1	N1	tangent ogive nose	3
N_2	N2	tangent ogive nose	3.5
N_3	N3	tangent ogive nose	5
N_4	N4	tangent ogive nose with rounded tip	3
N_5	N5	tangent ogive nose with tip strakes	3
N_6	N6	tangent ogive nose with side strakes	3
N_7	N7	tangent ogive nose	2.5
W_1	W1	wing of AR $\approx$ 4, $c_t/c_r = 0$	
W_2	W2	wing of AR $\approx$ 4, $c_t/c_r = 0.276$	
W_3	W3	wing of AR $\approx$ 4, $c_t/c_r = 0.533$	
W_4	W4	wing of AR $\approx$ 5, $c_t/c_r = 0.273$	
W_5	W5	wing of AR $\approx$ 3, $c_t/c_r = 0.280$	
T	T	tail, consisting of horizontal and vertical parts (see fig. 1(c))	

EXPERIMENTAL AERODYNAMIC CHARACTERISTICS FOR SLENDER BODIES WITH THIN WINGS AND TAIL AT ANGLES OF ATTACK FROM 0° TO 58° AND MACH NUMBERS FROM 0.6 TO 2.0

Leland H. Jorgensen and Edgar R. Nelson*

Ames Research Center

SUMMARY

An experimental investigation was conducted in the Ames 6- by 6-Foot Wind Tunnel to measure the static aerodynamic characteristics for bodies of circular and elliptic cross section with various thin flat-plate wings and a thin tail consisting of horizontal and vertical parts. Three wings had aspect ratios of 4 and taper ratios of about 0, 0.25, and 0.5. Two additional wings, which had taper ratios near 0.25 and aspect ratios of about 3 and 5, were also tested in combination with the bodies and tail. All wings had about the same planform area. The exposed area of the horizontal portion of the tail was about 33 to 36 percent of the exposed area of the wings. The exposed area of the vertical tail fin was about 22 to 24 percent of the exposed area of the wings. The elliptic body, with an a/b = 2 cross section, had the same length and axial distribution of cross sectional area as the circular body. The circular body had a cylindrical aftersection of fineness ratio 7, and it was tested with the wings and tail in combination with tangent ogive noses that had fineness ratios of 2.5, 3.0, 3.5, and 5.0. In addition, an ogive nose with a rounded tip and an ogive nose with two different nose strake arrangements were used.

Nineteen configuration combinations were tested at Mach numbers of 0.6, 0.9, 1.5, and 2.0 at angles of attack from 0° to 58°. The Reynolds numbers, based on body base diameter, were about 4.3×10^5.

The data demonstrate that taper ratio and aspect ratio had only small effect on the aerodynamic characteristics, especially at the higher angles of attack. Undesirable side forces and yawing moments, which developed at angles of attack greater than about 25°, were generally no greater than those for the bodies tested alone. As for the bodies alone and in combination with the wings, the side forces and yawing moments for the body-wing-tail combinations increased as the nose fineness ratio increased and/or as the subsonic Mach number decreased. It is virtually certain that the undesirable side forces and yawing moments originate with, or are caused by, the body nose.

INTRODUCTION

In the last several years high angle-of-attack aerodynamics has increased in importance because of the demand for greater maneuverability of missiles and aircraft (both manned and remotely

*Project engineer, ARO, Inc., Moffett Field, Calif. 94035.

piloted). Some recent introductory investigations in this field are reported in references 1 through 12. Most of the research reported in these references has been concerned with bodies and has been directed more toward missile applications than aircraft. The relatively small data base that existed several years ago for bodies alone and with strakes has been considerably enlarged, and work in this area seems to be continuing at a reasonable rate. However, there is still great need to enlarge the relatively small data base for bodies in combination with wings, tails, or both at subsonic, transonic, and supersonic Mach numbers. This data base, of course, is more applicable to aircraft than missiles.

To help enlarge this data base for basic bodies with wings, an investigation was recently conducted (ref. 12) to measure the force and moment characteristics for bodies of circular and elliptic cross section in combination with thin wings which had taper ratios of 0 to 0.5 and aspect ratios of 3 to 5. The bodies used were the same as those studied in references 8 and 10, and there were variations in nose fineness ratio, bluntness, and nose strake arrangement. All models were tested in the Ames 6- by 6-Foot Wind Tunnel at Mach numbers of 0.6, 0.9, 1.5, and 2.0 and angles of attack from 0° to 58°.

In the present investigation the tests in reference 12 have been repeated for the same body-wing models but with a tail added. Thus, the effects of body and wing variations on the aerodynamic characteristics of the body-wing-tail combinations can be studied, particularly at high angles of attack.

The purpose of this report is to present and discuss briefly the basic data that show the effects on the aerodynamic characteristics of wing taper ratio, wing aspect ratio, nose fineness ratio, nose bluntness, and nose strake arrangement with the tail present. The effect of removing the tail is also discussed.

TEST FACILITY

The experimental investigation was conducted in the Ames 6- by 6-Foot Wind Tunnel – a variable pressure, continuous flow, closed-return type facility. The nozzle ahead of the test section consists of an asymmetric sliding block that permits the Mach number to be continuously varied from 0.6 to 2.3. The test section has a perforated floor and ceiling so that boundary-layer flow can be removed for transonic testing.

MODEL AND BALANCE

Figure 1 shows the model components that were tested in various model combinations. These components include bodies, noses, wings, and tail.

The basic circular body (B_1) depicted in figure 1(a) consisted of a circular-arc tangent ogive of fineness ratio 3 followed by a cylindrical aftersection of fineness ratio 7. Body B_2 (fig. 1(a)) had an elliptic cross section of $a/b = 2$ and the same length and axial distribution of cross-sectional area as B_1. Hence, the fineness ratio of $\ell/d = 10$ for B_1 was also the equivalent fineness ratio for B_2. These

bodies were previously tested, and the results are reported in reference 10. The basic circular aftersection of B_1 (designated as C_1) was also tested (ref. 8) with ogive noses of fineness ratios of 2.5 to 5 (noses N_7, N_1, N_2, and N_3 in figure 1(b)). The circular aftersection C_1 was also tested (ref. 8) with a blunted nose (N_4) and noses with strakes (N_5 and N_6).

For the present test the bodies, noses, and tail in figures 1(a) through 1(c) were combined with five flat-plate wings (figures 1(c)–1(e)) that formed two families of wings. One family (W_1, W_2, and W_3) had an aspect ratio of about 4 and taper ratios (c_t/c_r) of 0, 0.276, and 0.533 (fig. 1(c)). The other family (W_4, W_2, and W_5) had aspect ratios of about 5, 4, and 3, respectively, and the taper ratios were all about 0.28 (fig. 1(d) and 1(e)).

All of the wings were designed to have the same planform area ($16\ d^2$) if the wings extended into the body B_1 to the axial centerline. Based on the phantom wing chord at the body centerline, the taper ratios for wings W_1, W_2, and W_3 were 0, 0.25, and 0.50, respectively. They were also 0.25 for W_4 and W_5. Pertinent planform dimensions of the exposed parts of the wings are given in the following table.

TABLE 1.– PLANFORM DIMENSIONS OF WINGS

Wing	AR	AR_e	ϵ,deg	(s-r)/d	c_r/d	c_t/d	c_t/c_r	A_w/d^2	A_w/A_r
W_1	4	4	45.00	3.5	3.5	0	0	12.250	15.598
W_2	4	3.784	59.03	3.5	2.9	0.800	0.276	12.950	16.488
W_3	4	3.653	71.57	3.5	2.5	1.333	0.533	13.412	17.076
W_4	5	4.761	64.36	3.972	2.622	0.715	0.273	13.254	16.876
W_5	3	2.810	51.33	2.964	3.295	0.924	0.280	12.506	15.924

AR = aspect ratio for wing extended into center of body B_1

AR_e = aspect ratio for two exposed wing panels joined together

d = diameter of body B_1

A_w = exposed wing planform area (2 panels)

A_r = reference area = body base area

The exposed area of the horizontal portion of the tail is $4.4\ d^2$, or about 36 percent of the exposed area of wing W_1. The exposed area of the vertical tail fin is $3\ d^2$, or about 24 percent of the exposed area of wing W_1.

Figure 2(a) shows the planform views of the 19 configurations that were tested in this study. All of these configurations are identified by the codes shown in figure 1, and these codes are used throughout the report.

All model parts were constructed of stainless steel, and all models were sting mounted (fig. 2(b)) through the base on a six-component, strain-gage "Task" balance. The balance force center was located inside each body at a position 4 base diameters forward of the base.

TESTS AND DATA REDUCTION

All model configurations shown in figure 2(a) were tested at angles of attack from 0° to about 58° on two model-support setups. One setup (fig. 2(b)) was used to test the models at angles of attack from 0° to about 27°, and the other (fig. 2(c)) was used for angles of attack from 27° to 58°. The models were tested at Mach numbers of 0.6, 0.9, 1.5, and 2.0. The Reynolds numbers, based on body diameter d, were about 4.3×10^5 for all of the body-wing-tail combinations. Several runs were also made with the bodies alone at Re = 3.8×10^5 and 6.5×10^5.

Six-component aerodynamic force and moment data were measured at each test condition, and all data were reduced to coefficient form and referred to the body axis coordinate system. The average base pressure from four base pressure tubes (at the sides, top, and bottom of the base) was used to compute the base drag. The base drag was subtracted from the total axial-force balance measurements, so that the data presented are for forces ahead of the body base. Rolling-moment coefficients were generally small and are omitted. Normal-force aerodynamic centers were computed from the normal-force and pitching-moment coefficients and are presented in lieu of the pitching-moment coefficients.

Lift coefficients and values of L/D referred to the wind axes were also computed and are presented. They were computed from the expressions:

$$C_L = C_N \cos\alpha - C_A \sin\alpha \tag{1}$$

$$C_D = C_N \sin\alpha + C_A \cos\alpha \tag{2}$$

and

$$\frac{L}{D} = \frac{C_L}{C_D} \tag{3}$$

The reference area A_r for all coefficients is the body base area (34.26 cm^2), and the reference length X for all moment coefficients is the body base diameter (6.60 cm). The coefficients, of course, can be easily recomputed based on wing area and an appropriate wing chord length, such as the root chord or mean aerodynamic chord. For example, the force coefficients based on exposed wing area can be obtained by dividing the presented values by the appropriate values of A_w/A_r tabulated in the previous section.

RESULTS AND DISCUSSION

In figures 3 through 24, experimental results for the numerous body-wing-tail configurations show the effects on the aerodynamic characteristics of wing taper ratio, wing aspect ratio, nose fineness ratio, nose rounding and nose strake arrangement. In figures 25 through 36 experimental results show the effects of removing the tail and the tail plus wing from selected body-wing-tail combinations. Each effect is discussed briefly with the aid of plots of C_N, x_{ac_N}/d, C_Y, C_Y/C_N, C_n, C_L, and L/D versus α for $\alpha = 0°$ to $60°$. Plots of C_A versus α are also presented but are not discussed. Because the models were sting supported from the rear, it is likely that the C_A data include effects of support interference. Any support effects are also included in the C_L and L/D data (obtained from C_N and C_A by eqs. (1)–(3)) but to a much smaller extent. Any effects of tunnel-blockage interference are unknown at present and are ignored.

Effect of Wing Taper Ratio

Data that show the effect of wing taper ratio on the aerodynamic characteristics for the winged circular body and tail (B_1T with W_1, W_2, and W_3) are presented in figures 3 through 6. Similar data for the winged elliptic body and tail (B_2T with W_1, W_2, and W_3) are presented in figures 7 through 10. Body alone data (refs. 8 and 10) for B_1 and B_2 are also shown for comparison.

For the change in taper ratio from 0 to about 0.5 (W_1 to W_3), there are generally only small effects on the aerodynamic characteristics. This is especially true for C_N and C_L at the subsonic Mach numbers (M = 0.6 and 0.9) and high angles of attack (greater than about $\alpha = 15°$). At the supersonic Mach numbers and high angles of attack, there is generally more variation in the C_N and C_L data, the coefficients being highest for the wing with the highest taper ratio (W_3, $c_t/c_r = 0.533$). This wing, however, has greater exposed wing area than the wing with no taper ratio (W_1). For example, $A_w/A_r = 17.076$ for W_3 as compared with $A_w/A_r = 15.598$ for W_1. If the C_N and C_L data were based on A_w instead of A_r, the differences at high α would be much less. Throughout the Mach number range most of the variations in C_N and C_L at low angles of attack probably can be attributed to flow separation effects from the wings.

It is interesting to note that the side-force coefficients (C_Y) for the body-wing-tail configurations are generally no greater and sometimes even smaller than for the bodies alone.[1] As discussed previously (refs. 8, 10), the undesirable side-force and yawing-moment coefficients that develop for the bodies alone at subsonic Mach numbers decrease with increase in subsonic Mach number and disappear with increase in Mach number into the supersonic flow regime. The same finding has been observed for the bodies with wings (ref. 12), and this finding again can be observed for the body-wing-tail models. However, for the body-wing-tail models the relative influence of C_Y to C_N is much smaller. In fact, the ratio (C_Y/C_N) appears to be negligible throughout the Mach number and angle of attack ranges studied.

[1] The signs of the side-force coefficients are sometimes different from run to run and from test of body alone to body with wing plus tail. It is believed that the signs result from the random asymmetric flow separation and vortex flow from the nose (observed from oil-flow tests).

Effect of Wing Aspect Ratio

Data are presented in figures 11 through 14 that show the effect of wing aspect ratio on the aerodynamic characteristics for the winged circular body with tail (B_1T) with W_5, W_2, and W_4 of AR $\approx$ 3, 4, and 5, respectively. Similar data for the winged elliptic body with tail (B_2T with W_5, W_2, and W_4) are presented in figures 15 through 18. Body-alone data (refs. 8 and 10) are also shown for comparison.

As for the case of taper ratio, there are no large effects of aspect ratio on the aerodynamic characteristics, especially the longitudinal characteristics. The undesirable side forces and yawing moments, which appear at the high angles of attack, are no larger and sometimes smaller than those shown for the bodies alone.

Effect of Nose Fineness Ratio

In figures 19 through 22, data are presented that show the effect on the aerodynamic characteristics of changing the nose fineness ratio from $\ell_N/d = 2.5$ (N_7) to $\ell_N/d = 5$ (N_3) for the circular cylinder (C_1) with W_2 (aspect ratio 4) and the tail (T).

As might be expected, there is little or no effect of nose fineness ratio on the longitudinal characteristics. However, there is a strong effect of nose fineness ratio on the characteristics of C_Y and C_n versus α for the wing-body-tail configuration at α greater than about 25° and M = 0.6 and 0.9. For example, in figures 19 and 20 it can be seen that the largest values of C_Y and C_n develop with the noses that have fineness ratios of 3.5 (N_2) and 5(N_3). These effects are similar to those reported in reference 9 for similar noses alone and in reference 8 for the same noses with the circular body. They are also similar to those reported in reference 12 for the winged body with the noses but without the tail. It thus can be concluded that the undesirable side-force and yawing-moment characteristics originate with, or are caused by, the body nose, and high fineness-ratio noses are the least desirable.

Effects of Nose Rounding and Strakes

Data are presented in figures 23 and 24 that show the effects of nose rounding and strakes on the body-wing-tail aerodynamic characteristics for M = 0.6 and 2.0. Results are compared for the circular cylinder C_1 plus wing W_2 and tail T with the basic nose N_1, the rounded nose N_4, the nose with tip strakes N_5, and the nose with strakes extending over its length N_6. All noses had a fineness ratio of about 3.

The results for the configuration with the rounded nose (N_4 C_1 W_2 T) are not significantly different from those for the configuration with the basic sharp nose (N_1 C_1 W_2 T), but both noses have a fineness ratio of 3. A different conclusion concerning the effect of bluntness is obtained if the results for the configuration with the rounded nose (N_4 C_1 W_2 T) are compared with those (figs. 19 and 20) for the configuration with the sharp fineness-ratio 3.5 nose (N_2 C_1 W_2 T). As previously discussed, undesirable side forces and yawing moments appeared with N_2 C_1 W_2 T at M = 0.6 and 0.9 (figs. 19 and 20). However, with the nose apex of N_2 C_1 W_2 T blunted by rounding to give a fineness ratio of 3 (configuration N_4 C_1 W_2 T), the side forces and yawing

moments essentially disappeared. The same thing was found (ref. 12) for these same configurations without the tail present.

There is an increase in C_N and C_L at high α and M = 0.6 resulting from the use of N_6, the nose with the side strakes extending over the nose length (fig. 23). This increase in C_N and C_L disappears at supersonic speeds (see fig. 24 for M = 2.0). The same result is reported in reference 12 for the configurations without the tail. There was no significant effect of the tip strakes from nose N_5 on any of the aerodynamic characteristics.

Effects of Removing Tail and Wing

Data are presented in figures 25 through 36 that show the effects on the aerodynamic characteristics of removing the tail, and the tail plus wing from selected body-wing-tail configurations. In figures 25 through 28, data are presented for N_1 C_1 W_2 T, N_1 C_1 W_2, and N_1 C_1 = B_1, configurations with the basic circular body. In figures 29 through 32, data are presented for N_3 C_1 W_2 T, N_3 C_1 W_2, and N_3 C_1, configurations with the circular body and fineness-ratio 5 nose. Finally, in figures 33 through 36, data are presented for B_2 W_2 T, B_2 W_2, and B_2, configurations with the elliptic body of a/b = 2 at $\phi = 0°$.

Generally, the magnitudes of the side-force and yawing-moment coefficients (C_Y and C_n) are about the same for the bodies alone as for the bodies with the wing and the wing plus tail. These undesirable coefficients are the largest for the body with the highest fineness-ratio nose (nose N_3 of $\ell_N/d = 5$). It is thus virtually certain that the undesirable C_Y and C_n characteristics originate with, or are caused by, the body nose. Fortunately, as observed previously (refs. 8, 10, 11, and 12), these undesirable characteristics decrease either with decrease in nose fineness ratio or with increase in Mach number. They essentially disappear at the supersonic Mach numbers.

There are numerous comparisons about the relative influence of the wing, tail, and body on the longitudinal characteristics that may be made from the data in figures 25 through 36. Only a few general comparisons concerning the C_N and C_L characteristics are cited herein as examples.

From the data comparisons, computations can be made which show that the wing develops greater than about 70 percent of the total C_N and C_L at α less than 20°. However, with increase in α from about 20° to 60°, the contributions to C_N and C_L from the wing decrease from about 70 percent to 45 percent.

Over this high α range (20° to 60°) the tail develops about 40 to 55 percent of the wing lift at M = 0.6 However, at M = 2.0, the tail only develops about 26 to 30 percent of the wing lift. It is interesting to note that the exposed horizontal tail area is 34 percent of the exposed area of wing W_2. Thus, from a relative standpoint, the tail is more efficient than the wing at M = 0.6 and less efficient at M = 2.0.

The data also can be used to demonstrate the well-known fact that a body is generally an efficient lifting component only at very high angles of attack. For example, at M = 0.6 and $\alpha = 20°$, body B_1 develops only about 4 percent of the total C_L; whereas, at M = 0.6 and $\alpha = 60°$, it develops about 24 percent.

CONCLUSIONS

1. Generally, changing the wing taper ratio from 0 to 0.5 had only small effects on the aerodynamic characteristics.

2. As was true for taper ratio, changing the wing aspect ratio from 3 to 5 resulted in no large effects on the aerodynamic characteristics.

3. Undesirable side forces and yawing moments for the body-wing-tail configurations were generally no greater than for the bodies alone. As for the bodies alone, they developed at subsonic Mach number for angles of attack above about 25°. Also, as for the bodies alone, the side forces and yawing moments increased with increase in nose fineness ratio. Fineness ratios greater than 3 produced the largest side forces.

4. The undesirable side forces and yawing moments decreased with increase in Mach number and virtually disappeared at supersonic Mach numbers.

5. Nose-tip rounding of a fineness ratio 3.5 ogive nose to give a fineness ratio 3 nose reduced the undesirable side forces and yawing moments. However, use of a sharp nose of fineness ratio 3 resulted in just as drastic a reduction in the side forces and yawing moments.

6. It is virtually certain that the undesirable side forces and yawing moments originate with, or are caused by, the body nose.

Ames Research Center
National Aeronautics and Space Administration
Moffett Field, California 94035, July 14, 1975

REFERENCES

1. Pick, George S.: Side Forces on Ogive-Cylinder Bodies at High Angles of Attack in Transonic Flow. J. Spacecraft and Rockets, vol. 9, no. 6, pp. 389–390, June 1972.

2. Clark, William H.; Peoples, John R.; and Briggs, M. Michael: Occurrence and Inhibition of Large Yawing Moments During High Incidence Flight of Slender Missile Configurations. AIAA Paper 72-968, 1972.

3. Coe, Paul L., Jr.; Chambers, Joseph R.; and Letko, William: Asymmetric Lateral-Directional Characteristics of Pointed Bodies of Revolution at High Angles of Attack. NASA TN D-7095, 1972.

4. Jorgensen, Leland H.: Prediction of Static Aerodynamic Characteristics for Space-Shuttle-Like and Other Bodies at Angles of Attack From 0° to 180°. NASA TN D-6996, 1973.

5. Jorgensen, Leland H.: Estimation of Aerodynamics for Slender Bodies Alone and With Lifting Surfaces at α's From 0° to 90°. AIAA Journal, vol. II, no. 3, pp. 409–412, March 1973.

6. Jorgensen, Leland H.: A Method for Estimating Static Aerodynamic Characteristics for Slender Bodies of Circular and Noncircular Cross Section Alone and With Lifting Surfaces at Angles of Attack from 0° to 90°. NASA TN D-7228, 1973.

7. Fleeman, E. L.; and Nelson, R. C.: Aerodynamic Forces and Moments on a Slender Body With a Jet Plume for Angles of Attack up to 180 Degrees. AIAA Paper 74-110, 1974.

8. Jorgensen, Leland H.; and Nelson, Edgar R.: Experimental Aerodynamic Characteristics for a Cylindrical Body of Revolution With Various Noses at Angles of Attack From 0° to 58° and Mach Numbers from 0.6 to 2.0. NASA TM X-3128, 1974.

9. Keener, Earl R.; and Chapman, Gary T.: Onset of Aerodynamic Side Forces at Zero Sideslip on Symmetric Forebodies at High Angles of Attack. AIAA Paper 74-770, 1974.

10. Jorgensen, Leland H.; and Nelson, Edgar R.: Experimental Aerodynamic Characteristics for Bodies of Elliptic Cross Section at Angles of Attack from 0° to 58° and Mach Numbers From 0.6 to 2.0. NASA TM X-3129, 1975.

11. Jorgensen, Leland H.; and Nelson, Edgar R.: Experimental Aerodynamic Characteristics for a Cylindrical Body of Revolution With Side Strakes and Various Noses at Angles of Attack From 0° to 58° and Mach numbers from 0.6 to 2.0. NASA TM X-3130, 1975.

12. Jorgensen, Leland H.; and Howell, Michael H.: Experimental Aerodynamic Characteristics for Slender Bodies With Thin Wings at Angles of Attack From 0° to 58° and Mach Numbers From 0.6 to 2.0. NASA TM X-3309, 1976.

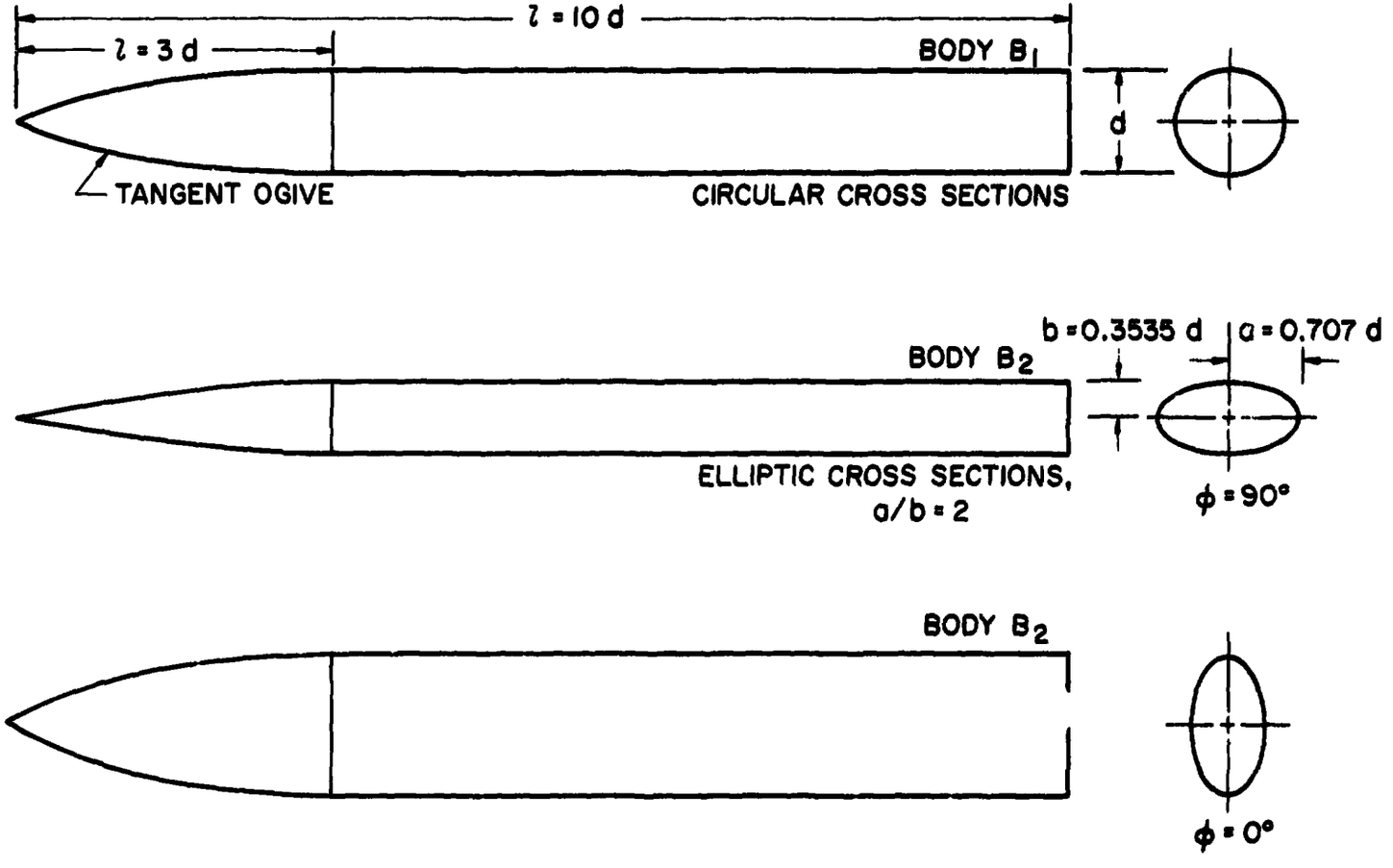

(a) Basic bodies of circular and elliptic cross section.

Figure 1.– Model components; d = 6.60 cm (2.60 in.).

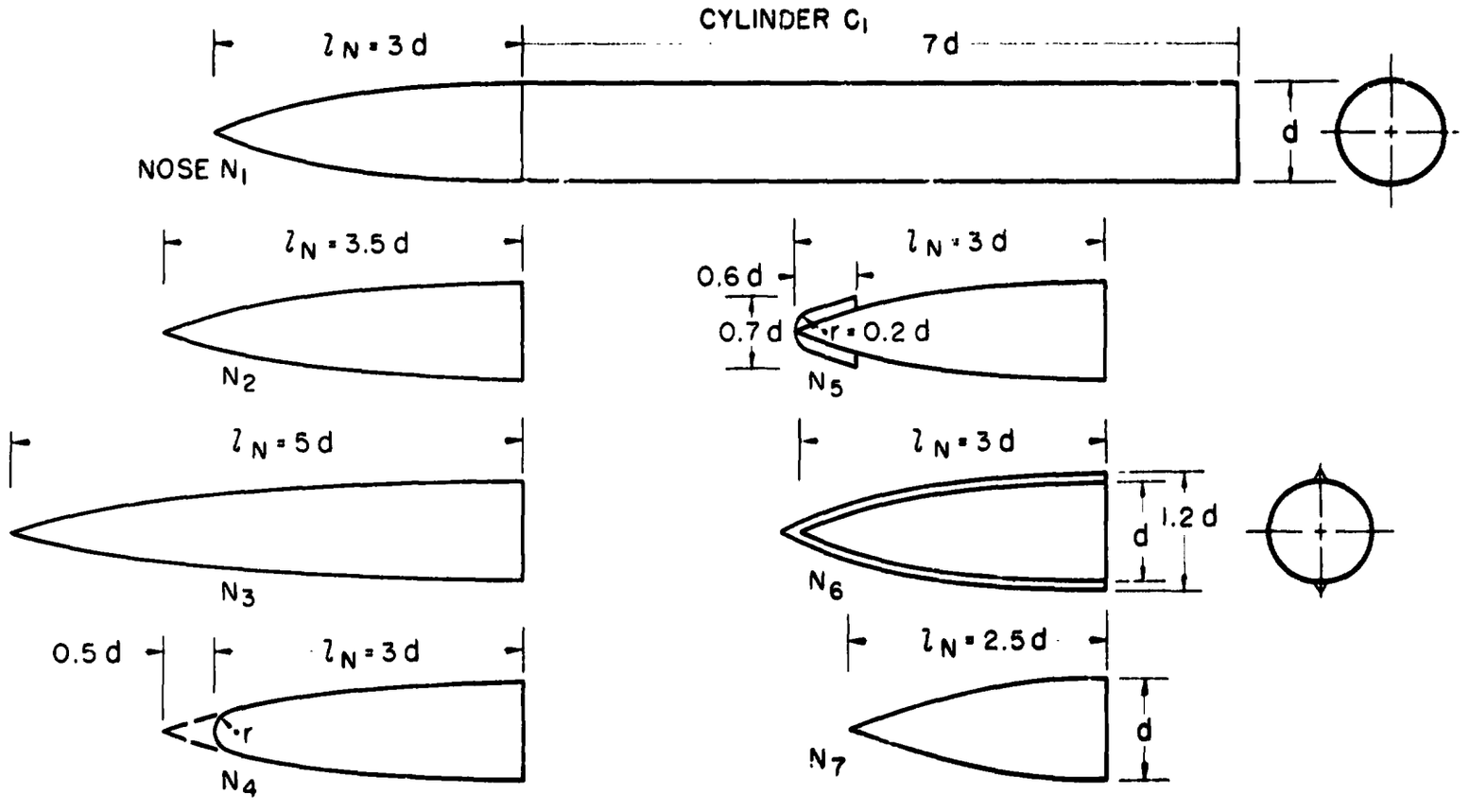

(b) Additional noses for modification of body $B_1 = N_1 C_1$.

Figure 1. - Continued.

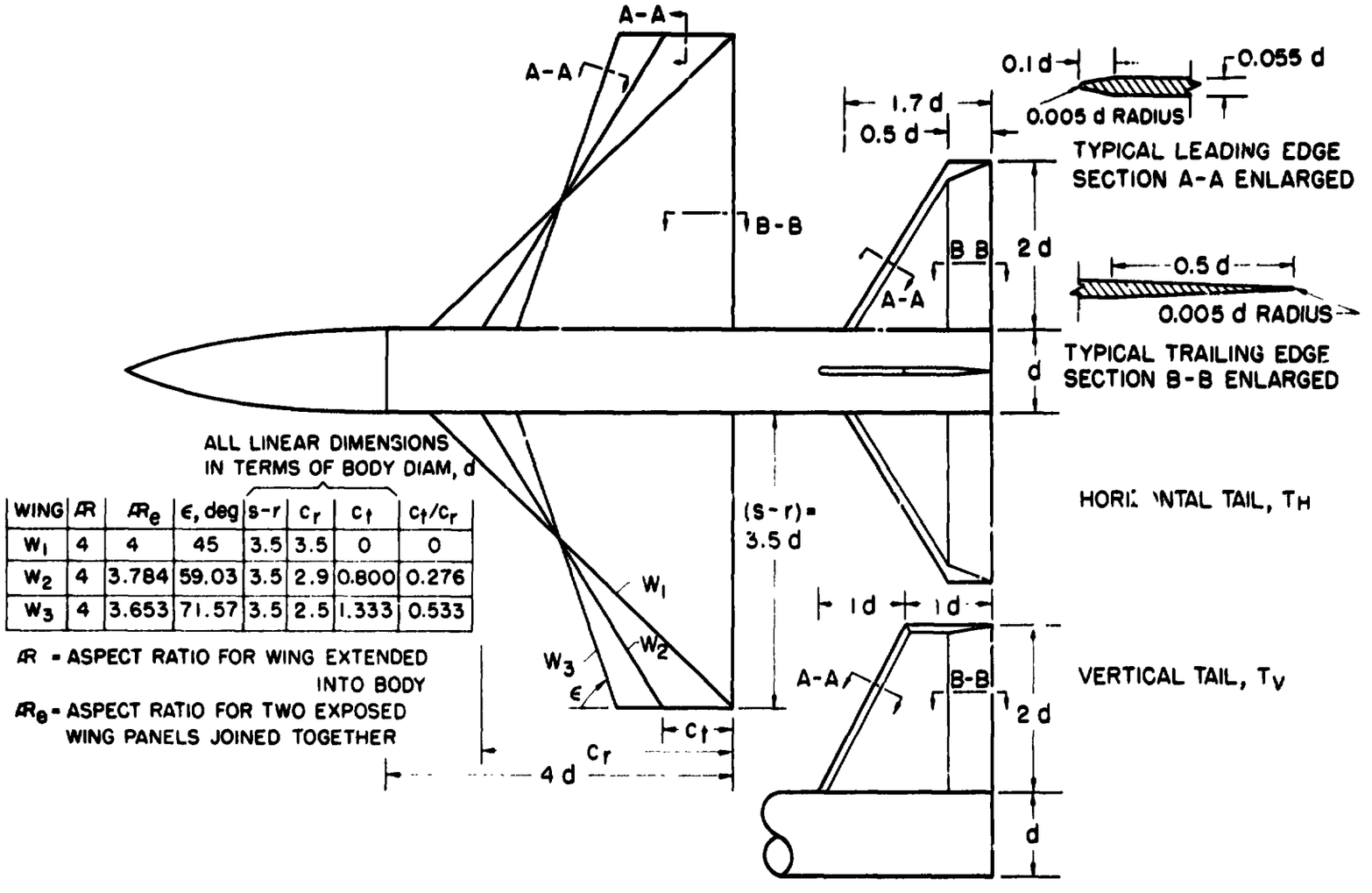

WING	AR	ARe	ϵ, deg	s-r	cr	ct	ct/cr
W1	4	4	45	3.5	3.5	0	0
W2	4	3.784	59.03	3.5	2.9	0.800	0.276
W3	4	3.653	71.57	3.5	2.5	1.333	0.533

AR = ASPECT RATIO FOR WING EXTENDED INTO BODY

ARe = ASPECT RATIO FOR TWO EXPOSED WING PANELS JOINED TOGETHER

(c) Body B_1 with aspect-ratio 4 wings of various taper ratios and tail arrangement.

Figure 1.– Continued.

NOTE: TYPICAL LEADING AND TRAILING EDGE SECTIONS SHOWN IN FIG. 2

HORIZONTAL AND VERTICAL TAILS CAN BE ATTACHED AT POSITIONS SHOWN IN FIG. 2

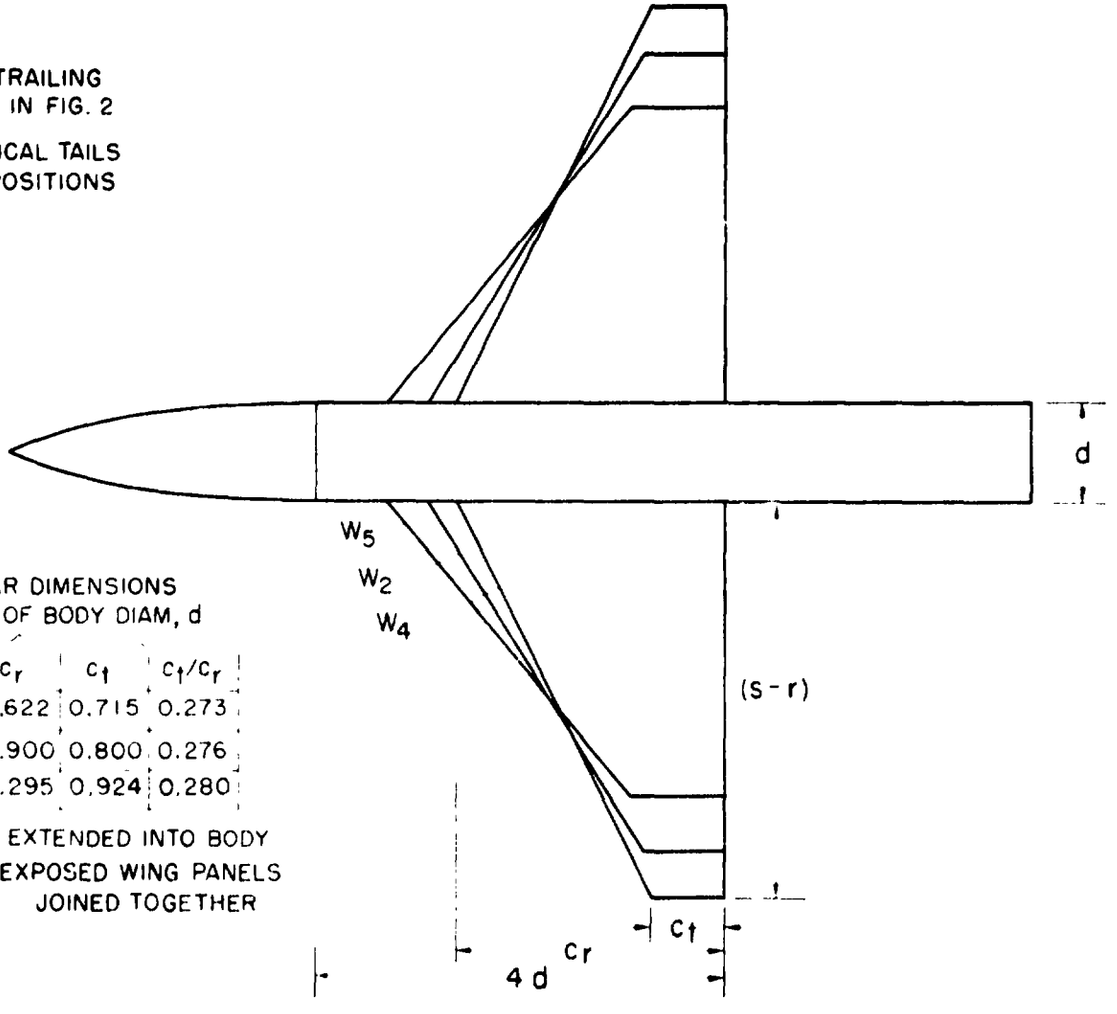

ALL LINEAR DIMENSIONS IN TERMS OF BODY DIAM, d

WING	$\mathcal{AR}$	$\mathcal{AR}_e$	ϵ, deg	s-r	c_r	c_t	c_t/c_r
W_4	5	4.761	64.36	3.972	2.622	0.715	0.273
W_2	4	3.784	59.03	3.500	2.900	0.800	0.276
W_5	3	2.810	51.33	2.964	3.295	0.924	0.280

$\mathcal{AR}$ = ASPECT RATIO FOR WING EXTENDED INTO BODY

$\mathcal{AR}_e$ = ASPECT RATIO FOR TWO EXPOSED WING PANELS JOINED TOGETHER

(d) Body B_1 with wings of aspect ratio 3, 4, and 5 (referring to wings W_2, W_4, and W_5).

Figure 1.– Continued.

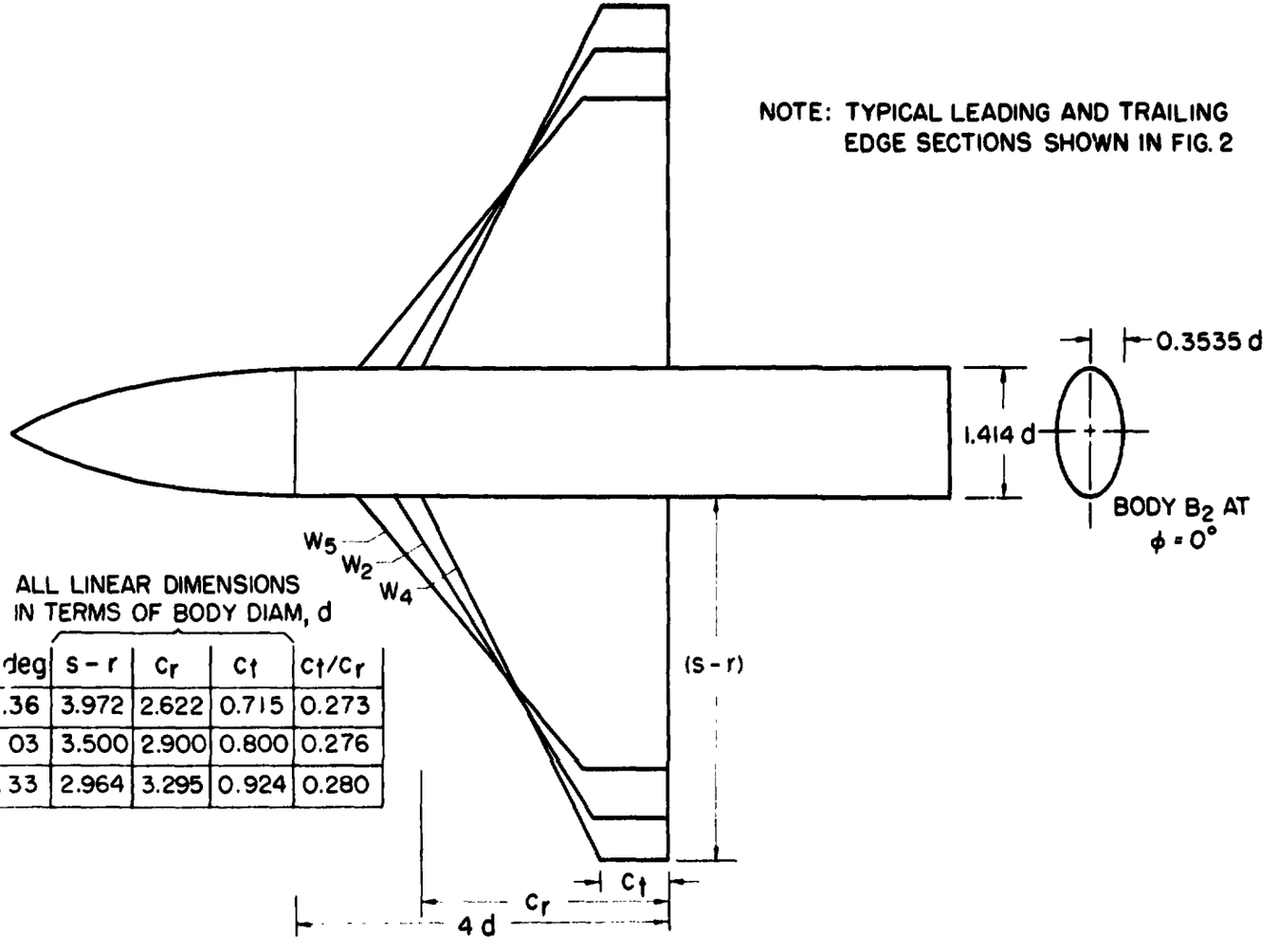

ALL LINEAR DIMENSIONS IN TERMS OF BODY DIAM, d

WING	AR$_e$	ϵ, deg	s - r	c_r	c_t	c_t/c_r
W_4	4.761	64.36	3.972	2.622	0.715	0.273
W_2	3.784	53 03	3.500	2.900	0.800	0.276
W_5	2.810	51.33	2.964	3.295	0.924	0.280

(e) Body B_2 with wings W_2, W_4, and W_5.

Figure 1.– Concluded.

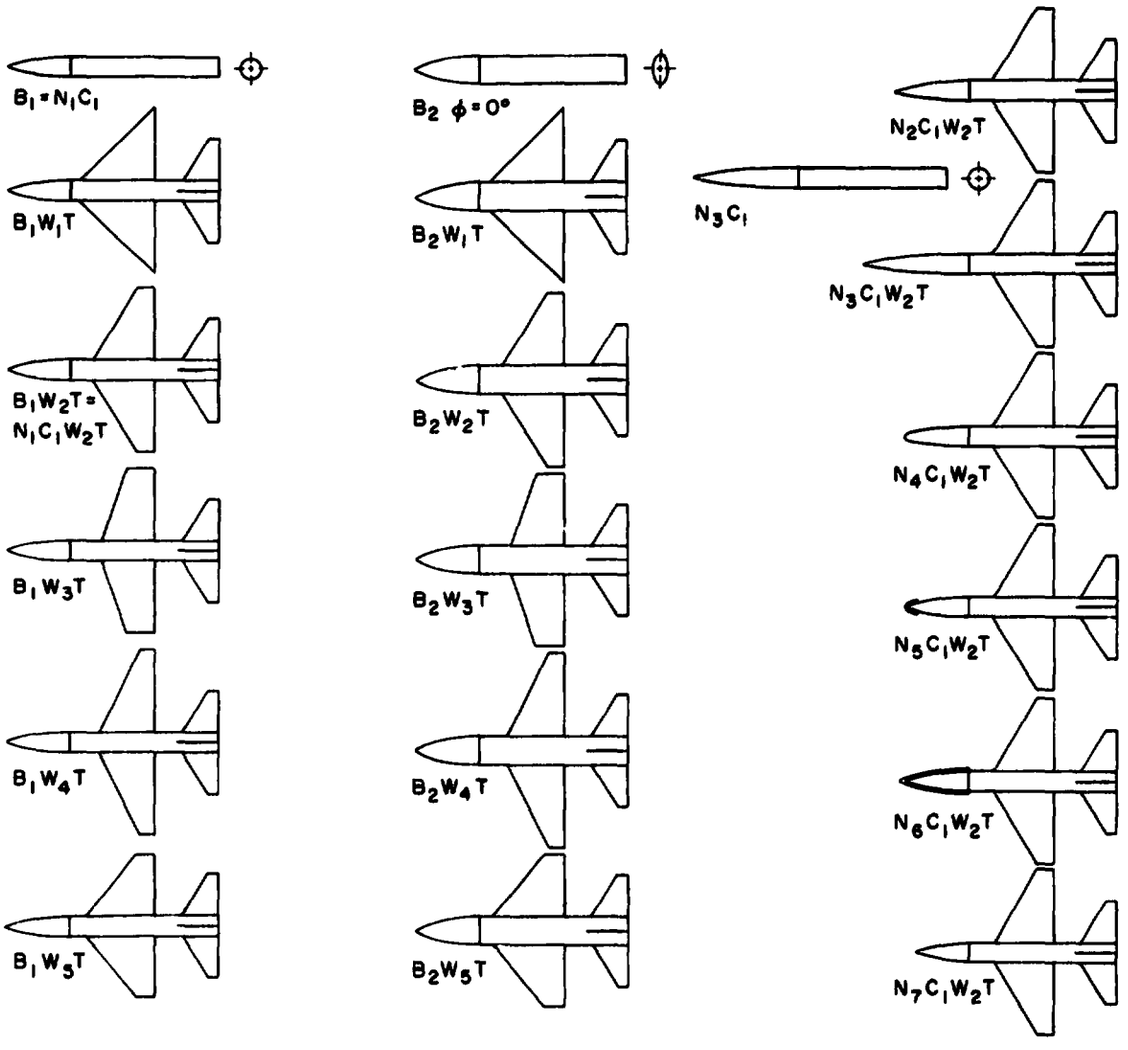

(a) Planform views of configurations tested.

Figure 2.– Planform views of configurations tested and typical model-support setups in the Ames 6- by 6-Foot Wind Tunnel.

(b) Test Model (B_2 W_5 T) on support setup for $\alpha = 0°$ to about 27° in the Ames 6- by 6-Foot Wind Tunnel.

Figure 2. – Continued.

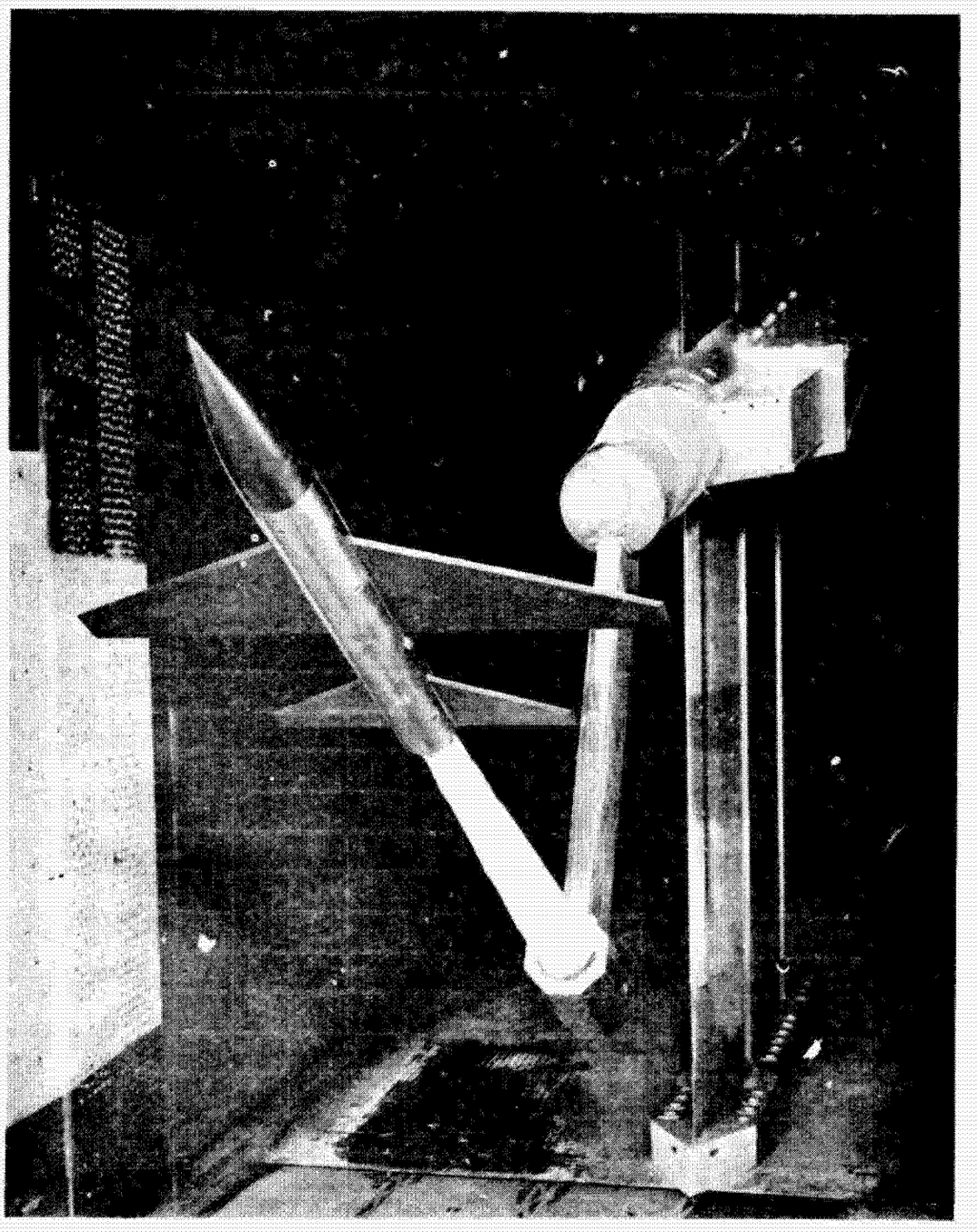

(c) Test model (B_1, W_4, T) on support setup for $\alpha = 27°$ to 58° in the Ames 6- by 6-Foot Wind Tunnel.

Figure 2. Concluded.

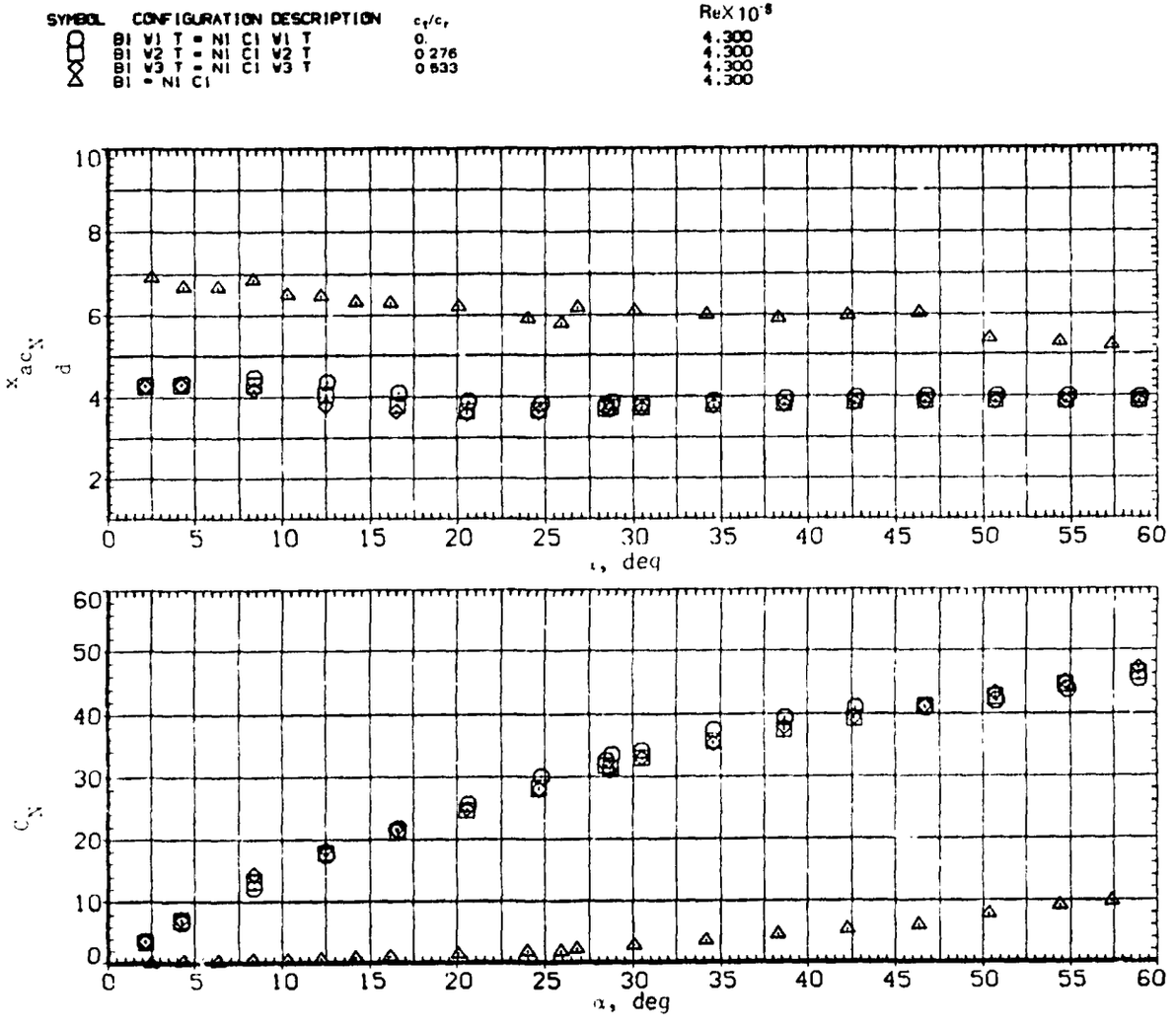

(a) x_{ac_N}/d and C_N versus α.

Figure 3.– Effect of wing taper ratio with circular body and tail; M = 0.6.

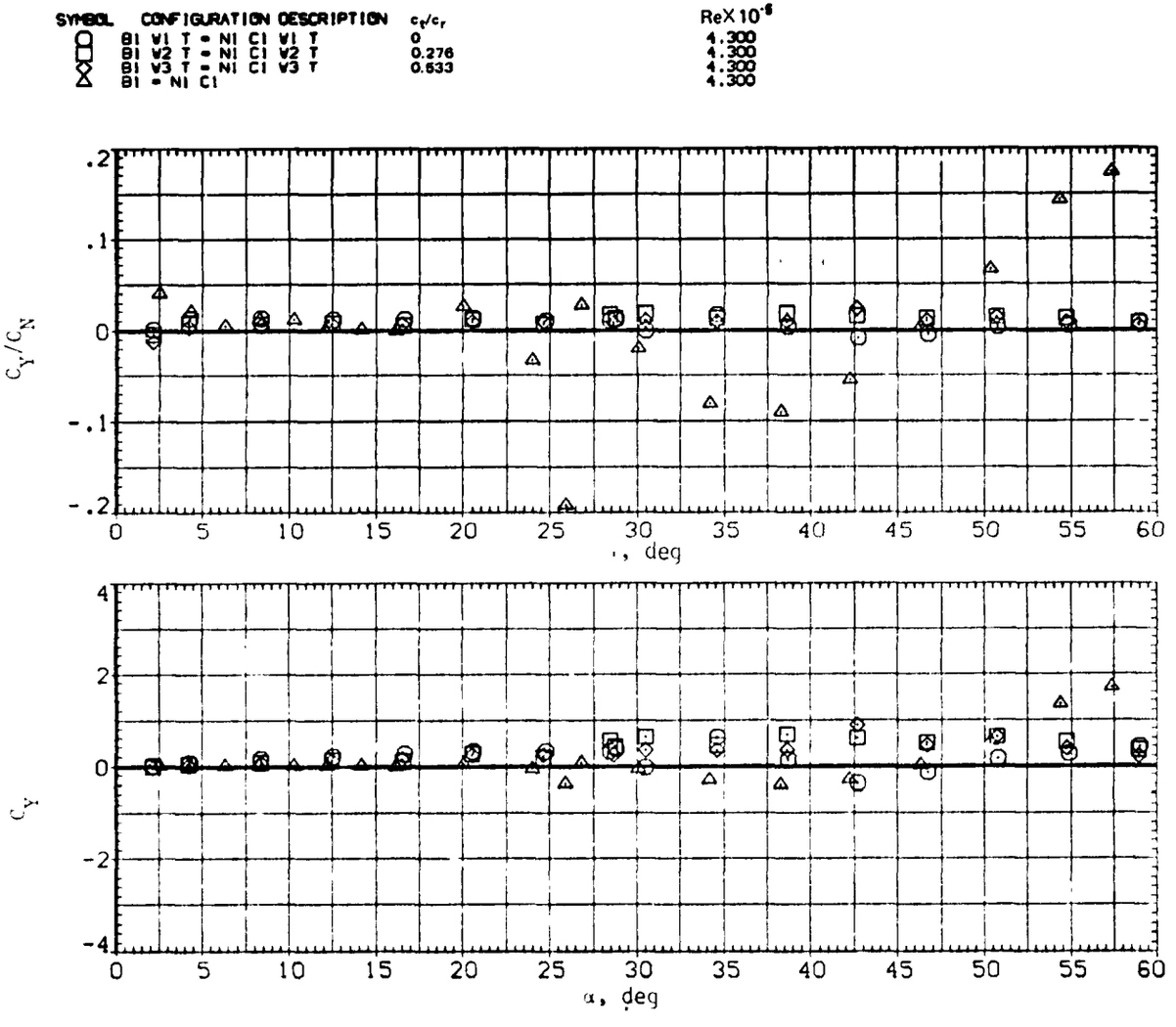

(b) C_Y/C_N and C_Y versus α.

Figure 3.– Continued.

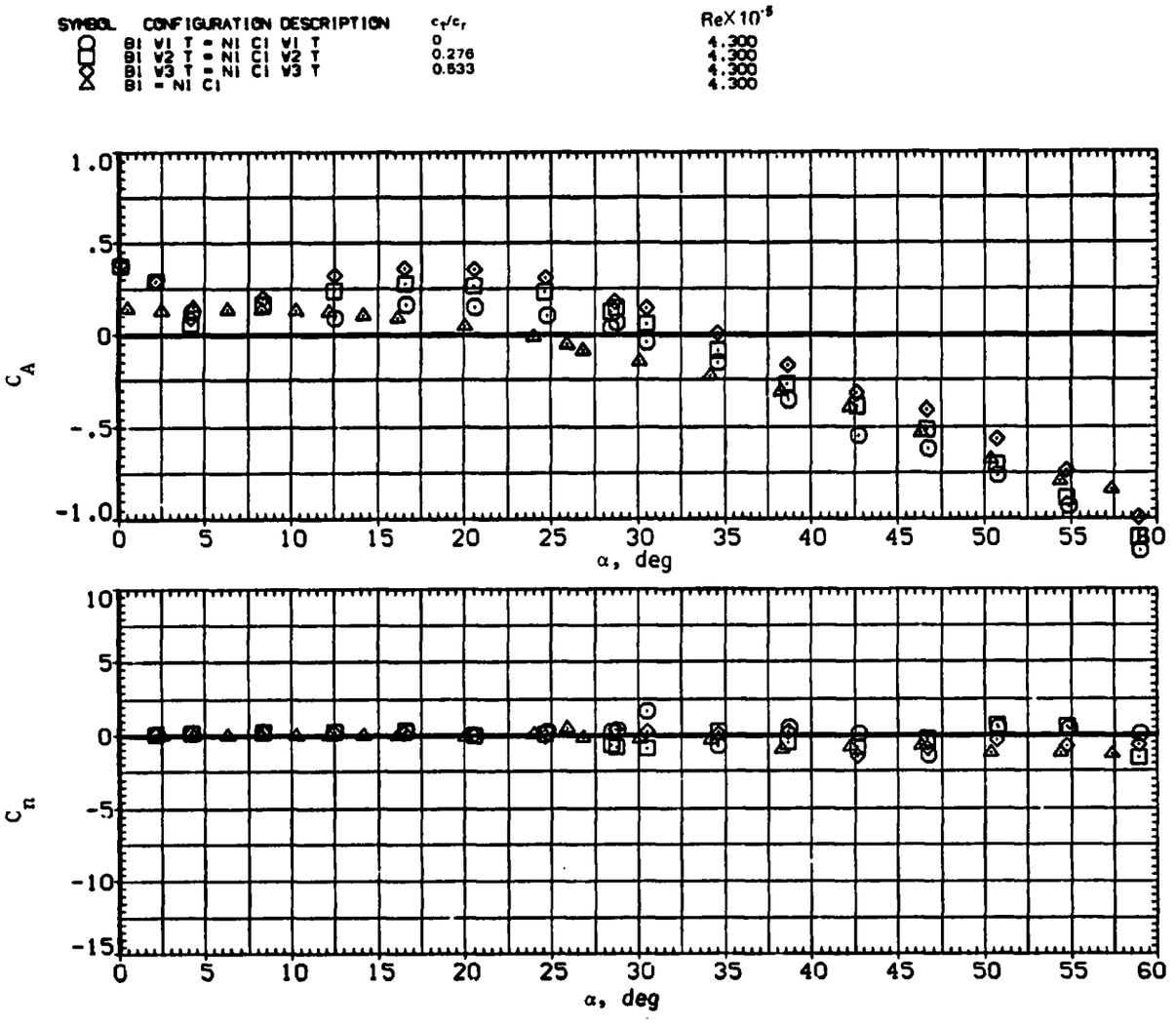

(c) C_A and C_n versus α.

Figure 3.– Continued.

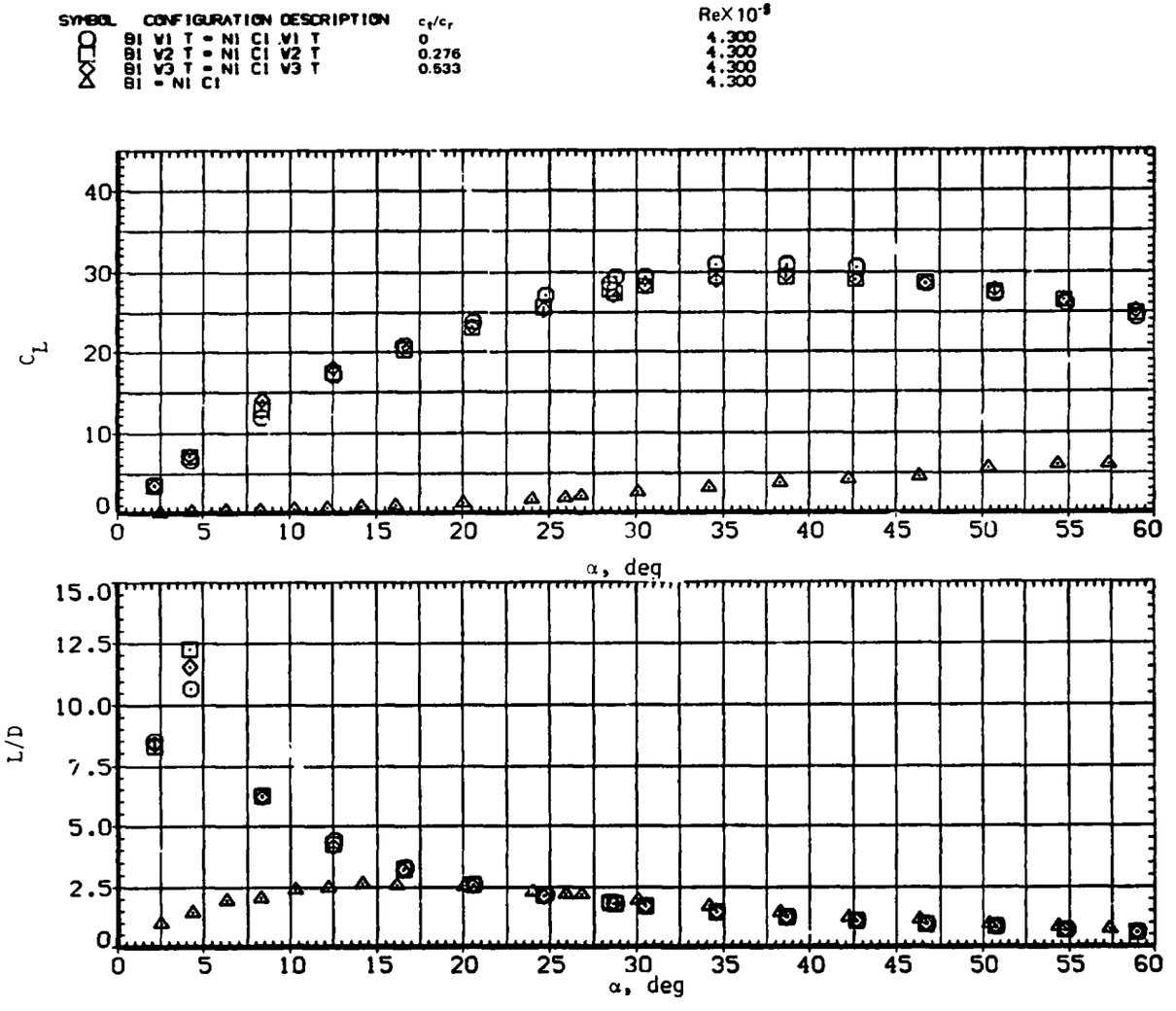

(d) C_L and L/D versus α.

Figure 3.– Concluded.

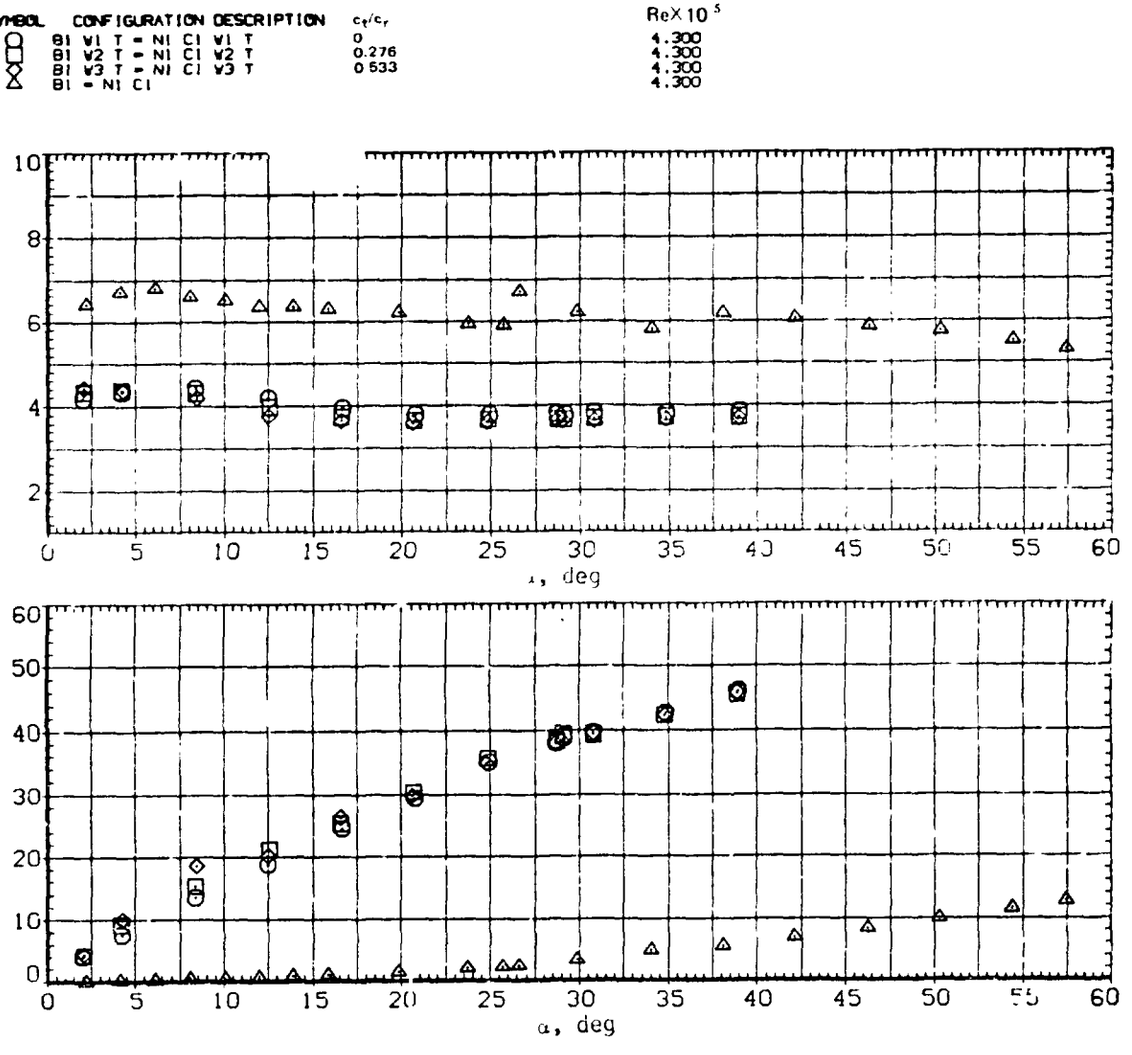

(a) x_{ac_N}/d and C_N versus α.

Figure 4.– Effect of wing taper ratio with circular body and tail; M = 0.9.

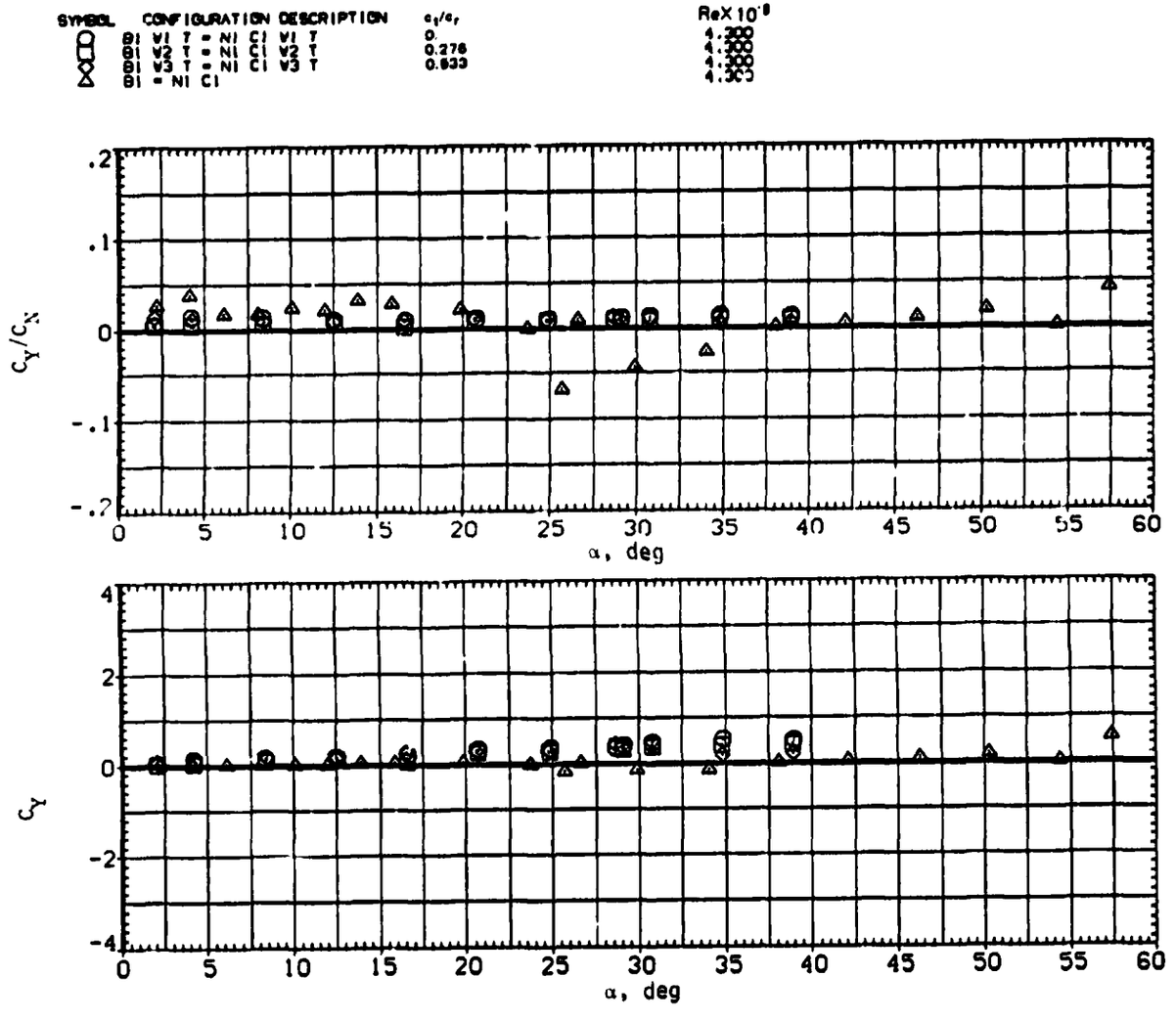

(b) C_Y/C_N and C_Y versus α.

Figure 4.– Continued.

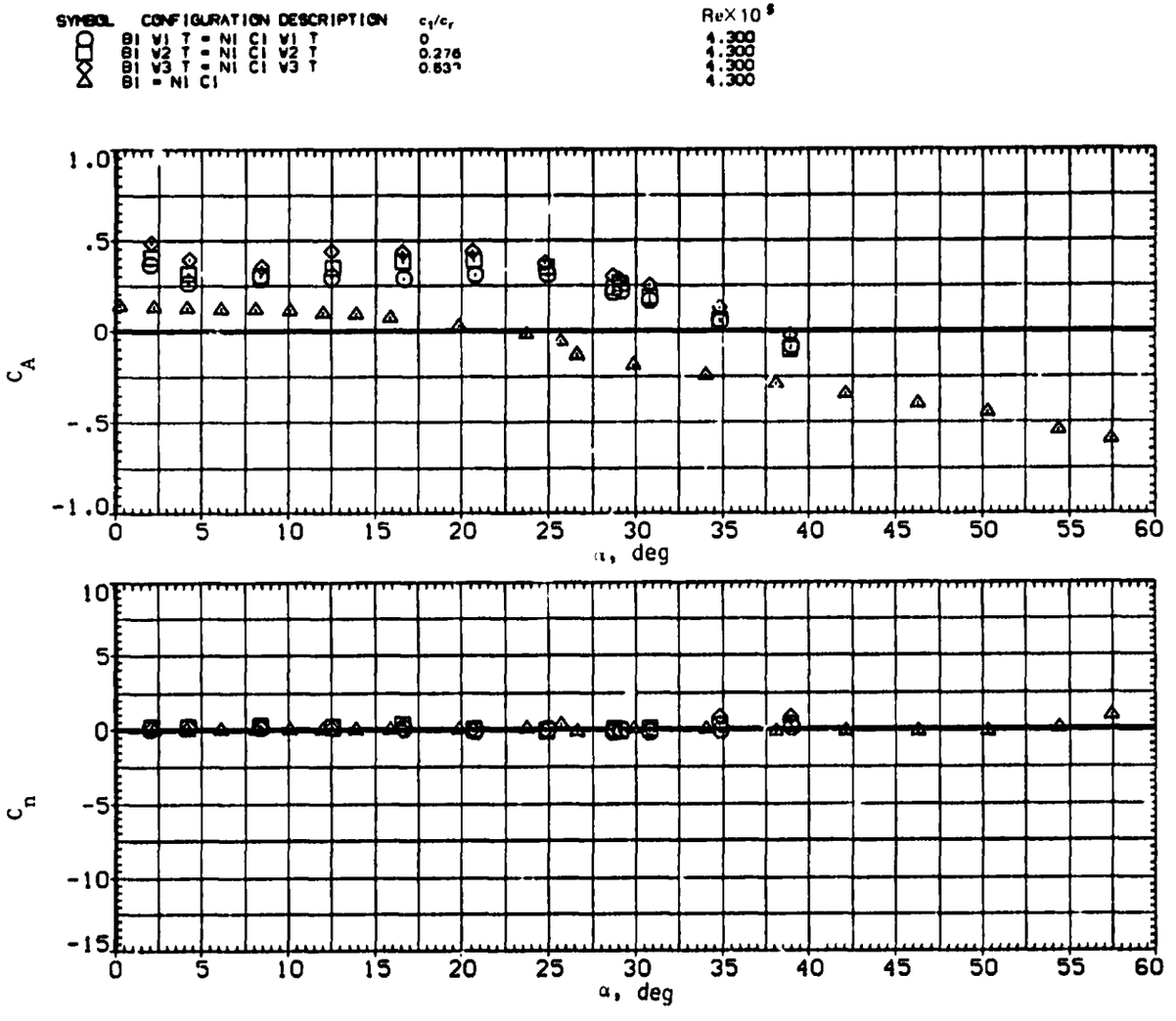

(c) C_A and C_n versus α.

Figure 4.– Continued.

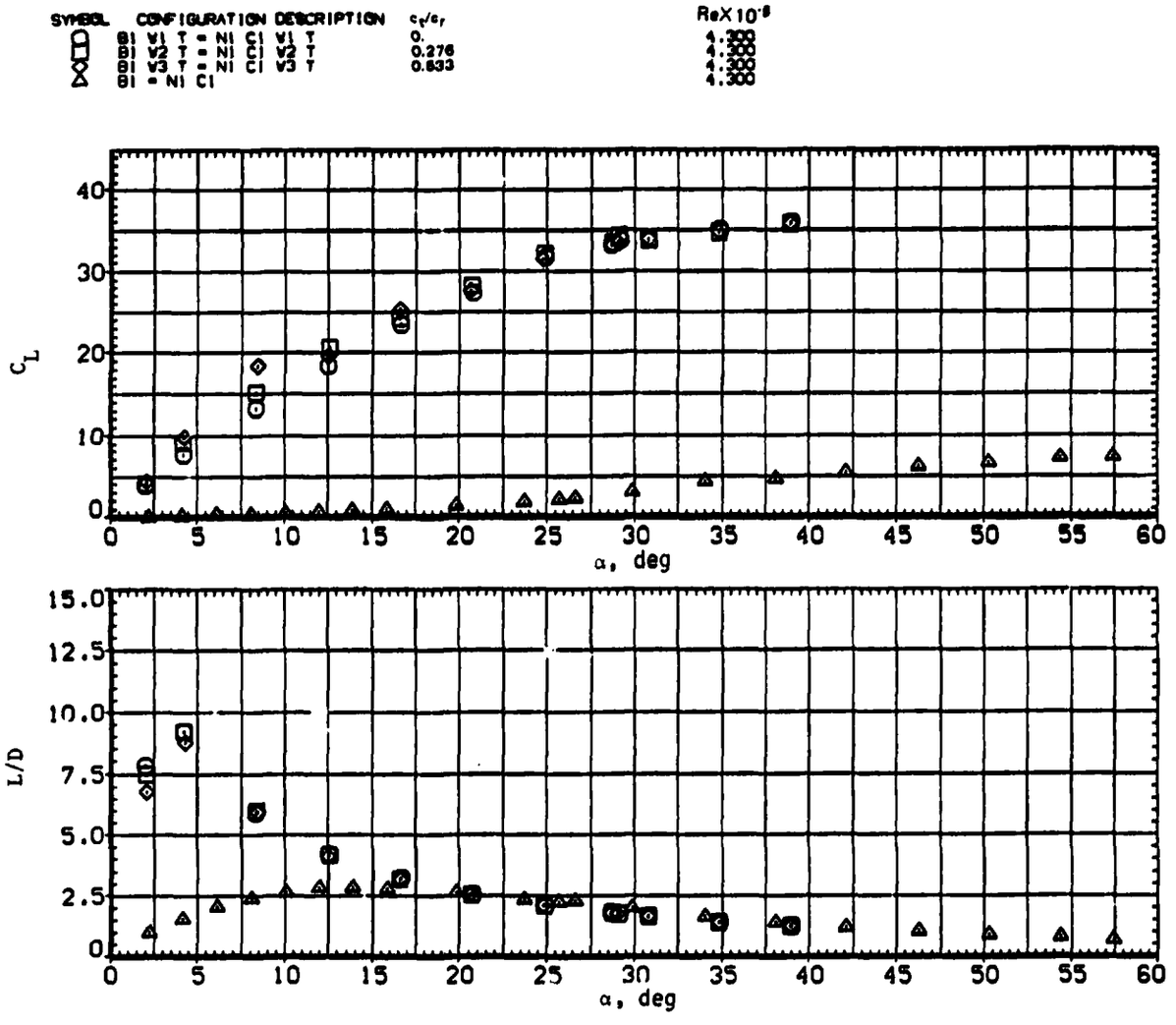

(d) C_L and L/D versus α.

Figure 4.– Concluded.

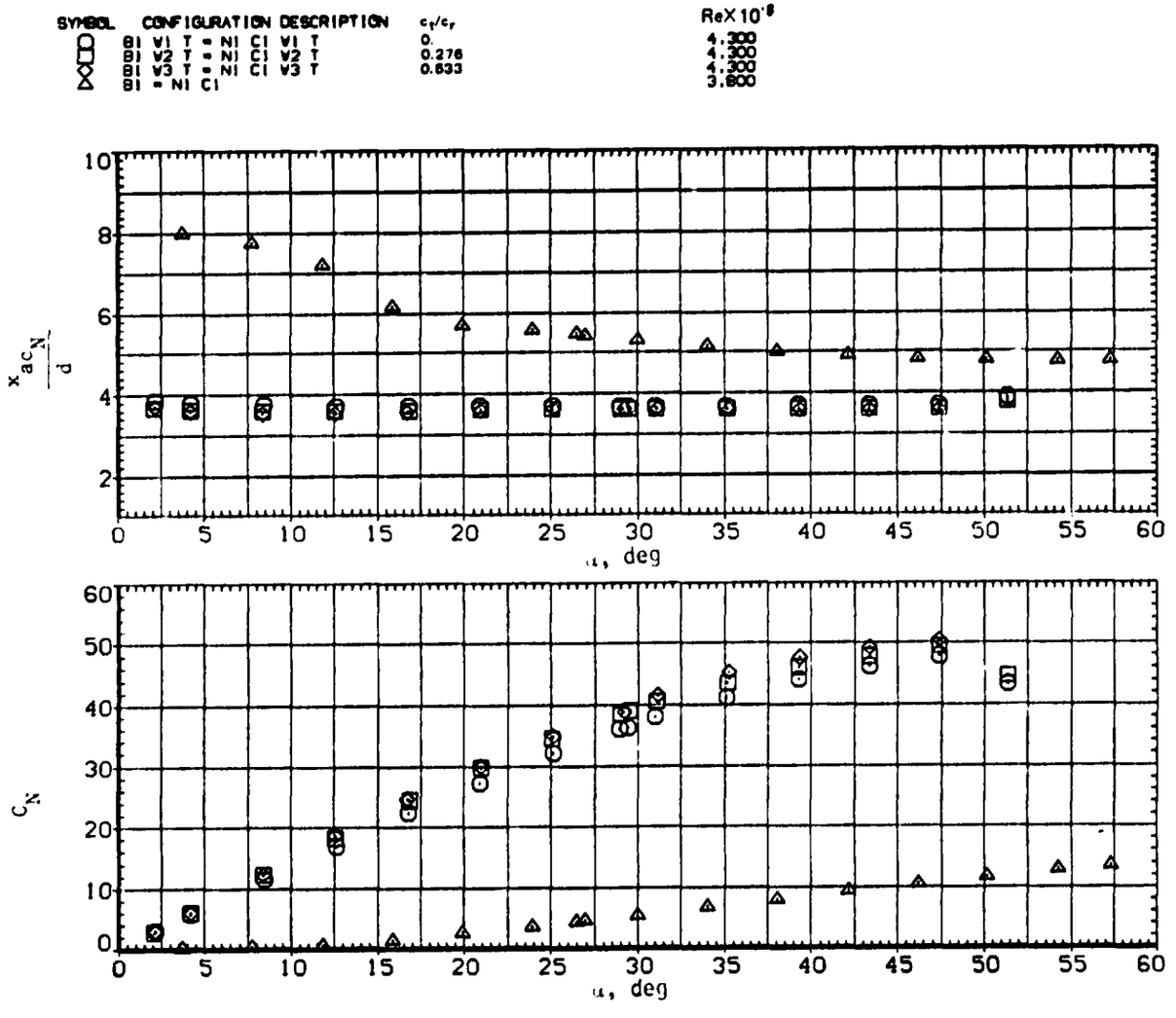

(a) x_{ac_N}/d and C_N versus α.

Figure 5.– Effect of wing taper ratio with circular body and tail; M = 1.5.

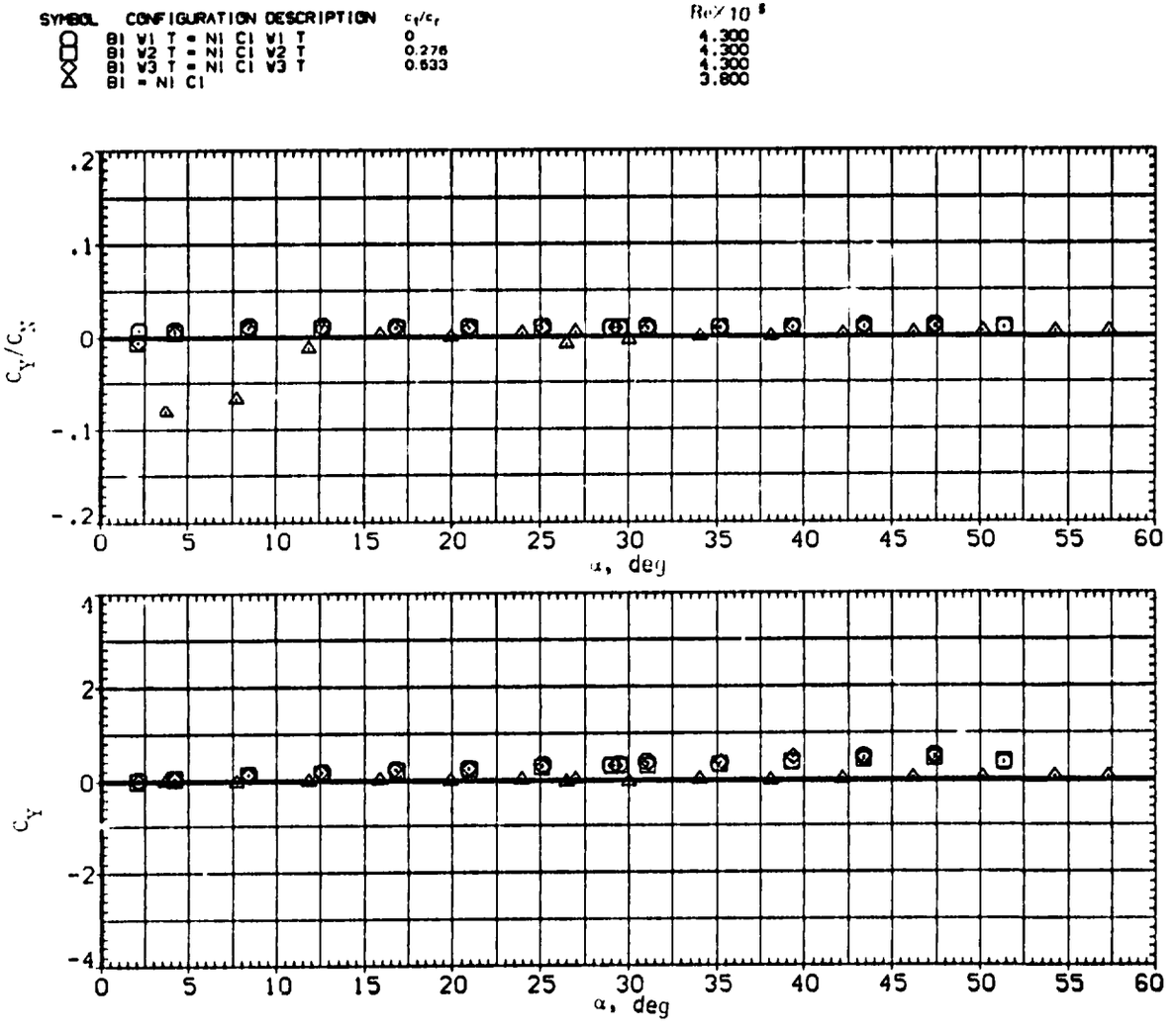

(b) C_Y/C_N and C_Y versus α.

Figure 5.– Continued.

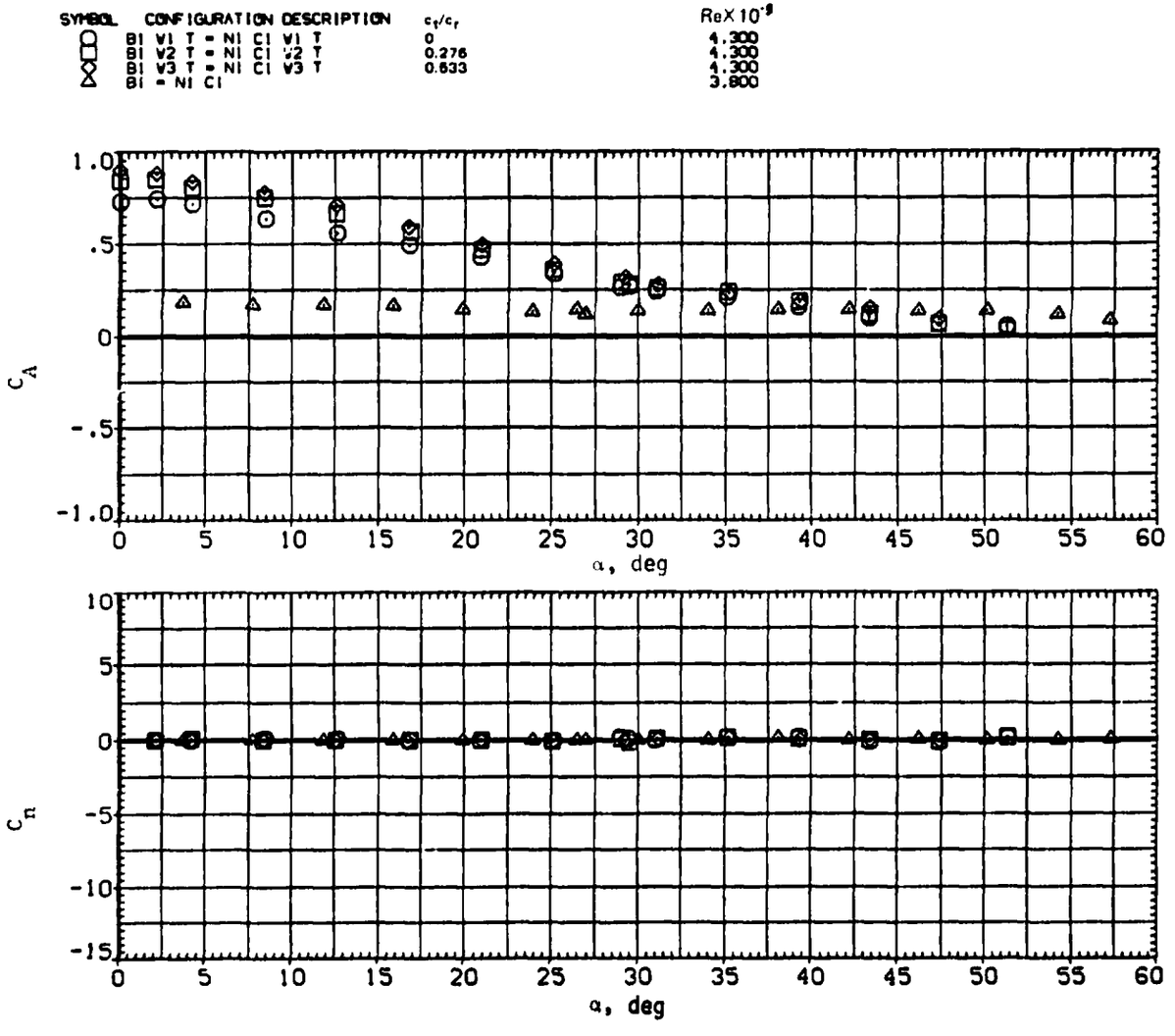

(c) C_A and C_n versus α.

Figure 5.– Continued.

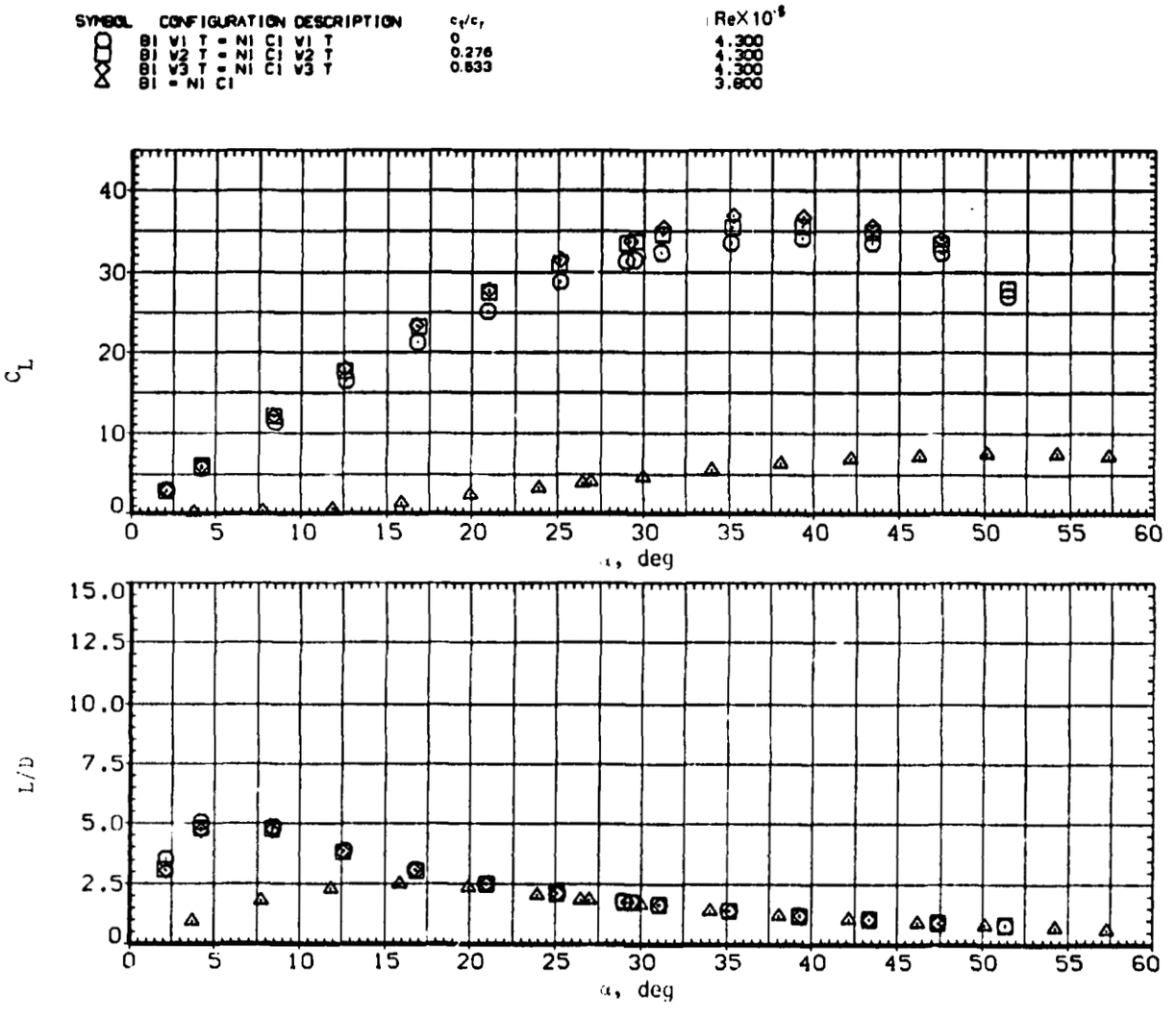

(d) C_L and L/D versus α.

Figure 5.– Concluded.

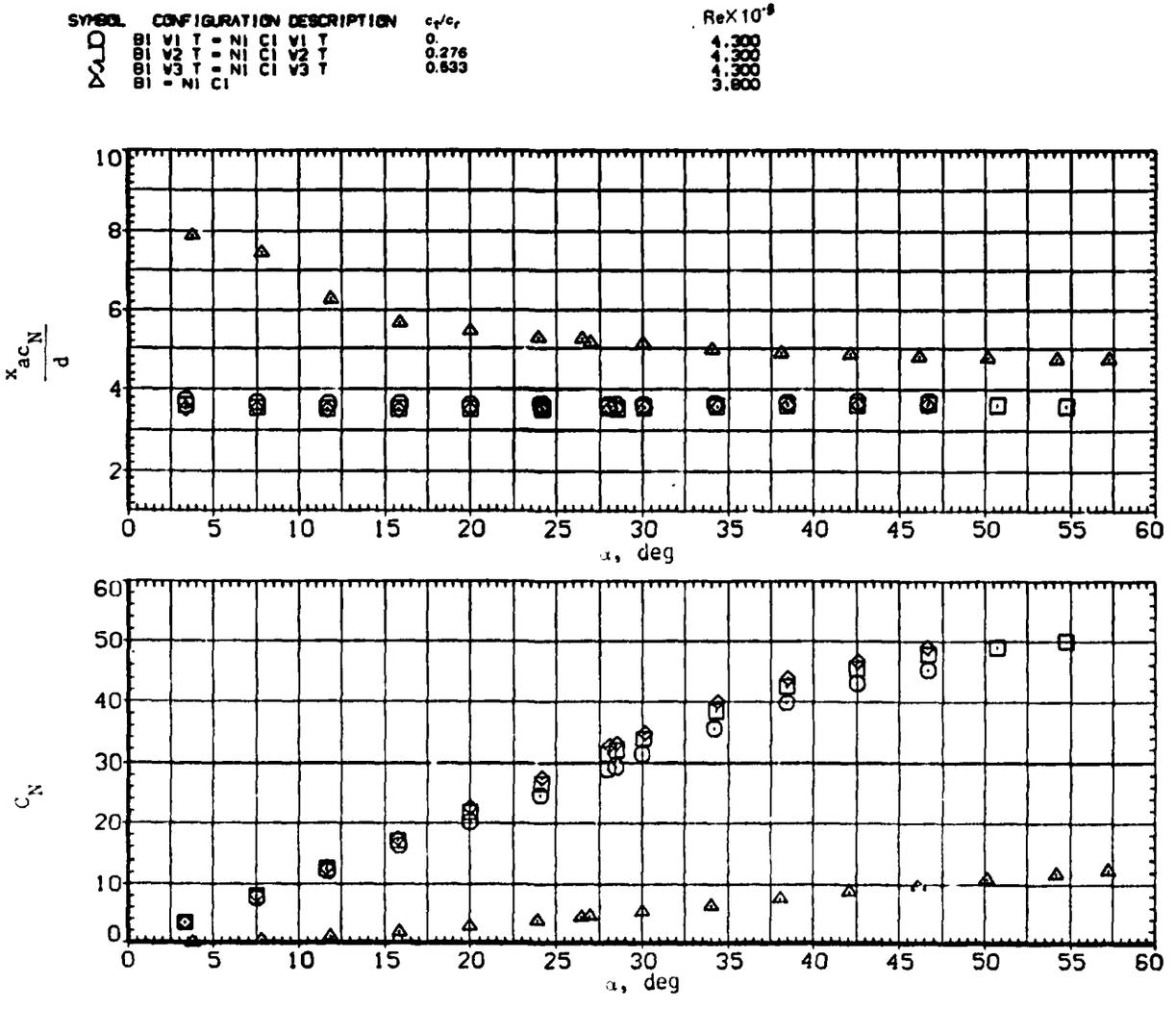

(a) x_{ac_N}/d and C_N versus α.

Figure 6.– Effect of wing taper ratio with circular body and tail; M = 2.0.

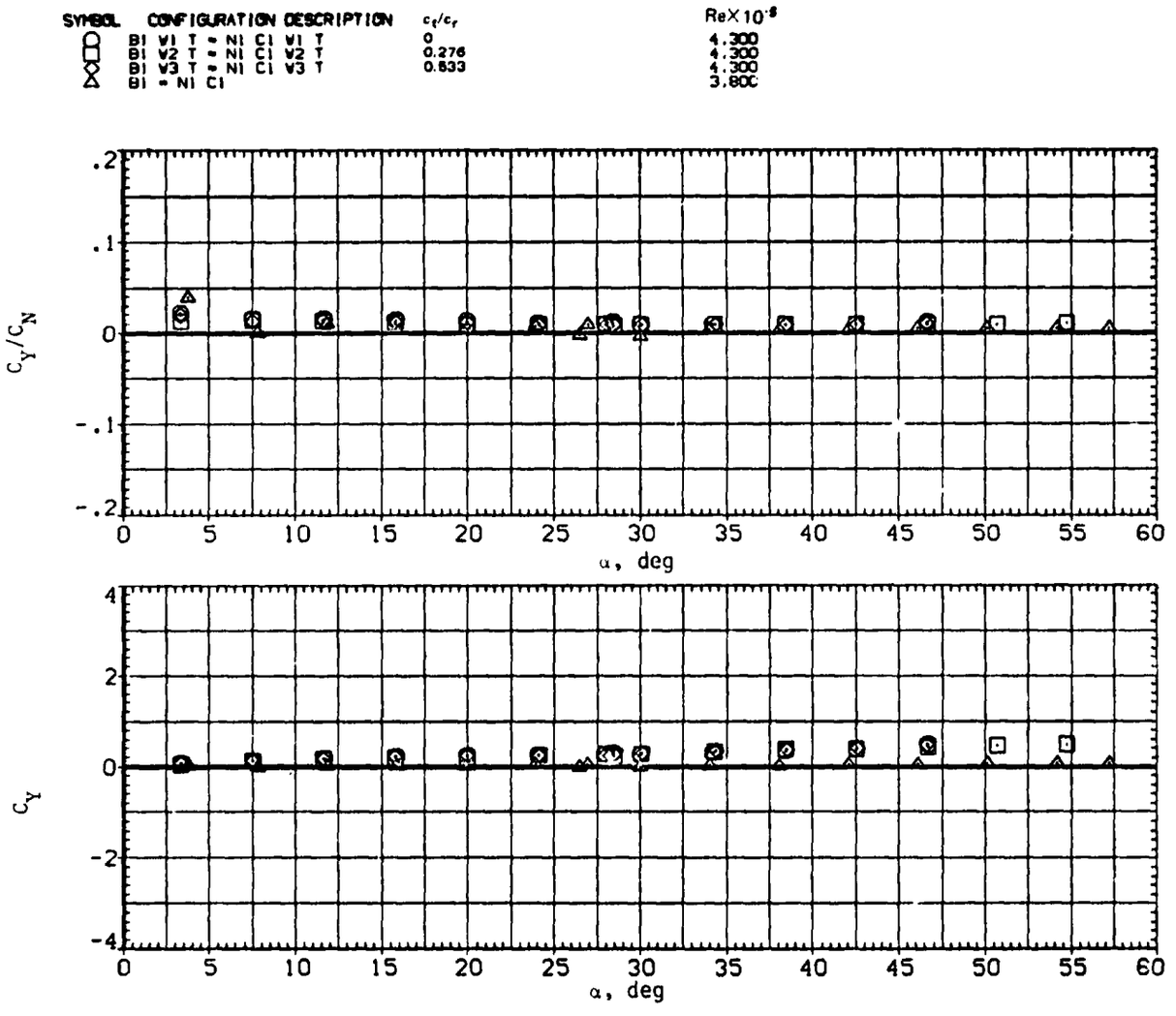

(b) C_Y/C_N and C_Y versus α.

Figure 6.– Continued.

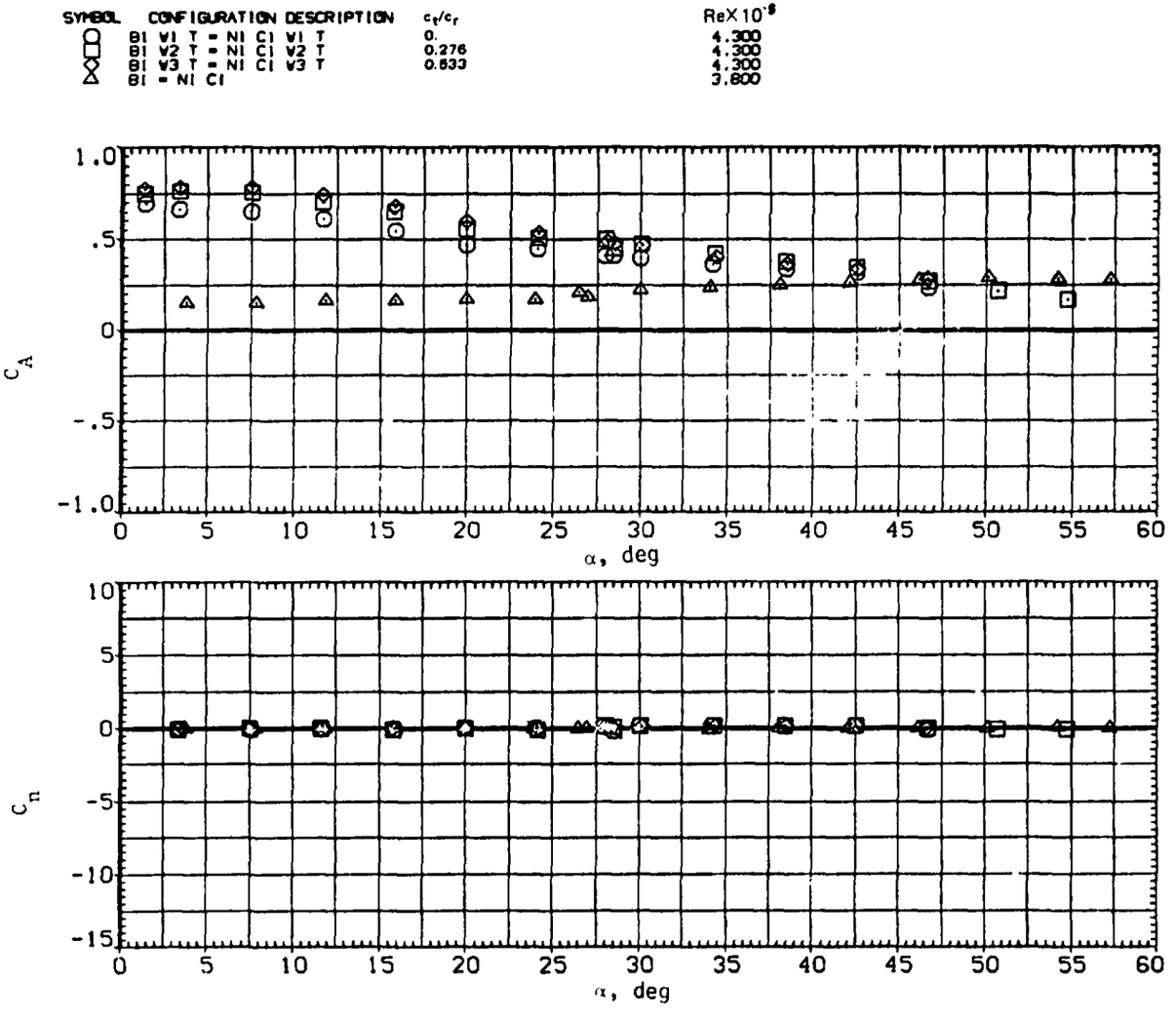

(c) C_A and C_n versus α.

Figure 6.– Continued.

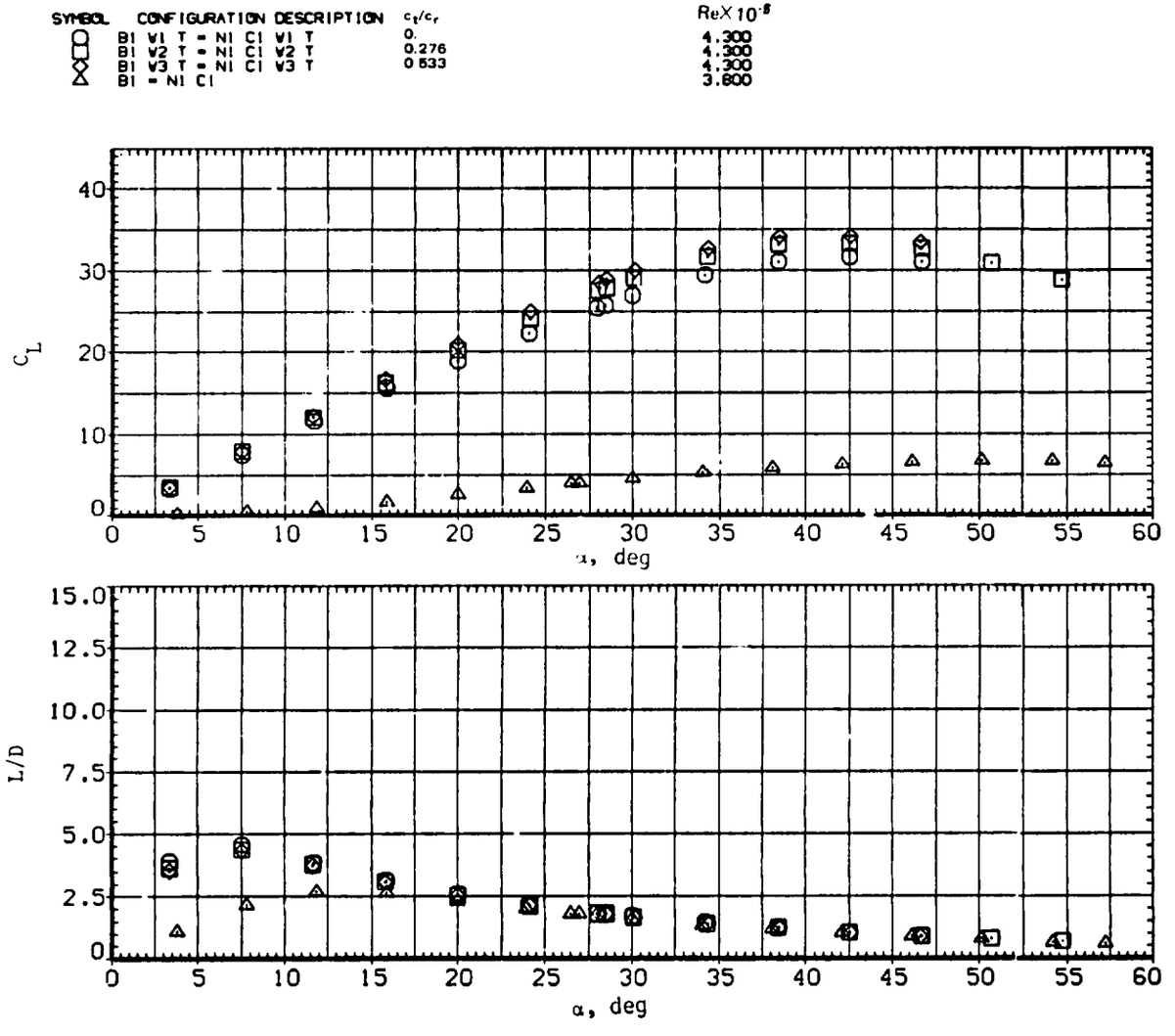

(d) C_L and L/D versus α.

Figure 6.– Concluded.

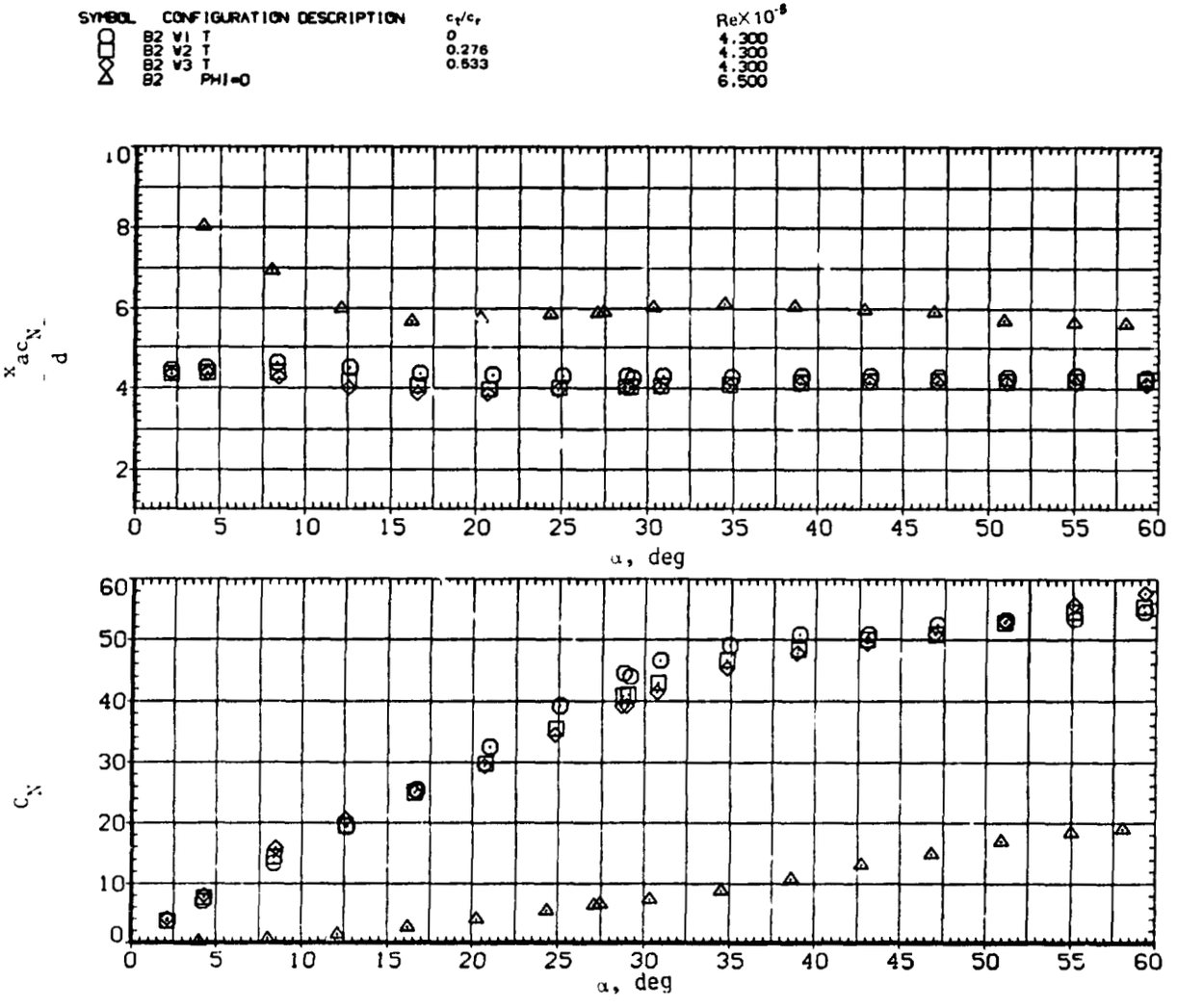

(a) x_{ac_N}/d and C_N versus α.

Figure 7. – Effect of wing taper ratio with elliptic body and tail; M = 0.6.

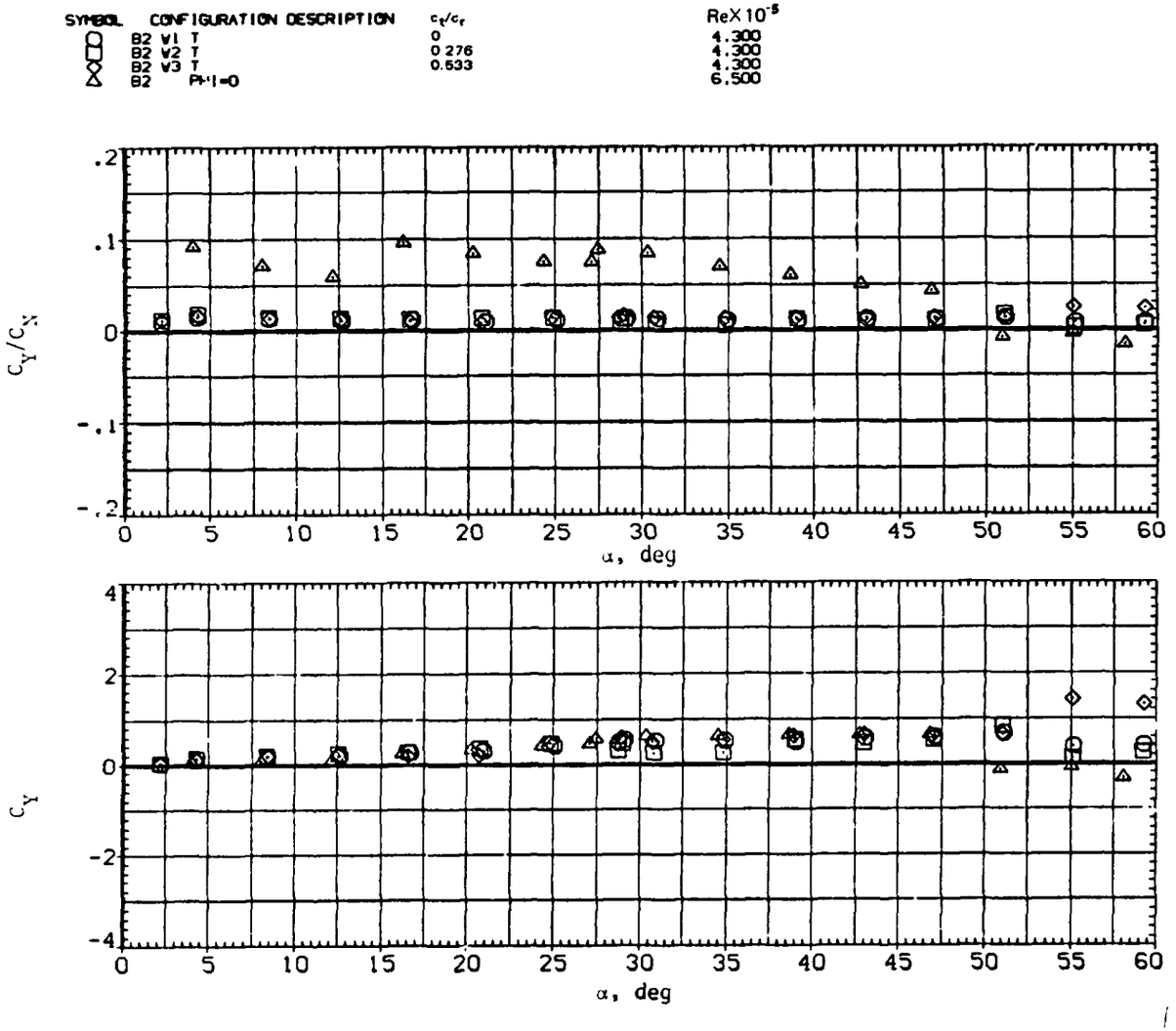

(b) C_Y/C_N and C_Y versus α.

Figure 7.– Continued.

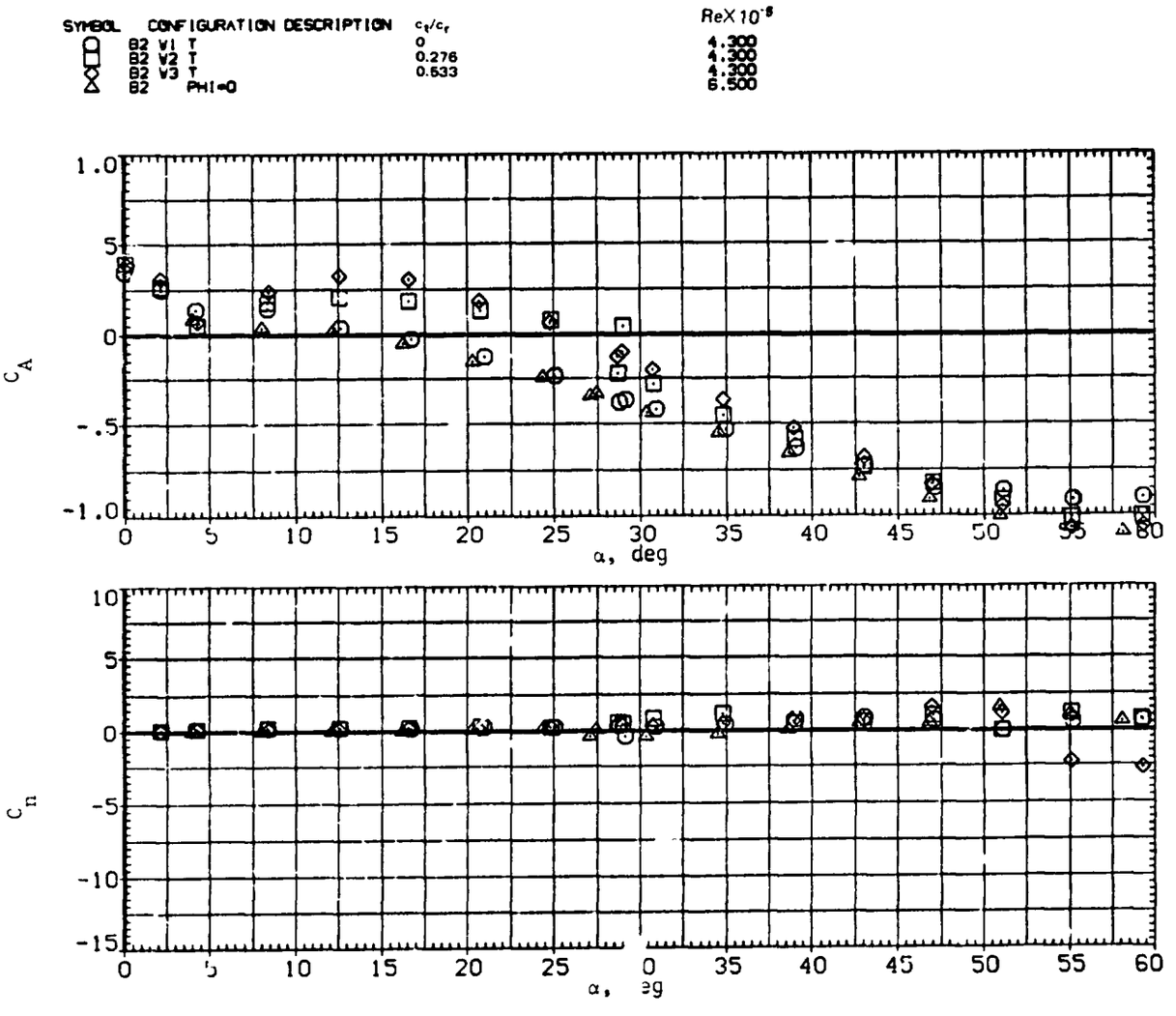

(c) C_A and C_n versus α.

Figure 7.-- Continued.

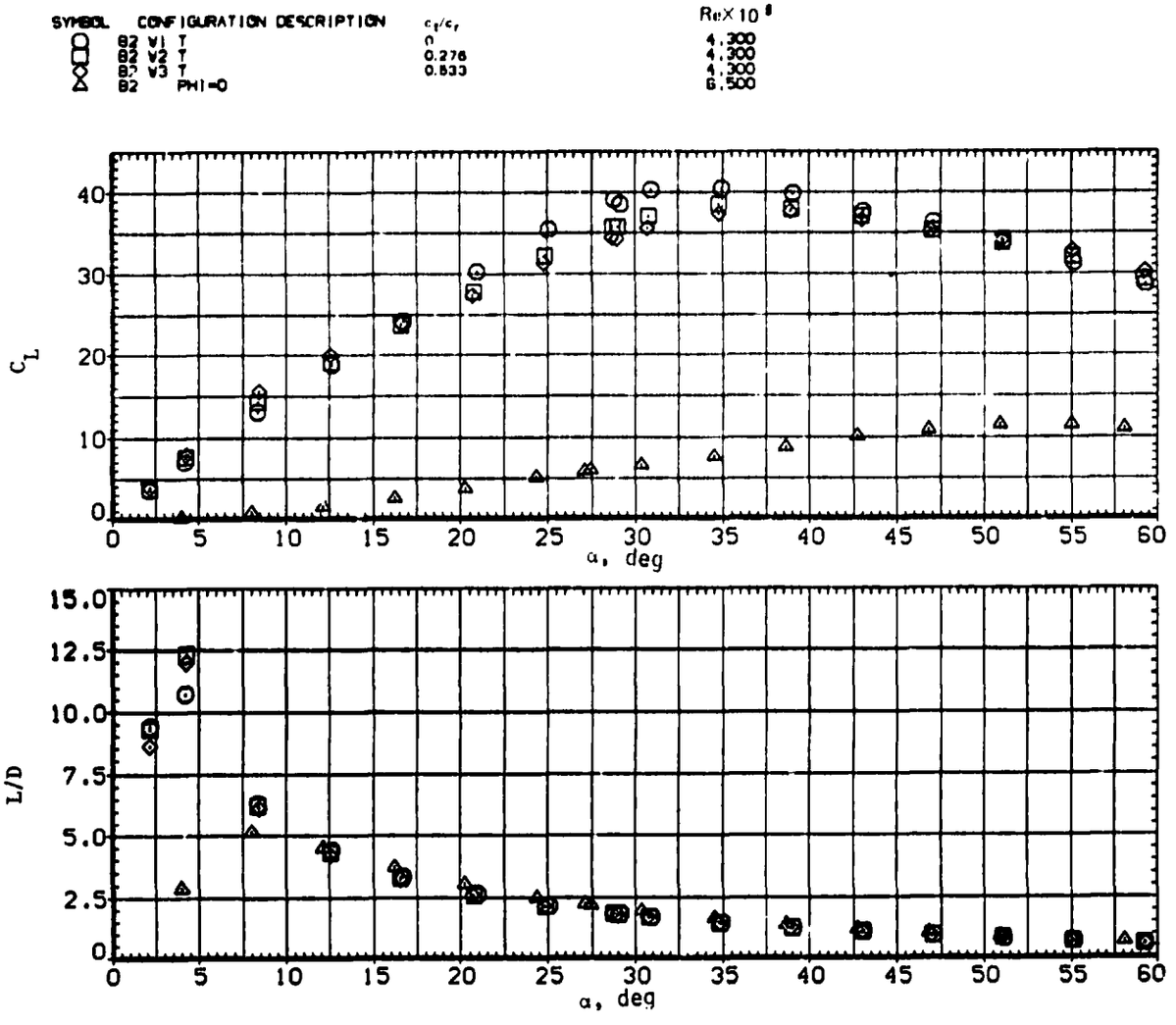

(d) C_L and L/D versus α.

Figure 7.– Concluded.

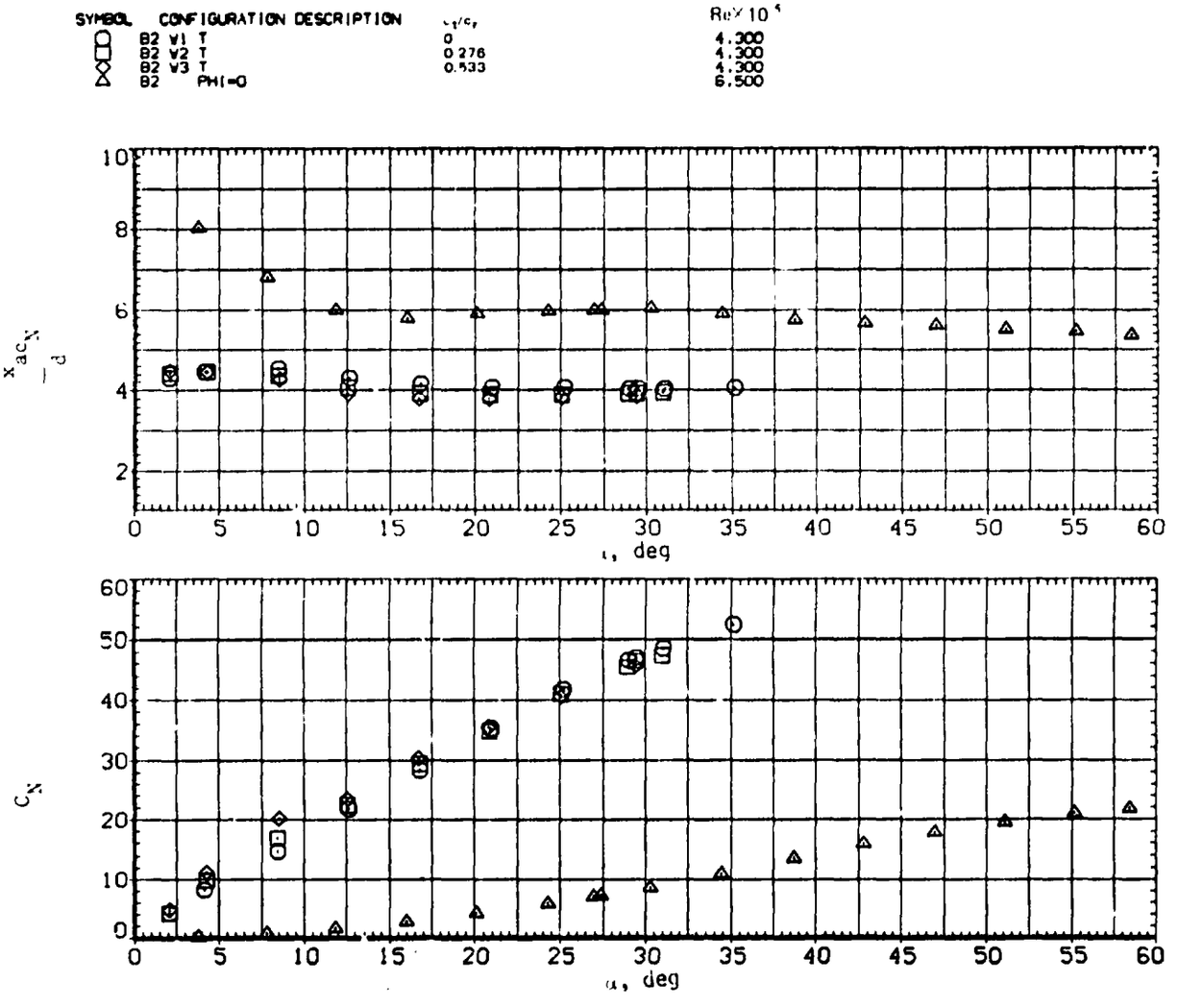

(a) x_{ac_N}/d and C_N versus α.

Figure 8. - Effect of wing taper ratio with elliptic body and tail; M = 0.9.

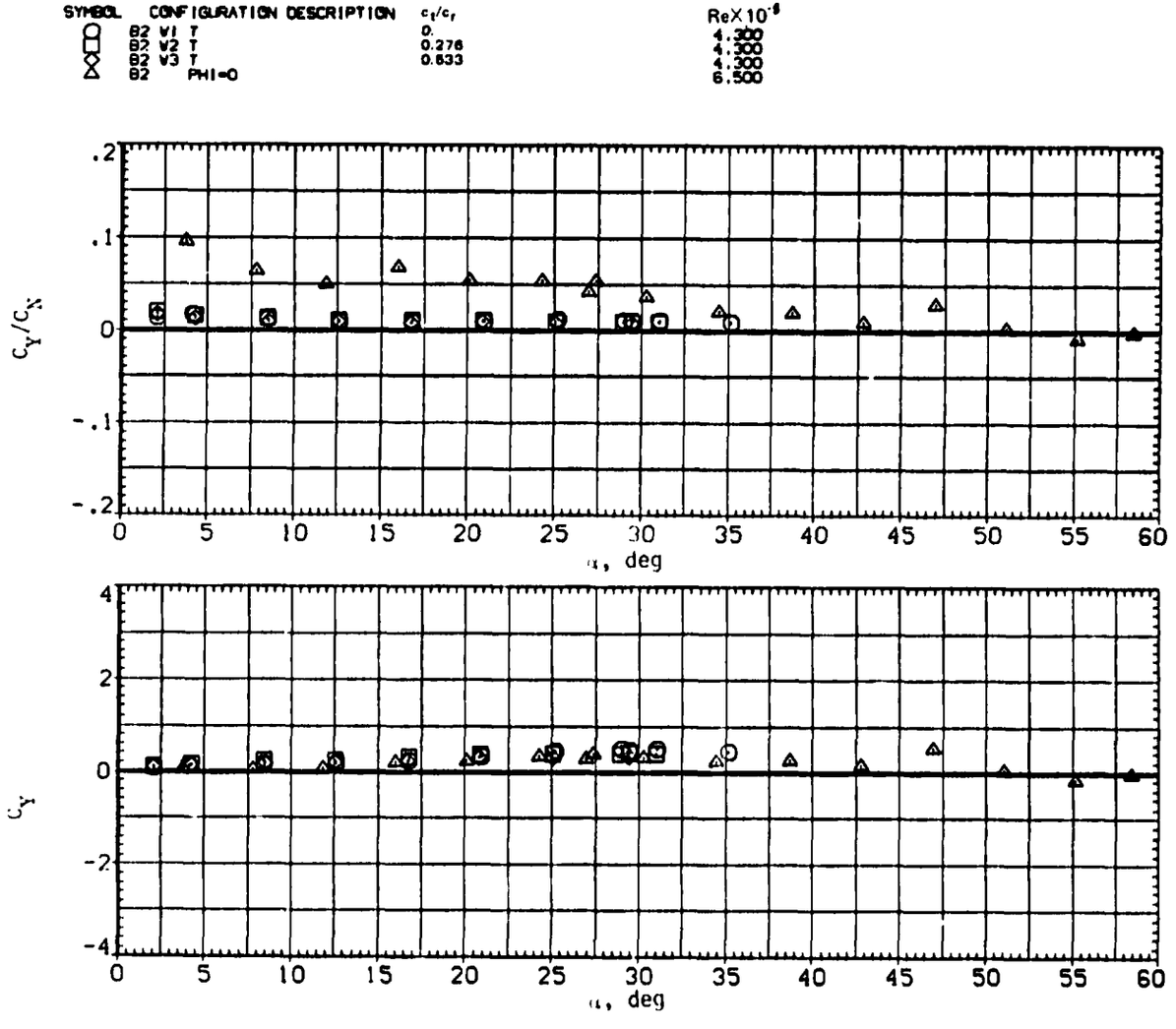

(b) C_Y/C_N and C_Y versus α.

Figure 8. Continued.

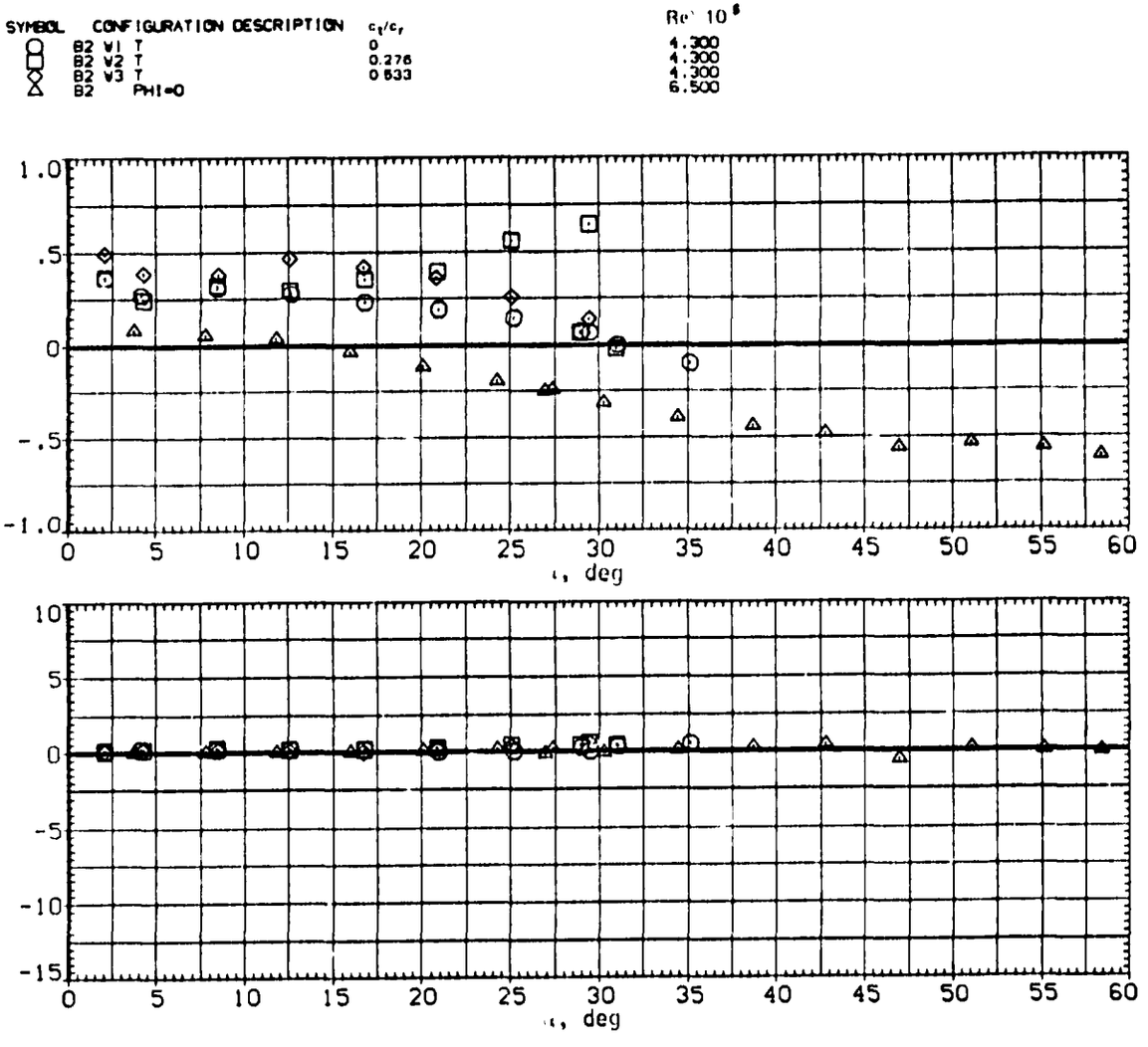

(c) C_A and C_n versus α.

Figure 8. Continued.

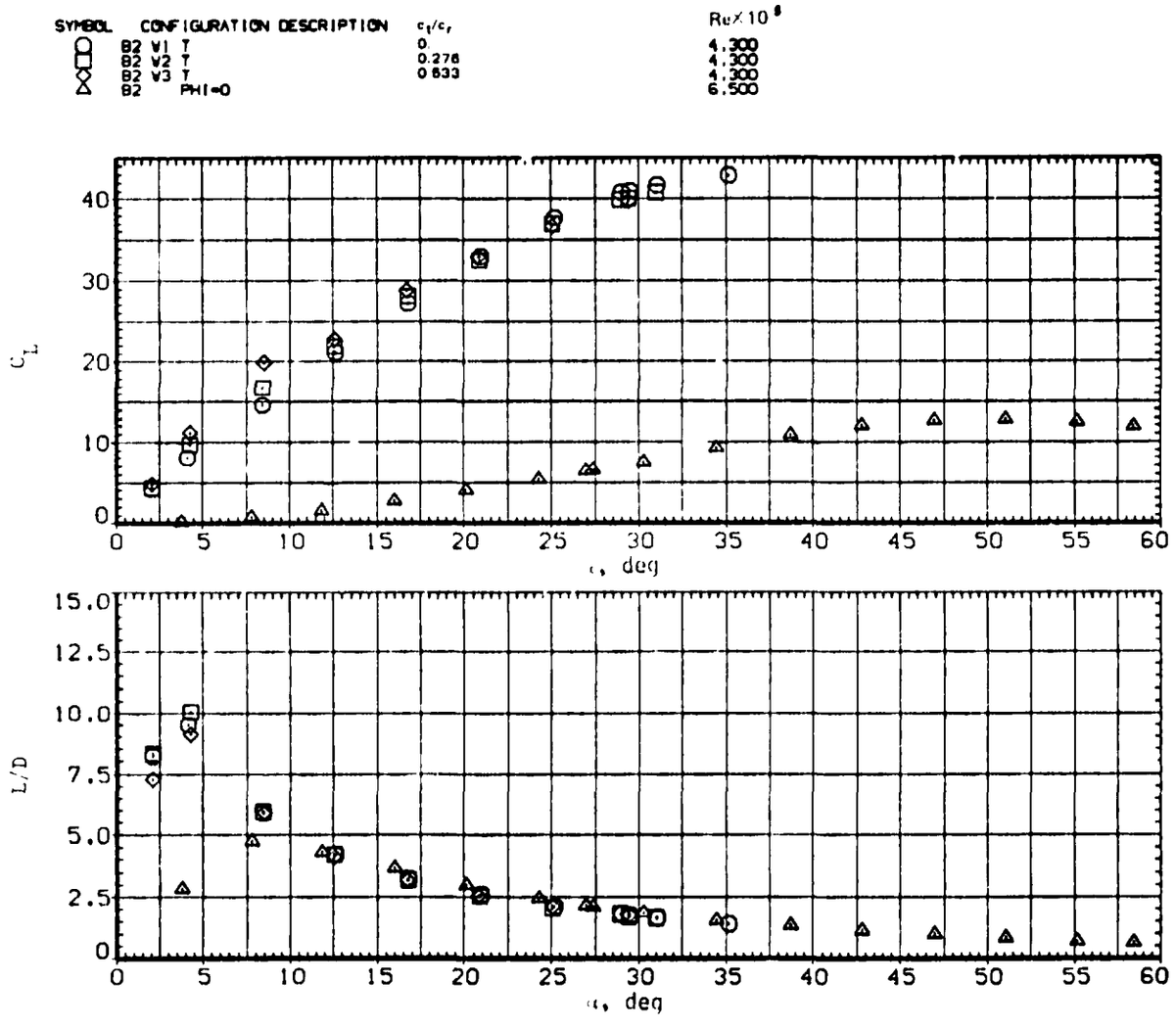

(d) C_L and L/D versus α.

Figure 8. Concluded.

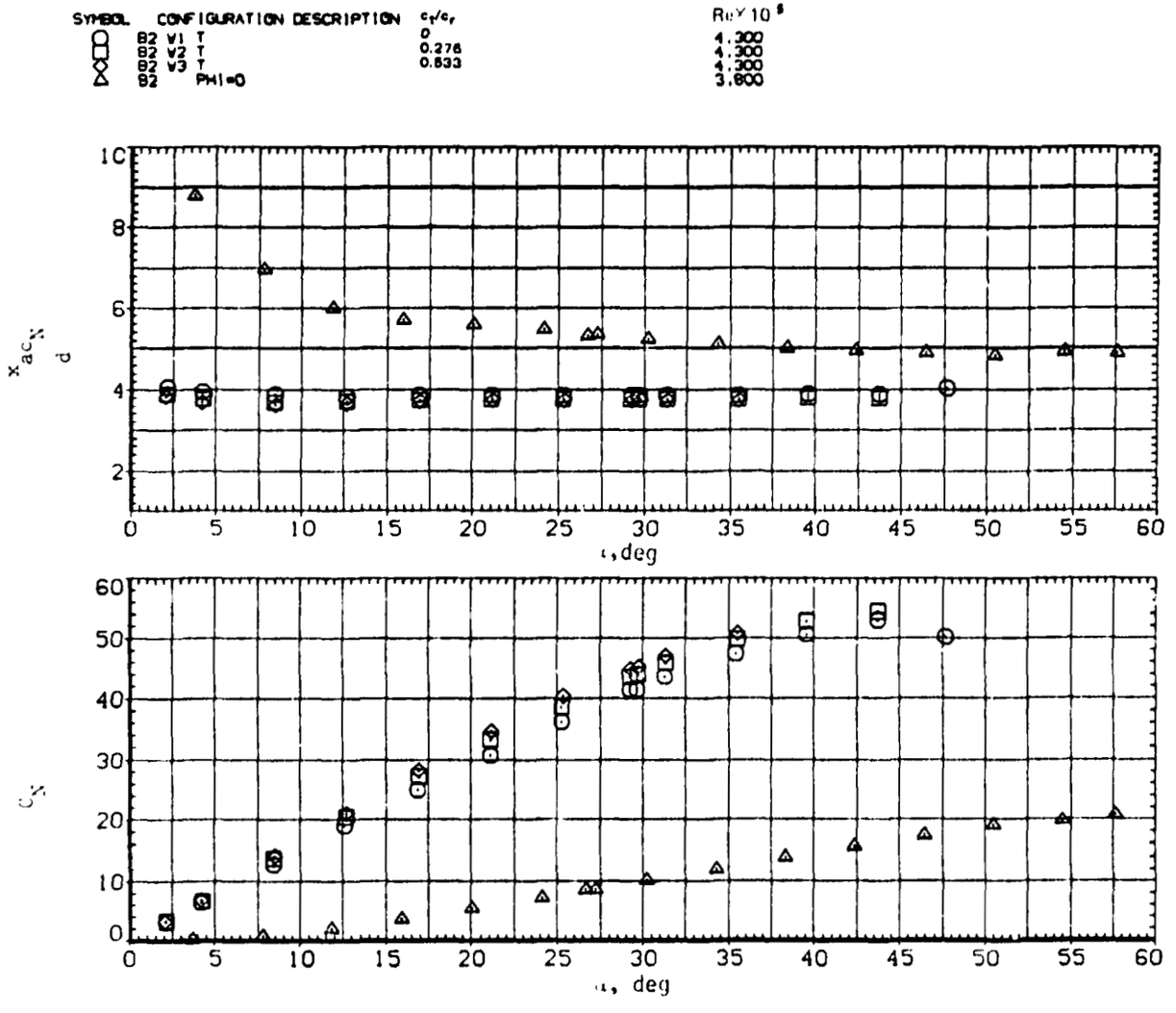

(a) x_{ac_N}/d and C_N versus α.

Figure 9. Effect of wing taper ratio with elliptic body and tail. M = 1.5.

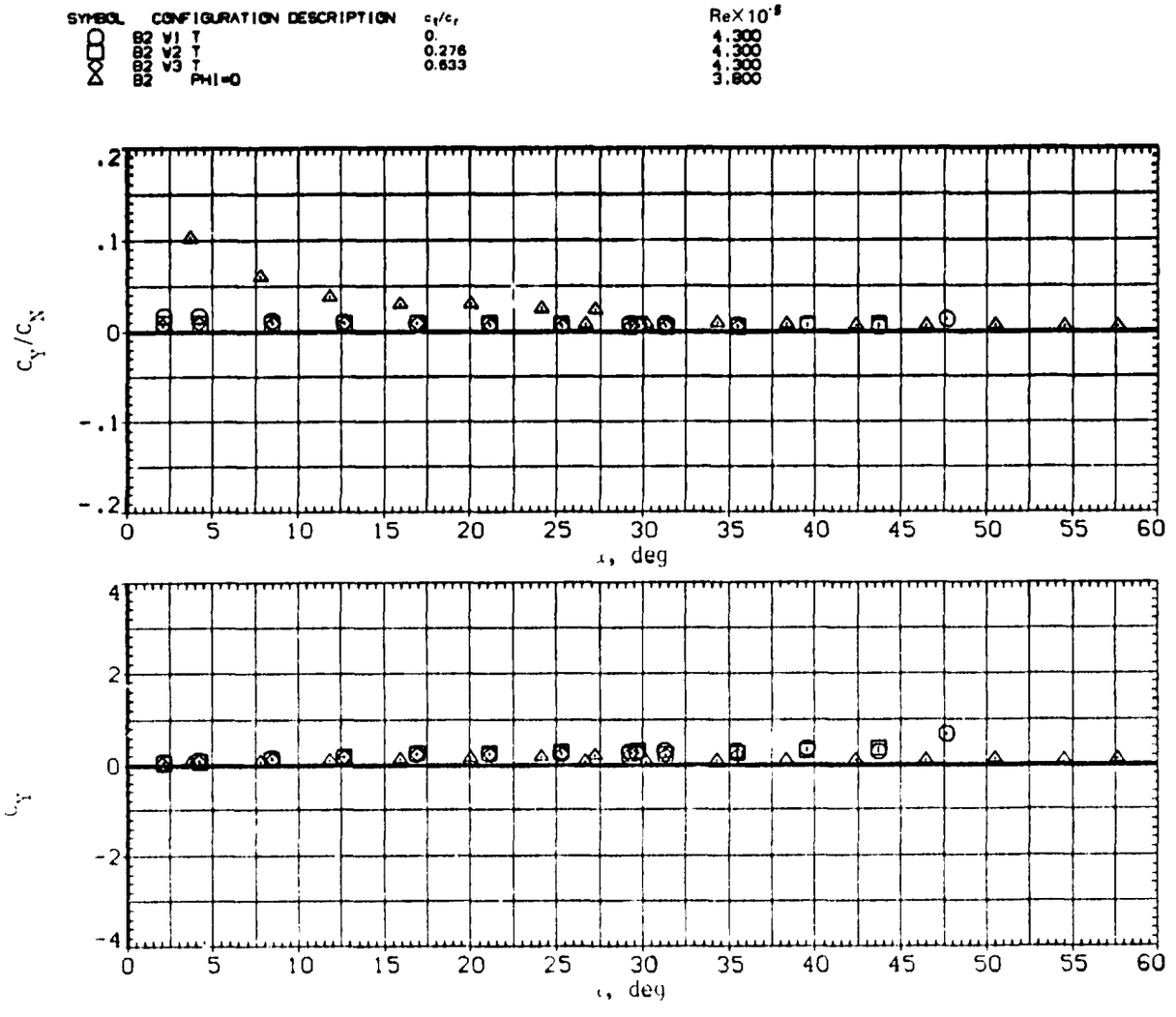

(b) C_Y/C_N and C_Y versus α.

Figure 9. Continued.

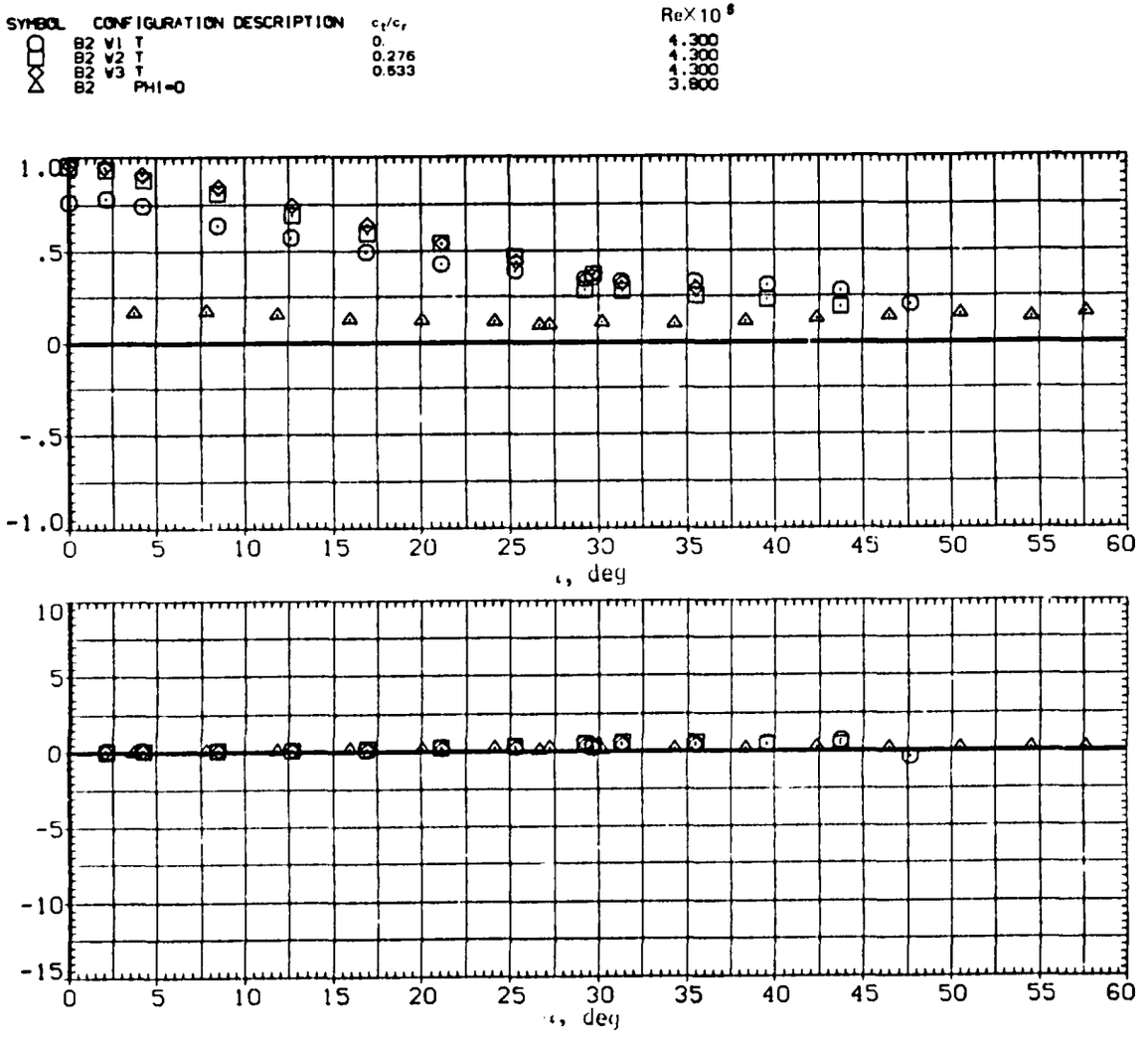

(c) C_A and C_n versus α.

Figure 9. Continued.

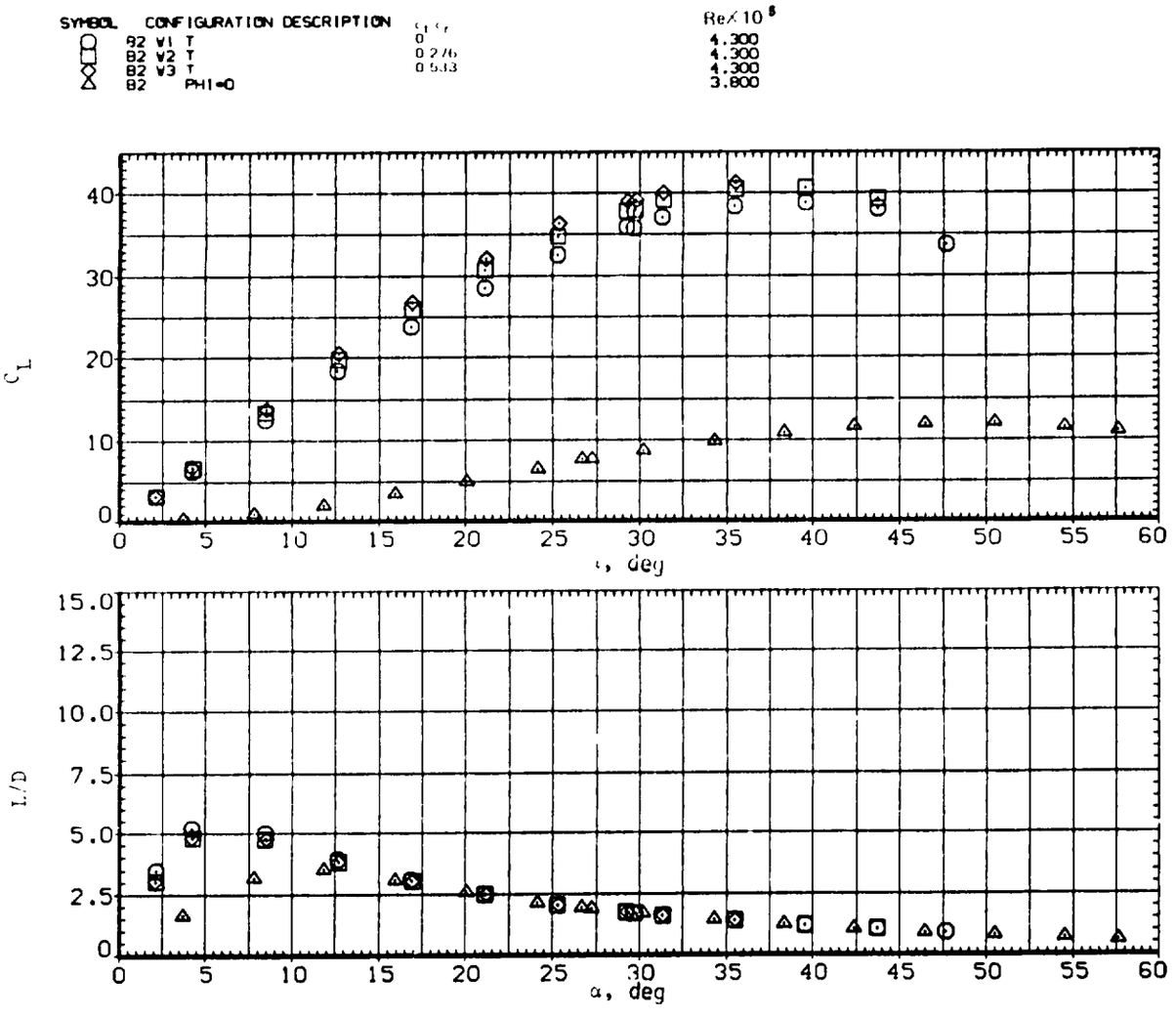

(d) C_L and L/D versus α.

Figure 9. – Concluded.

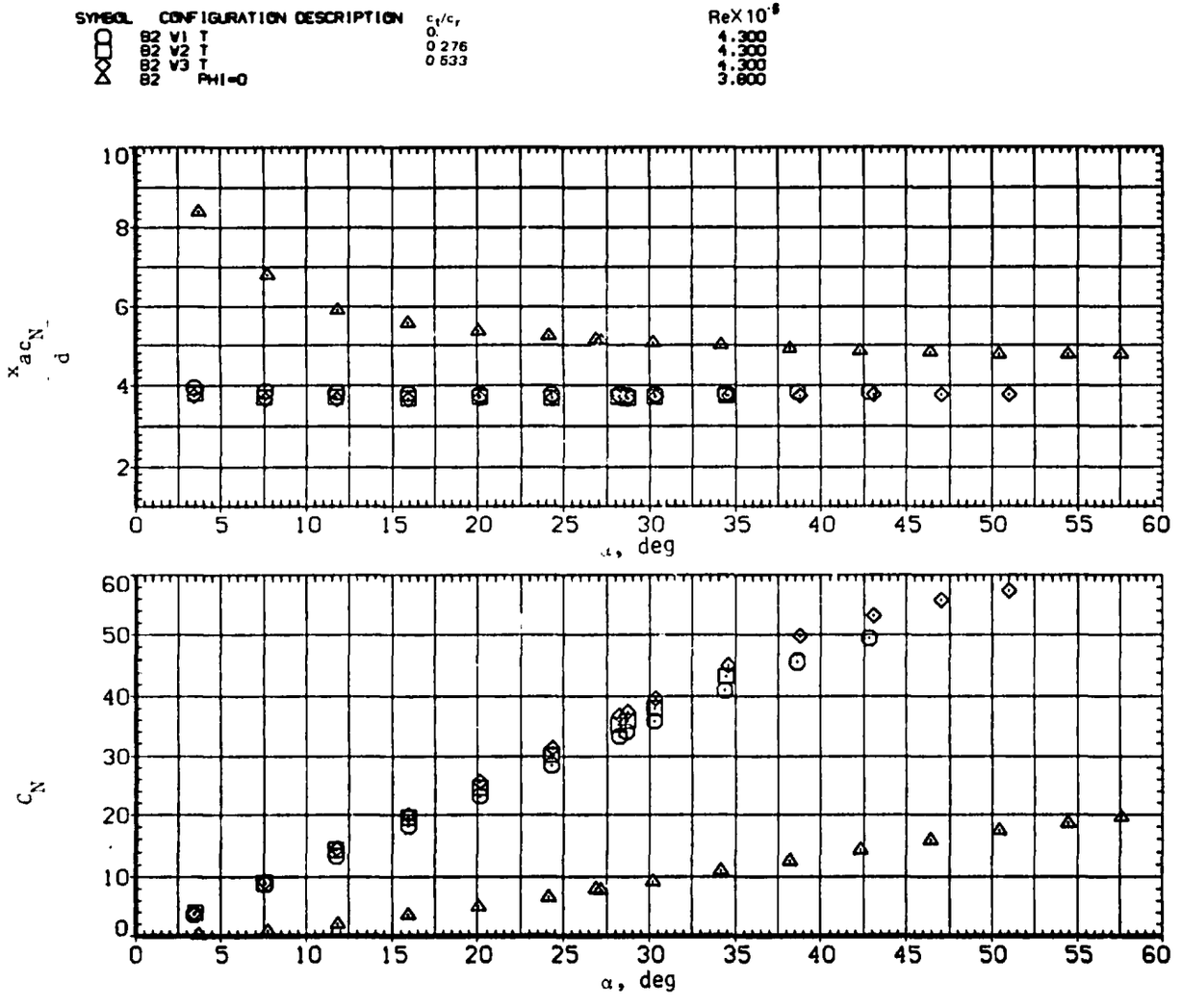

(a) x_{ac_N}/d and C_N versus α.

Figure 10.– Effect of wing taper ratio with elliptic body and tail, M = 2.0.

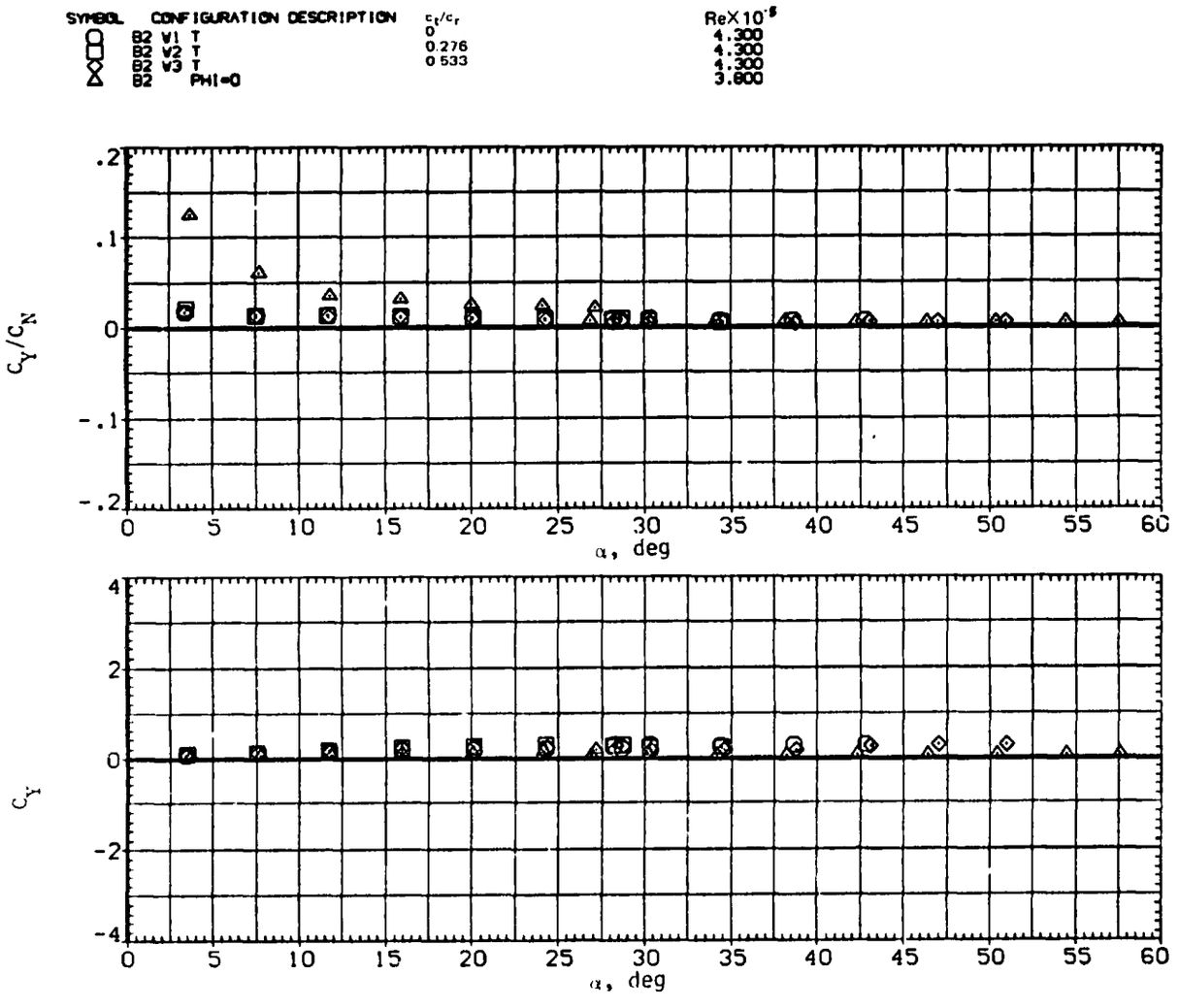

(b) C_Y/C_N and C_Y versus α.

Figure 10.– Continued.

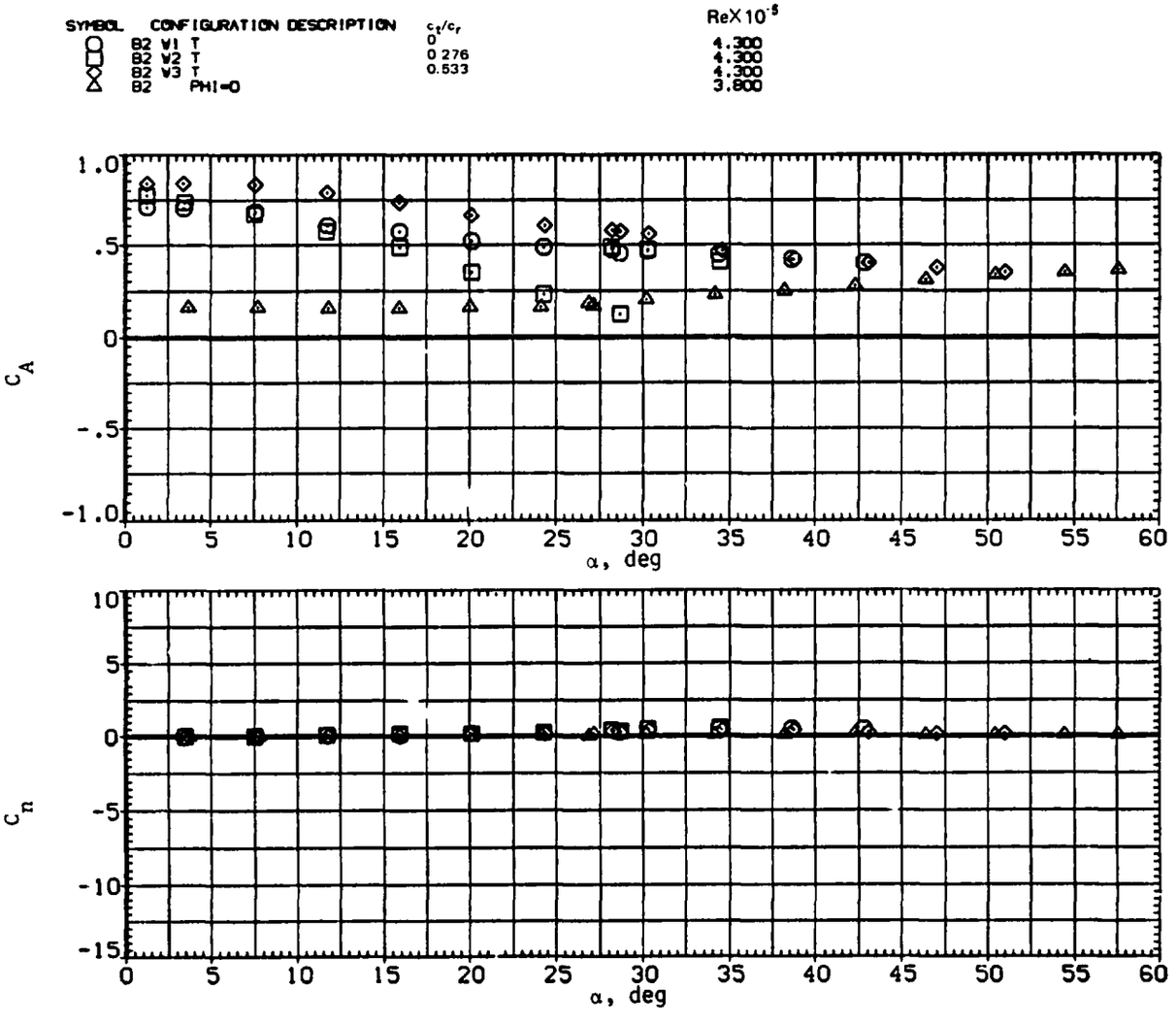

(c) C_A and C_n versus α.

Figure 10.– Continued.

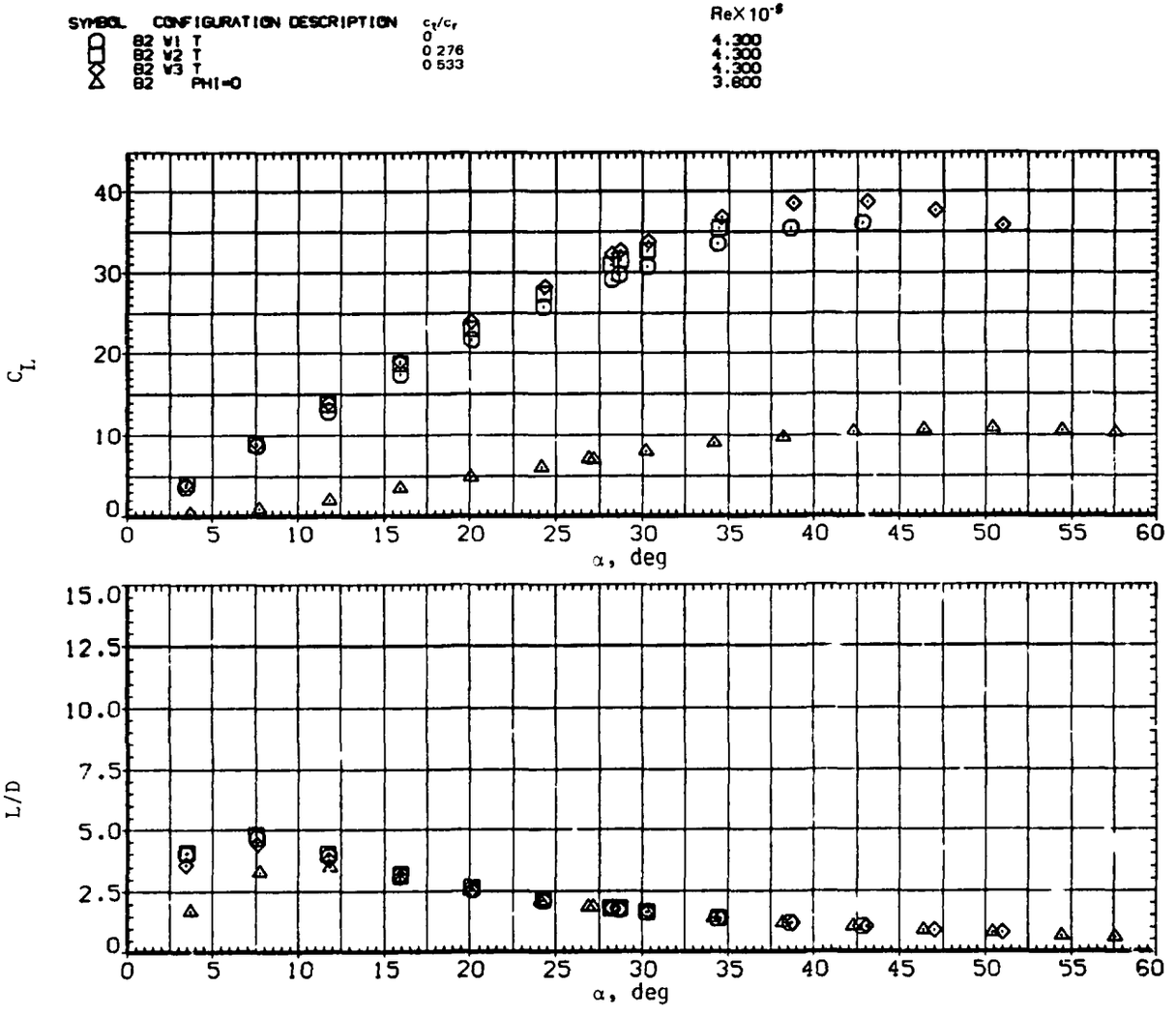

(d) C_L and L/D versus α.

Figure 10. – Concluded.

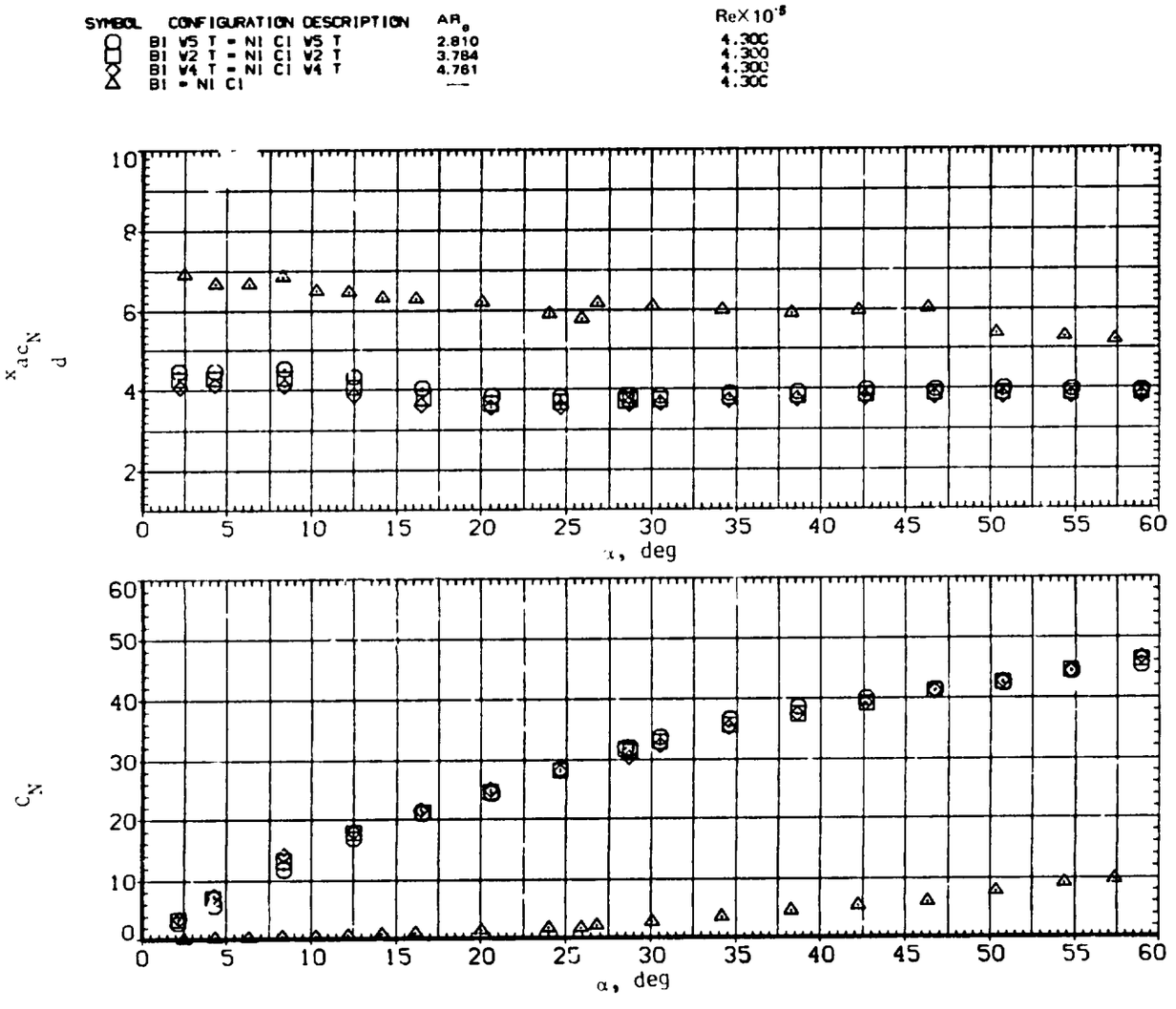

(a) x_{ac_N}/d and C_N versus α.

Figure 11. - Effect of wing aspect ratio with circular body and tail, M = 0.6.

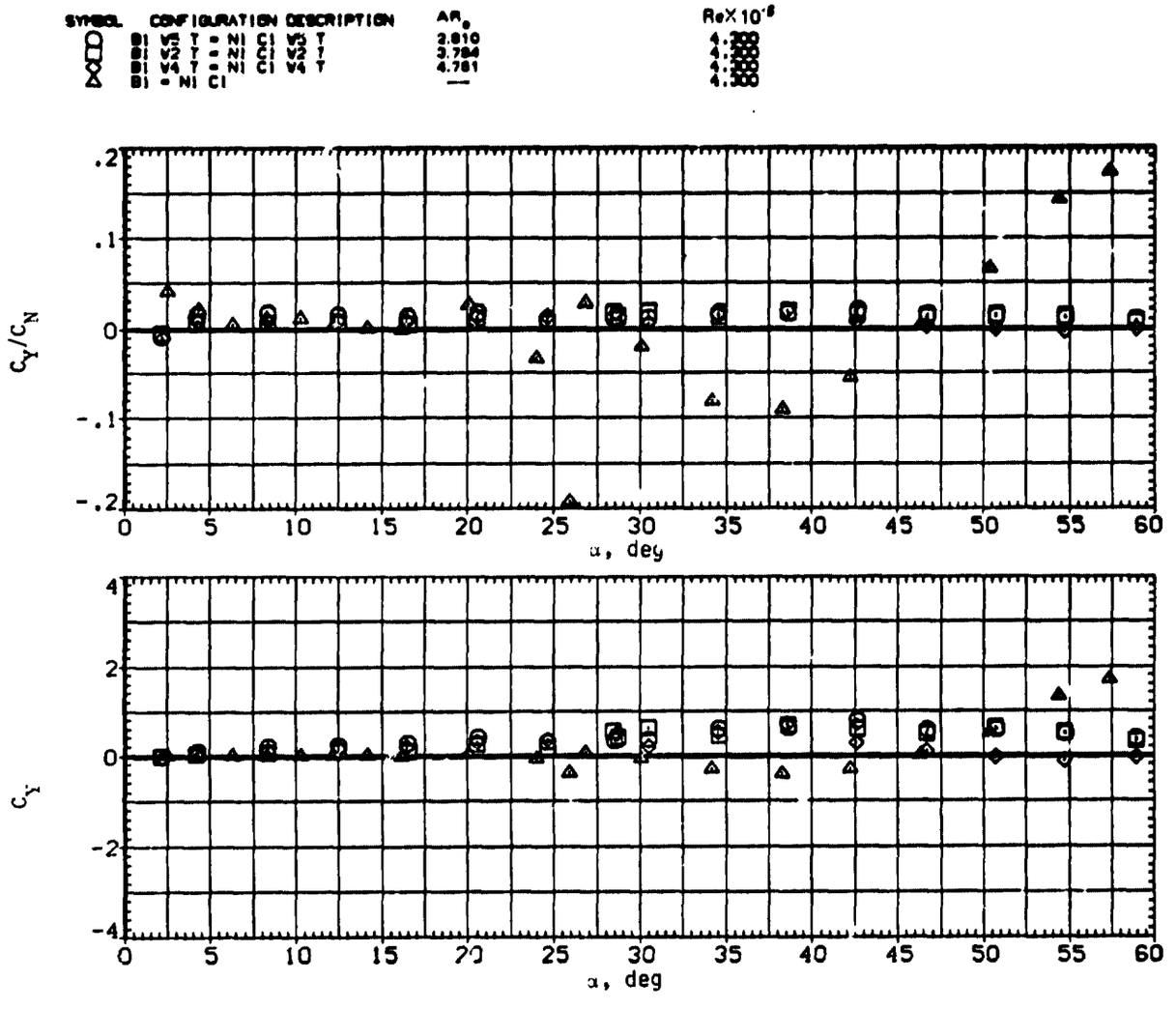

(b) C_Y/C_N and C_Y versus α.

Figure 11.– Continued.

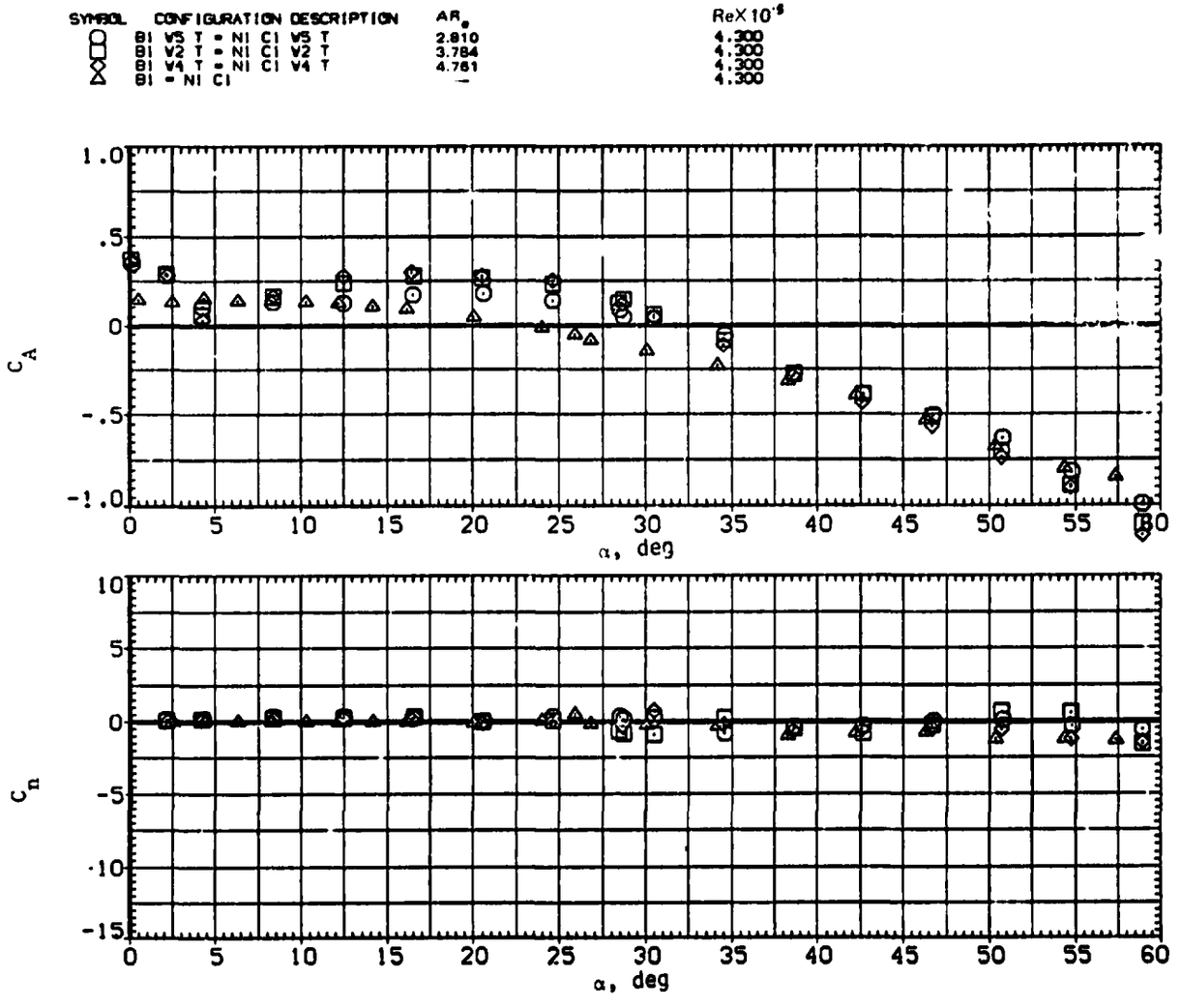

(c) C_A and C_n versus α.

Figure 11.– Continued.

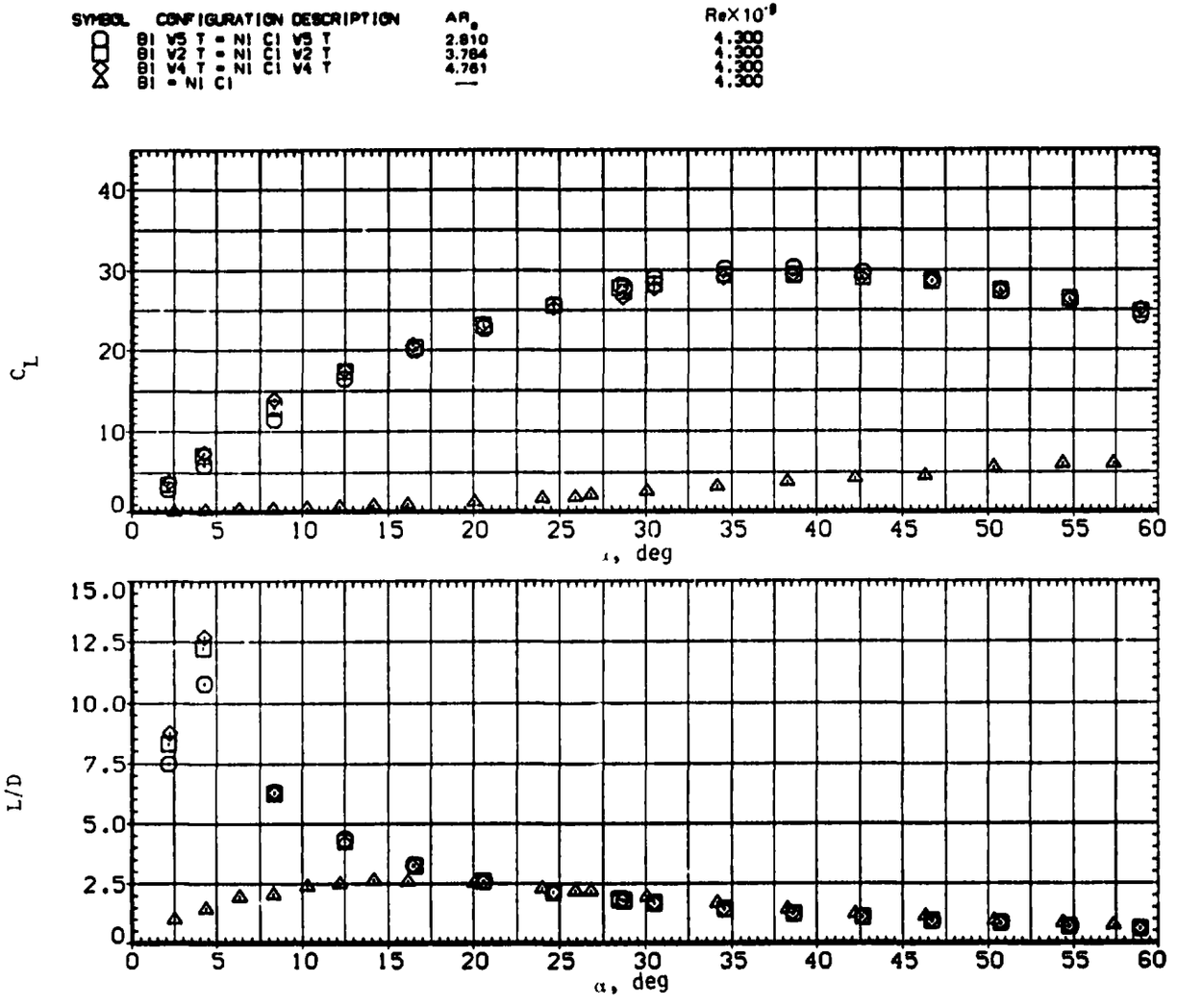

(d) C_L and L/D versus α.

Figure 11.– Concluded.

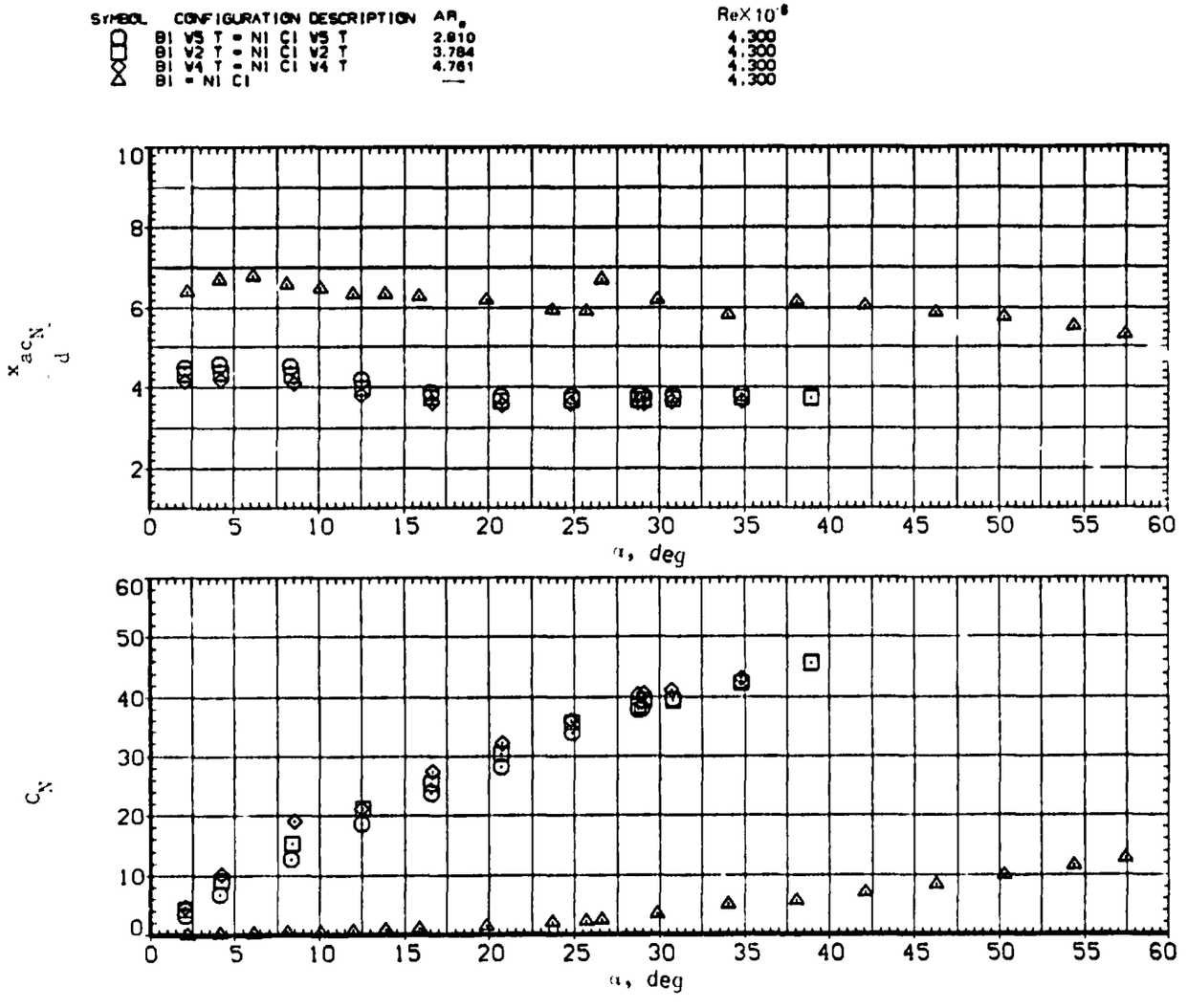

(a) x_{ac_N}/d and C_N versus α.

Figure 12. Effect of wing aspect ratio with circular body and tail, M = 0.9.

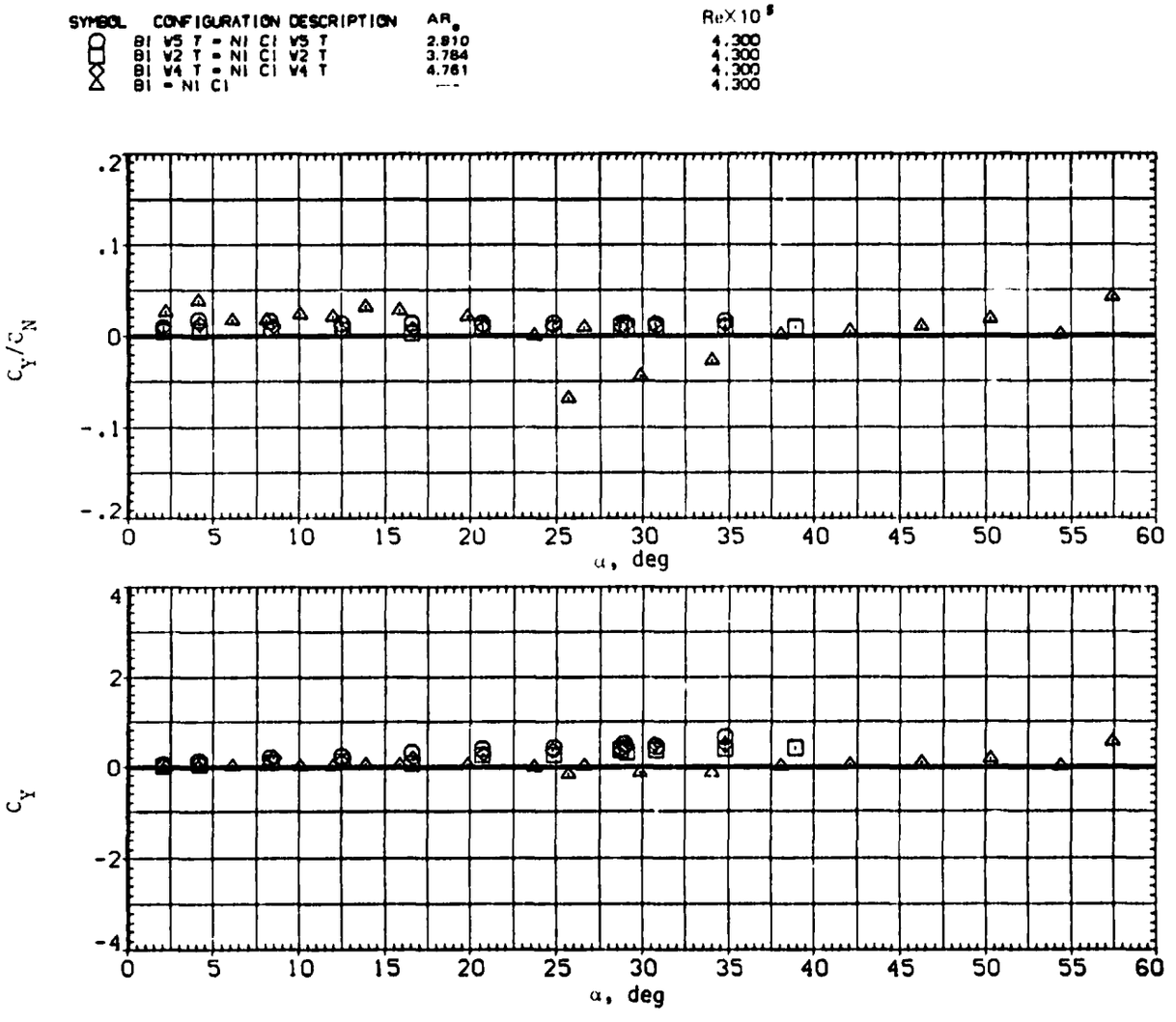

(b) C_Y/C_N and C_Y versus α.

Figure 12. Continued.

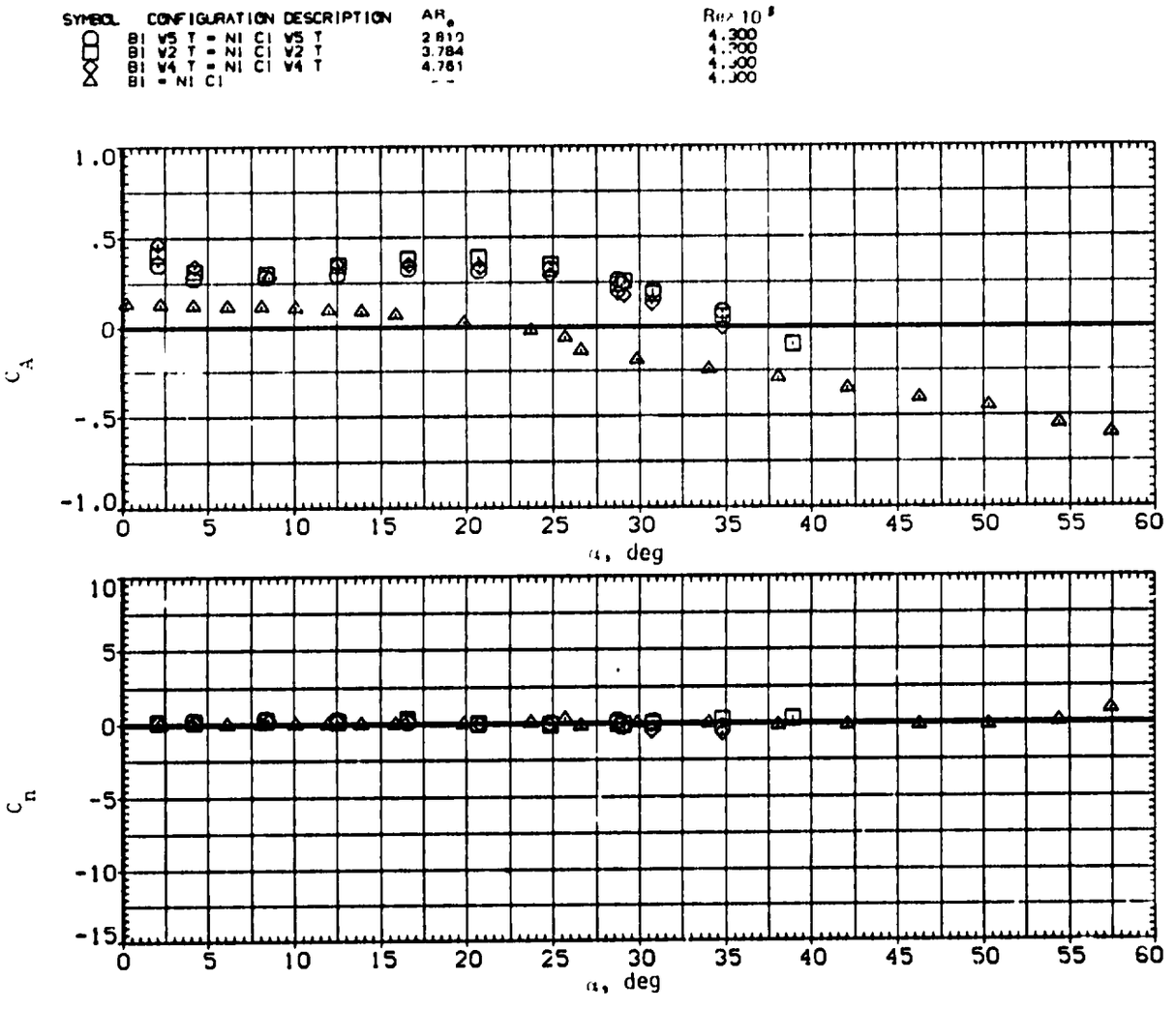

(c) C_A and C_n versus α.

Figure 12. Continued.

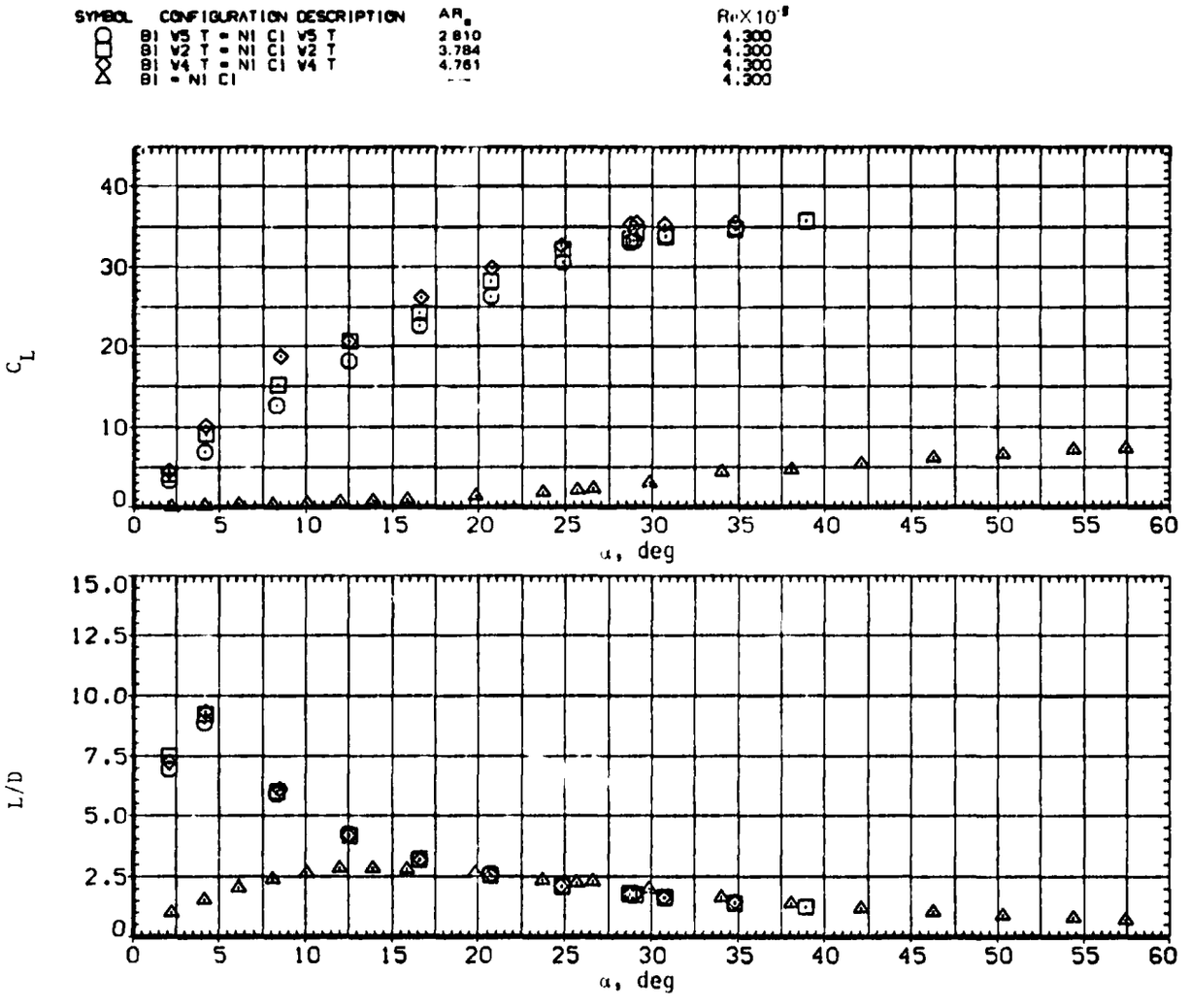

(d) C_L and L/D versus α.

Figure 12. - Concluded.

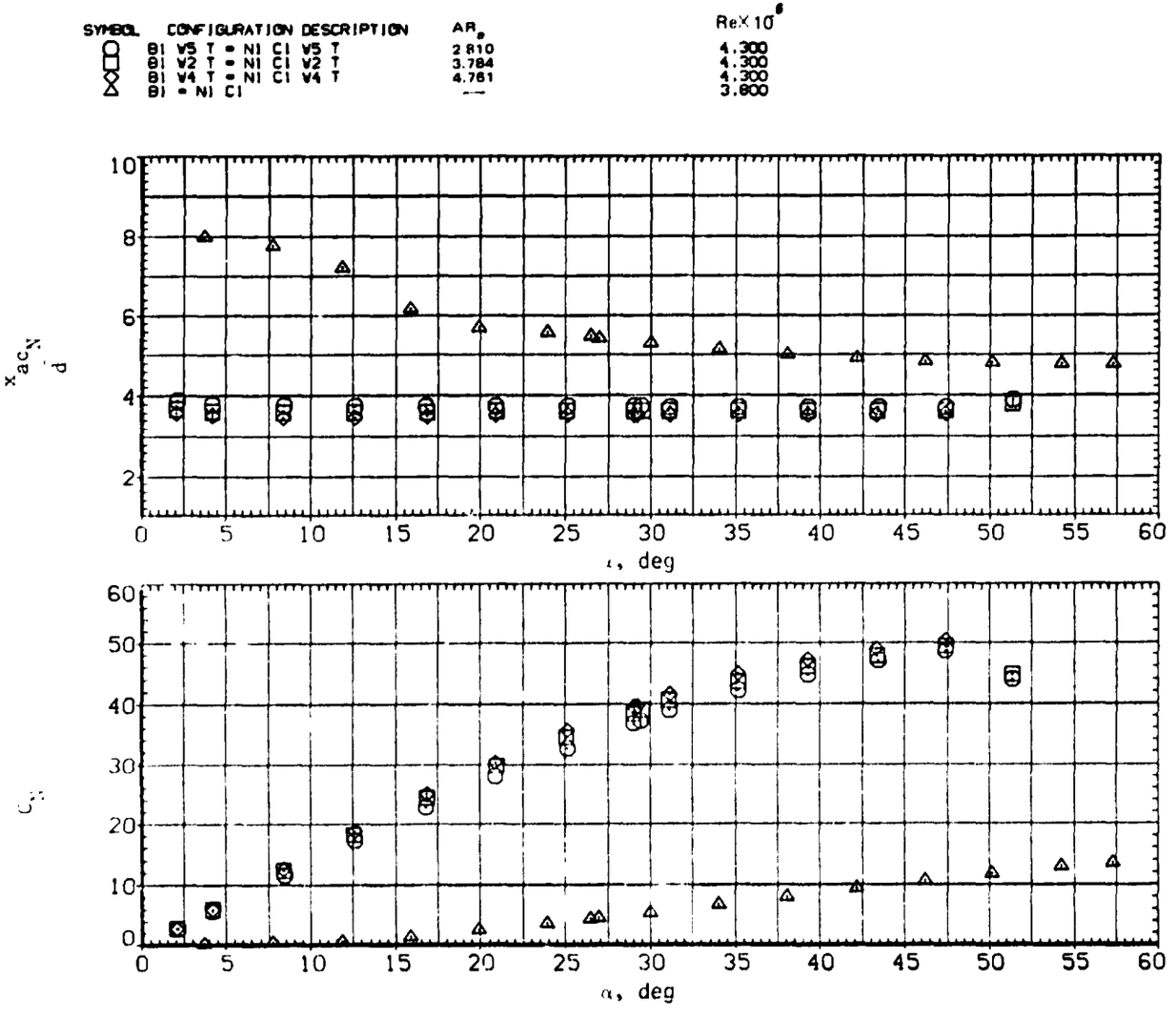

(a) x_{ac_N}/d and C_N versus α.

Figure 13. Effect of wing aspect ratio with circular body and tail, M = 1.5.

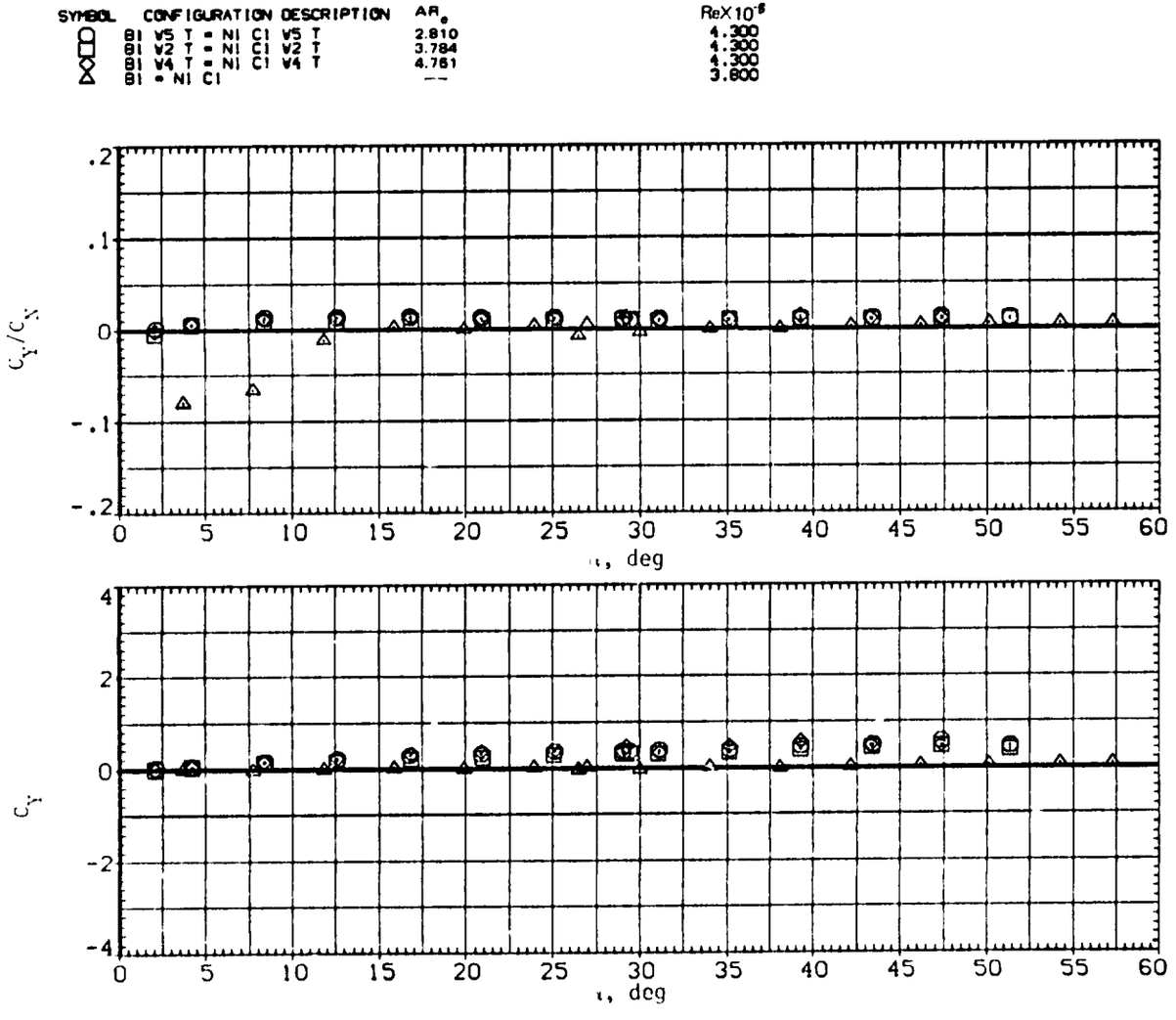

(b) C_Y/C_N and C_Y versus α.

Figure 13. Continued.

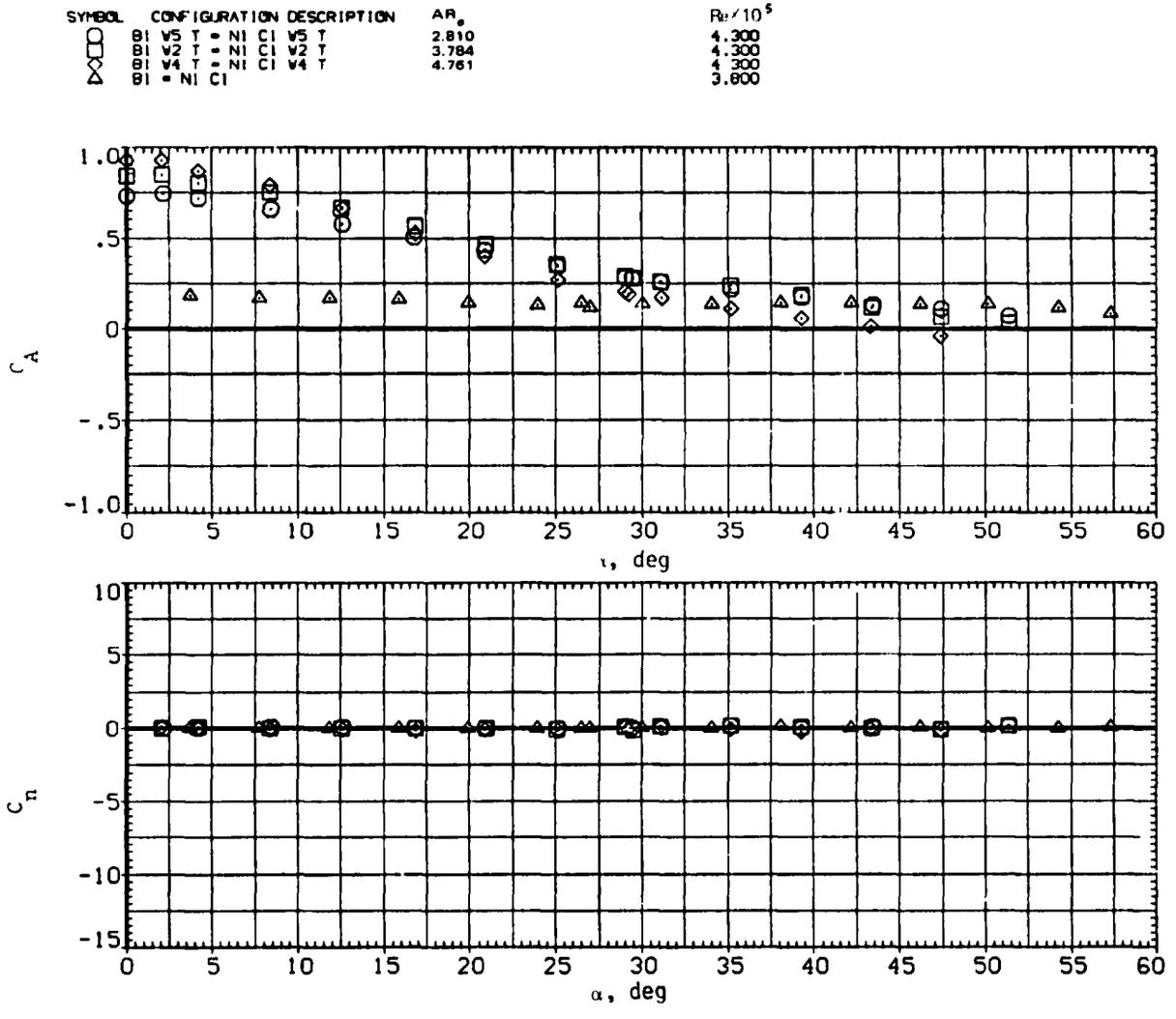

(c) C_A and C_n versus α.

Figure 13. – Continued.

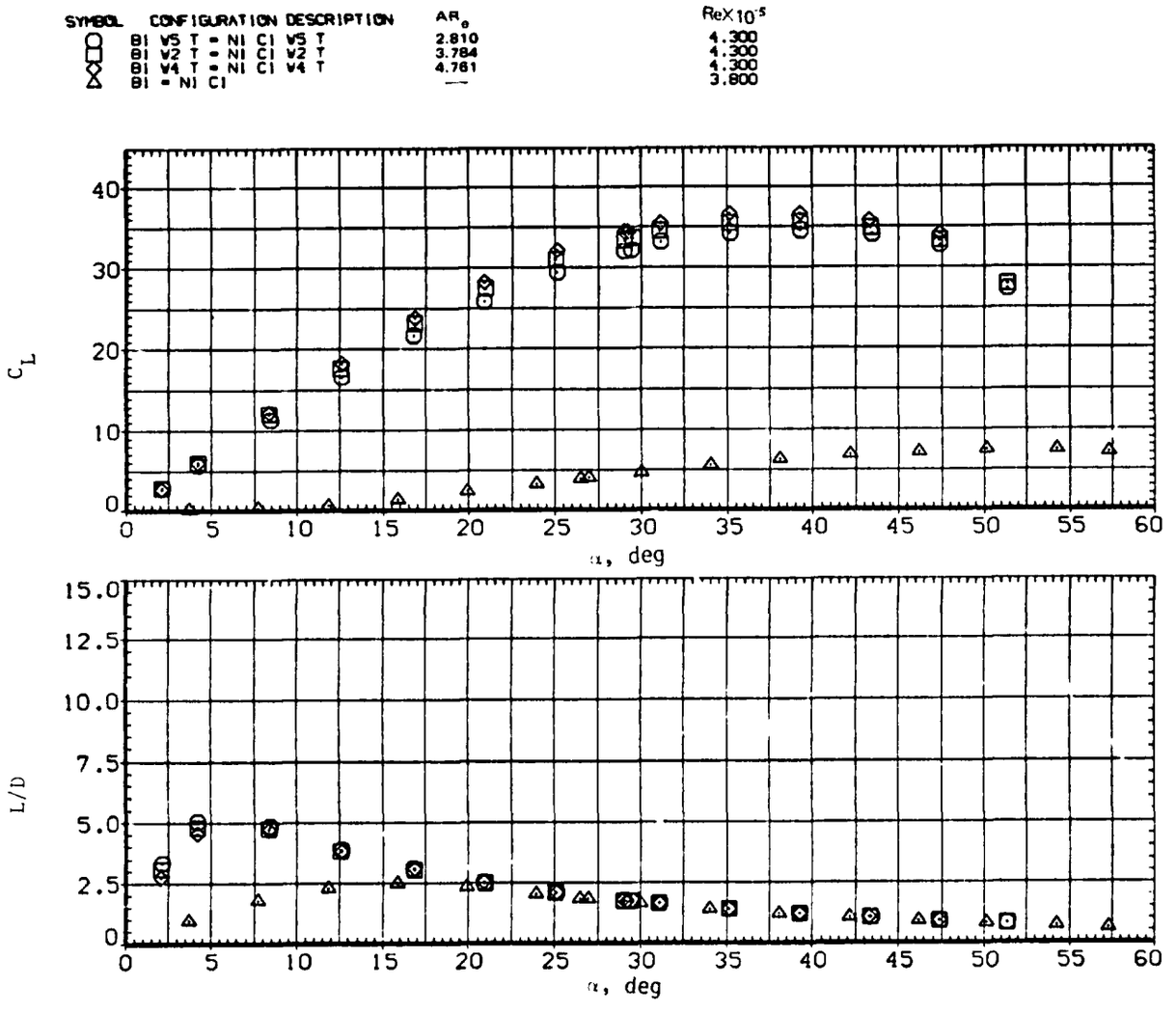

(d) C_L and L/D versus α.

Figure 13.– Concluded.

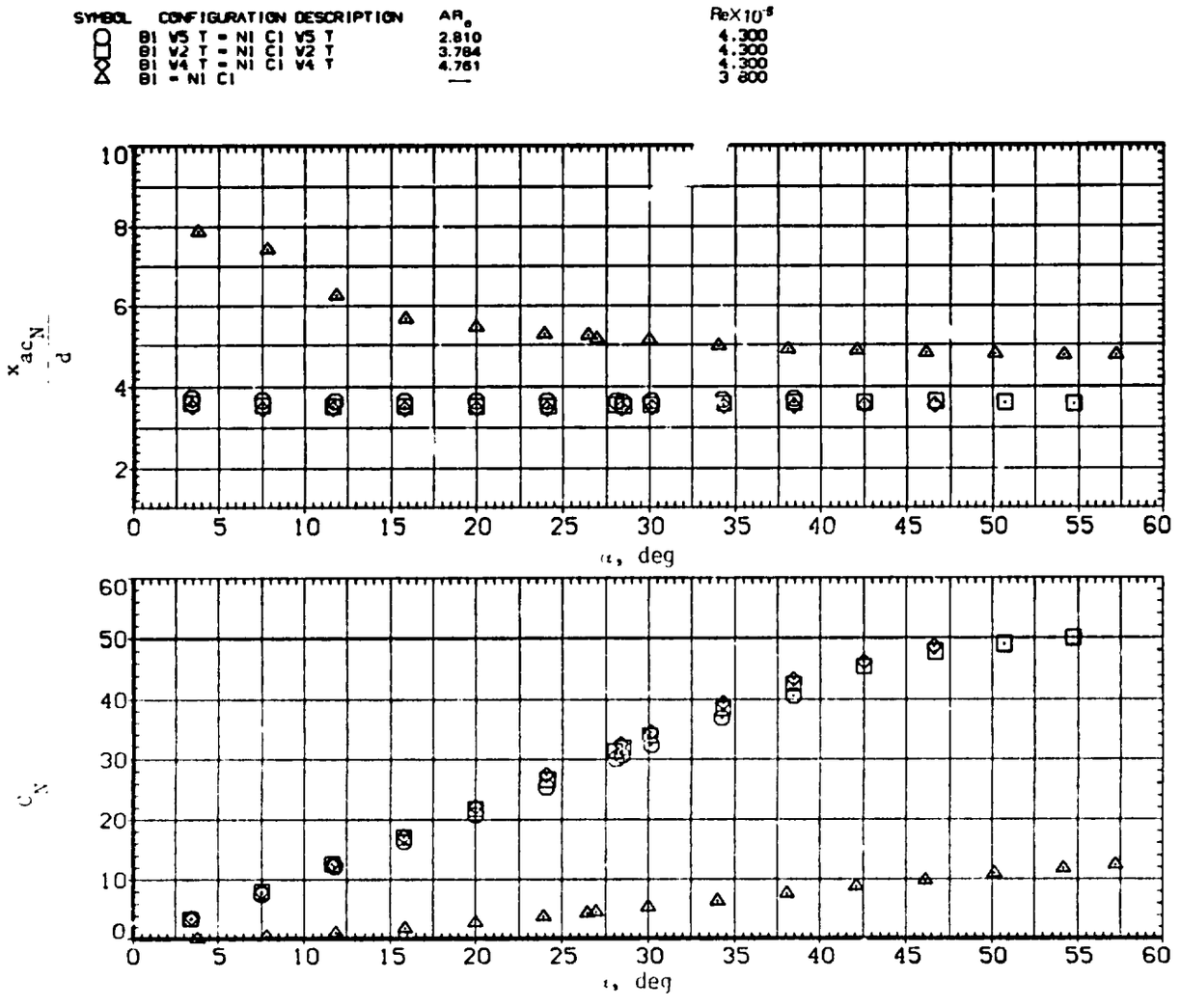

(a) x_{ac_N}/d and C_N versus α.

Figure 14. Effect of wing aspect ratio with circular body and tail, M = 2.0.

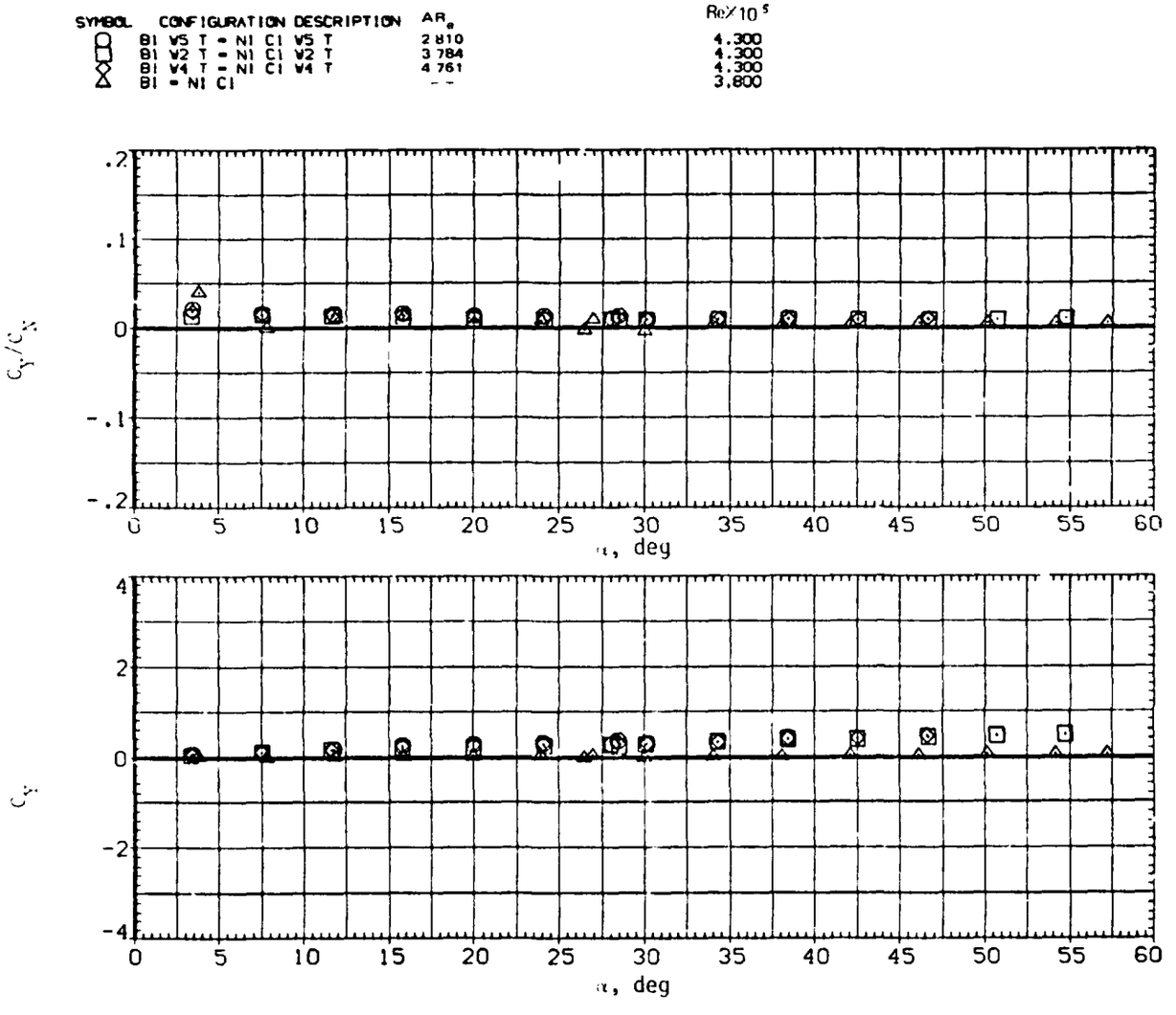

(b) C_Y/C_N and C_Y versus α.

Figure 14. - Conti l.

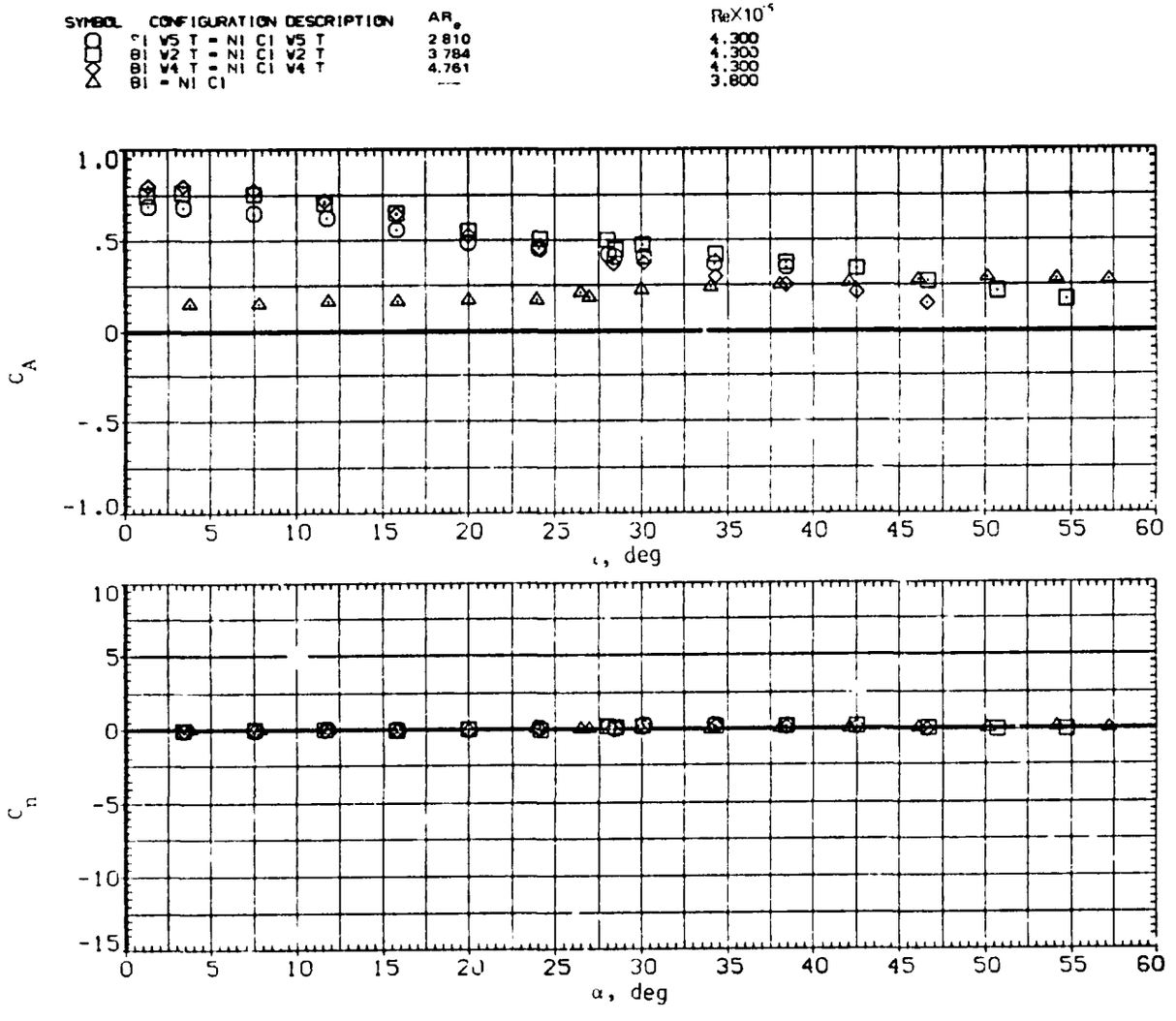

(c) C_A and C_n versus α.

Figure 14. Continued.

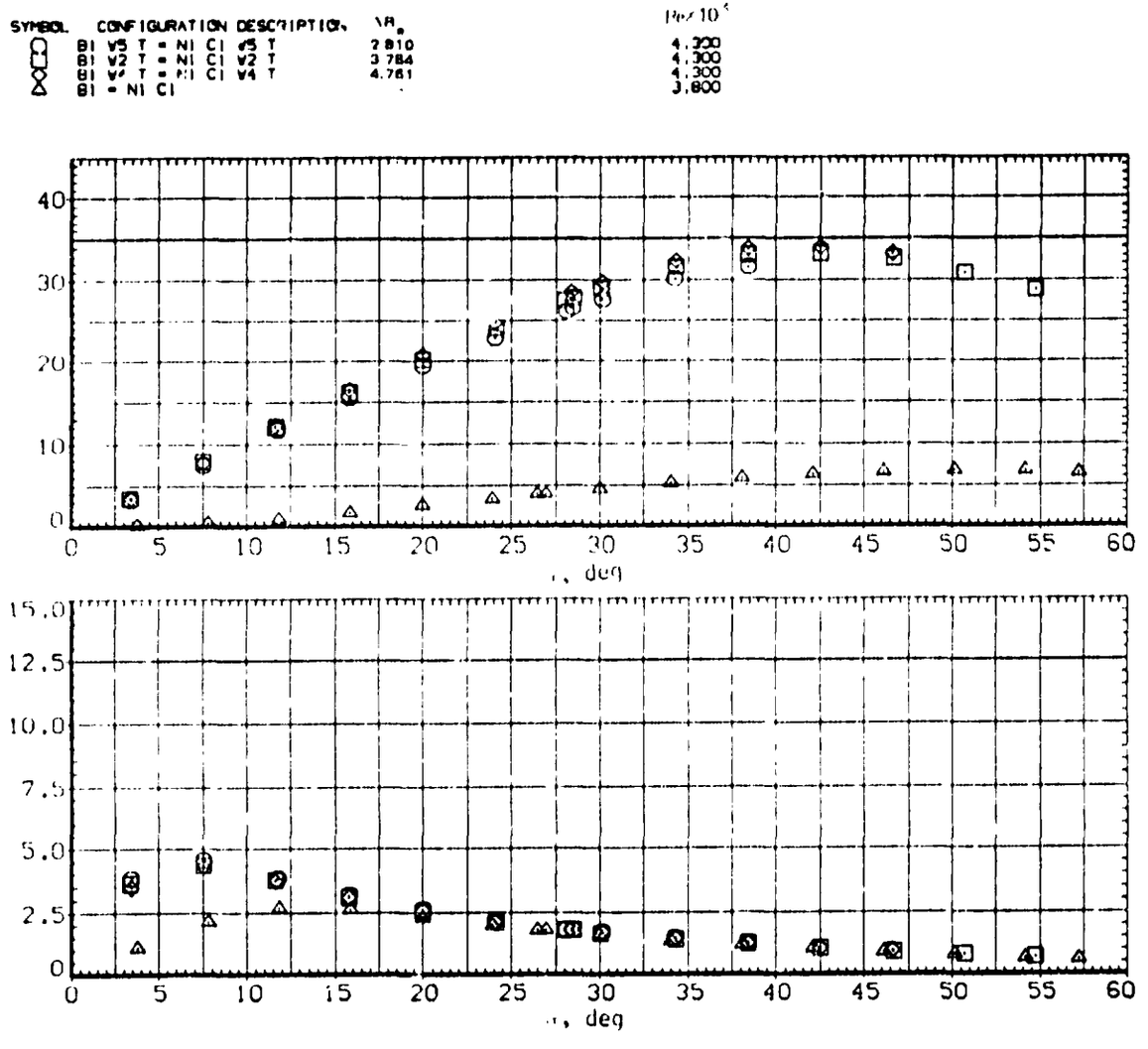

(d) C_L and L/D versus α.

Figure 14. Concluded.

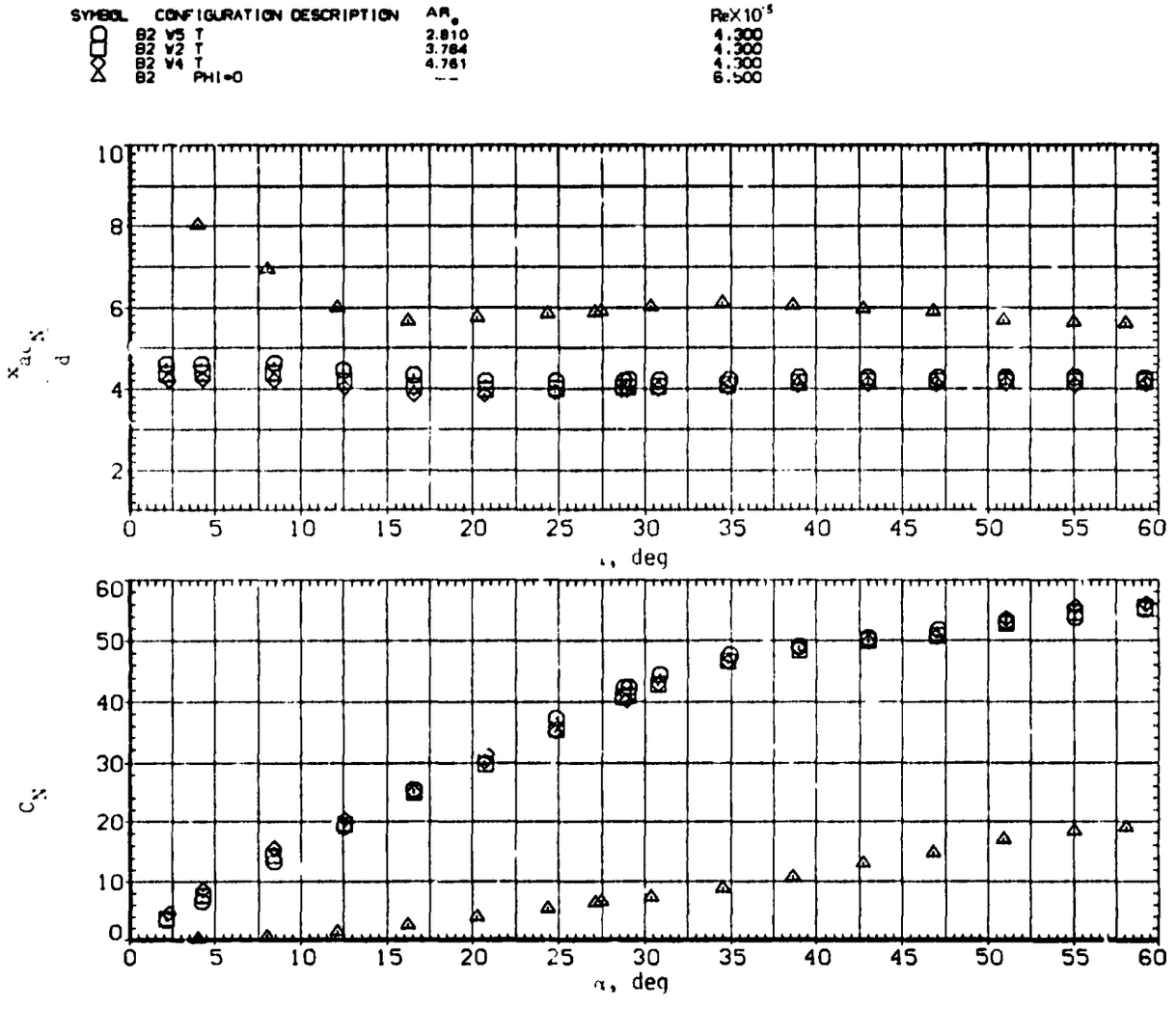

(a) x_{ac_N}/d and C_N versus α.

Figure 15 Effect of wing aspect ratio with elliptic body and tail, M = 0.6.

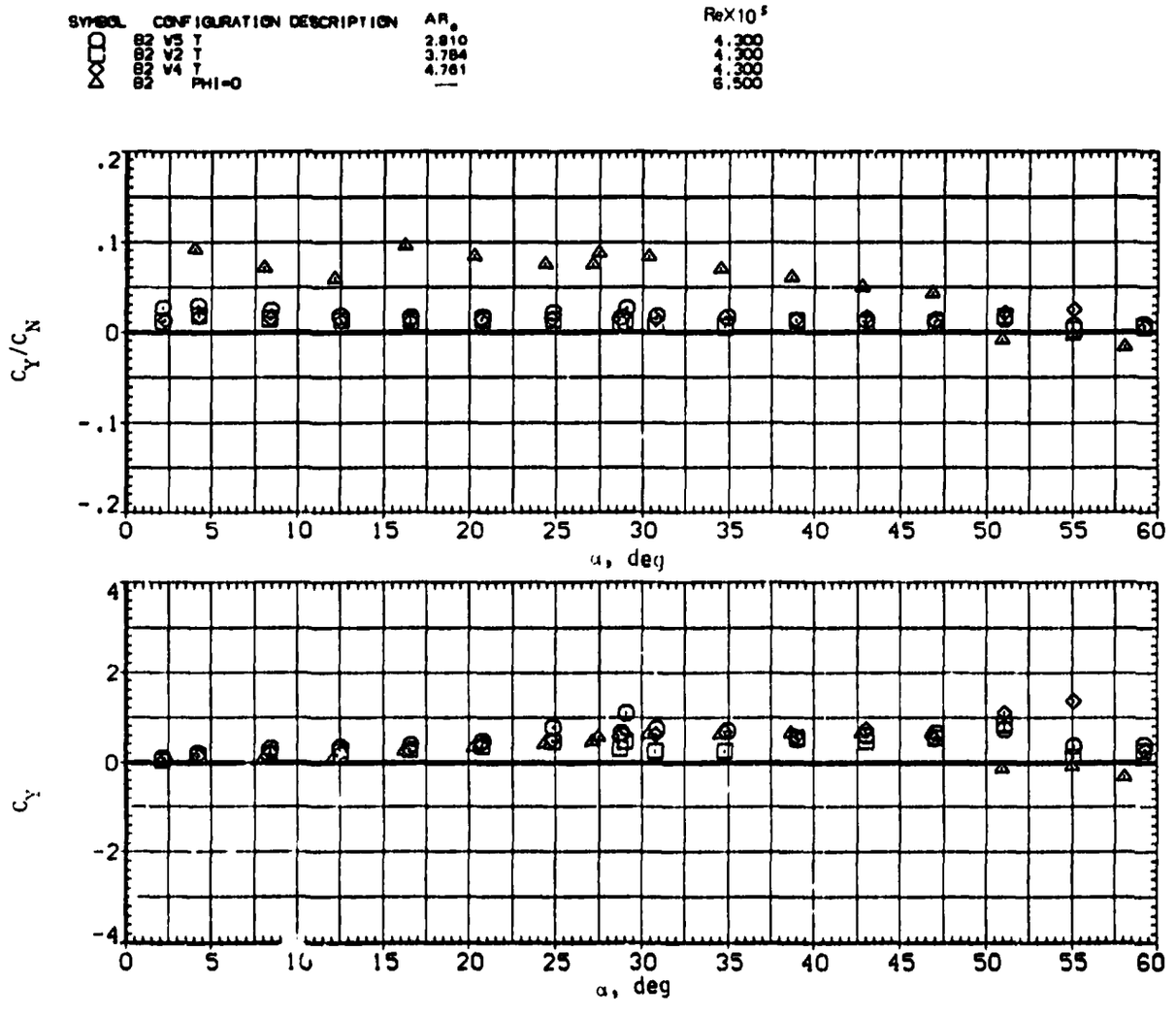

(b) C_Y/C_N and C_Y versus α.

Figure 15. Continued.

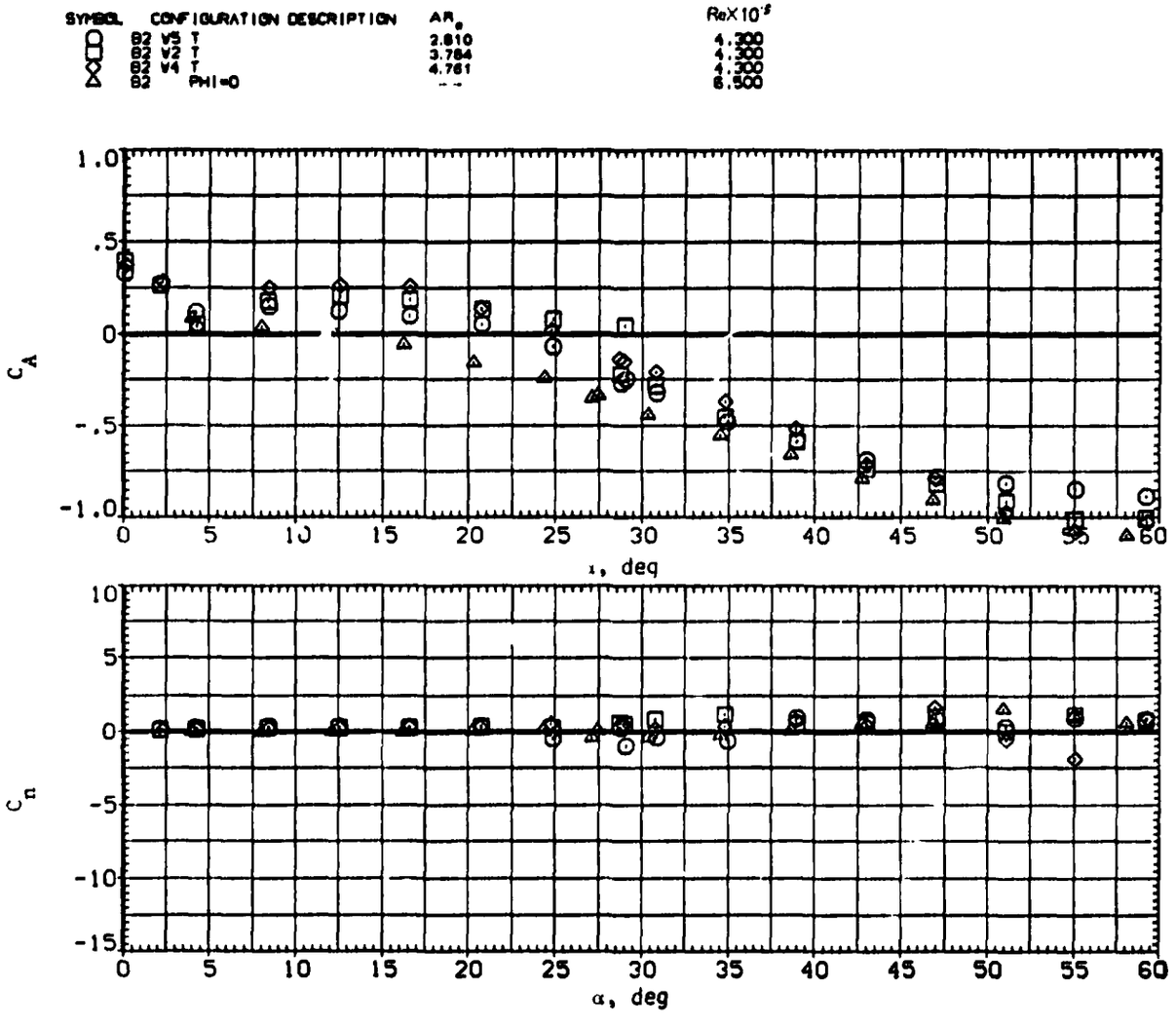

(c) C_A and C_n versus α.

Figure 15. Continued.

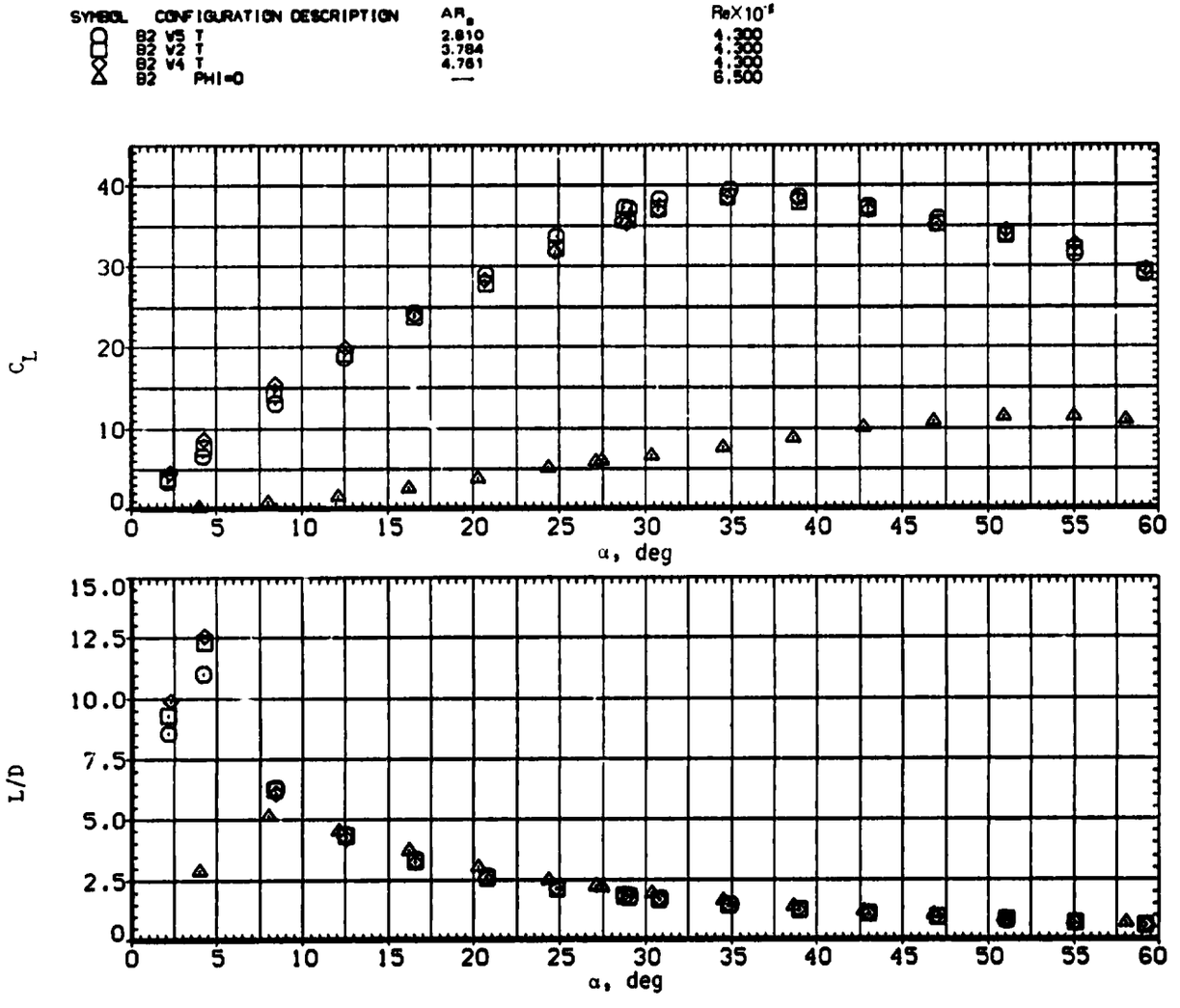

(d) C_L and L/D versus α.

Figure 15.– Concluded.

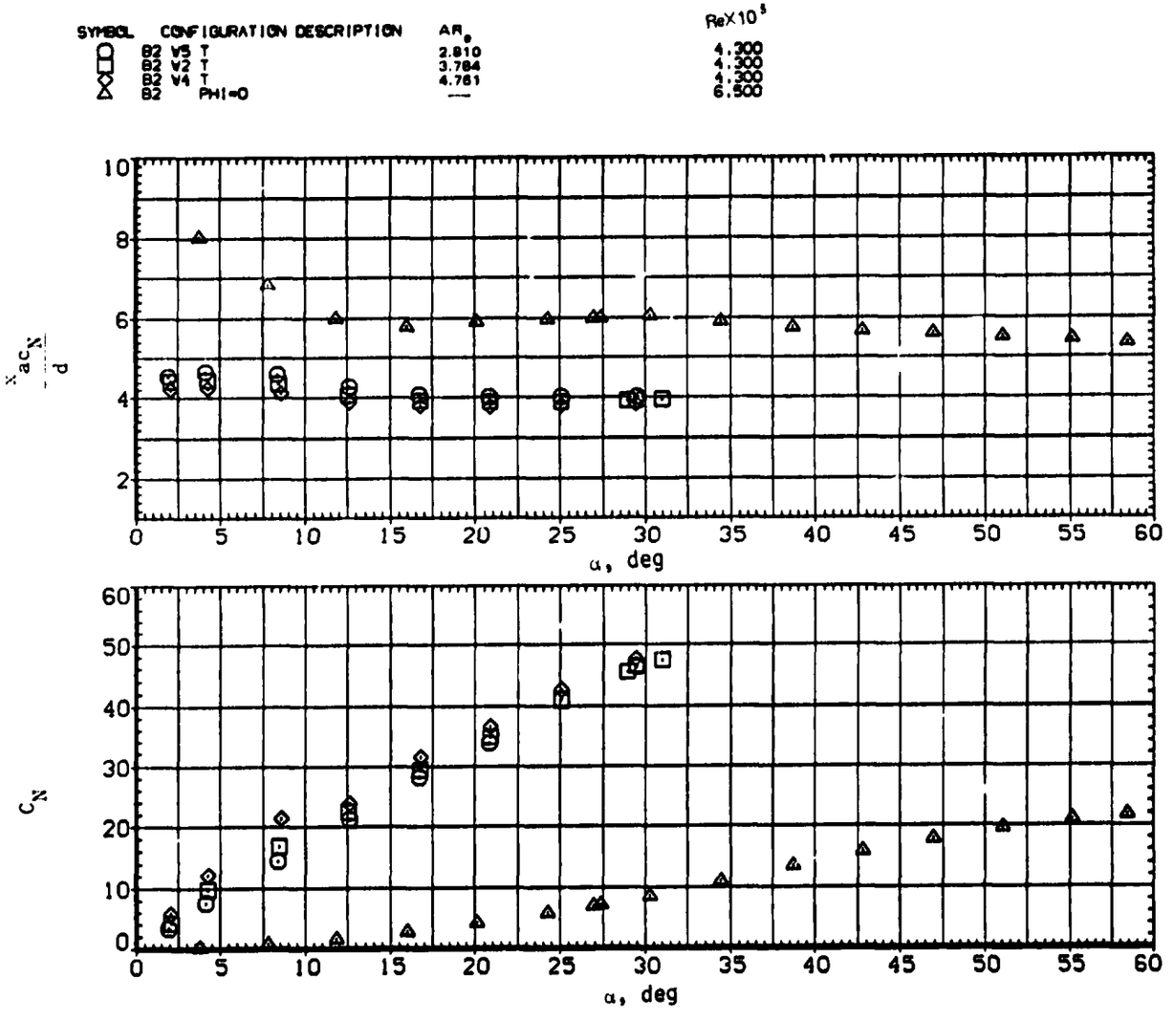

(a) x_{ac_N}/d and C_N versus α.

Figure 16.- Effect of wing aspect ratio with elliptic body and tail, M = 0.9.

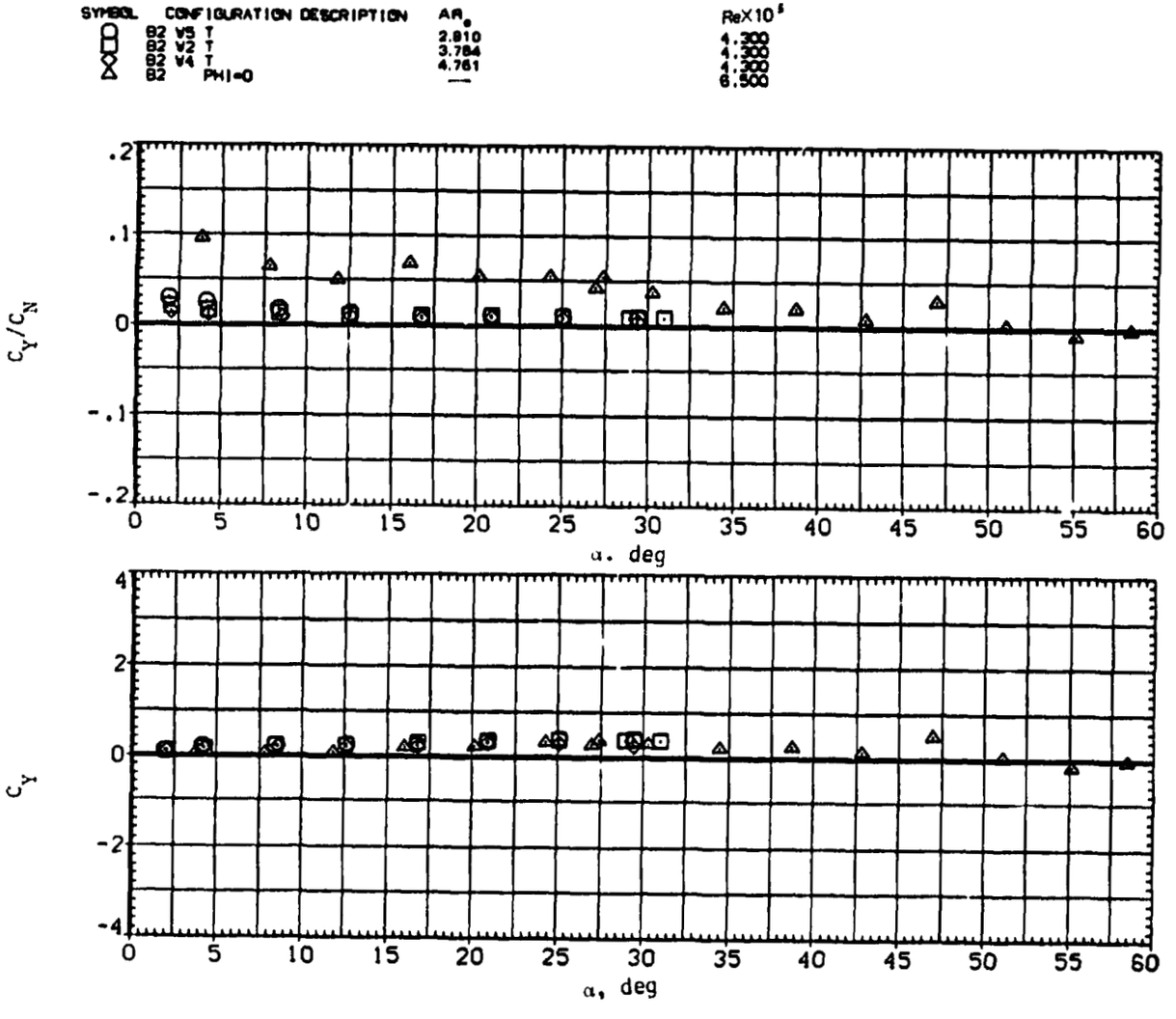

(b) C_Y/C_N and C_Y versus α.

Figure 16. - Continued.

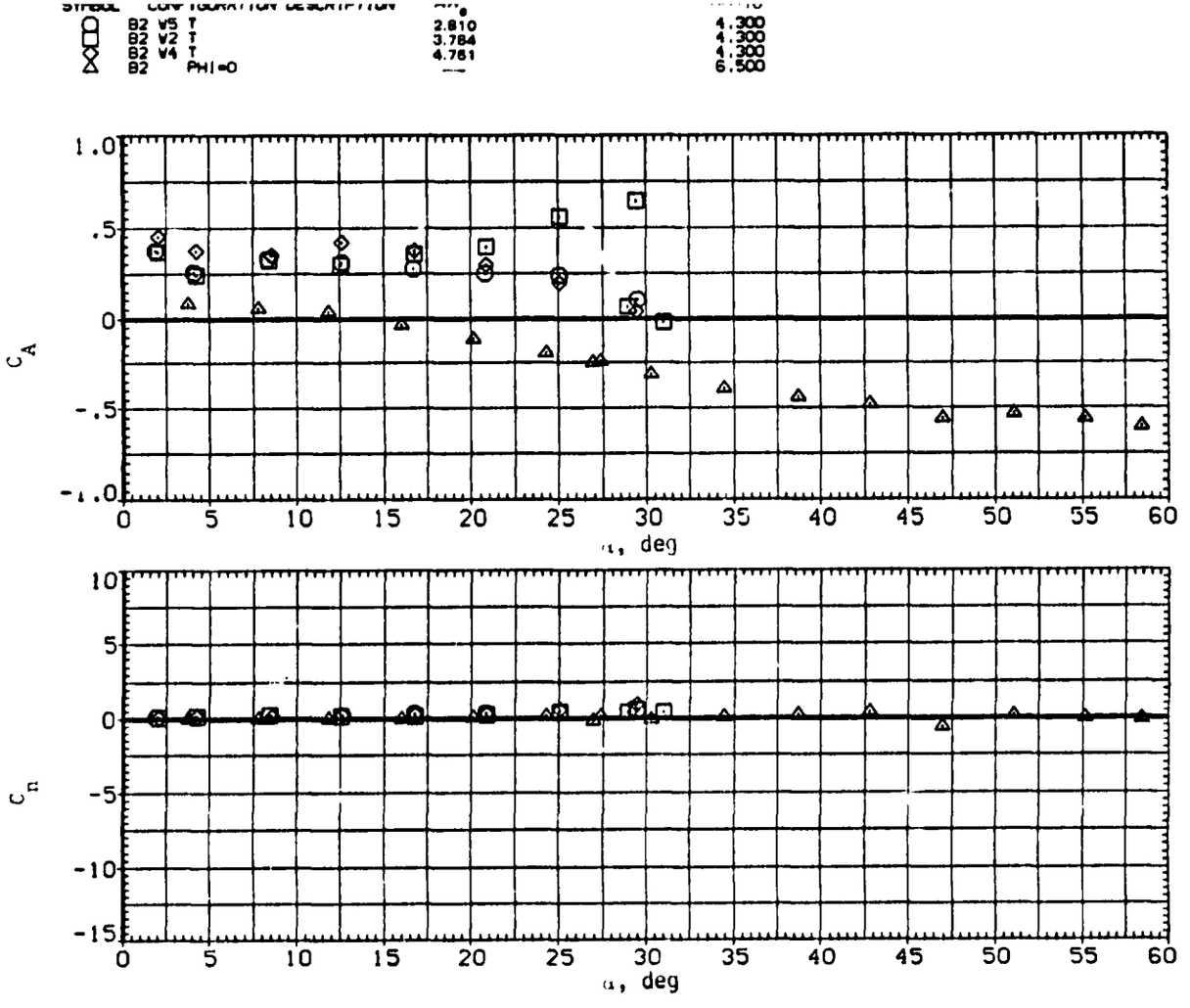

(e) C_A and C_n versus α.

Figure 16.– Continued.

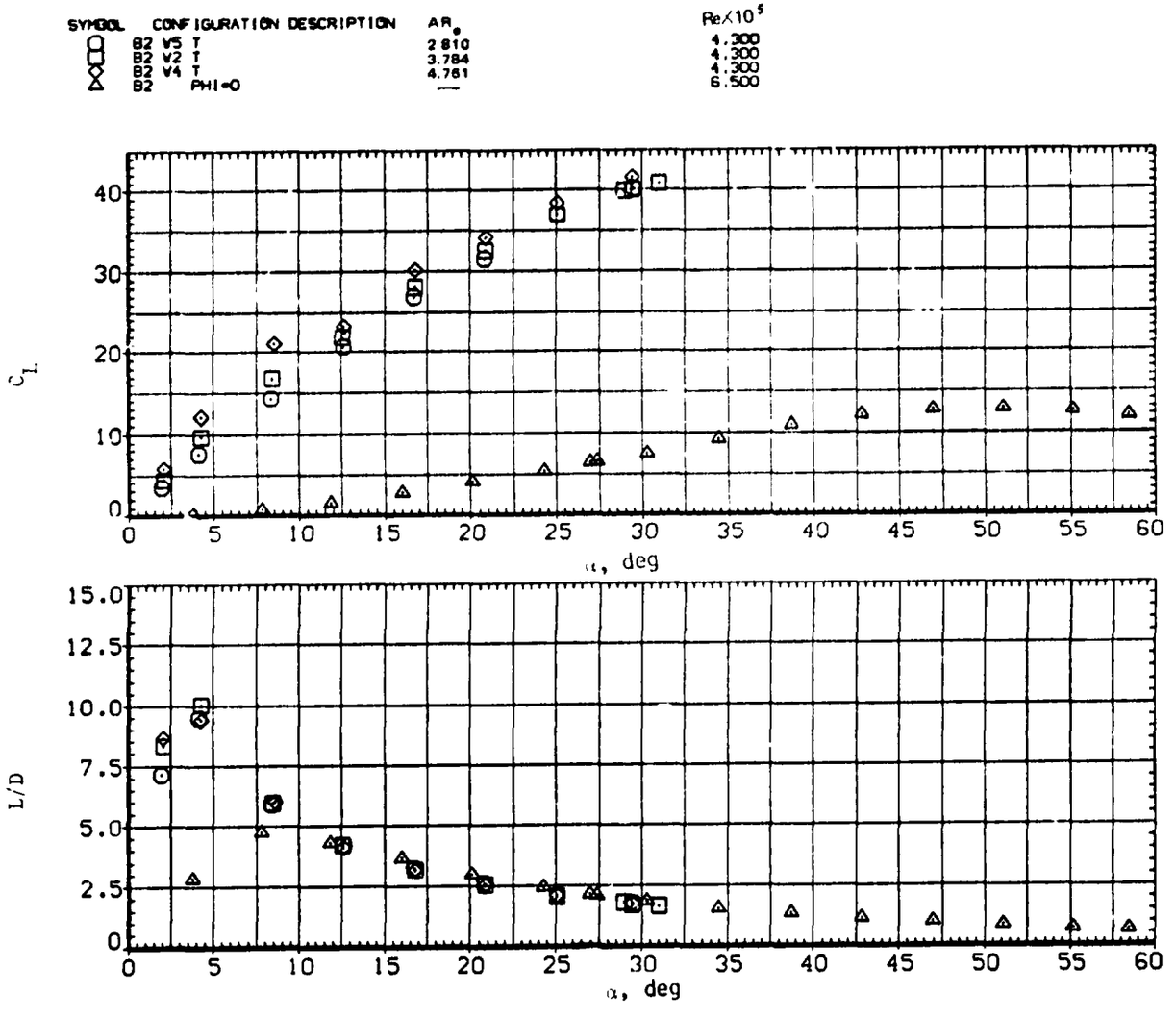

(d) C_L and L/D versus α.

Figure 16. Concluded.

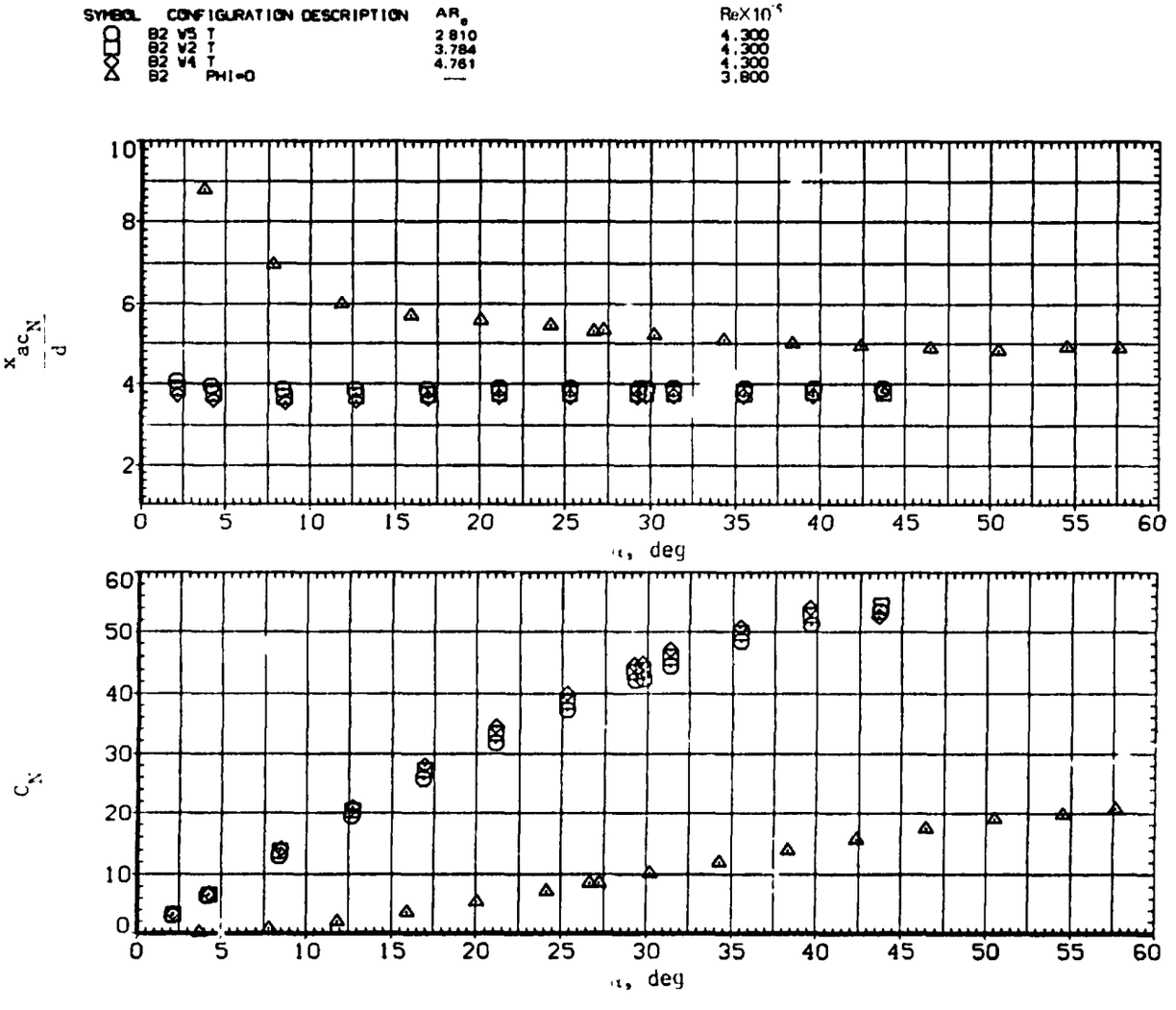

(a) x_{ac_N}/d and C_N versus α.

Figure 17. - Effect of wing aspect ratio with elliptic body and tail, M = 1.5.

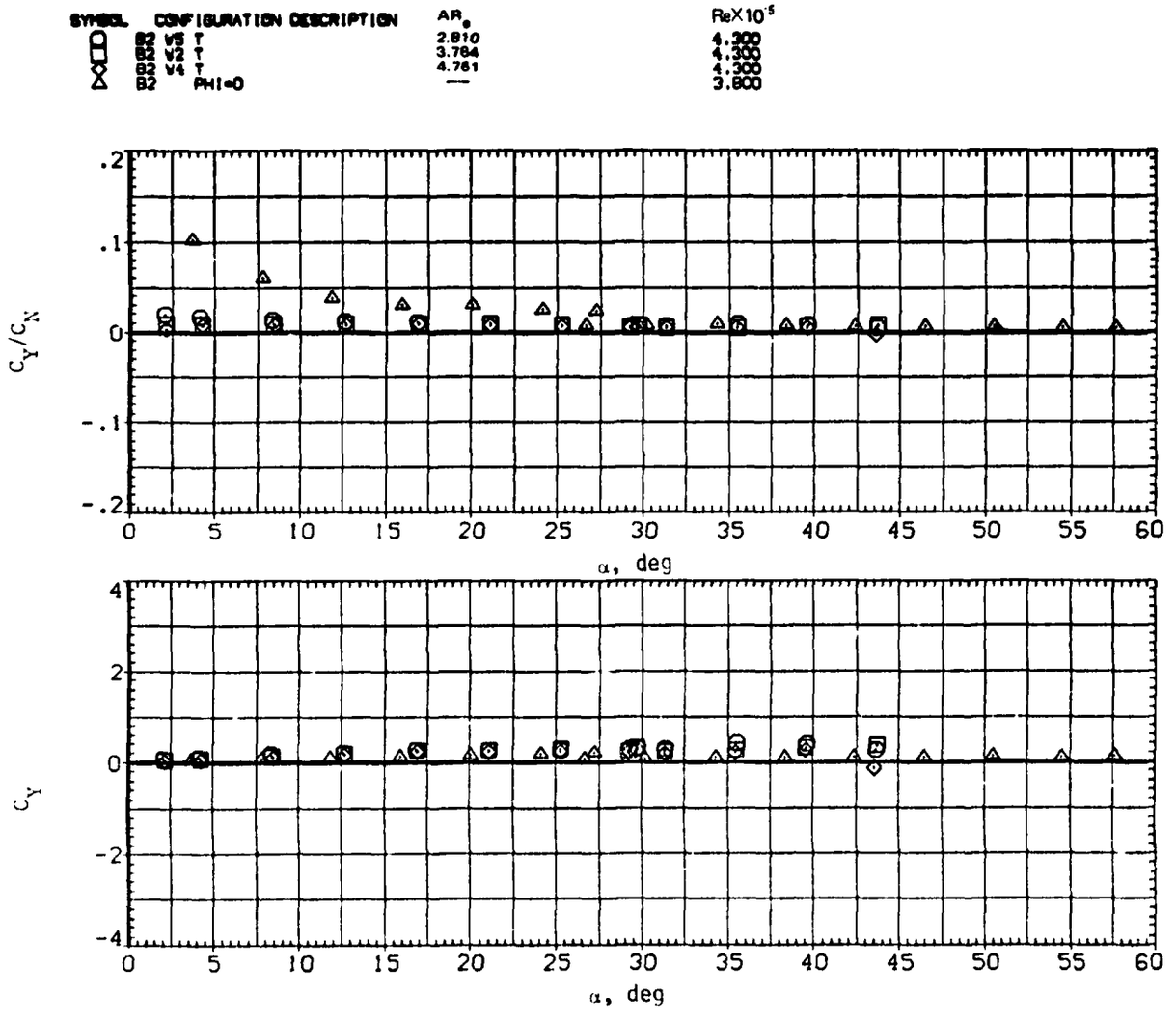

(b) C_Y/C_N and C_Y versus α.

Figure 17. Continued.

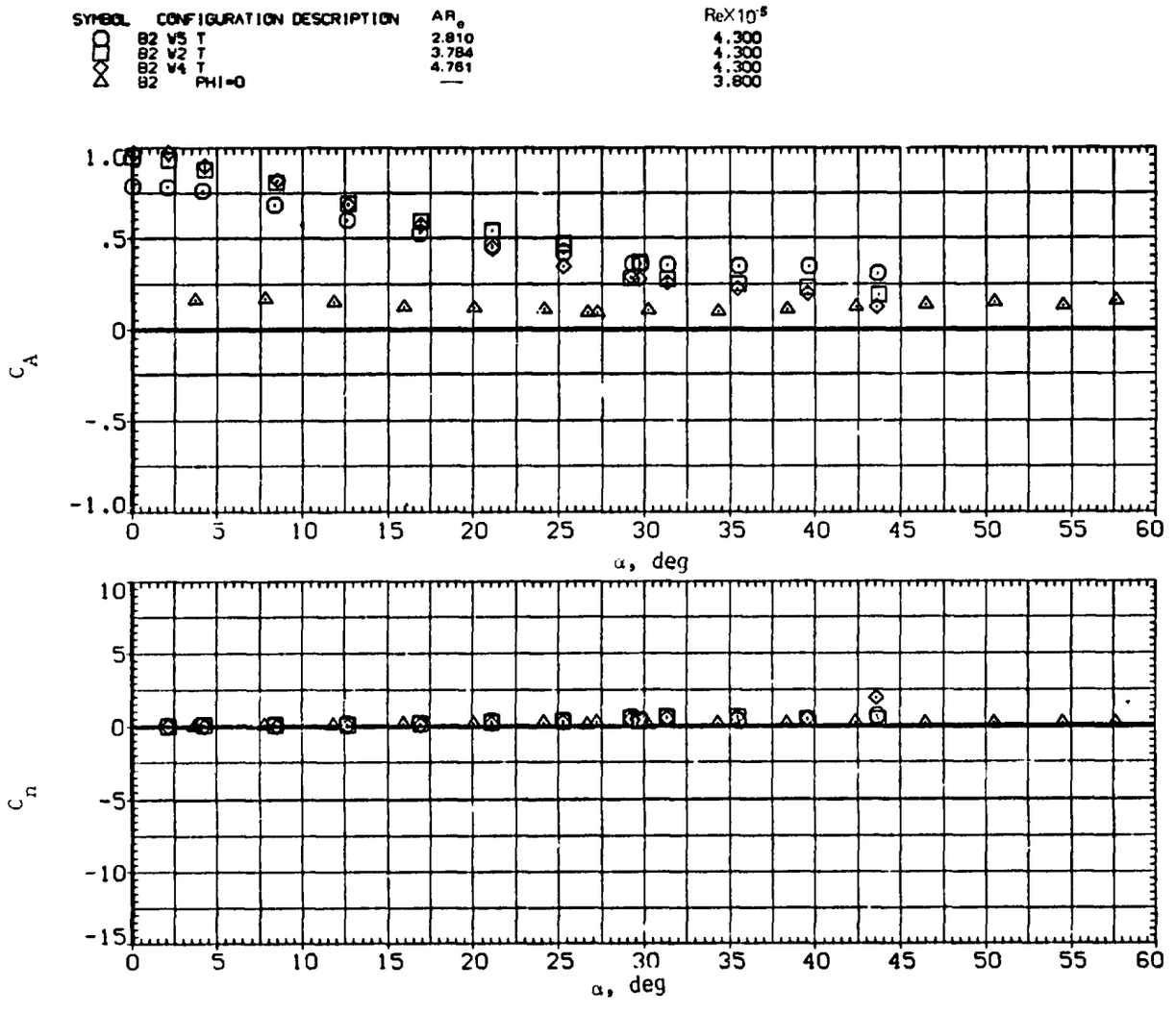

(c) C_A and C_n versus α.

Figure 17. Continued.

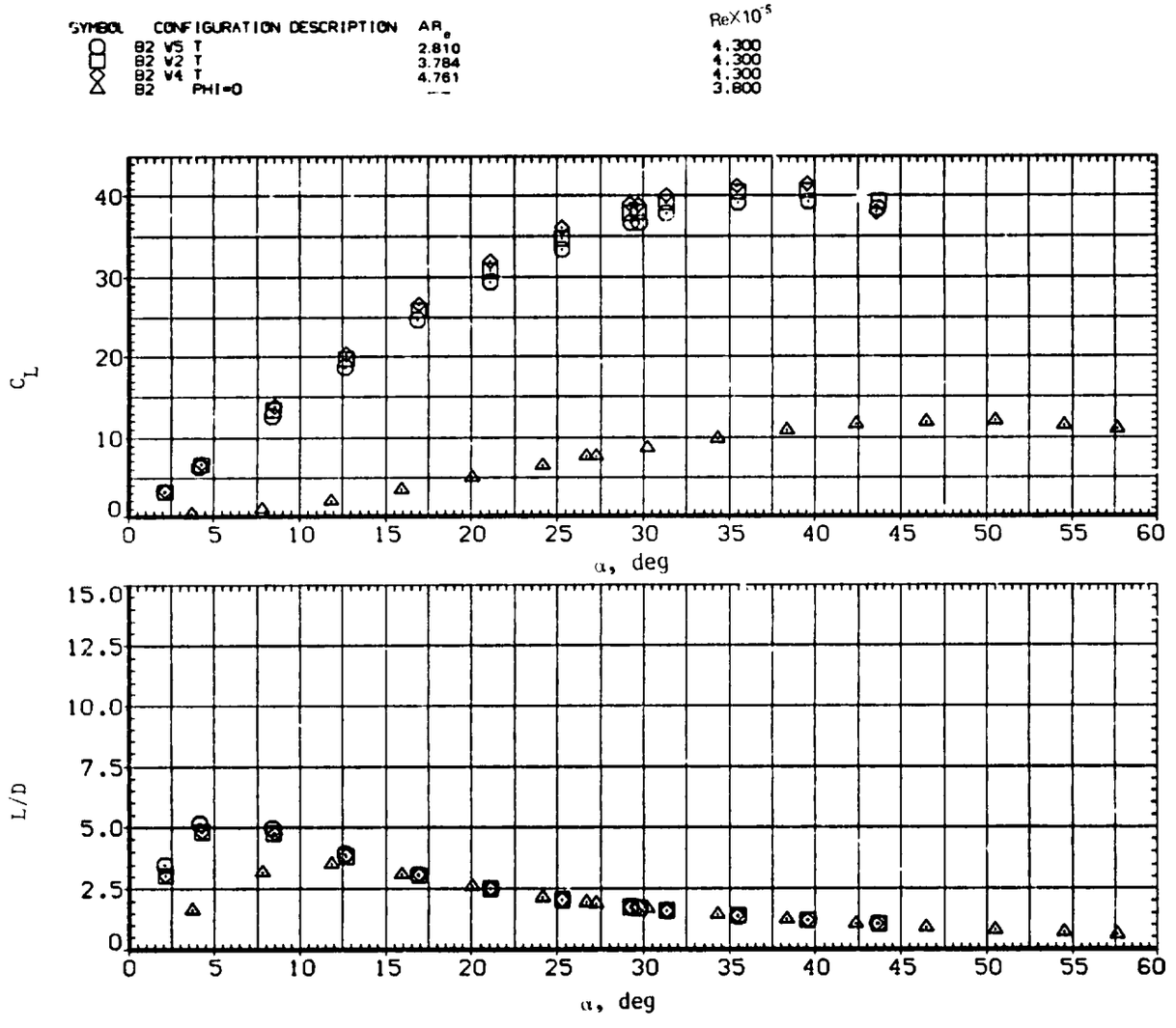

(d) C_L and L/D versus α.

Figure 17.– Concluded.

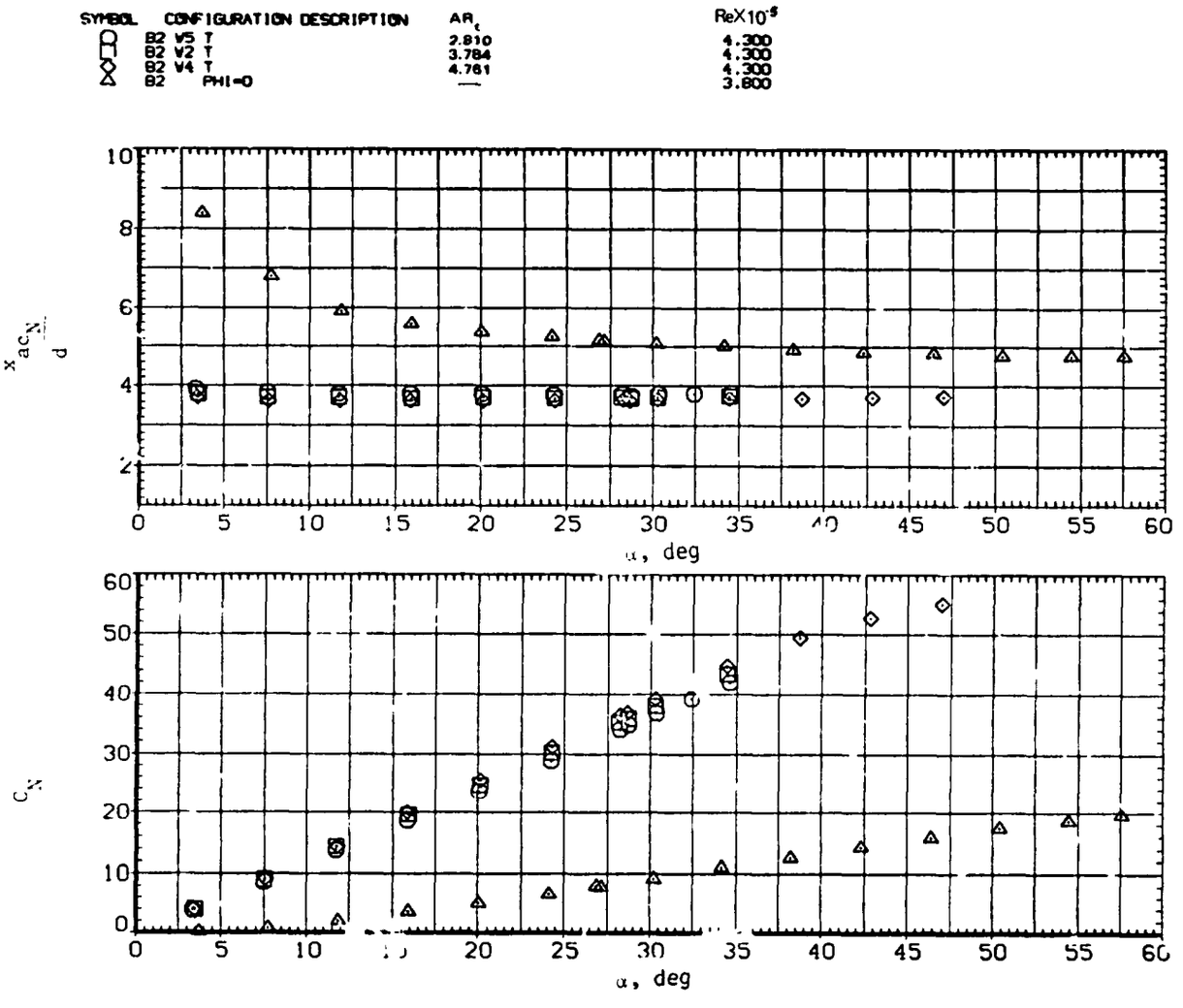

(a) x_{ac_N}/d and C_N versus α.

Figure 18. Effect of wing aspect ratio with elliptic body and tail, M = 2.0.

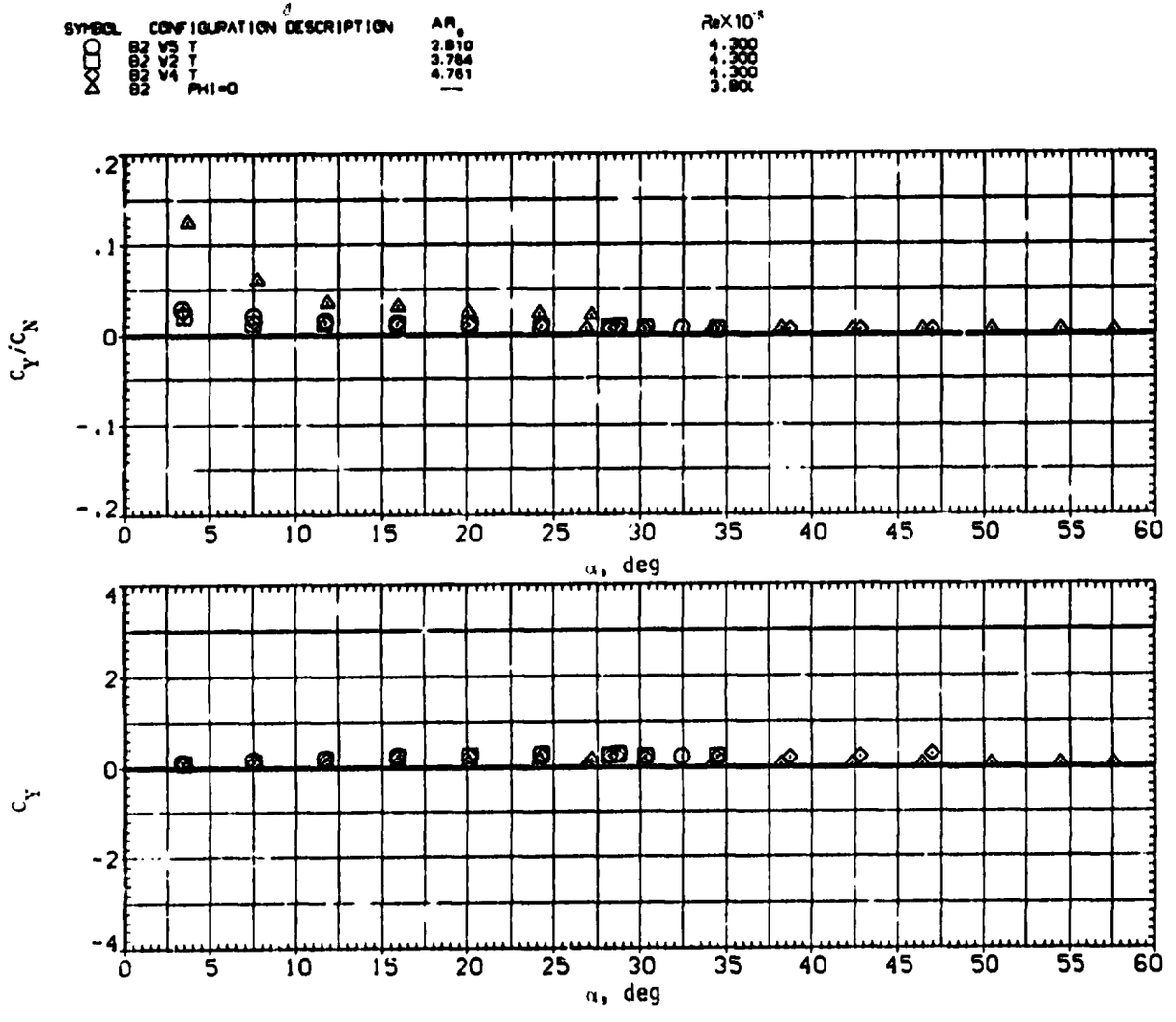

(b) C_Y/C_N and C_Y versus α.

Figure 18. Continued.

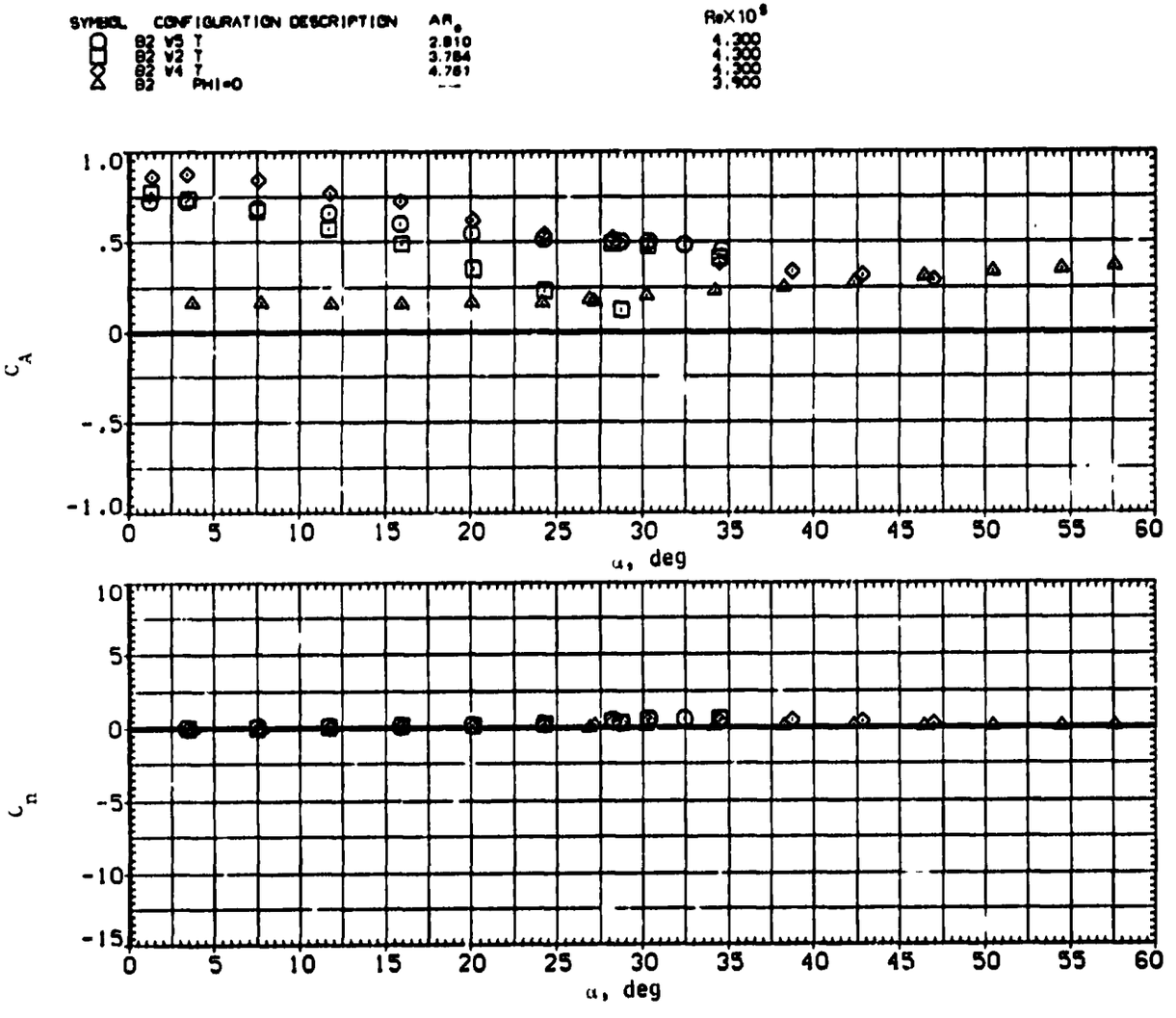

(c) C_A and C_n versus α.

Figure 18.– Continued.

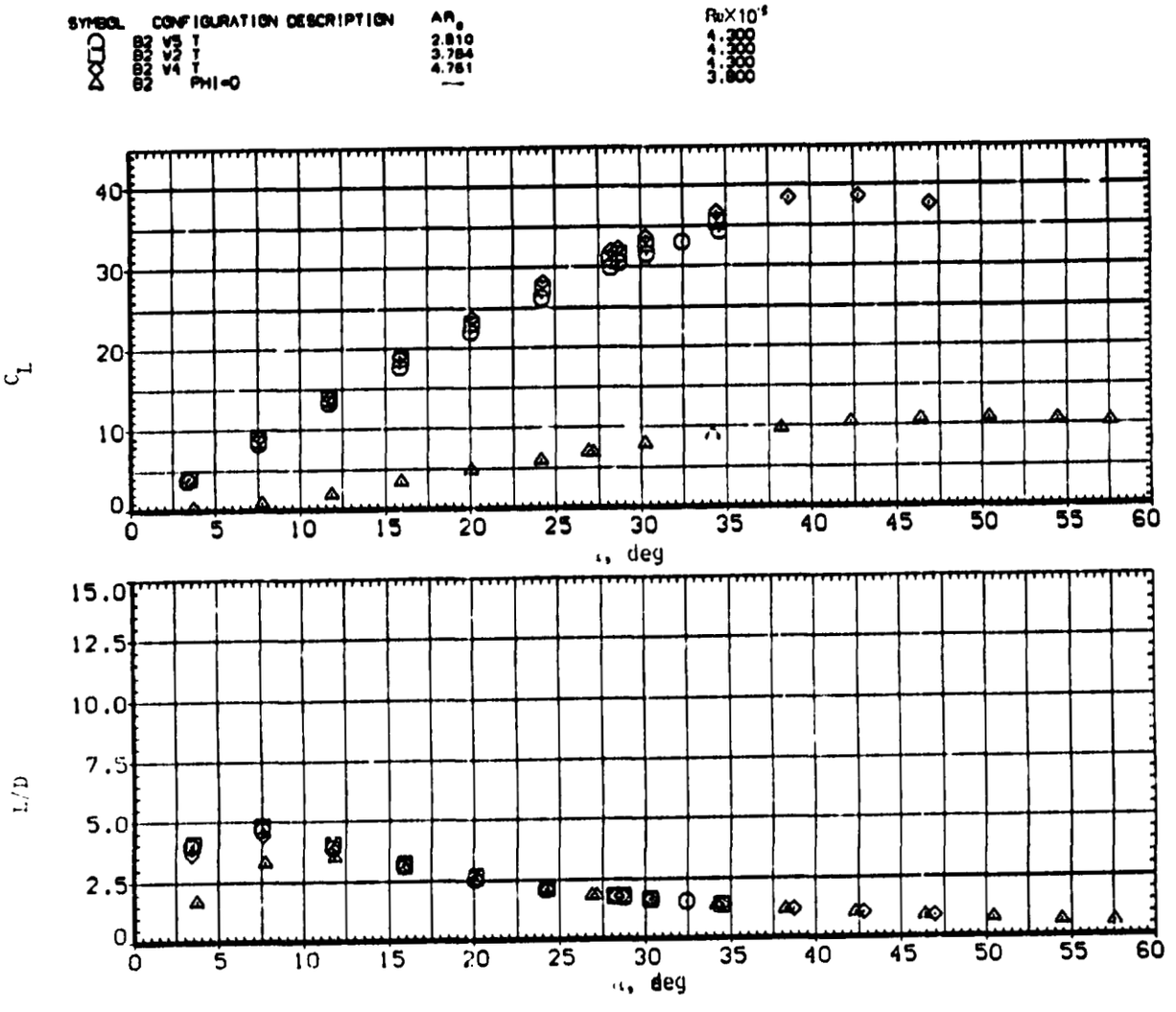

(d) C_L and L/D versus α.

Figure 18. Concluded.

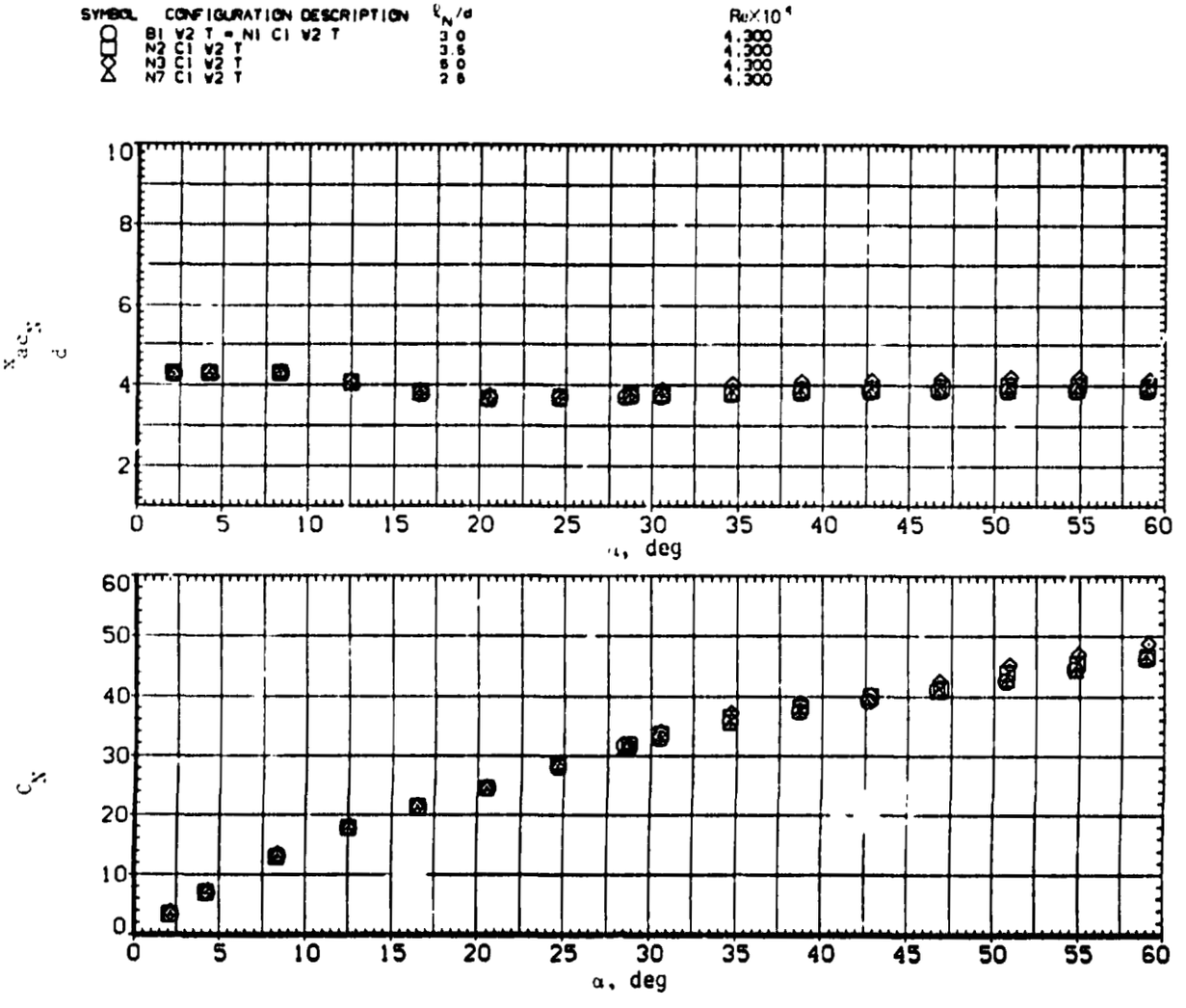

(a) x_{ac_N}/d and C_N versus α.

Figure 19.- Effect of nose fineness ratio on wing-body-tail characteristics, M = 0.6.

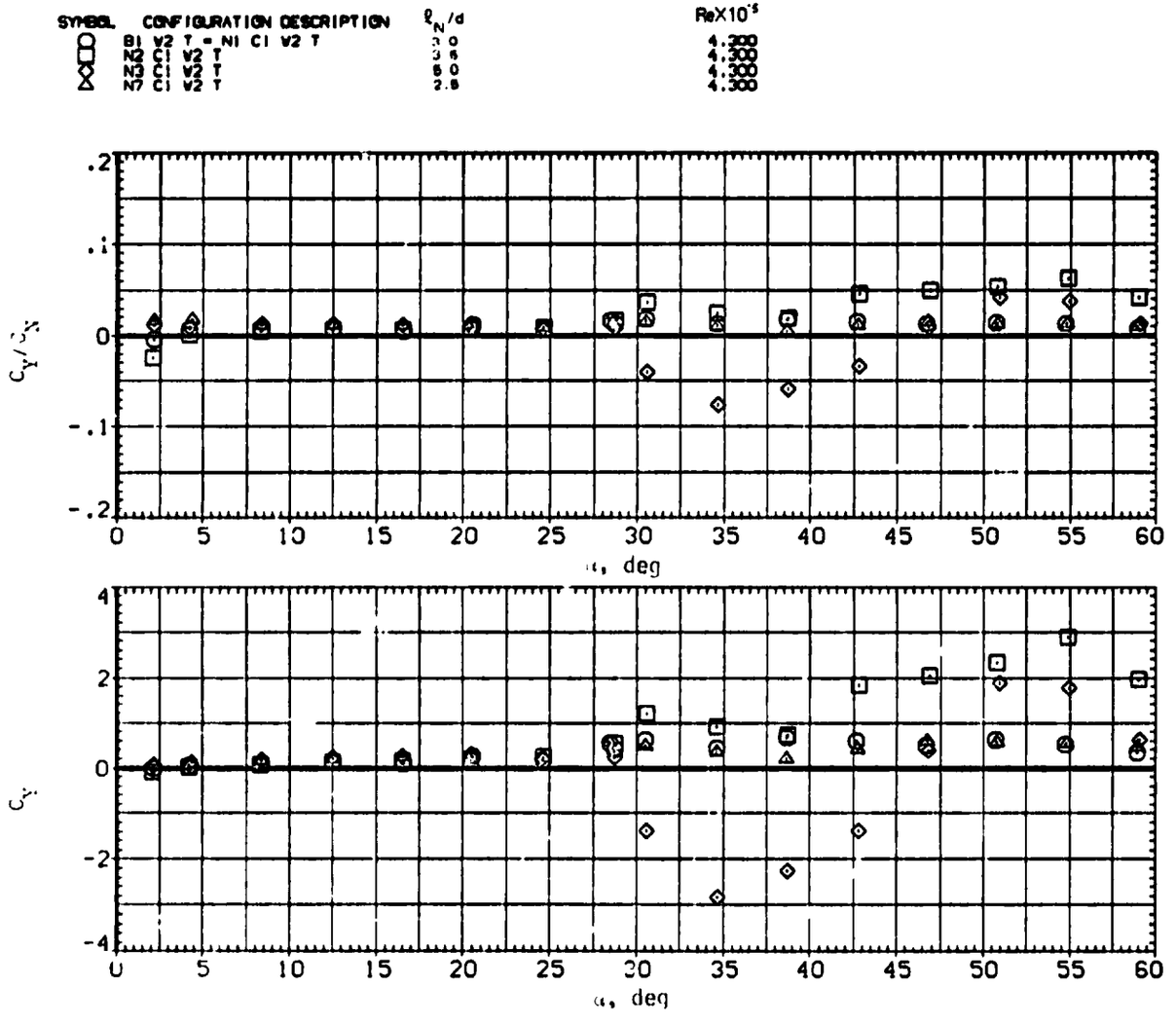

(b) C_Y/C_N and C_Y versus α.

Figure 19.- Continued.

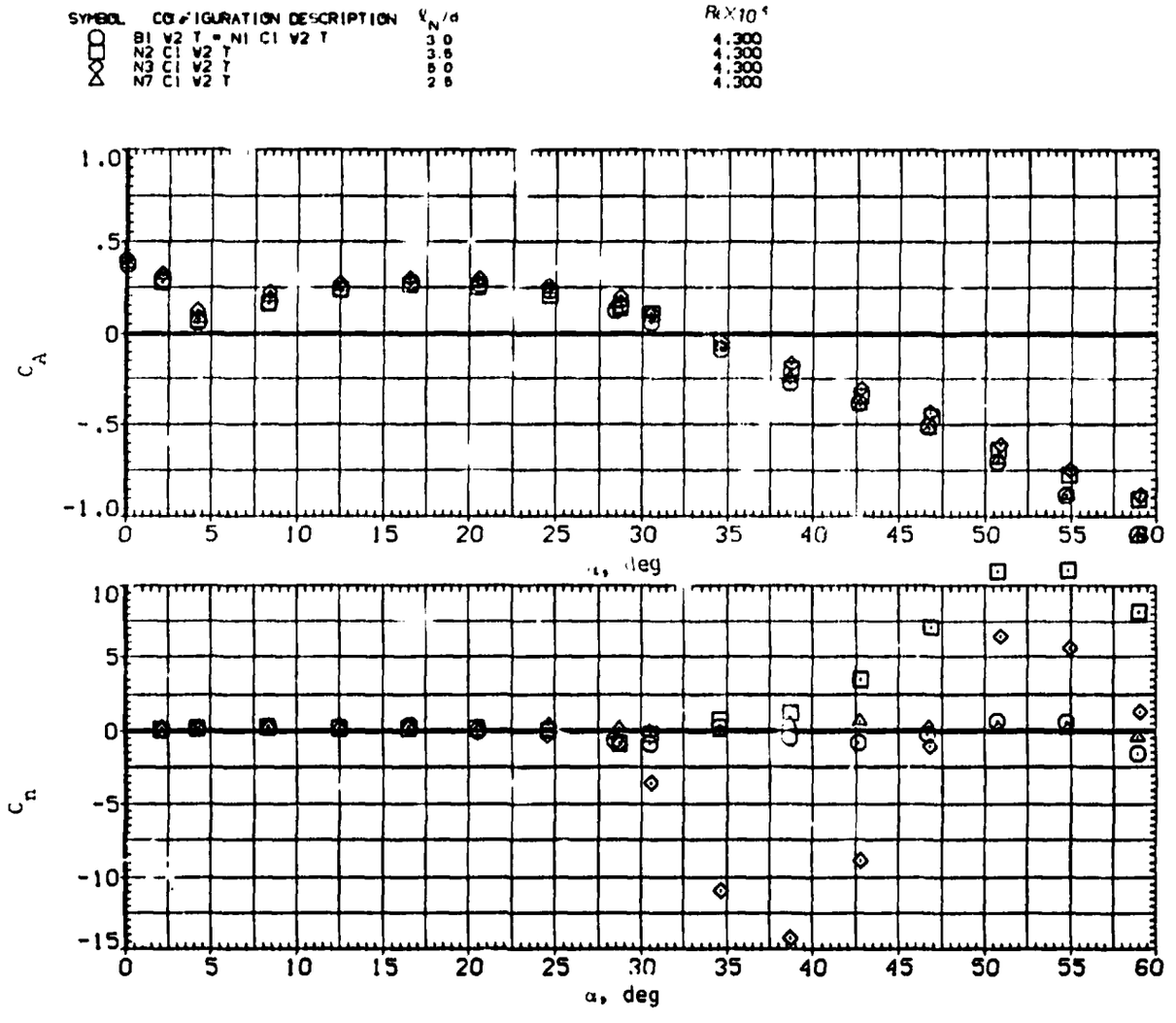

(c) C_A and C_n versus α.

Figure 19.– Continued.

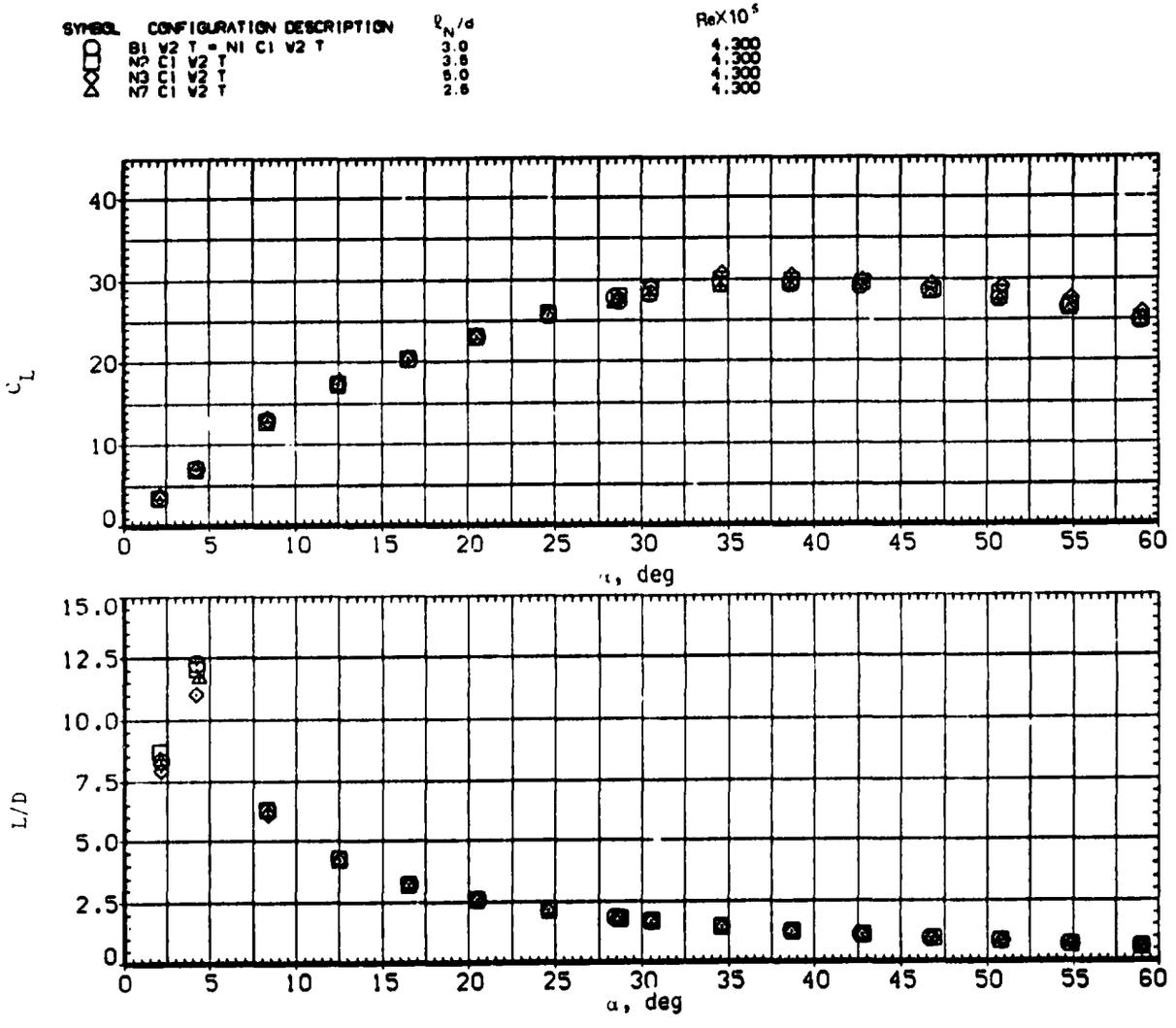

(d) C_L and L/D versus α.

Figure 19.– Concluded.

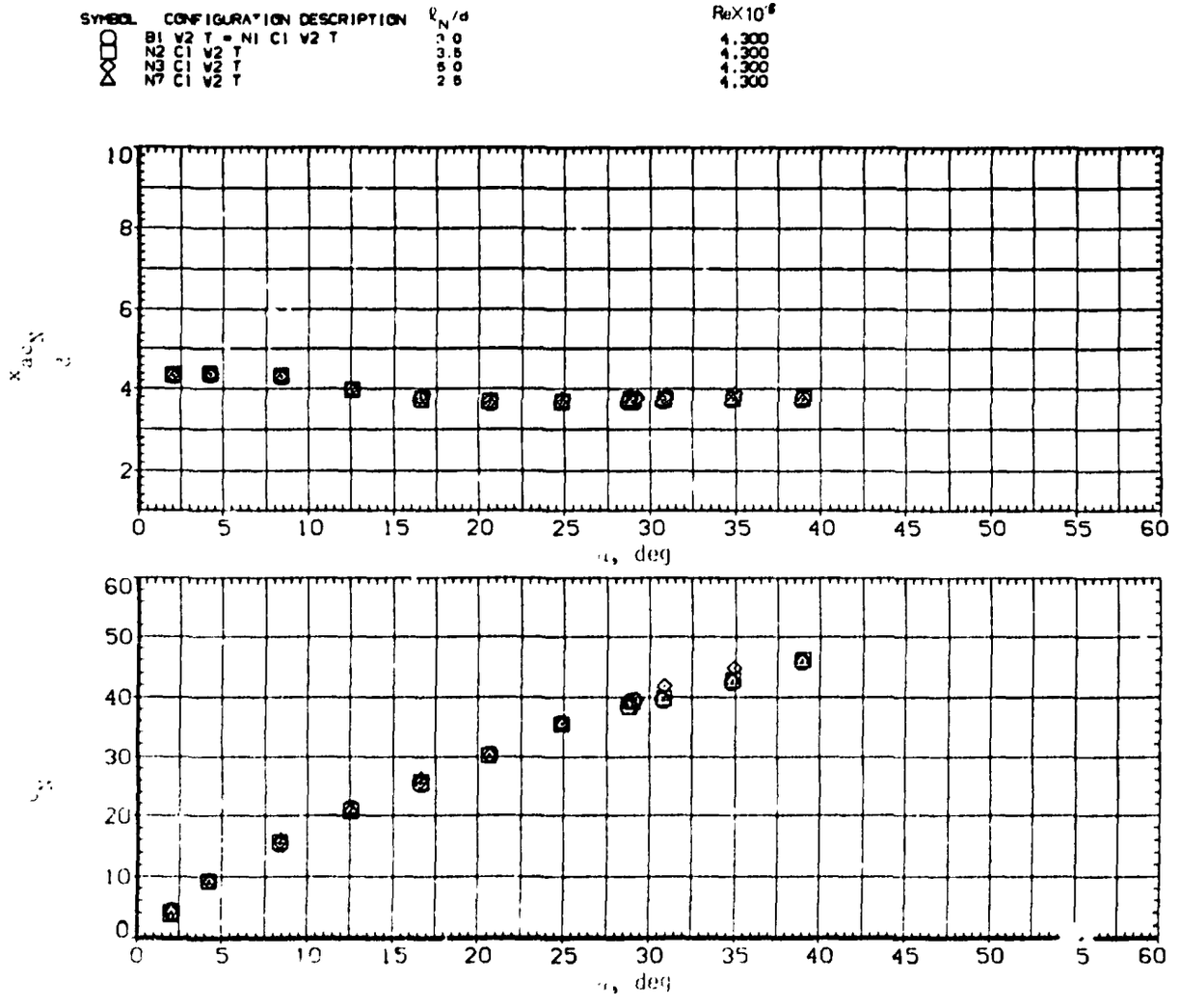

(a) x_{ac_N}/d and C_N versus α.

Figure 20 Effect of nose fineness ratio on wing-body-tail characteristics, M = 0.9.

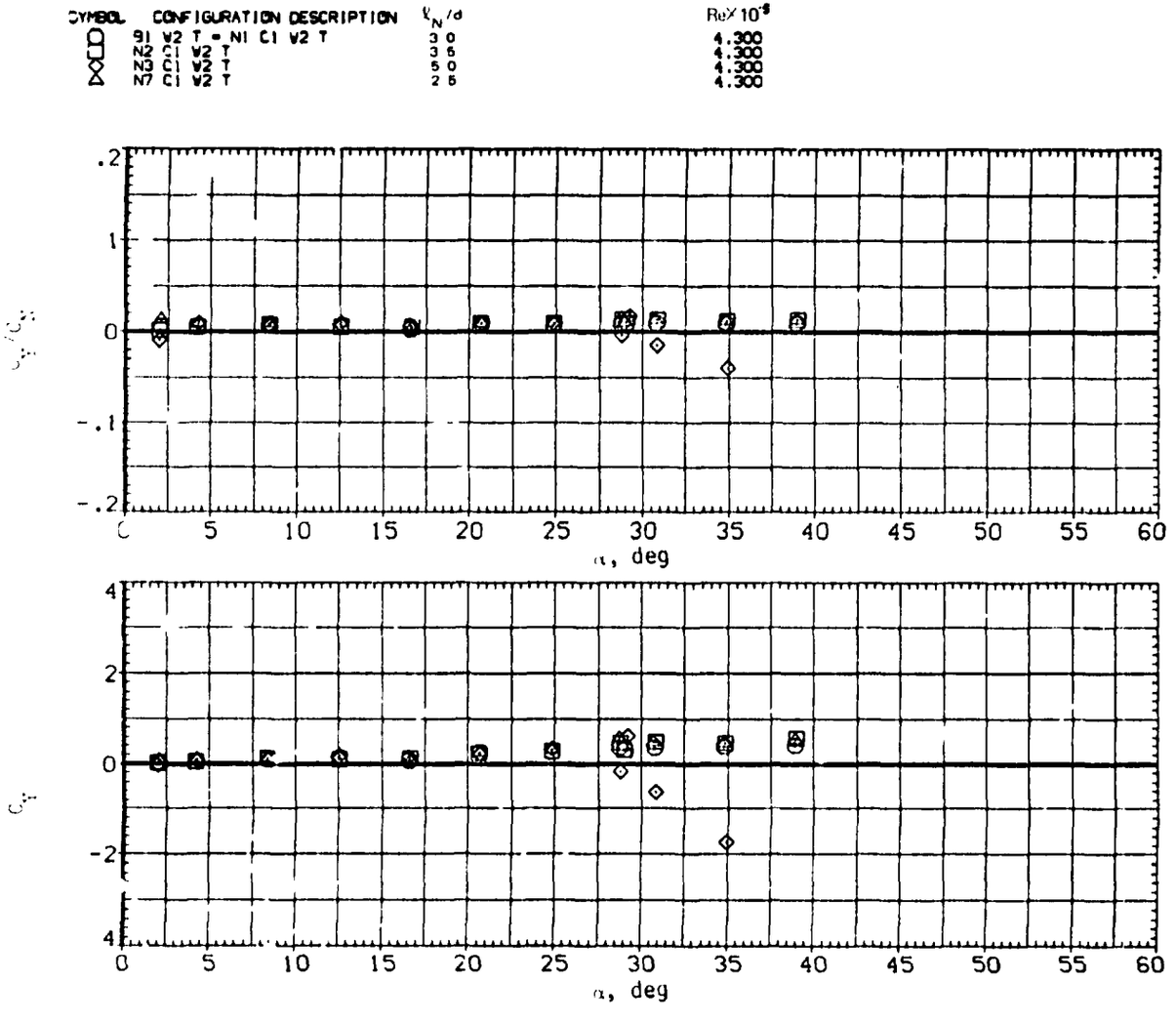

(b) C_Y/C_N and C_Y versus α.

Figure 20. - Continued.

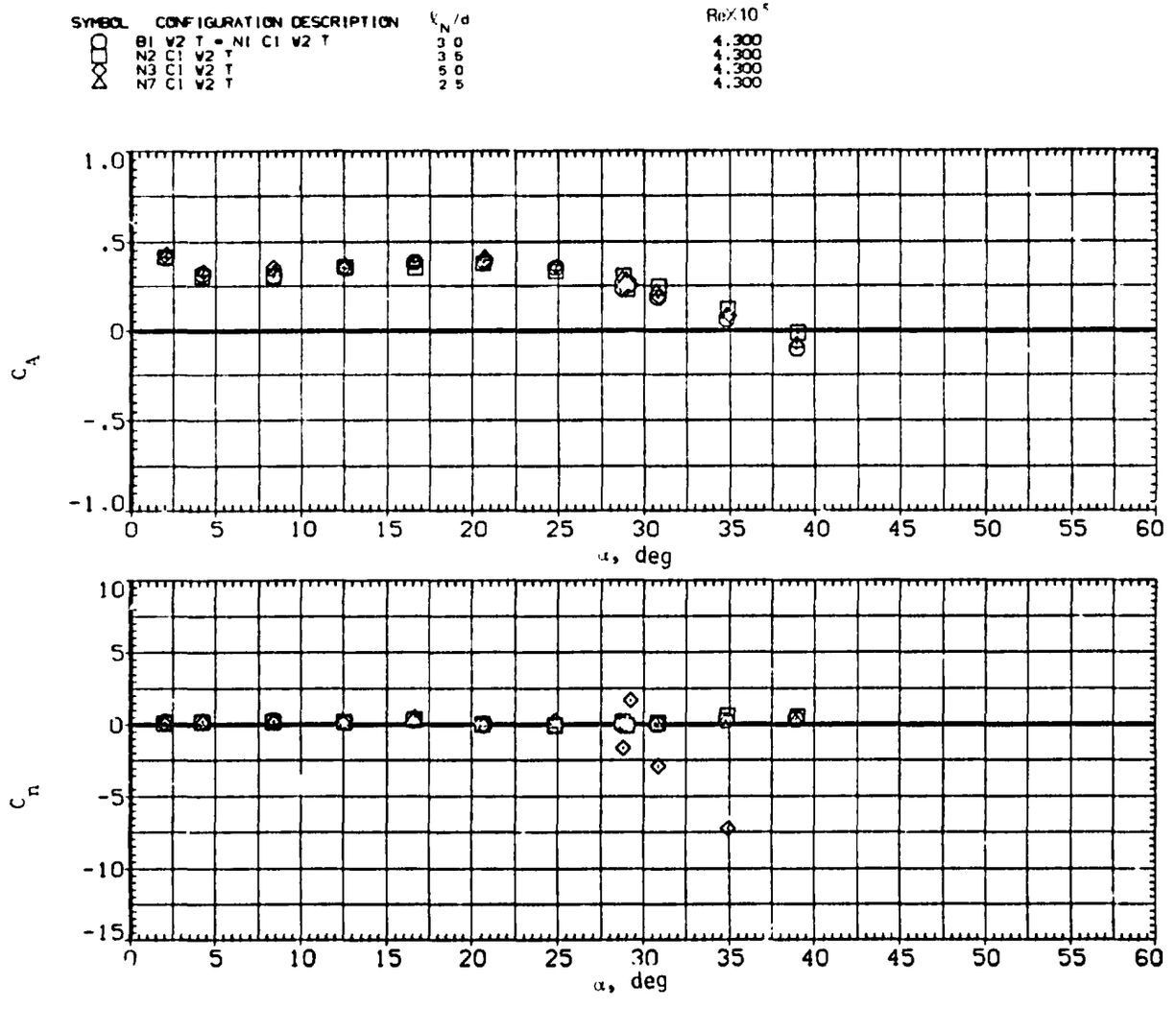

(c) C_A and C_n versus α.

Figure 20. – Continued.

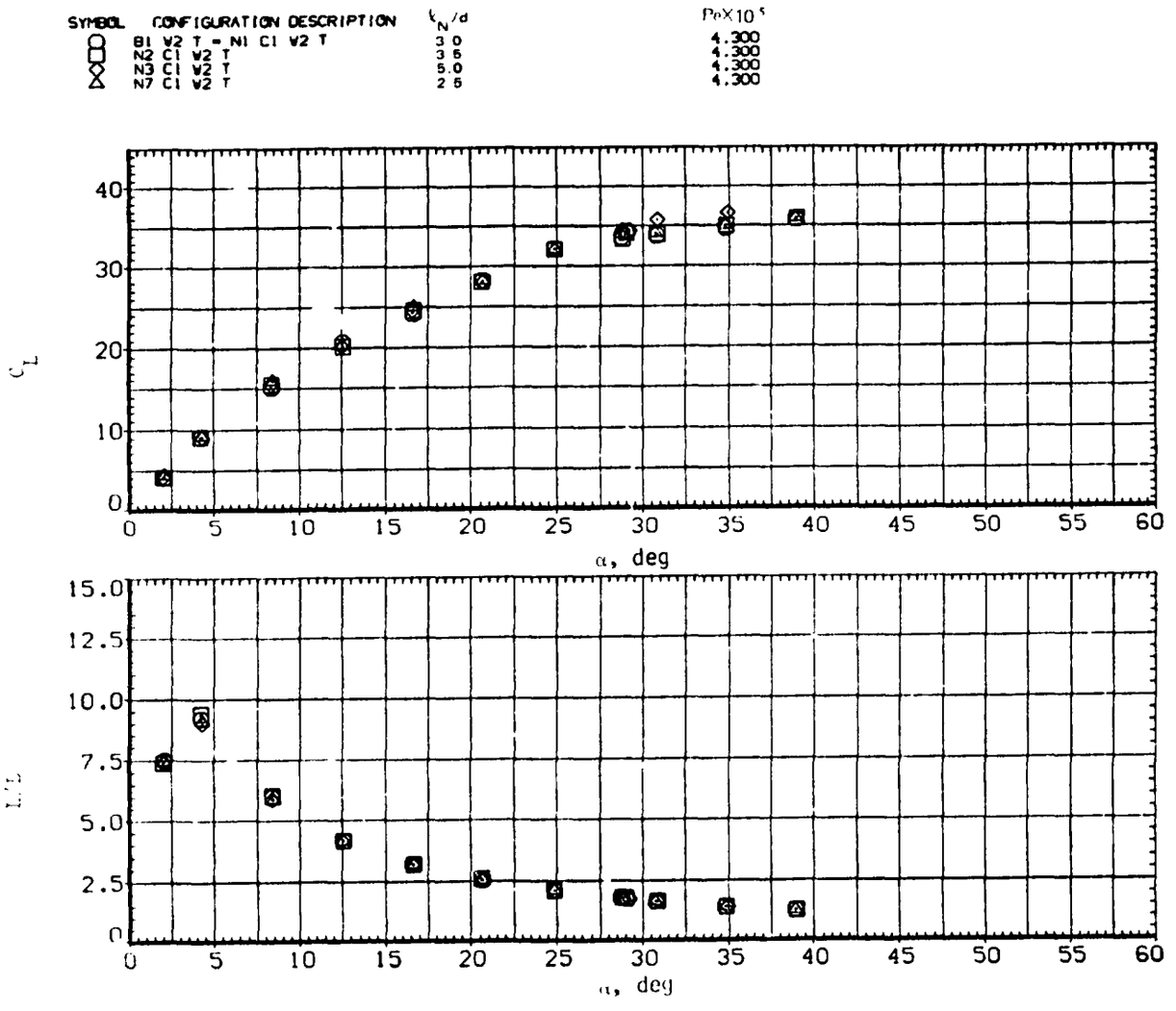

(d) C_L and L/D versus α.

Figure 20. Concluded.

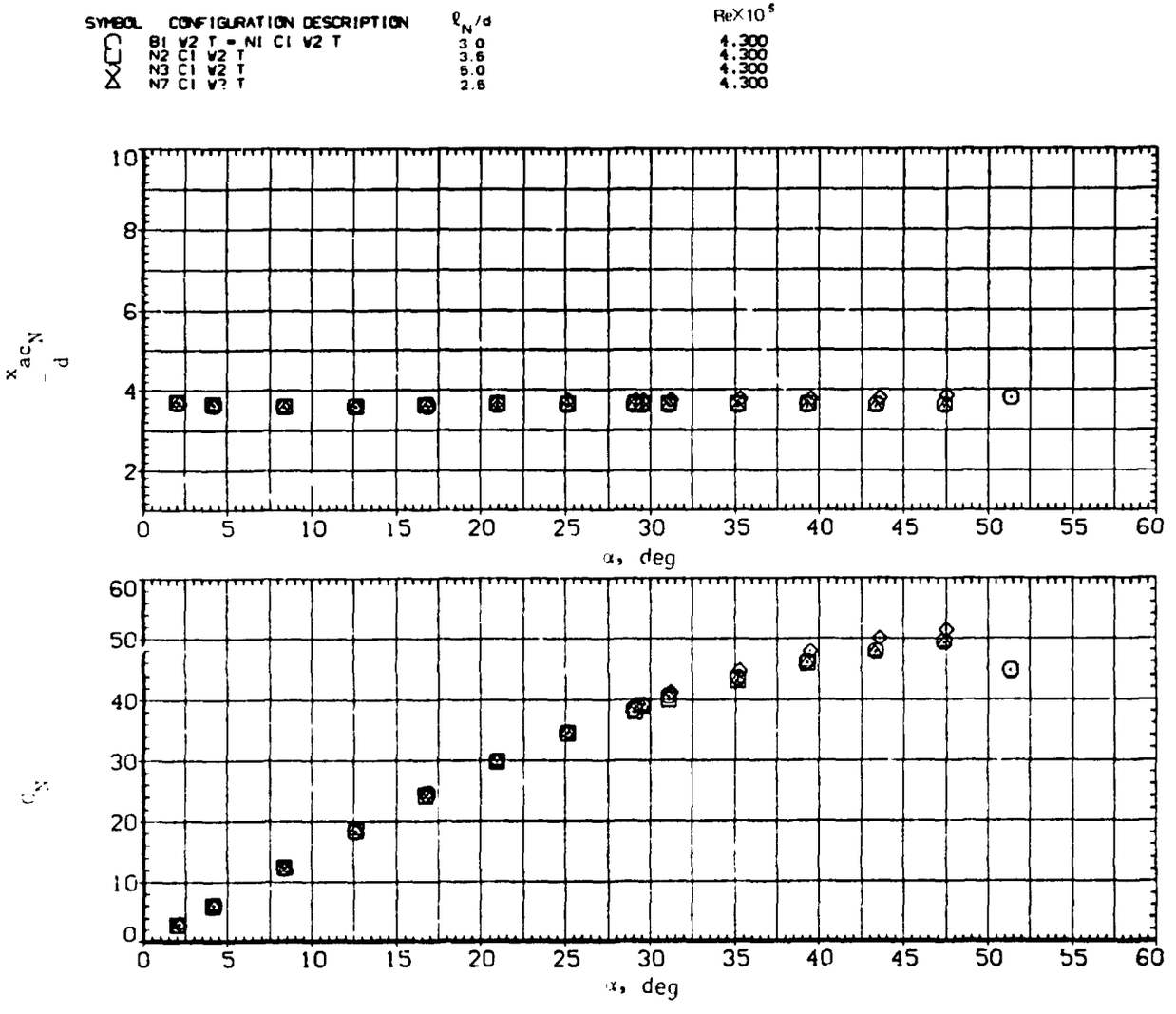

(a) x_{ac_N}/d and C_N versus α.

Figure 21. Effect of nose fineness ratio on wing-body-tail characteristics, M = 1.5.

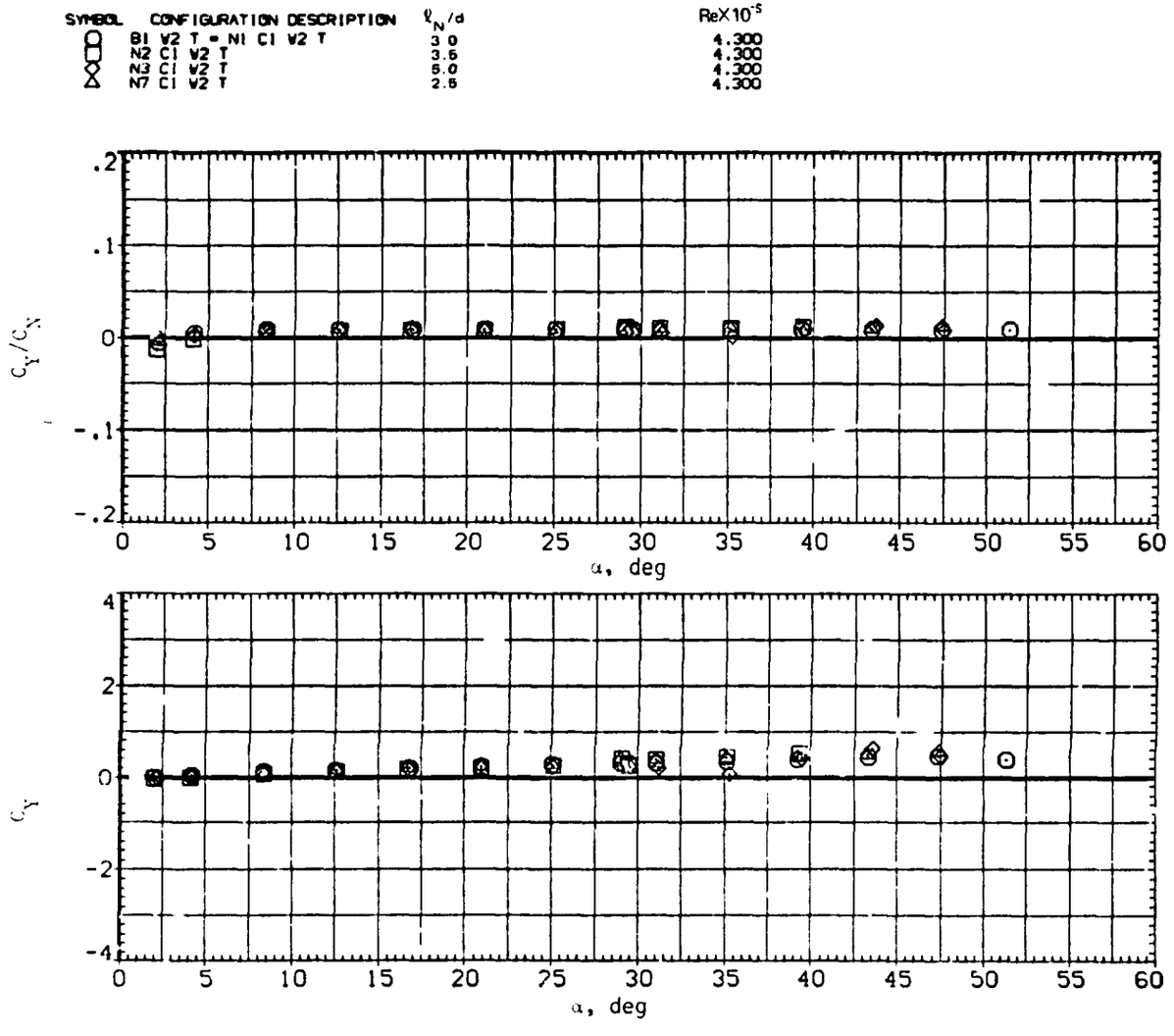

(b) C_Y/C_N and C_Y versus α.

Figure 21. Continued.

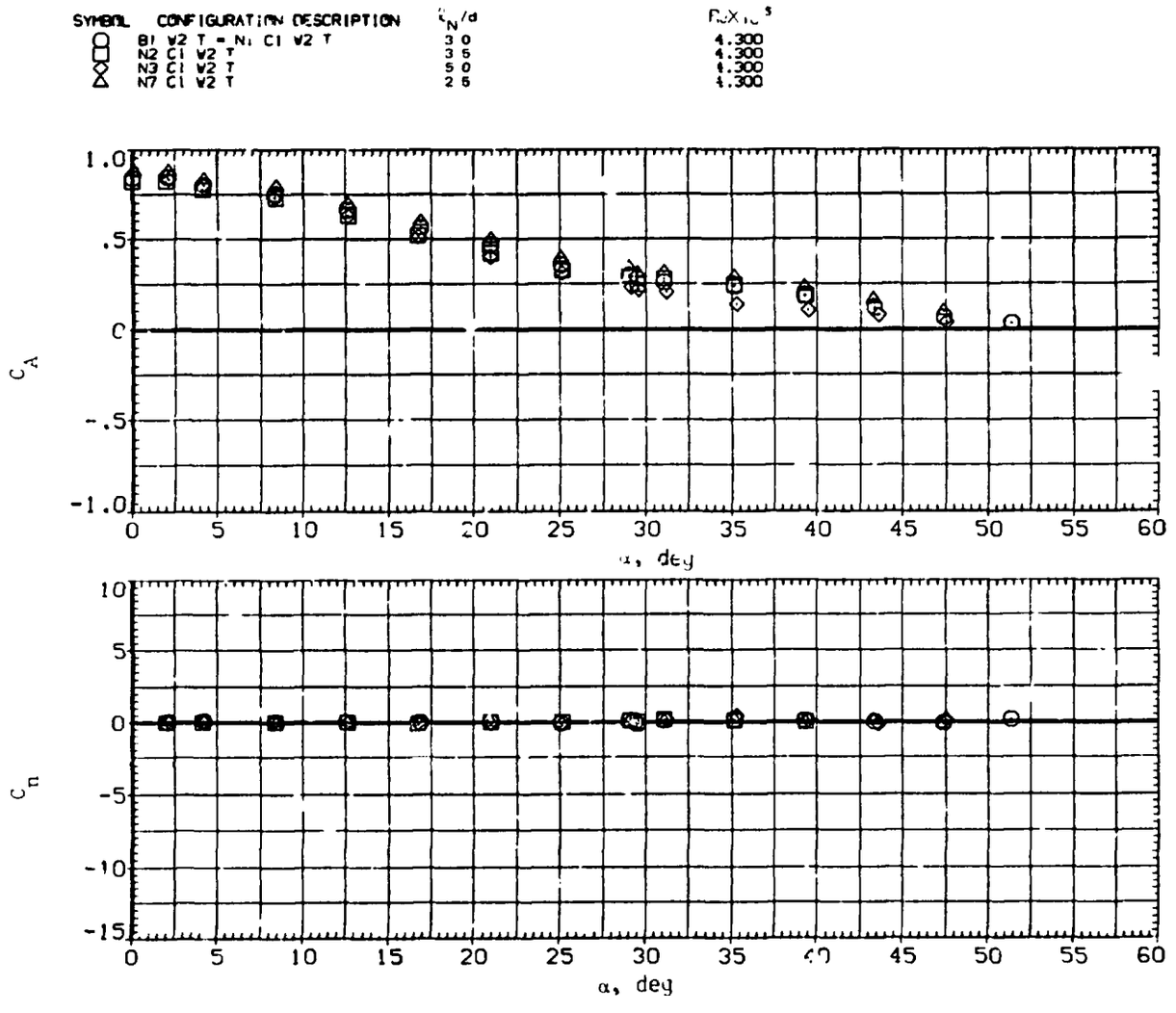

(c) C_A and C_n versus α.

Figure 21. - Continued.

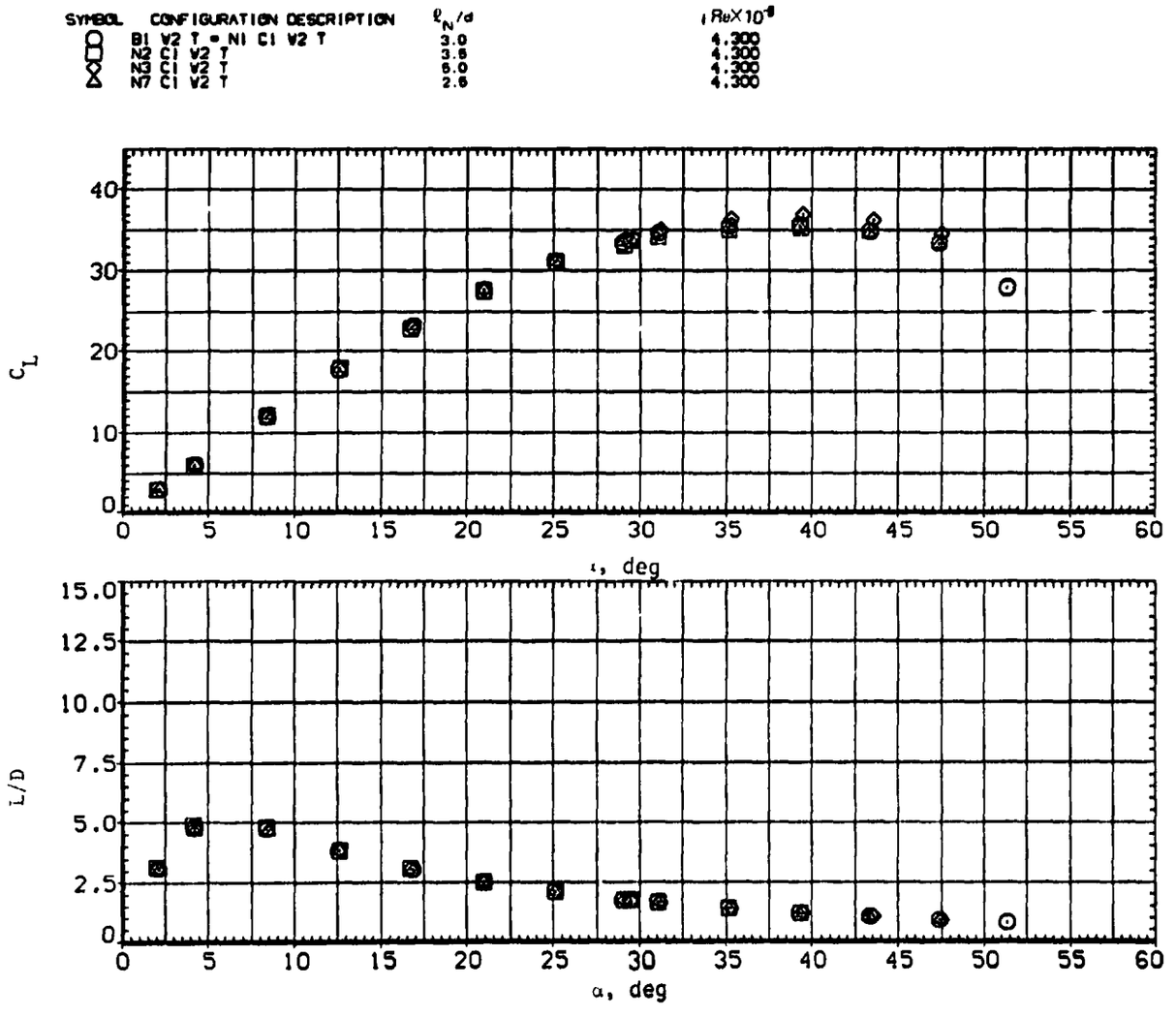

(d) C_L and L/D versus α.

Figure 21. Concluded.

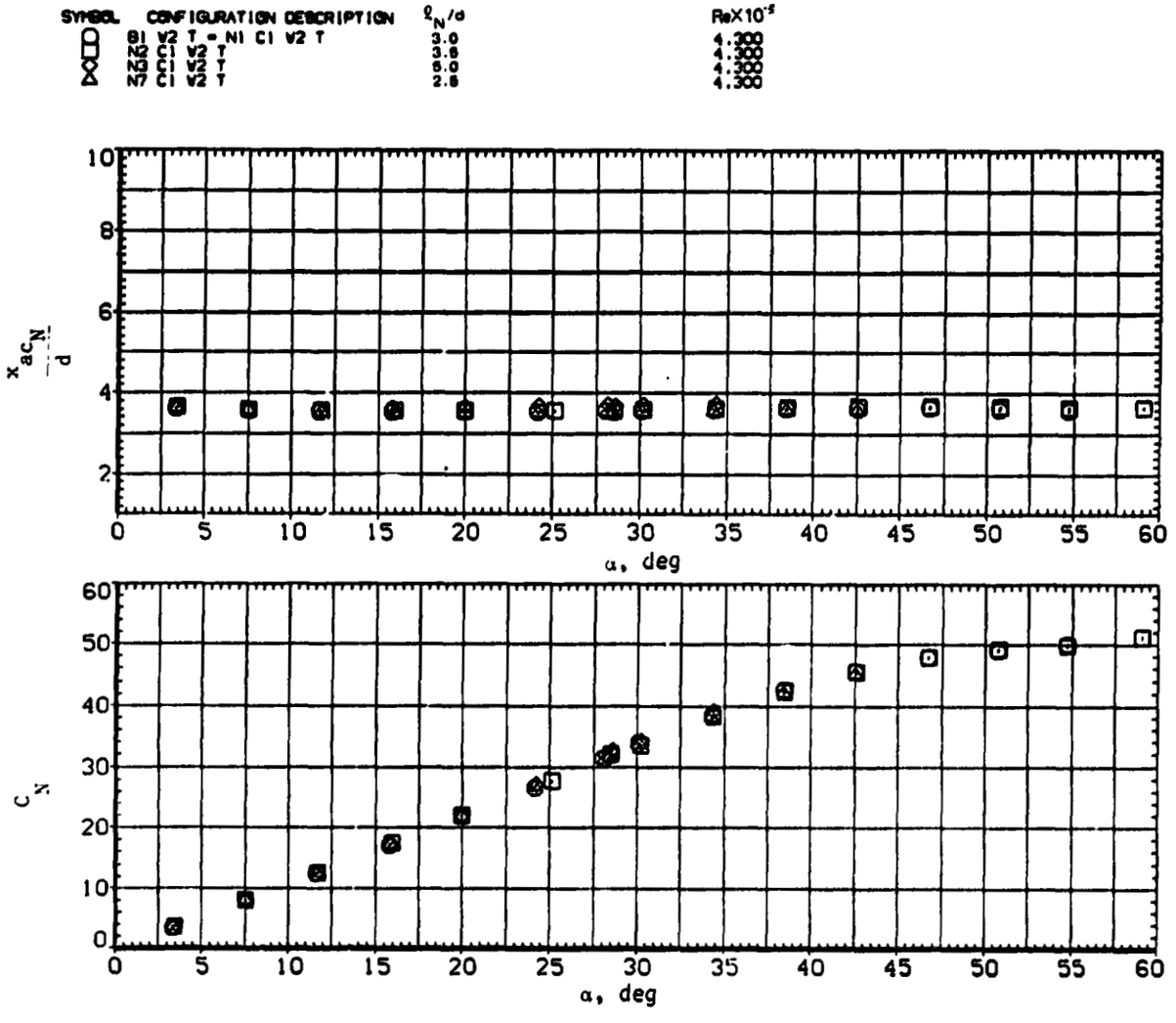

(a) x_{ac_N}/d and C_N versus α.

Figure 22. Effect of nose fineness ratio on wing-body-tail characteristics, M = 2.0.

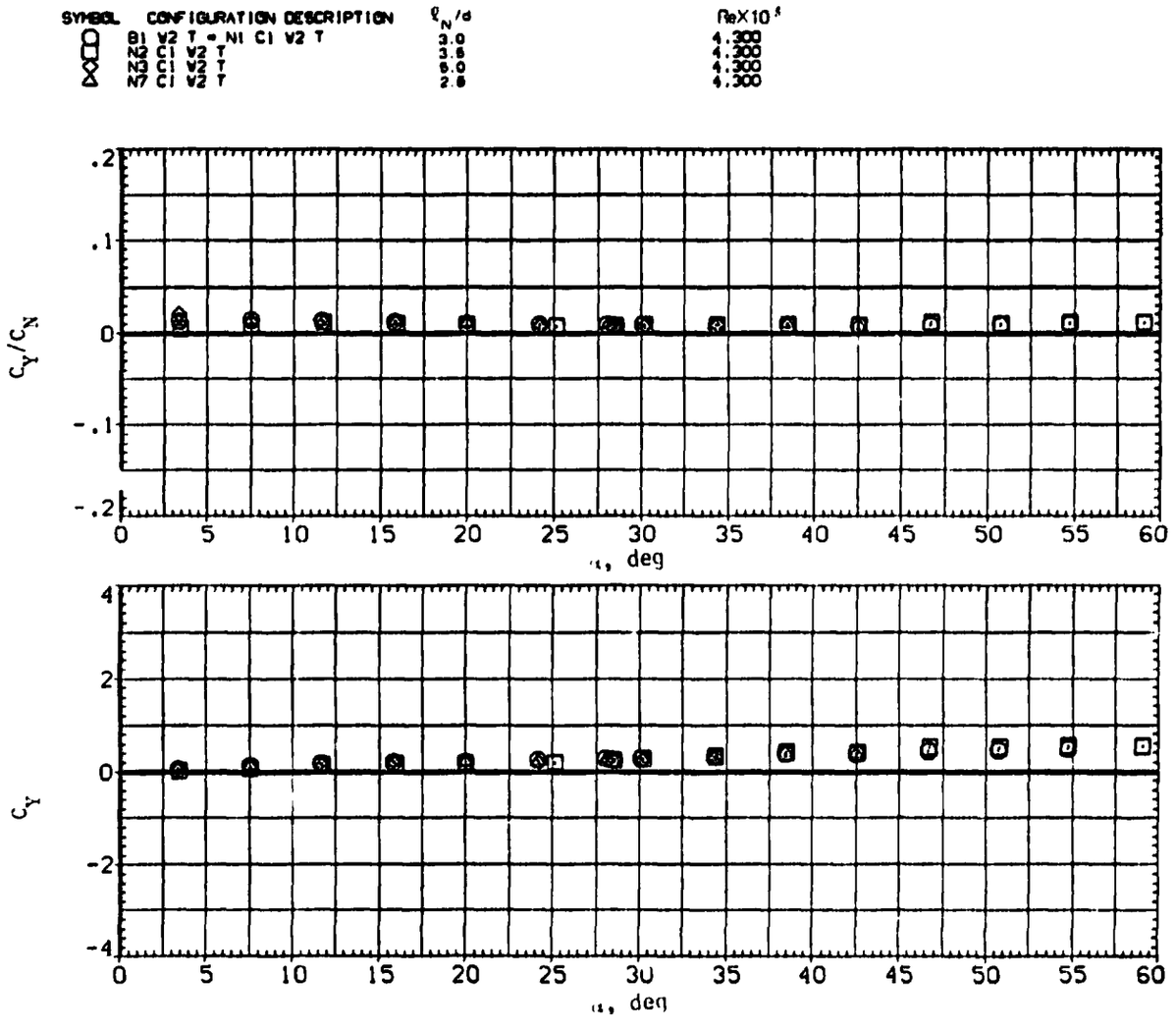

(b) C_Y/C_N and C_Y versus α.

Figure 22.– Continued.

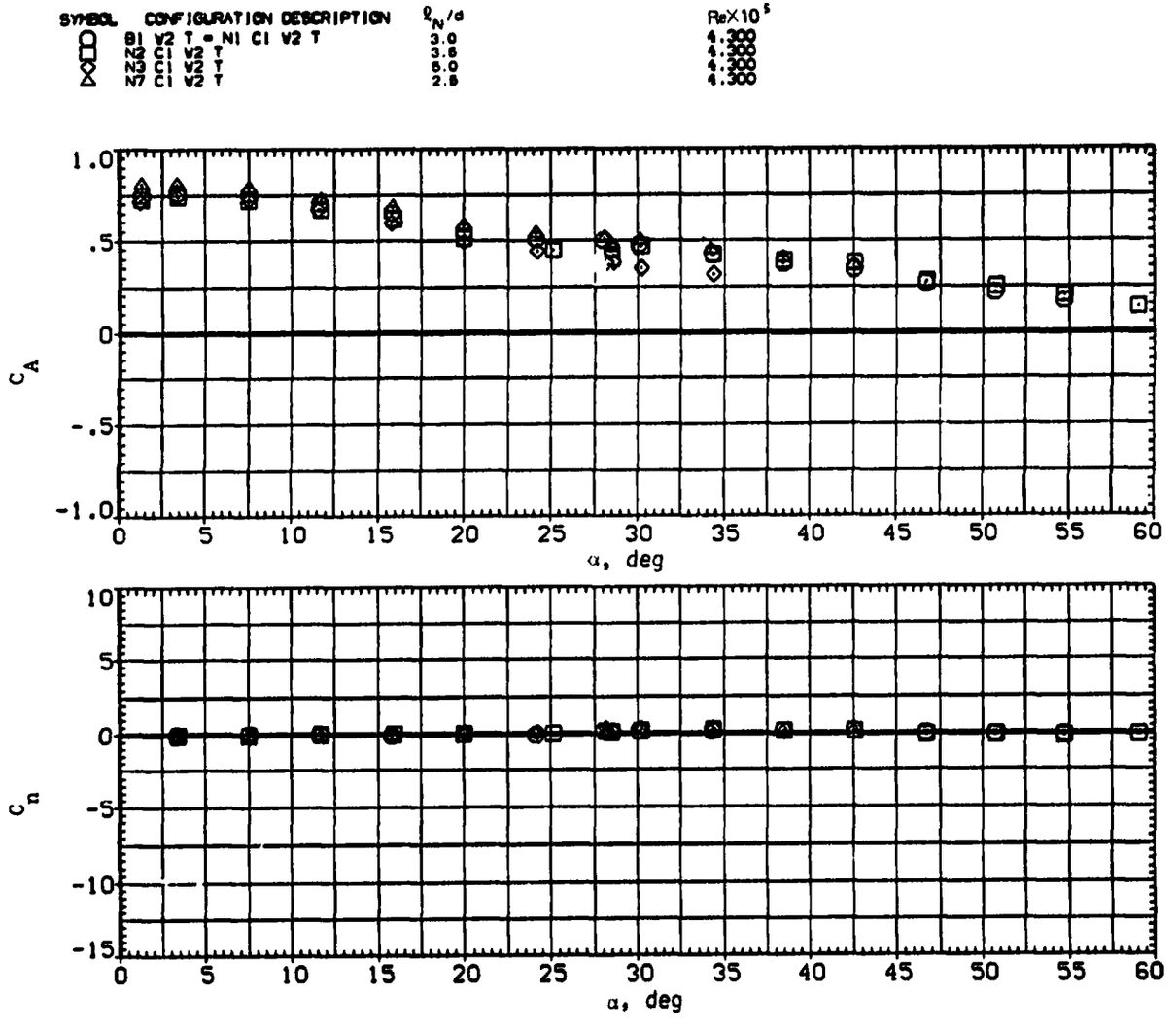

(c) C_A and C_n versus α.

Figure 22. Continued.

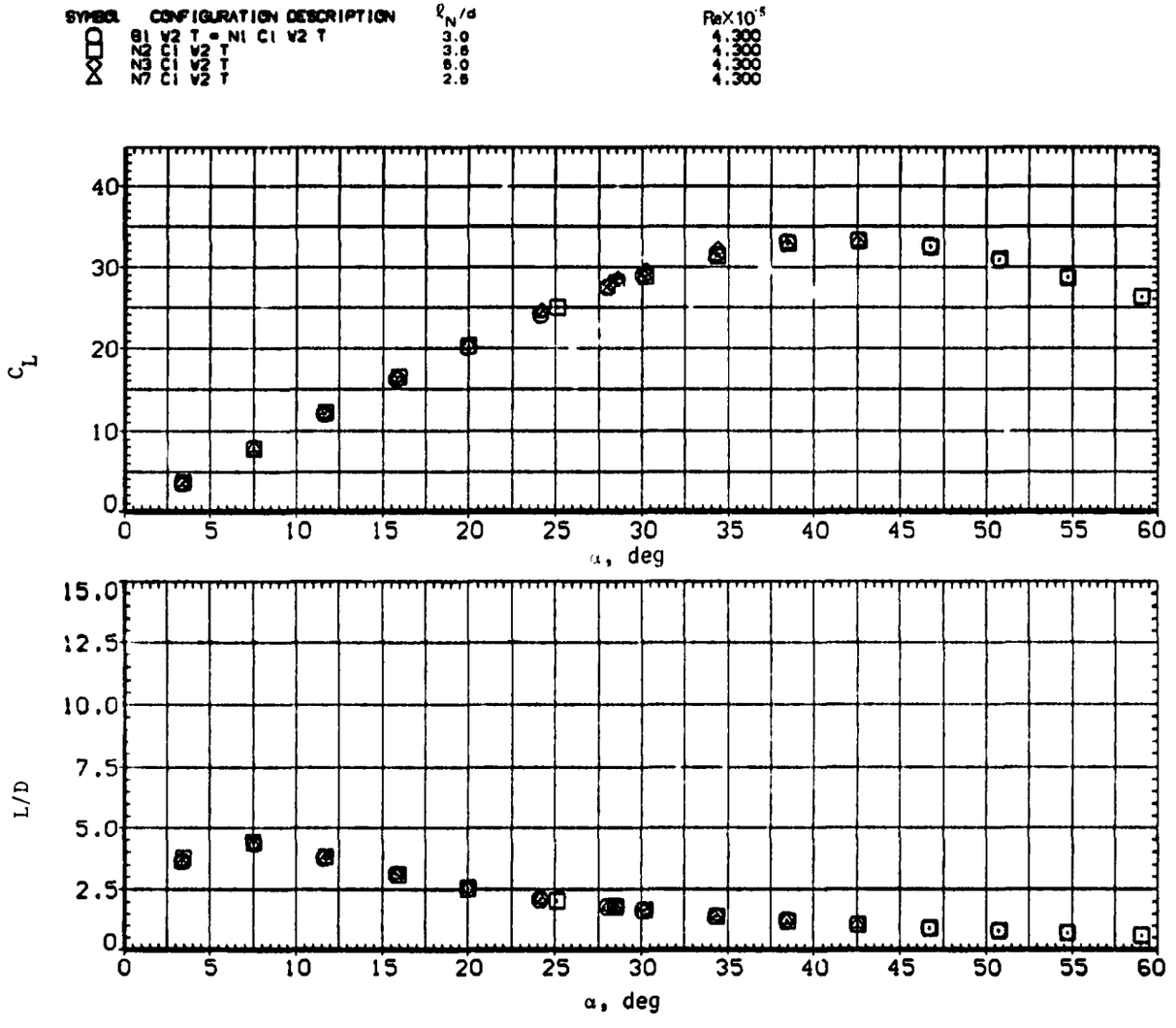

(d) C_L and L/D versus α.

Figure 22.– Concluded.

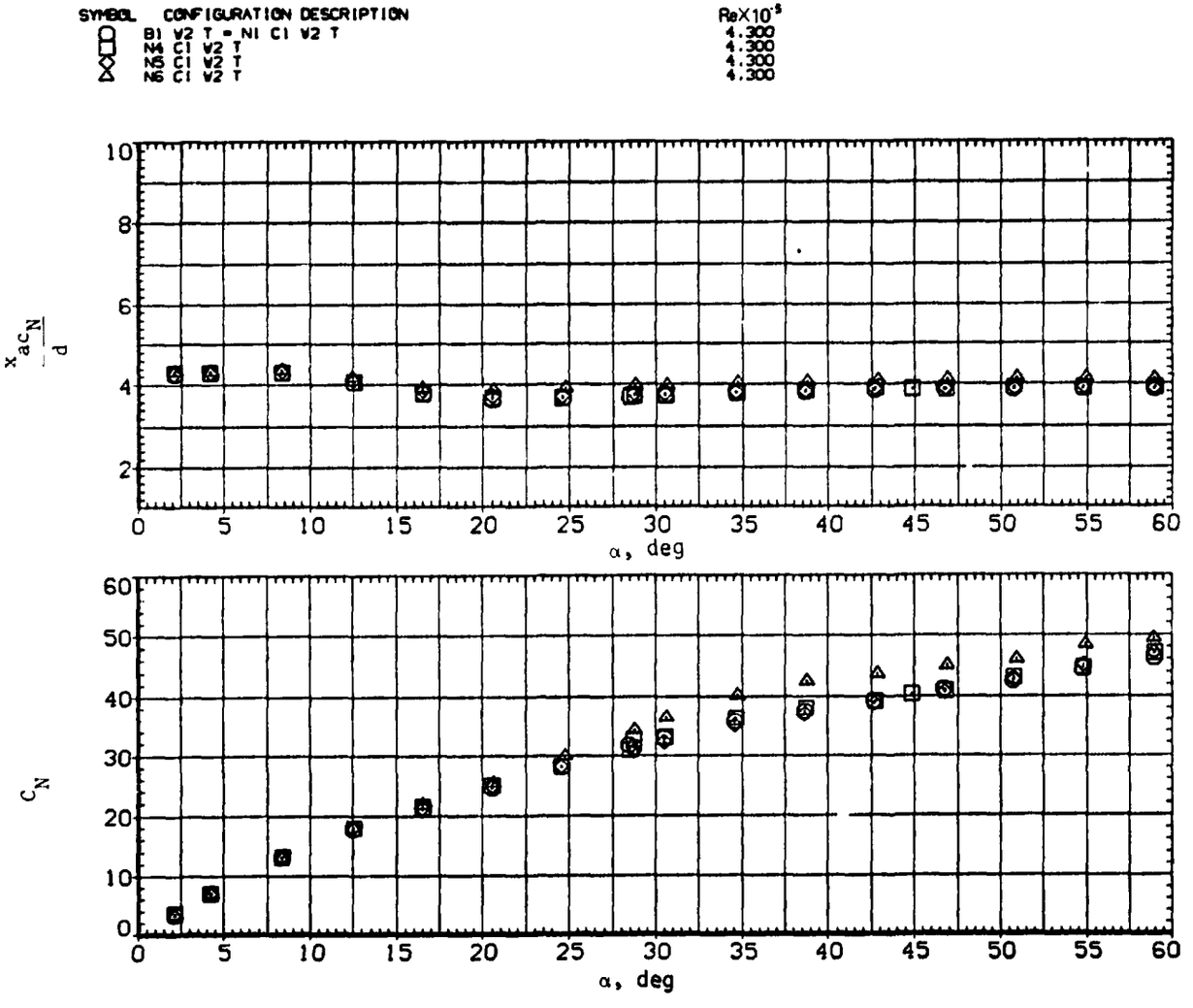

(a) x_{ac_N}/d and C_N versus α.

Figure 23. Effect of nose rounding and strakes on wing-body-tail characteristics, M = 0.6.

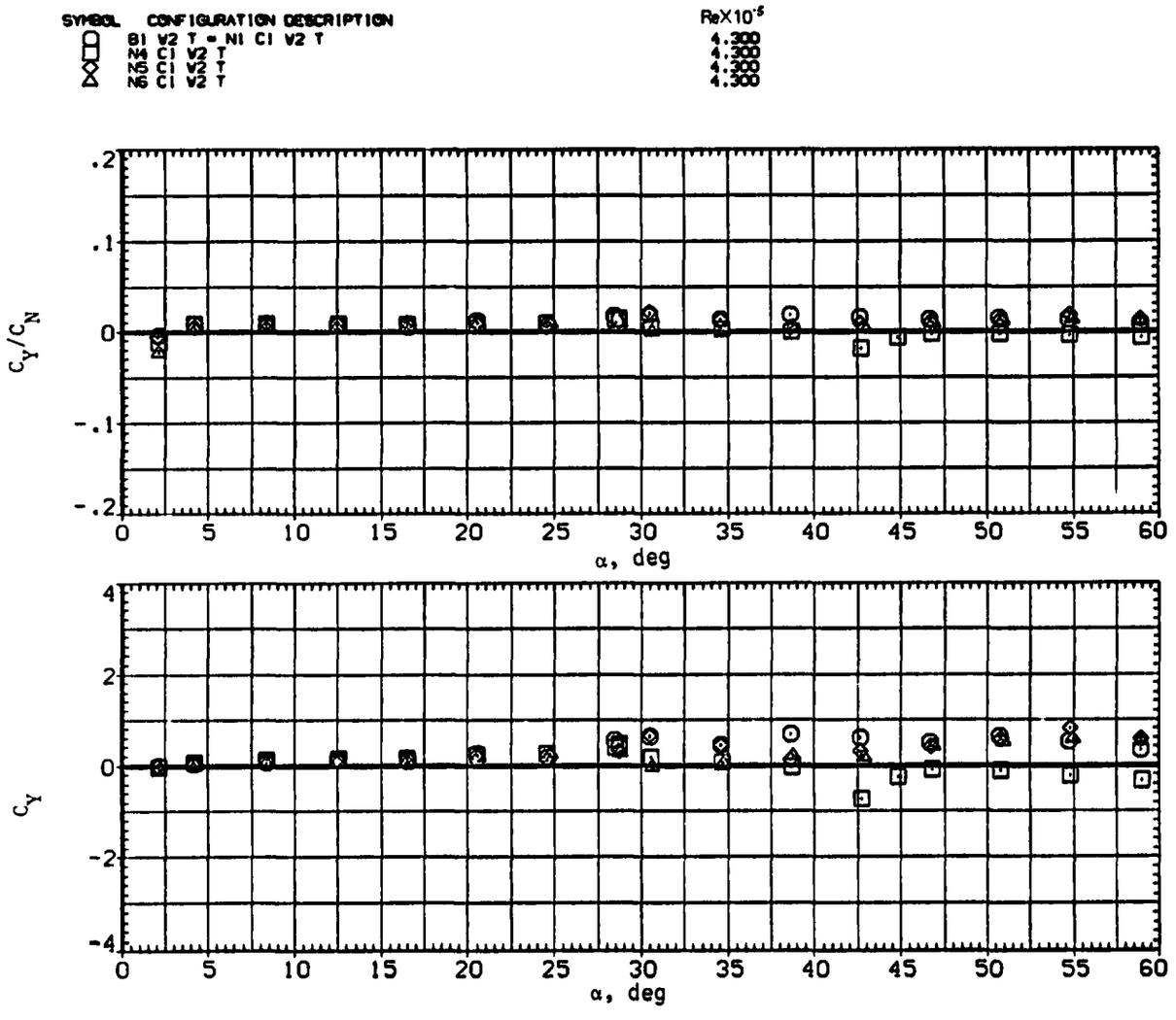

(b) C_Y/C_N and C_Y versus α.

Figure 23.– Continued.

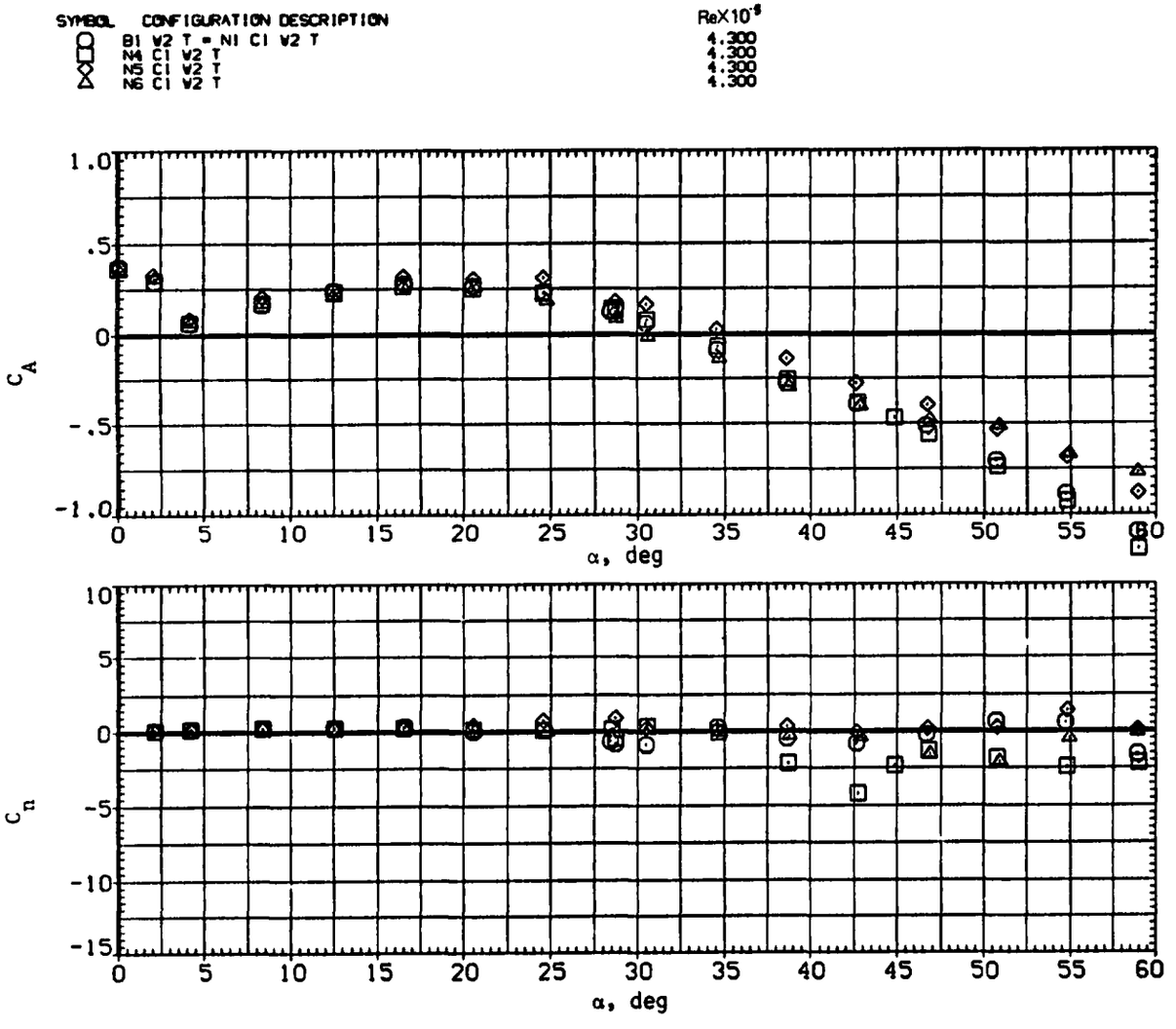

(c) C_A and C_n versus α.

Figure 23.– Continued.

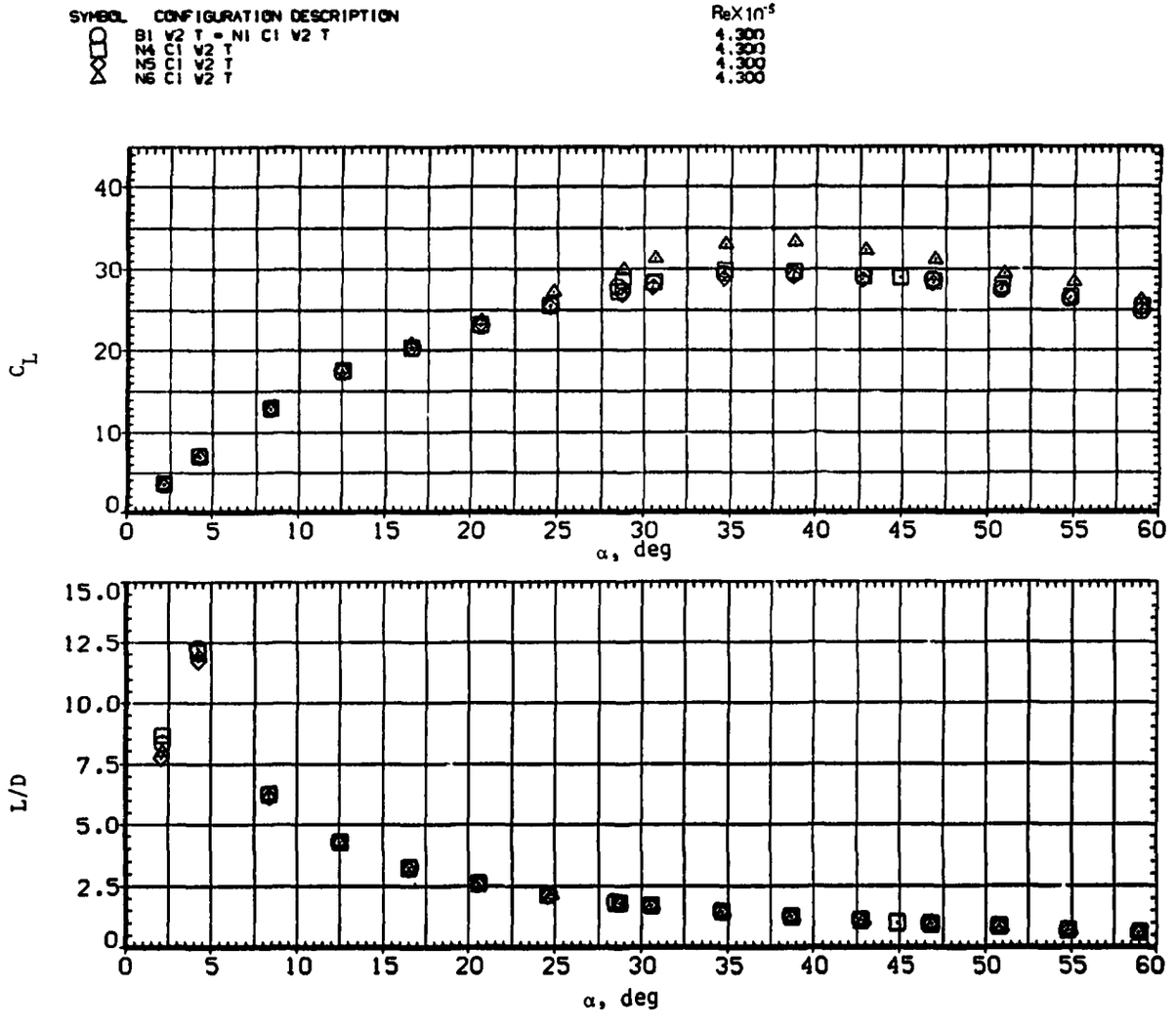

(d) C_L and L/D versus α.

Figure 23.– Concluded.

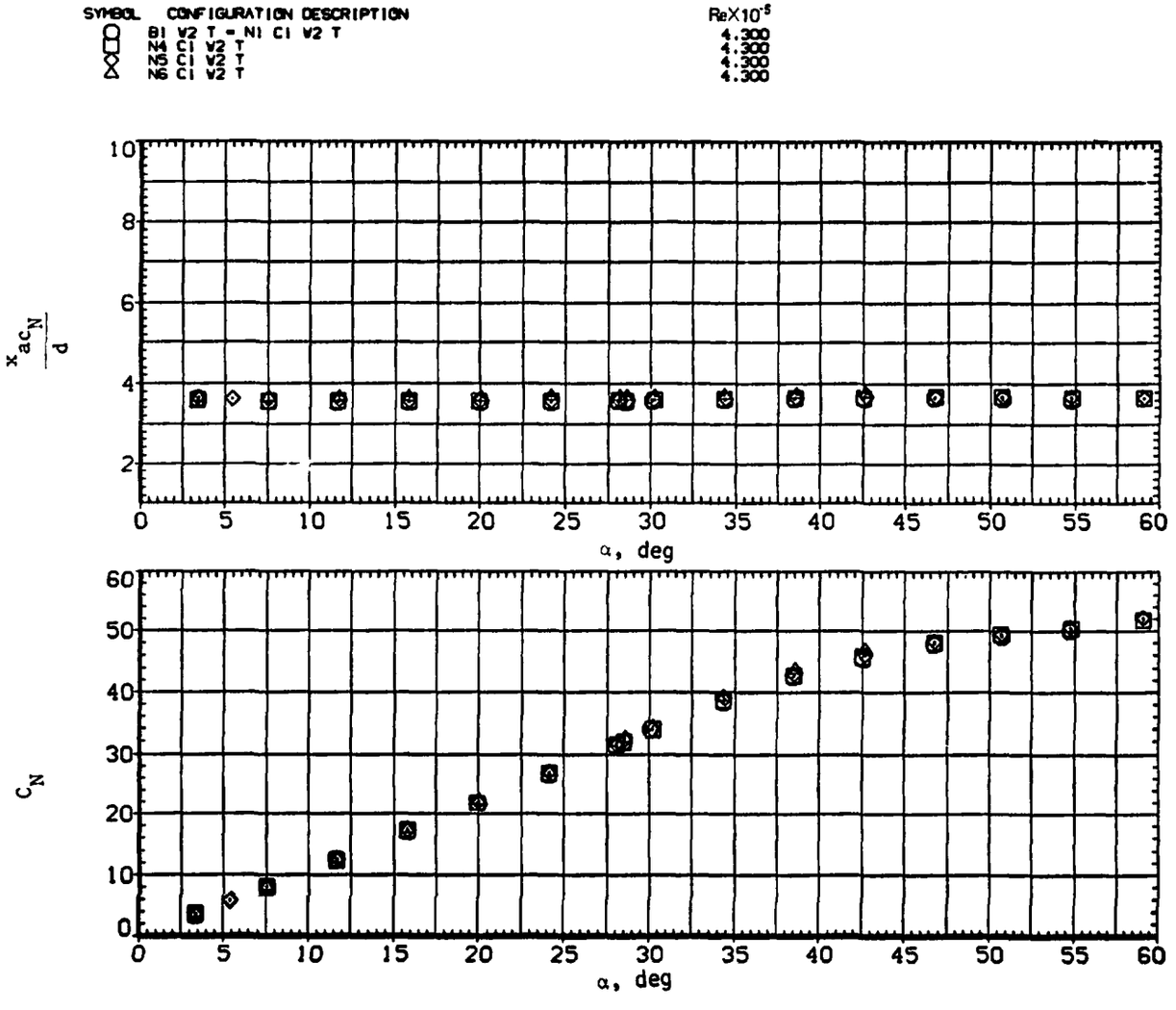

(a) x_{ac_N}/d and C_N versus α.

Figure 24.– Effect of nose rounding and strakes on wing-body-tail characteristics, M = 2.0.

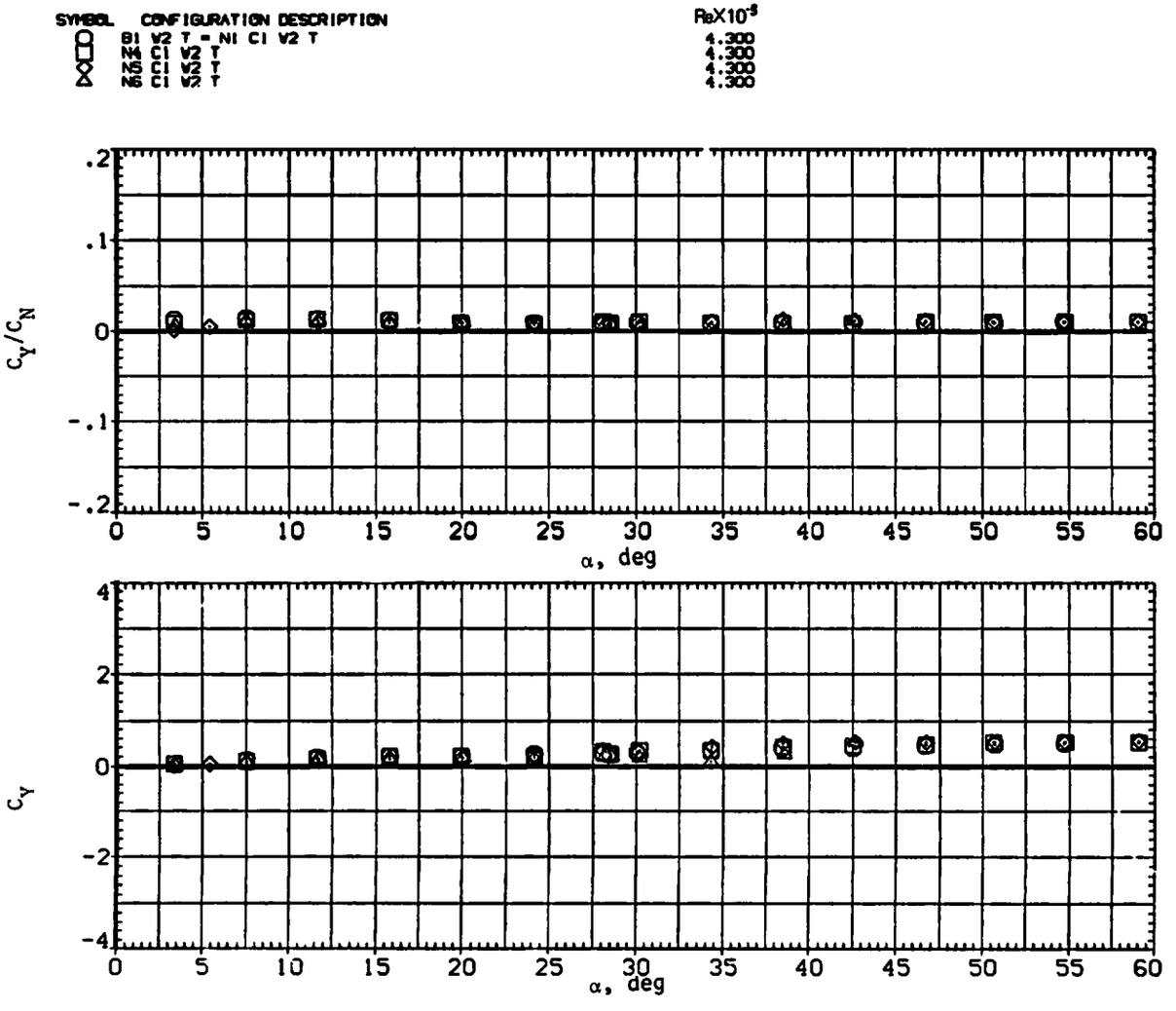

(b) C_Y/C_N and C_Y versus α.

Figure 24.– Continued.

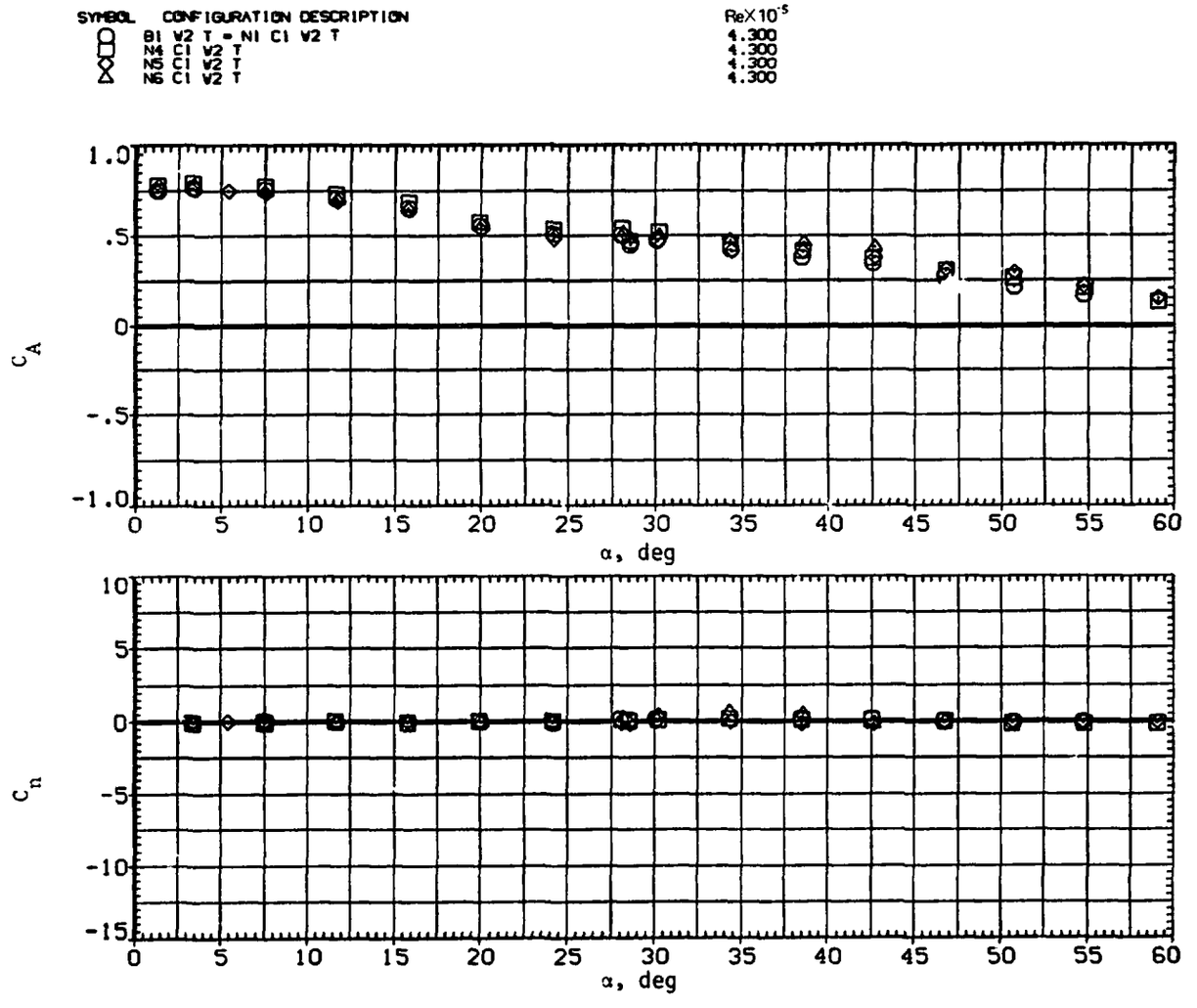

(c) C_A and C_n versus α.

Figure 24.– Continued.

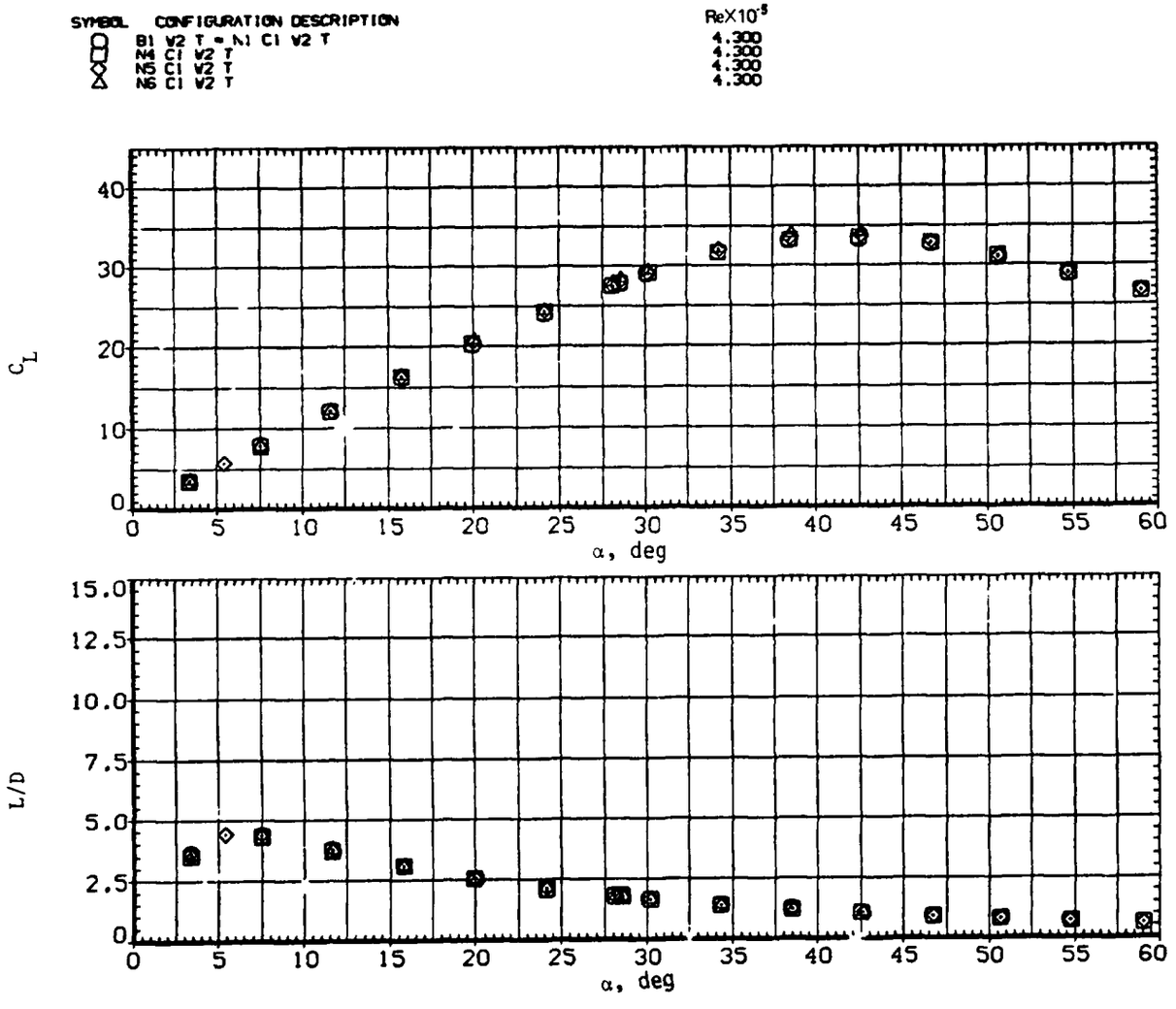

(d) C_L and L/D versus α.

Figure 24.– Concluded.

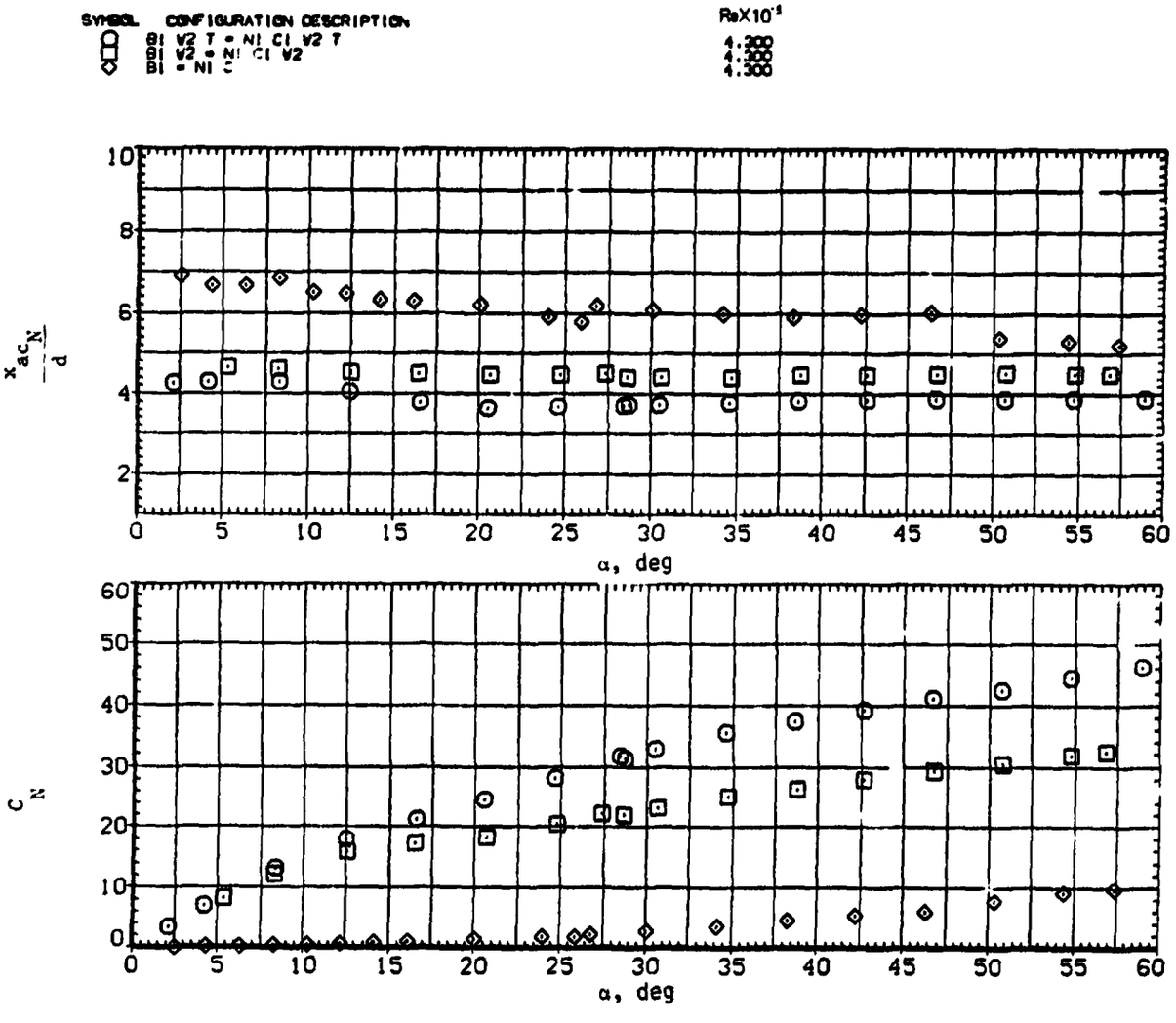

(a) x_{ac_N}/d and C_N versus α.

Figure 25.– Effect of removing tail and wing from a circular body N_1 C_1 ($\ell_N/d = 3$); $M = 0.6$.

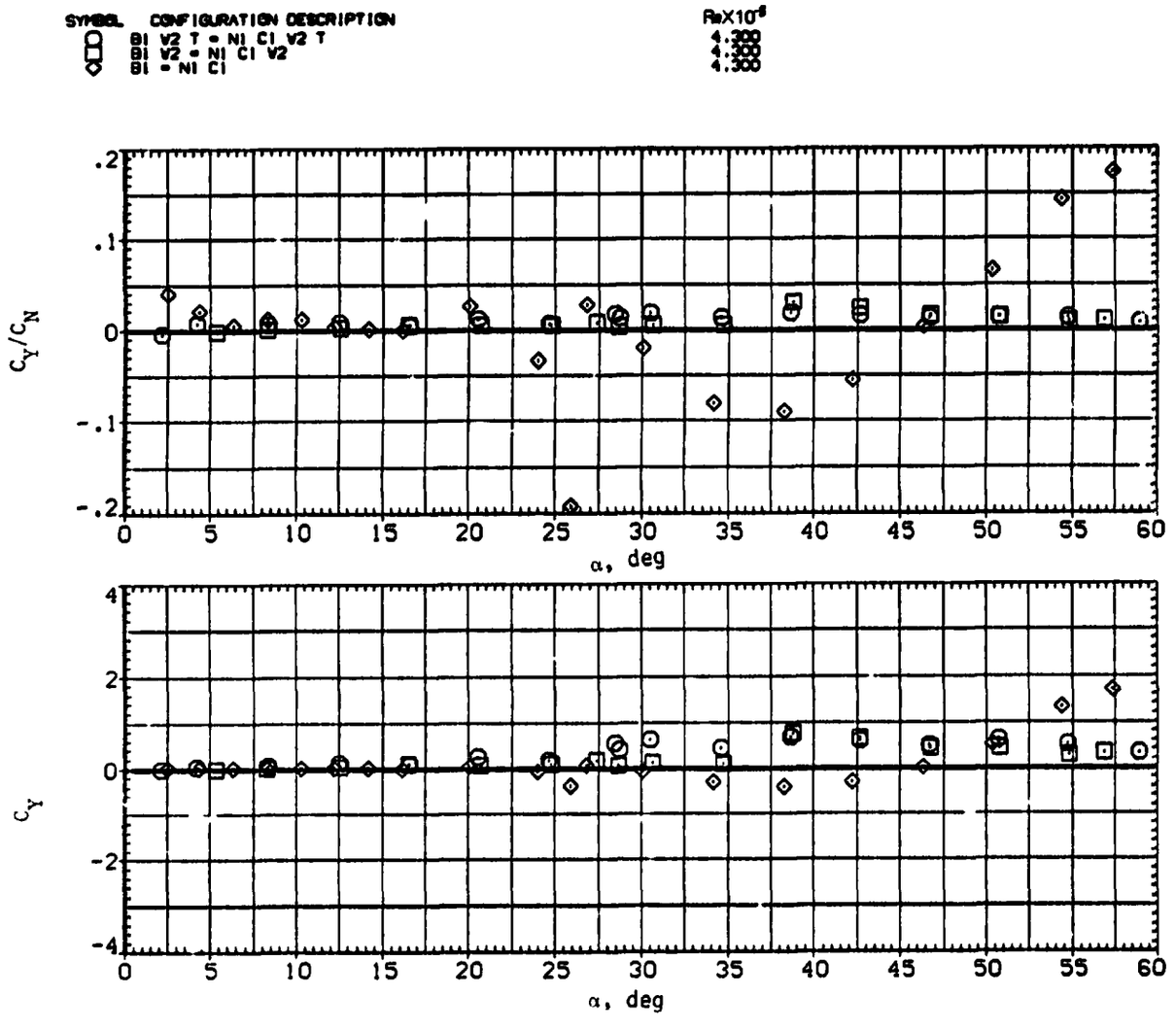

(b) C_Y/C_N and C_Y versus α.

Figure 25.– Continued.

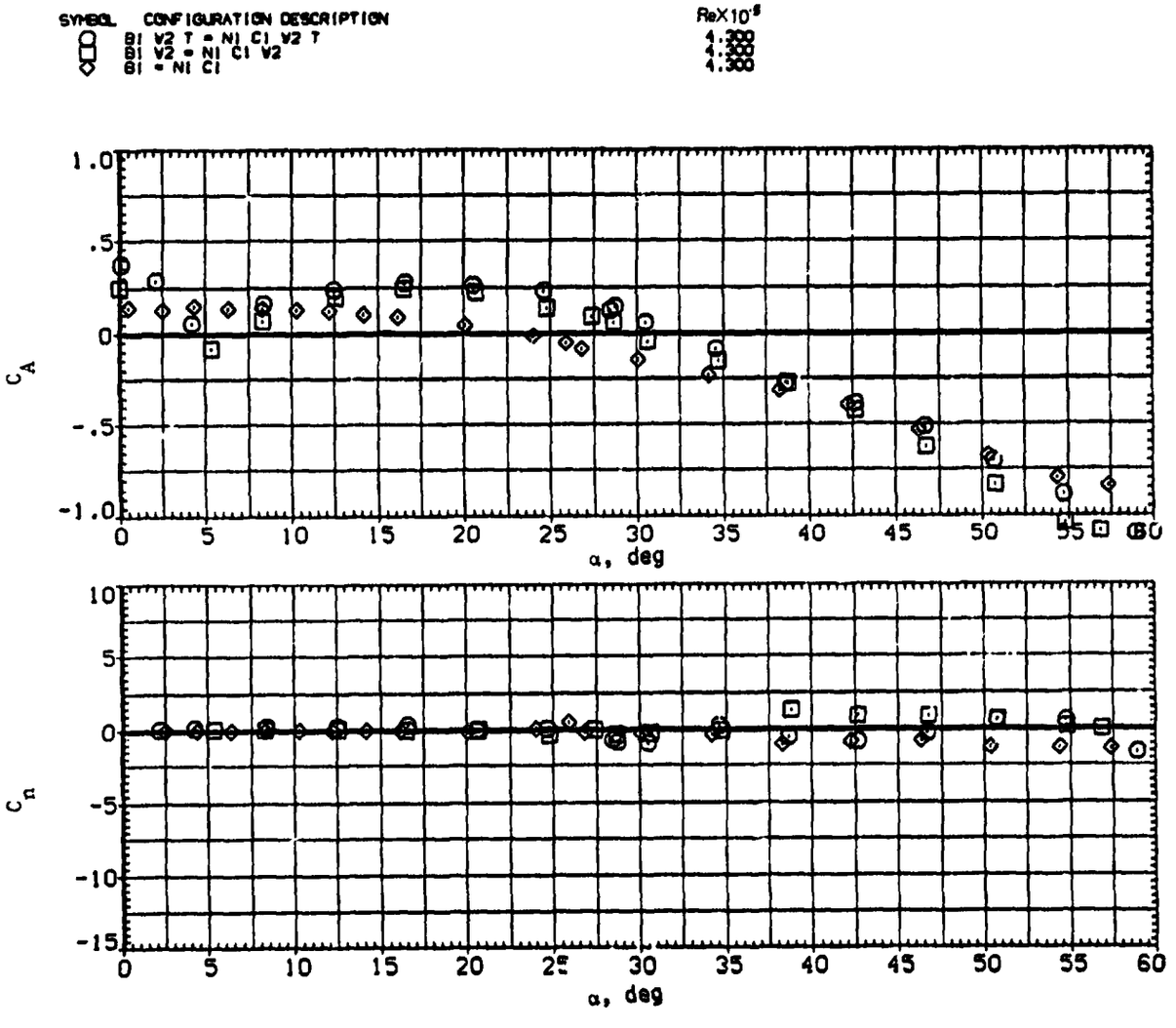

(c) C_A and C_n versus α.

Figure 25.– Continued.

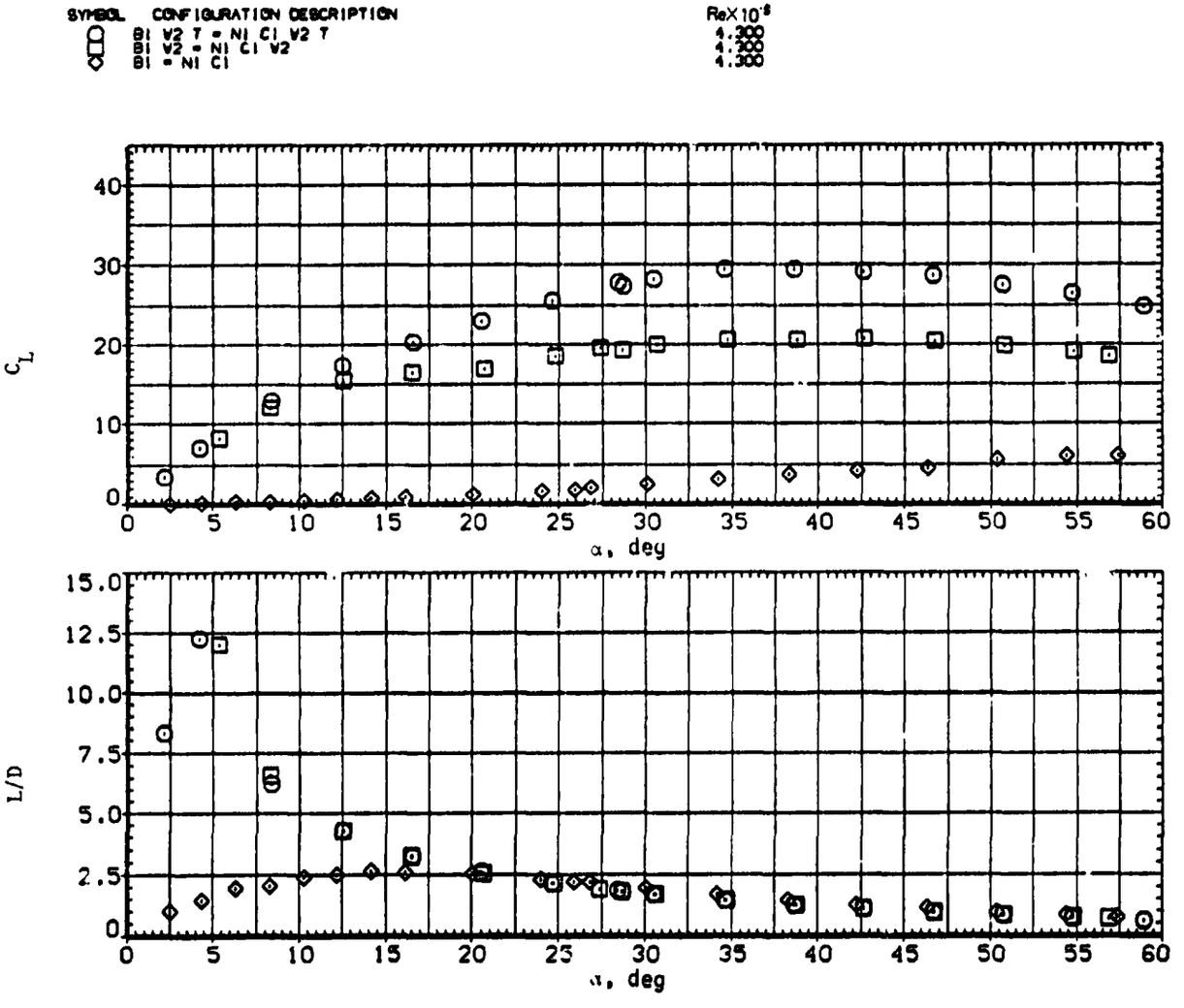

(d) C_L and L/D versus α.

Figure 25.-- Concluded.

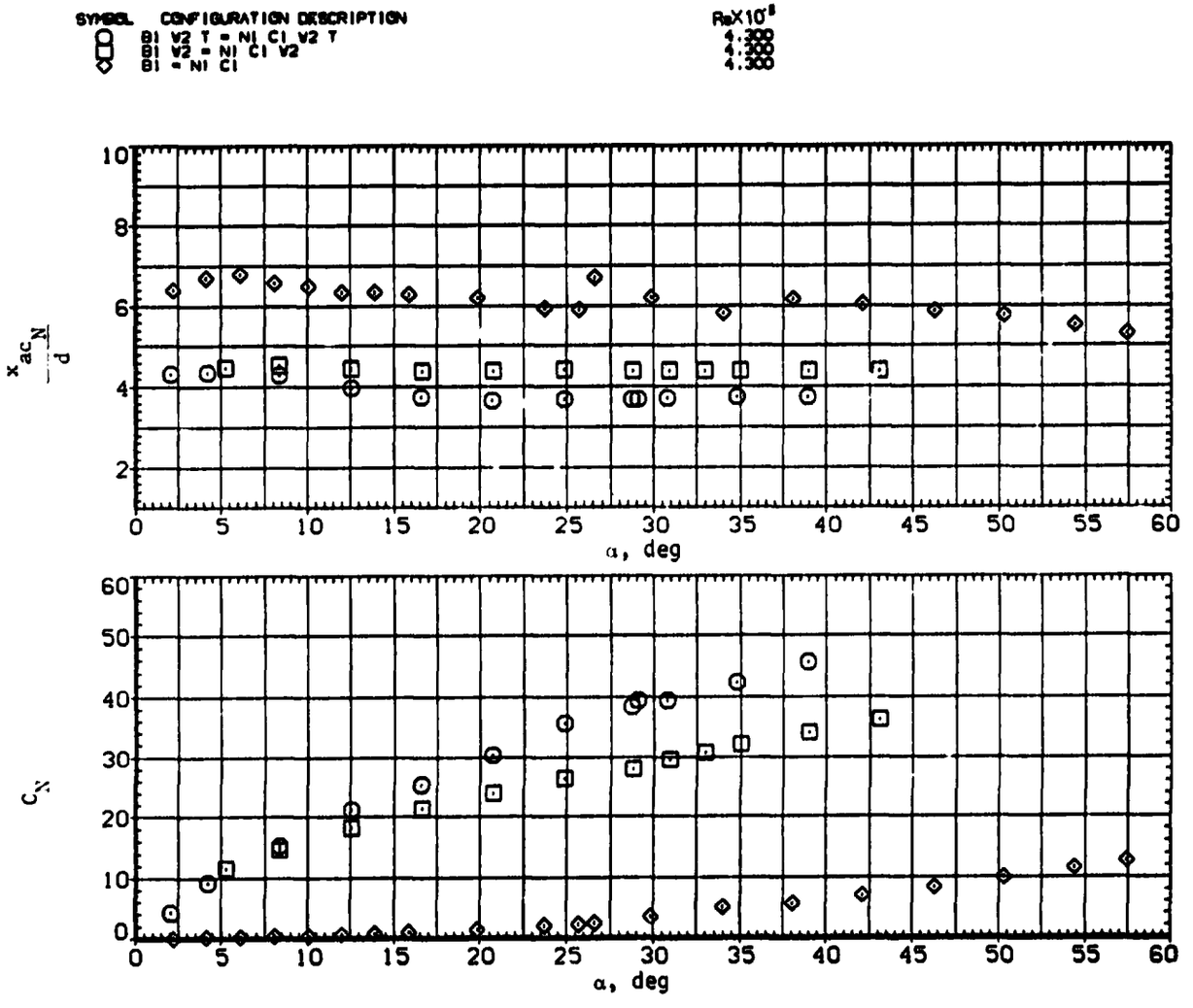

(a) x_{ac_N}/d and C_N versus α.

Figure 26.– Effect of removing tail and wing from a circular body N_1 C_1 ($\ell_N/d = 3$); $M = 0.9$.

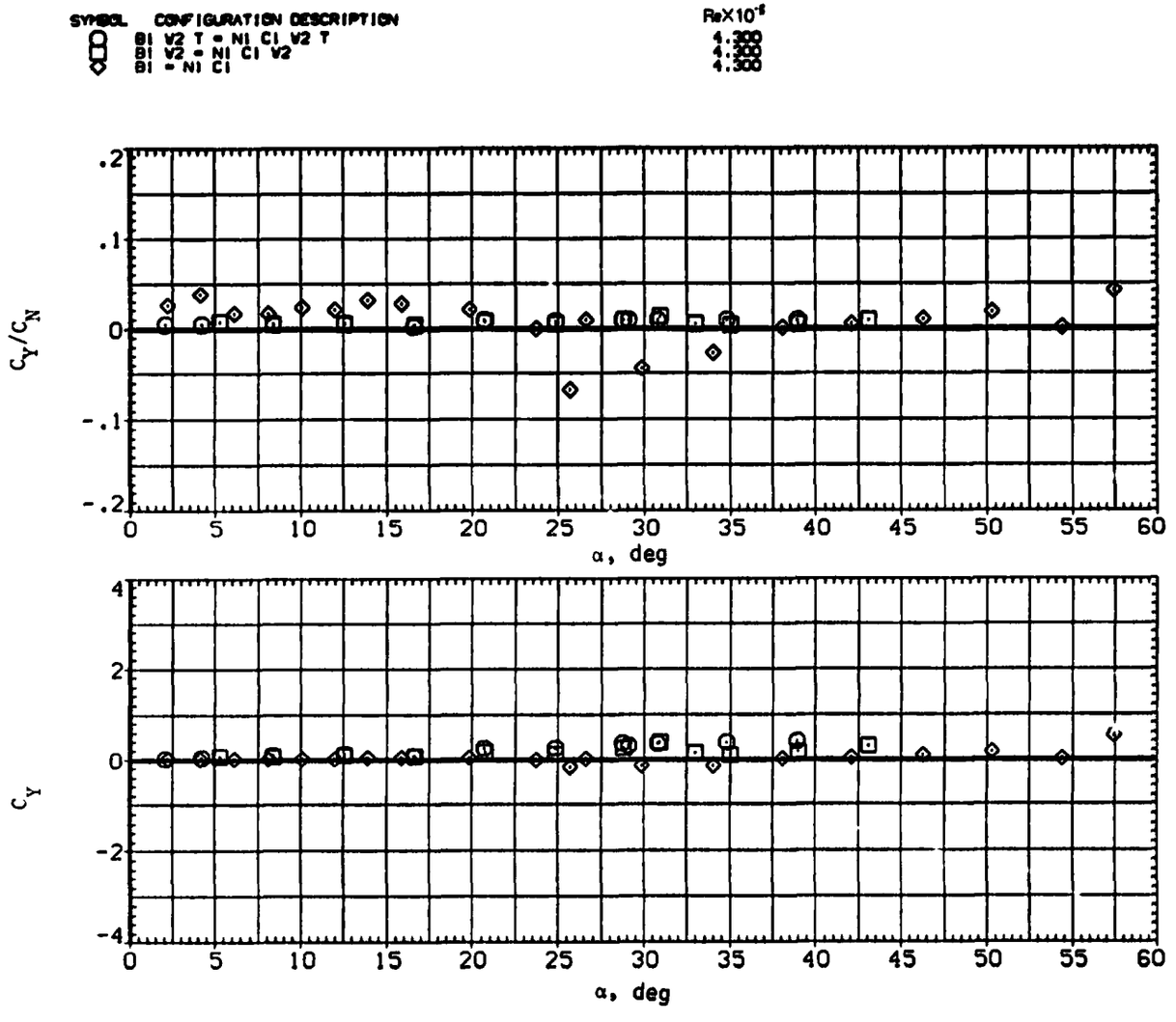

(b) C_Y/C_N and C_Y versus α.

Figure 26.– Continued.

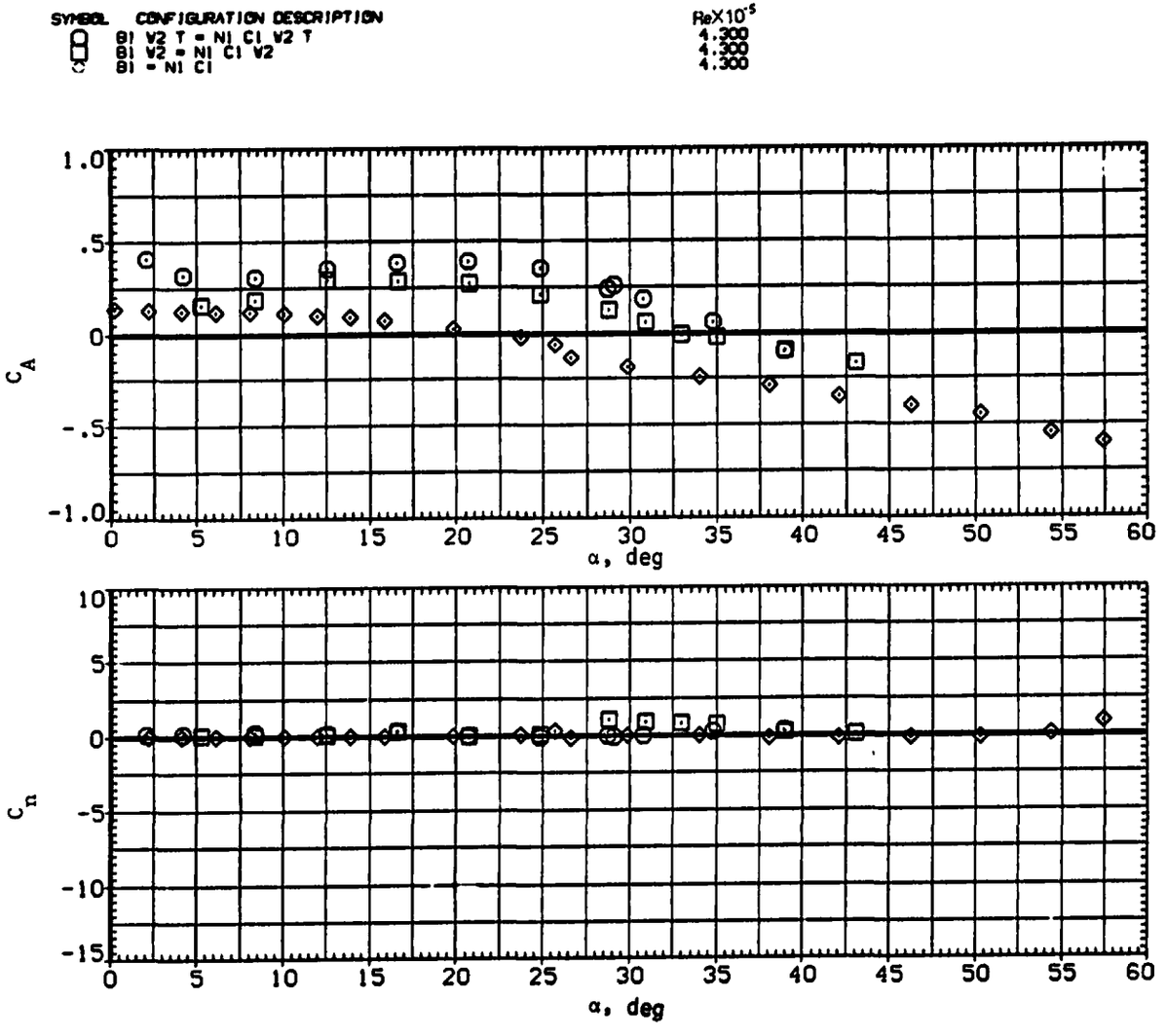

(c) C_A and C_n versus α.

Figure 26.– Continued.

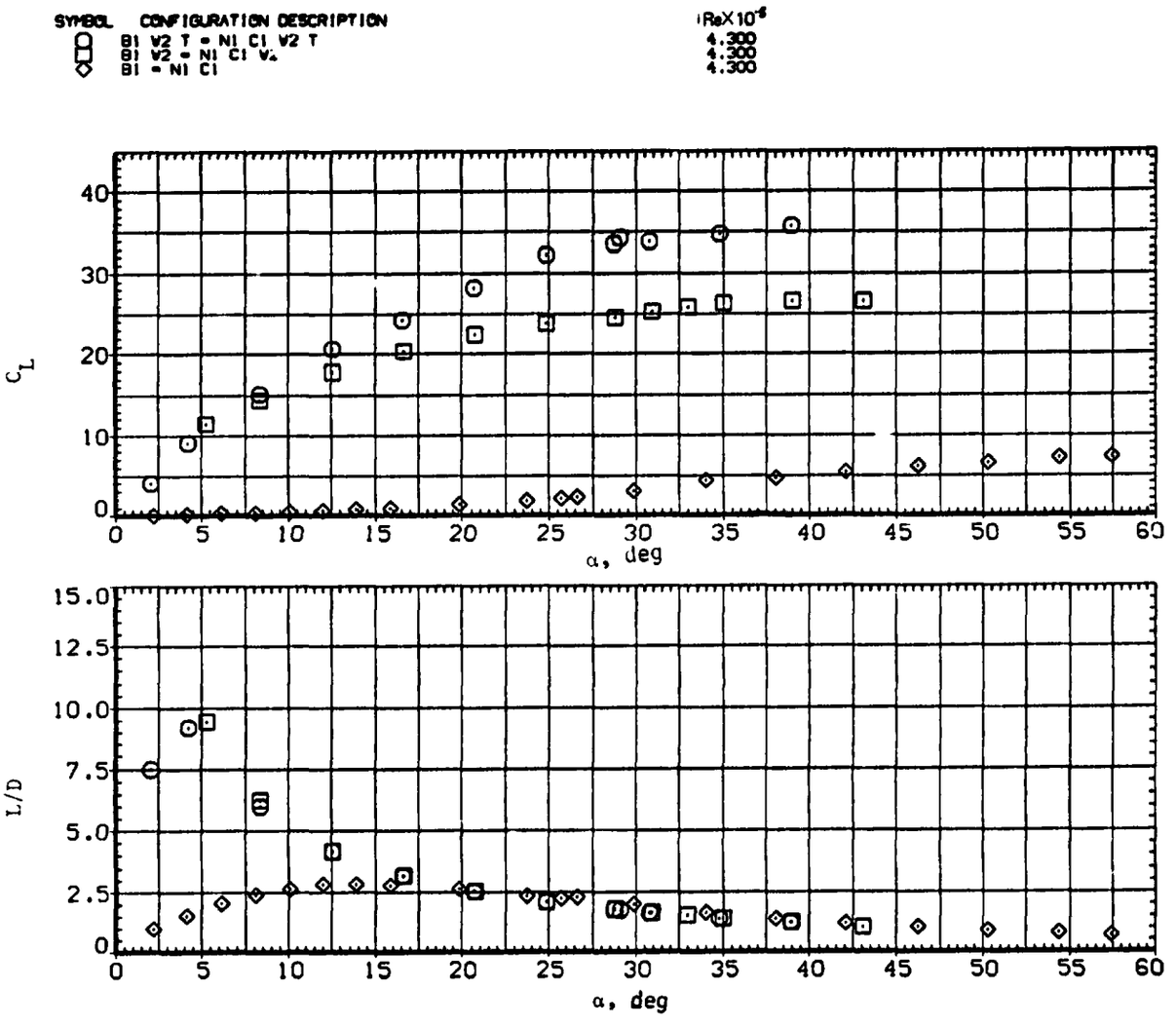

(d) C_L and L/D versus α.

Figure 26.– Concluded.

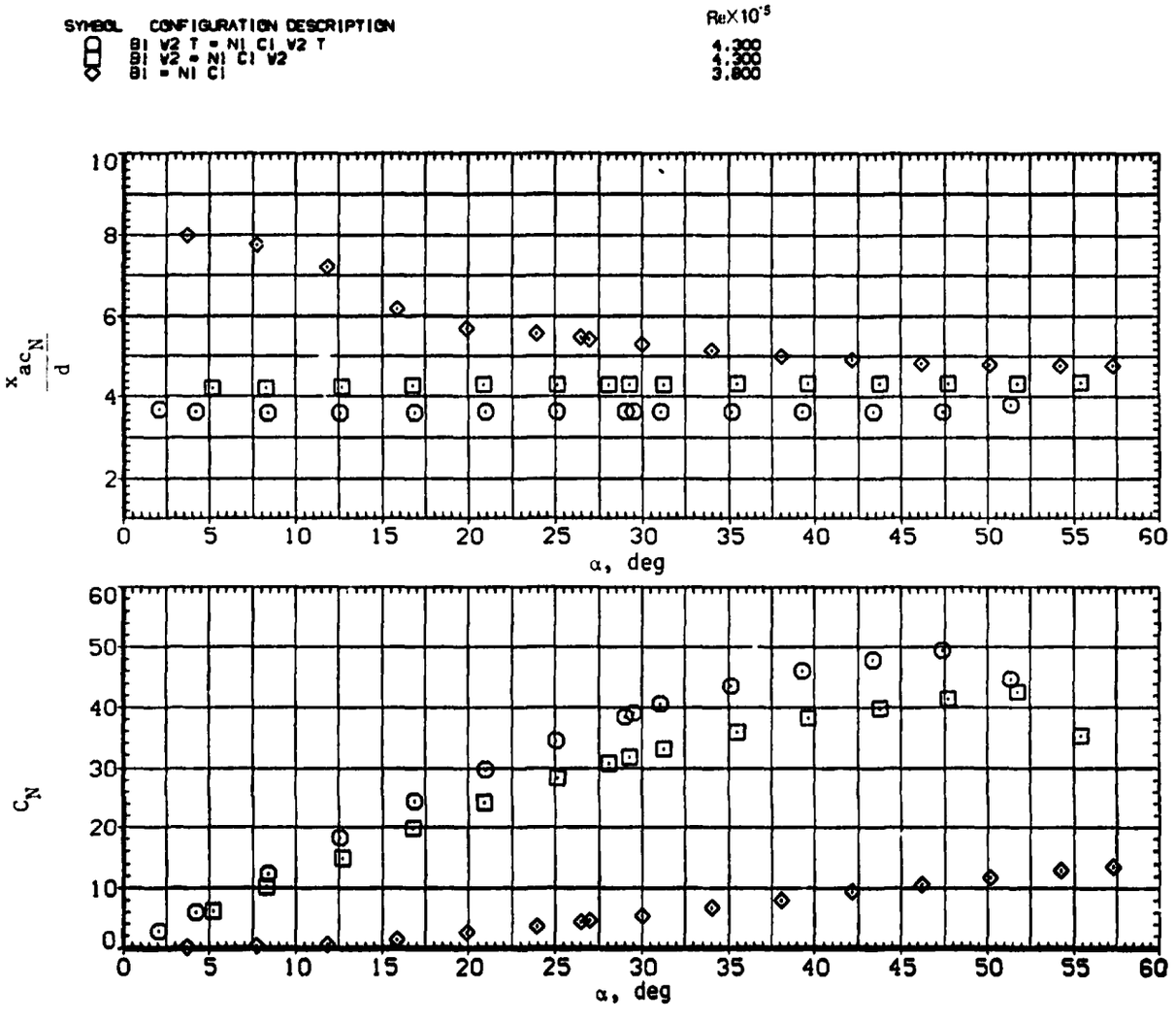

(a) x_{ac_N}/d and C_N versus α.

Figure 27.– Effect of removing tail and wing from a circular body N_1 C_1 ($\ell_N/d = 3$); M = 1.5.

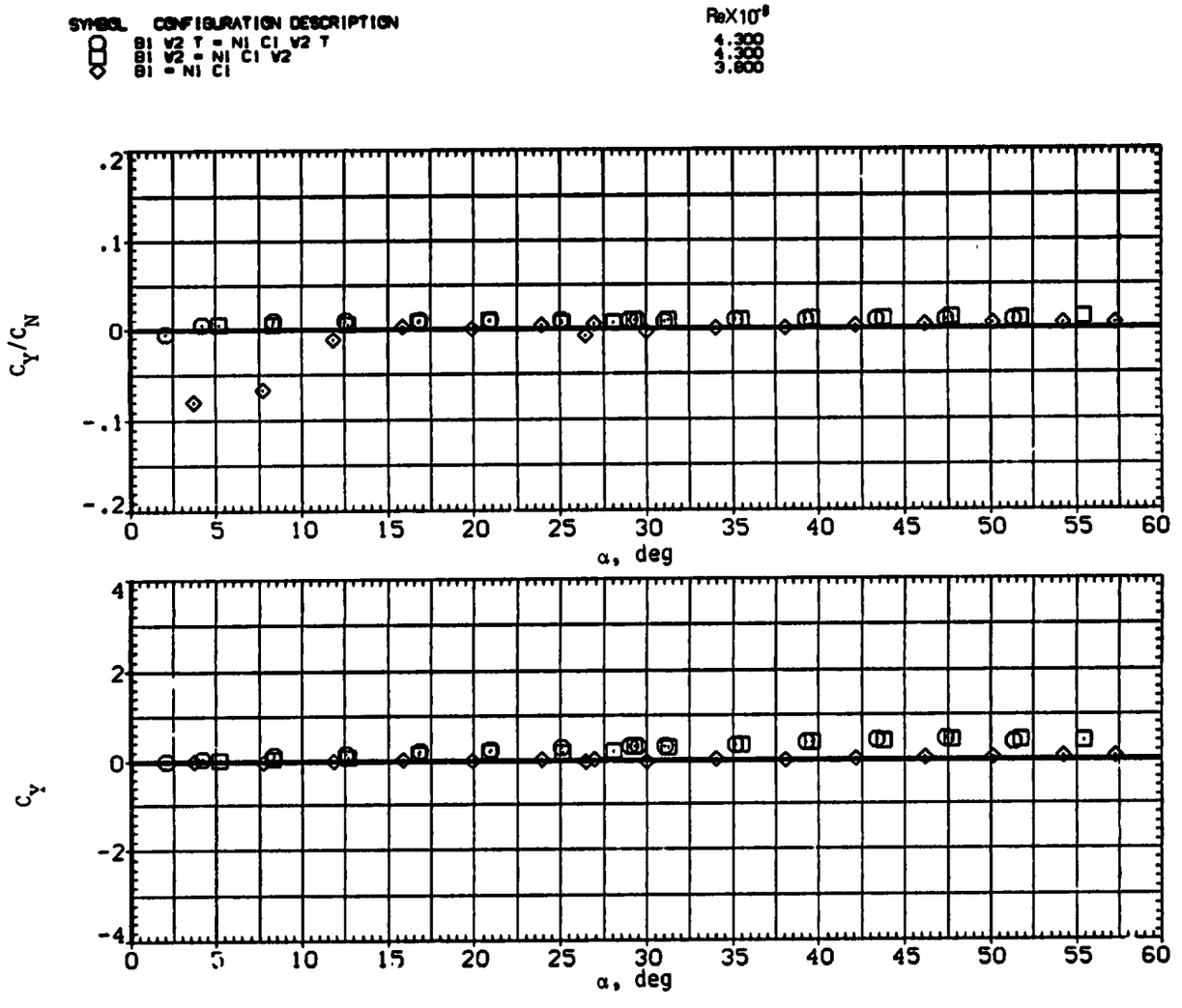

(b) C_Y/C_N and C_Y versus α.

Figure 27.– Continued.

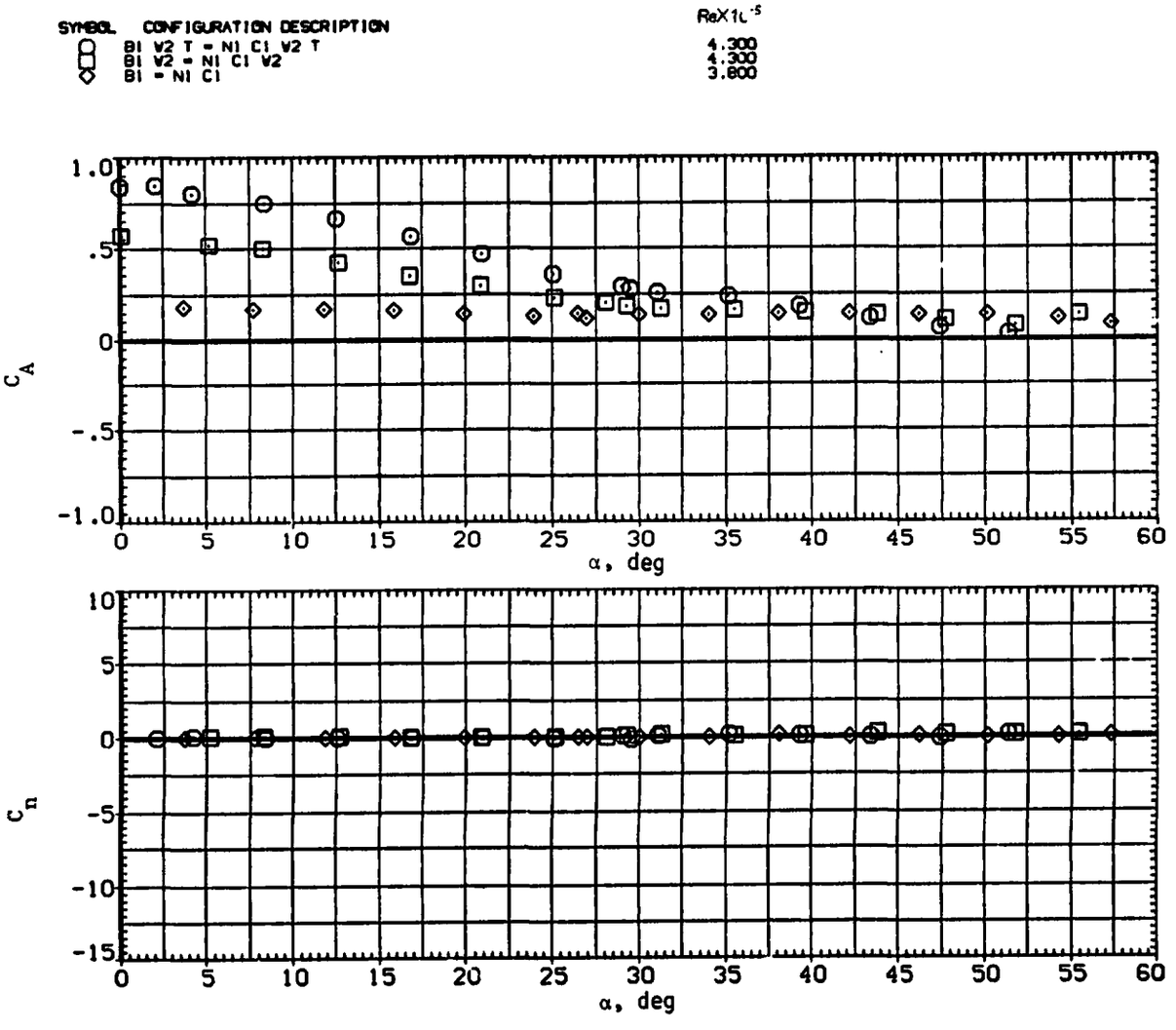

(c) C_A and C_n versus α.

Figure 27.– Continued.

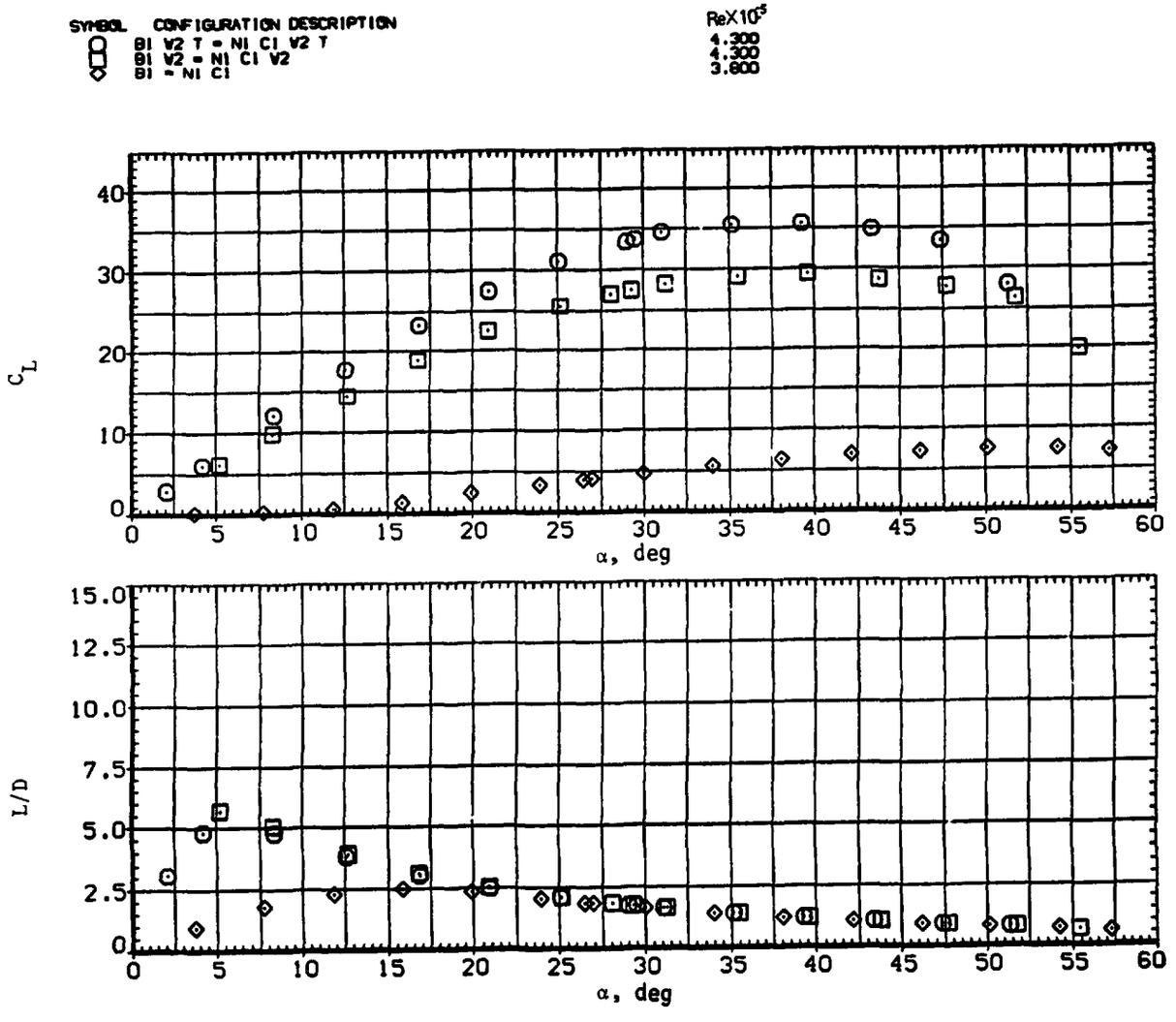

(d) C_L and L/D versus α.

Figure 27.– Concluded.

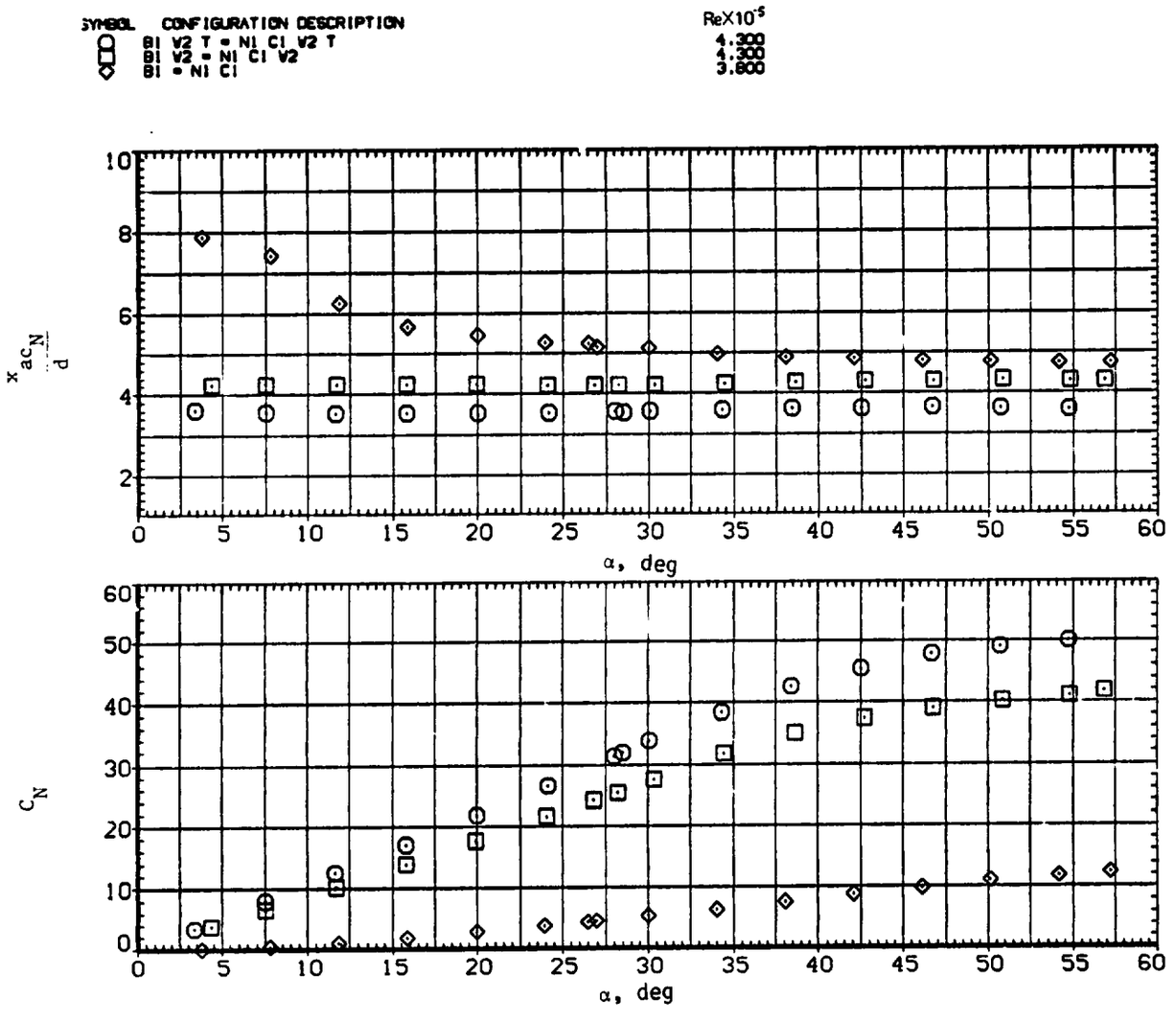

(a) x_{ac_N}/d and C_N versus α.

Figure 28.– Effect of removing tail and wing from a circular body N_1 C_1 ($\ell_N/d = 3$); M = 2.0.

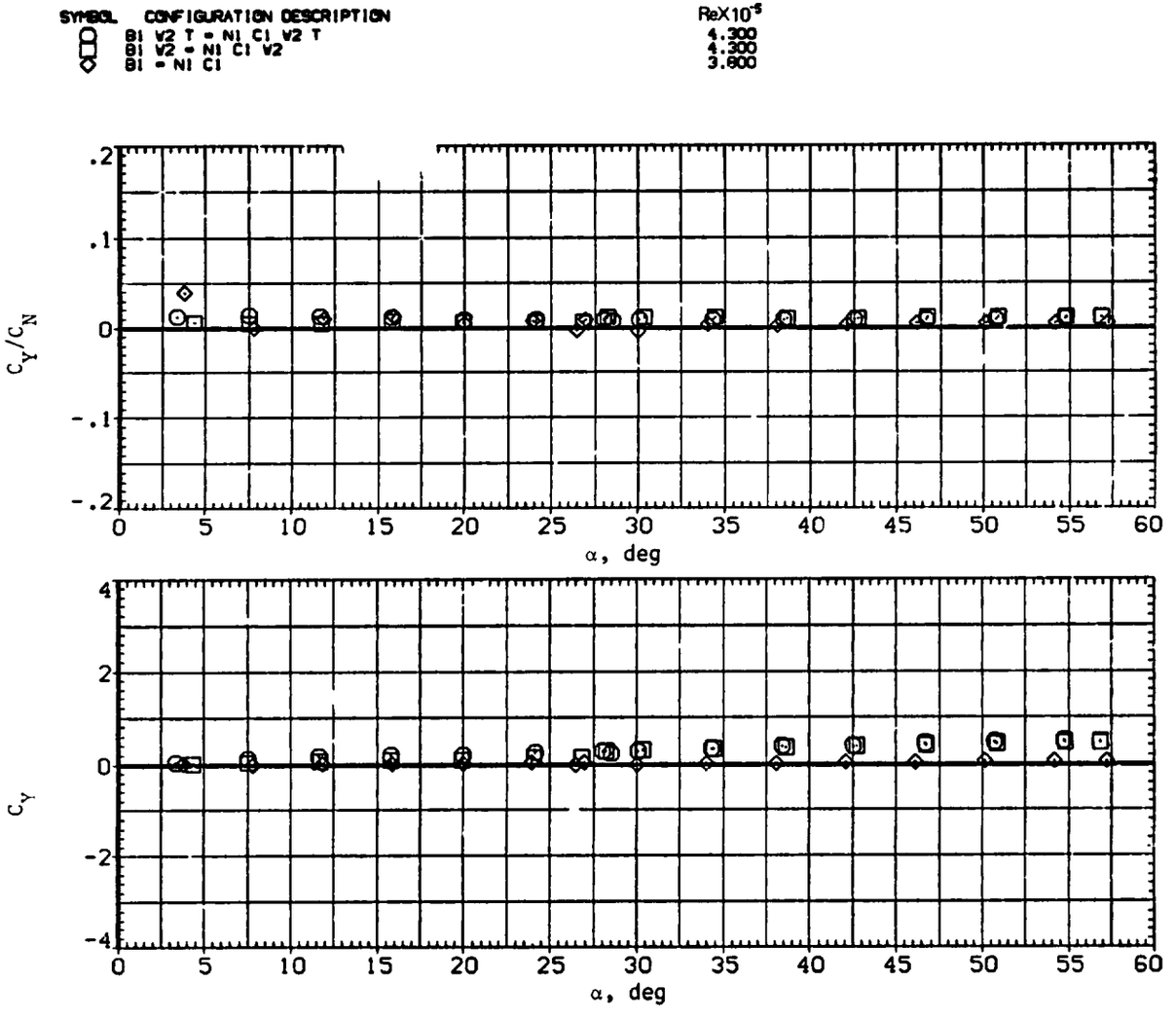

(b) C_Y/C_N and C_Y versus α.

Figure 28.– Continued.

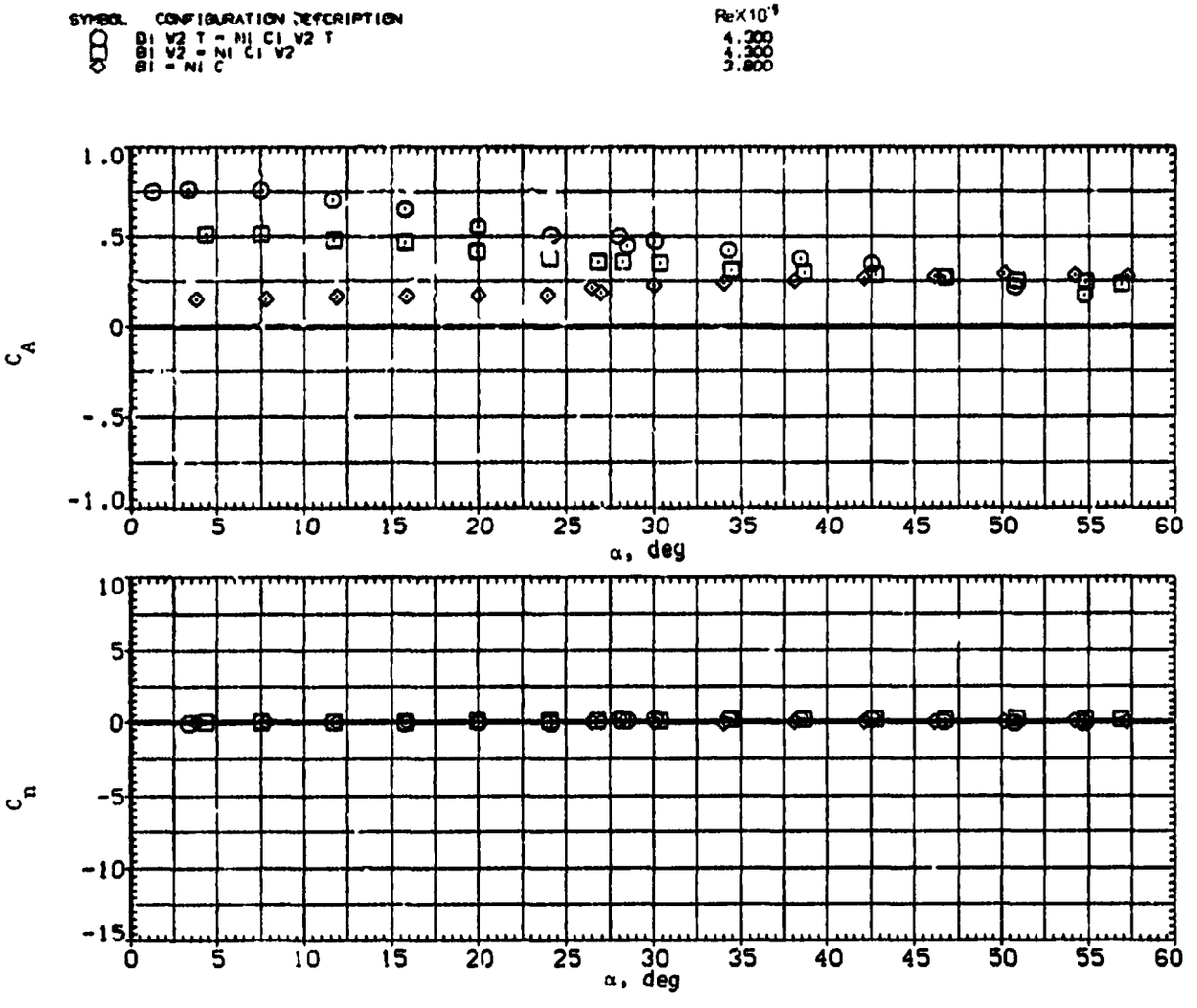

(c) C_A and C_n versus α.

Figure 28.– Continued.

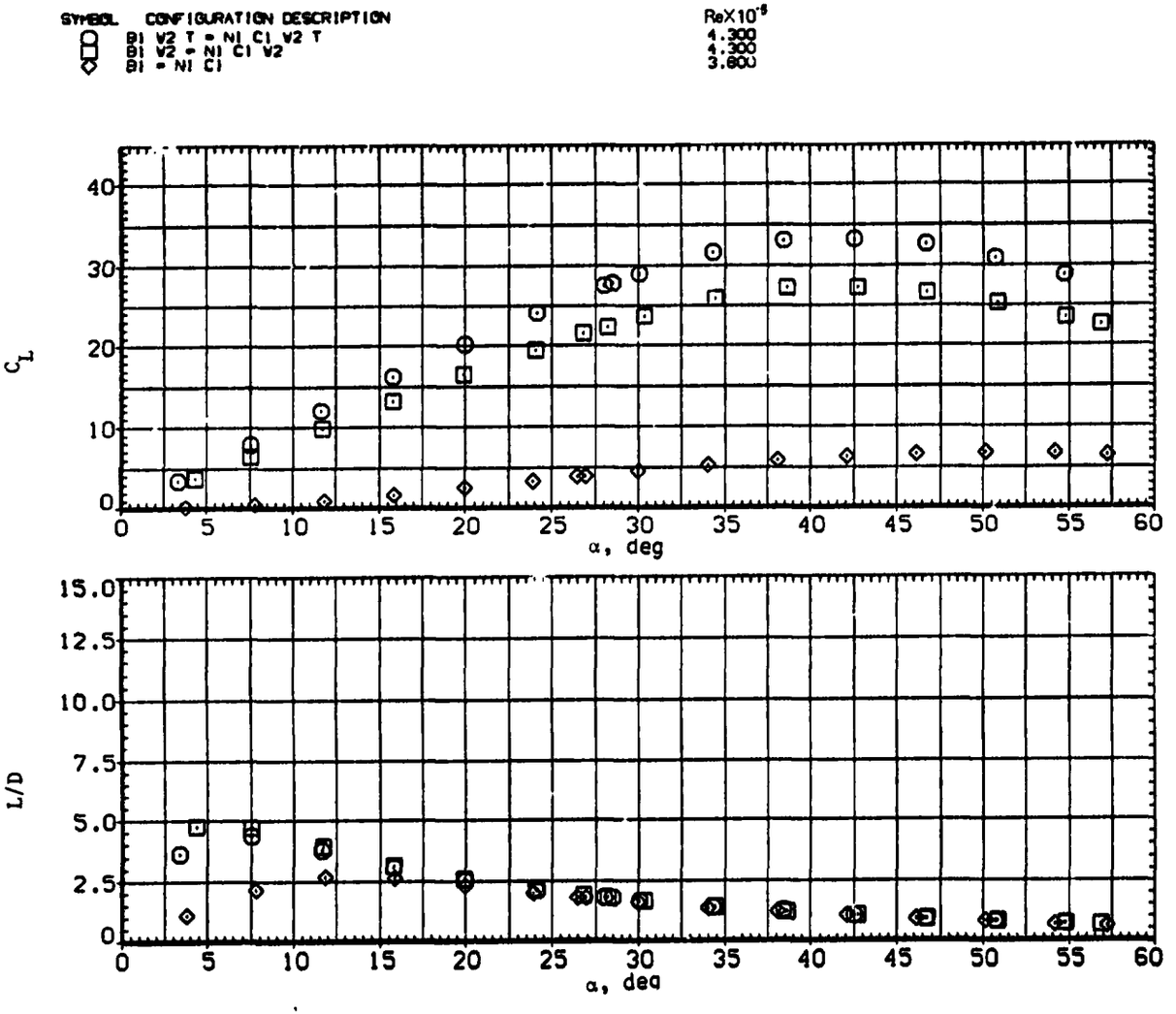

(d) C_L and L/D versus α.

Figure 28.– Concluded.

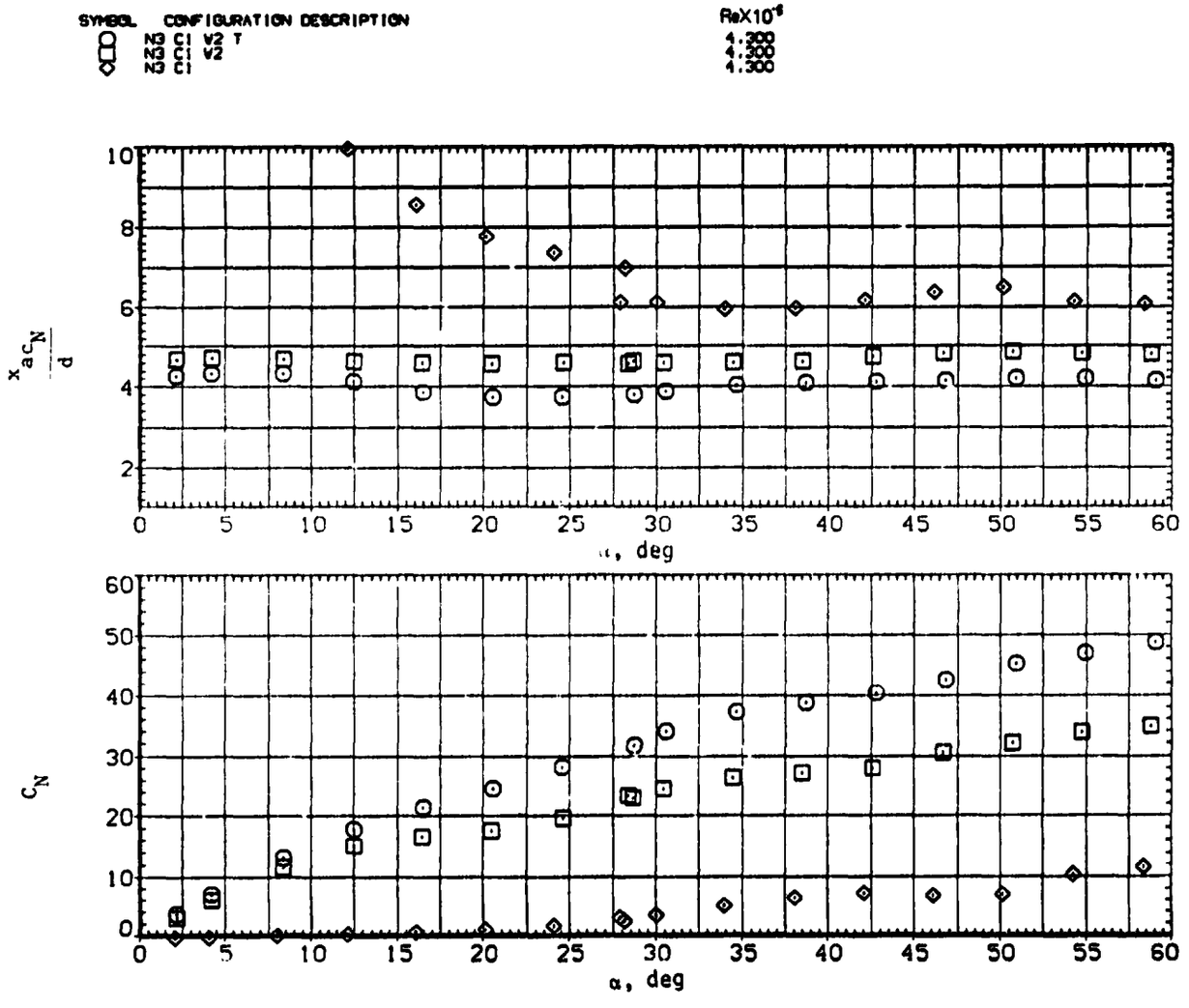

(a) x_{ac_N}/d and C_N versus α.

Figure 29.– Effect of removing tail and wing from a circular body N_3 C_1 ($\ell_N/d = 5$); M = 0.6.

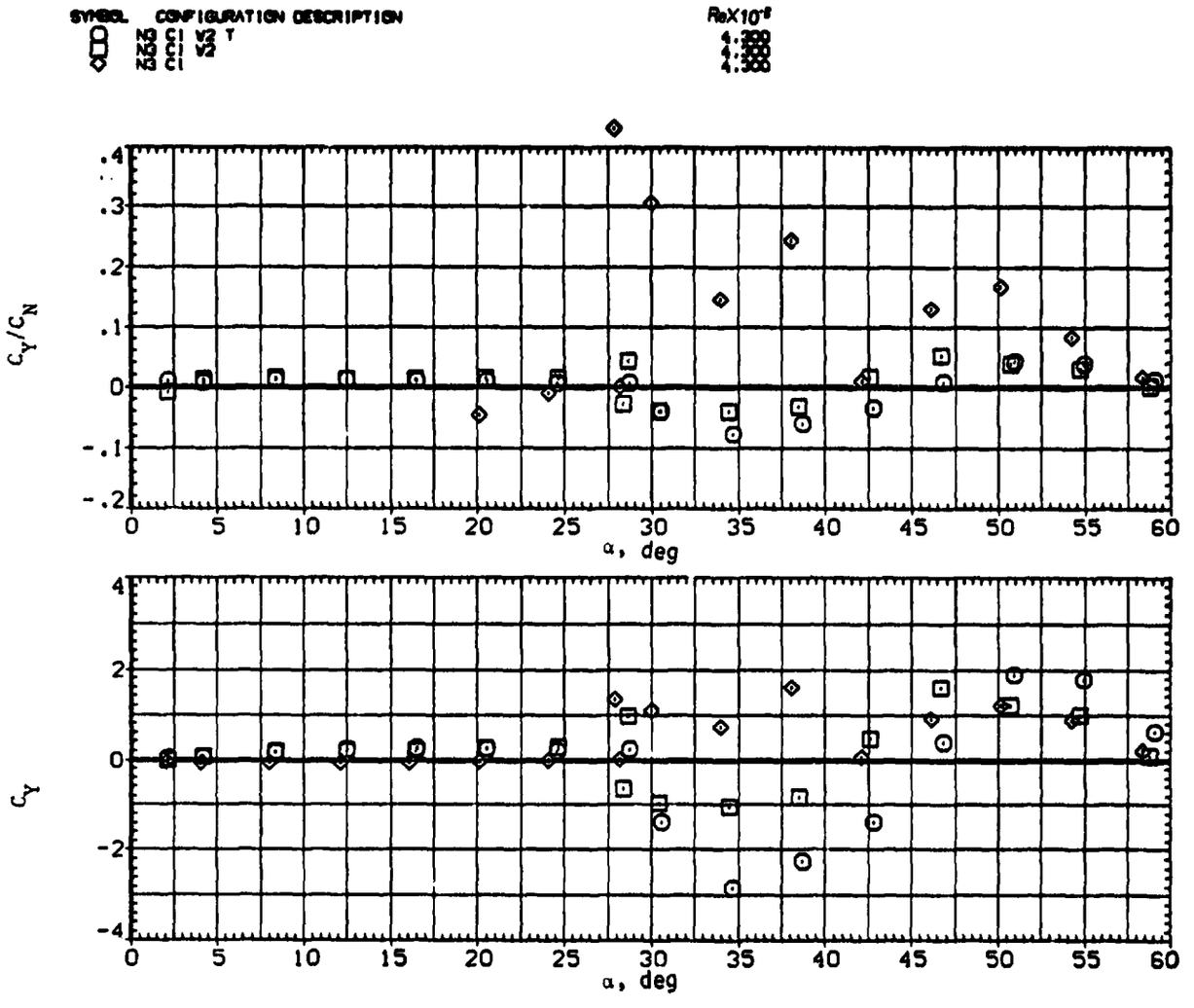

(b) C_Y/C_N and C_Y versus α.

Figure 29.– Continued.

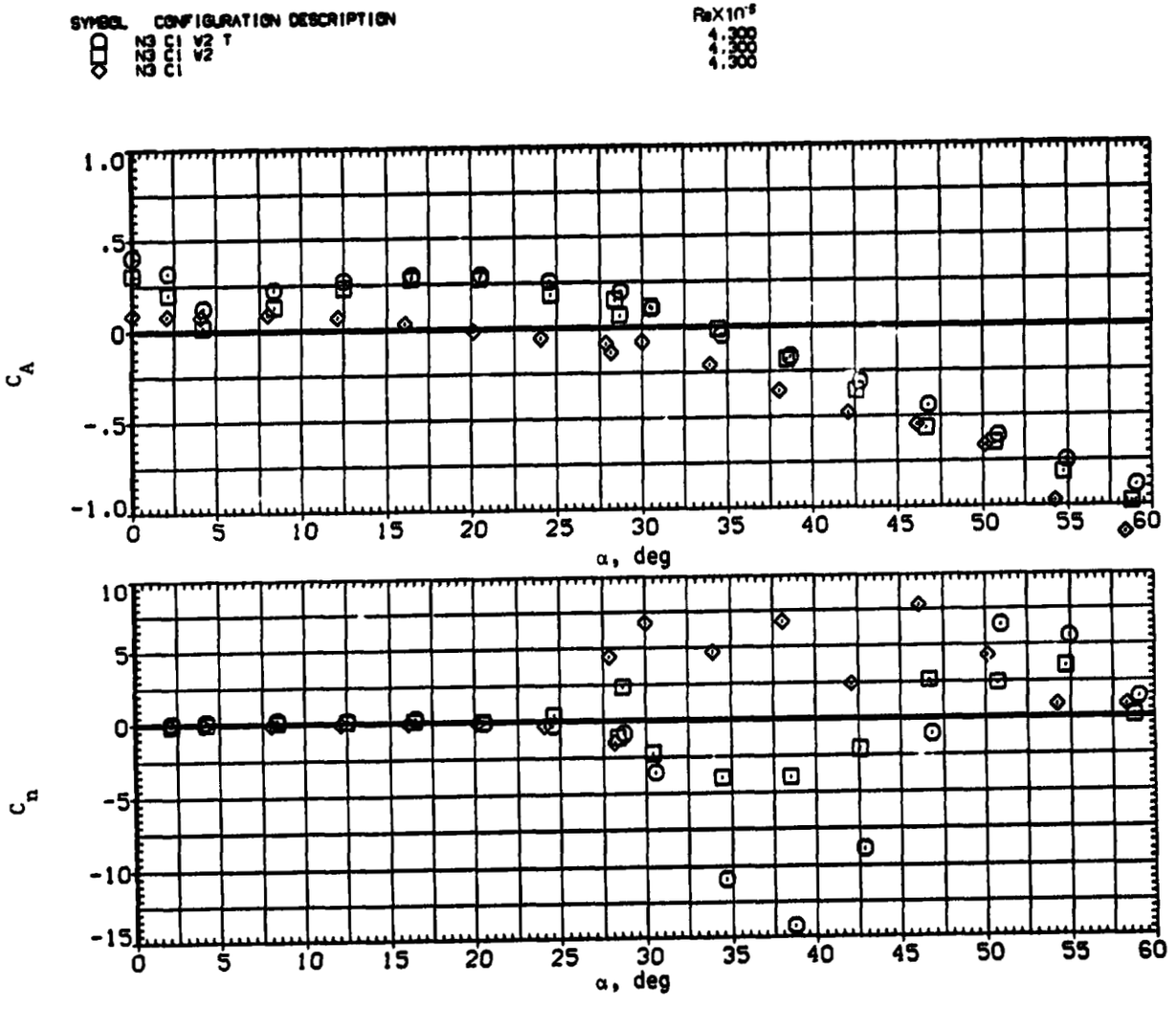

(c) C_A and C_n versus α.

Figure 29.– Continued.

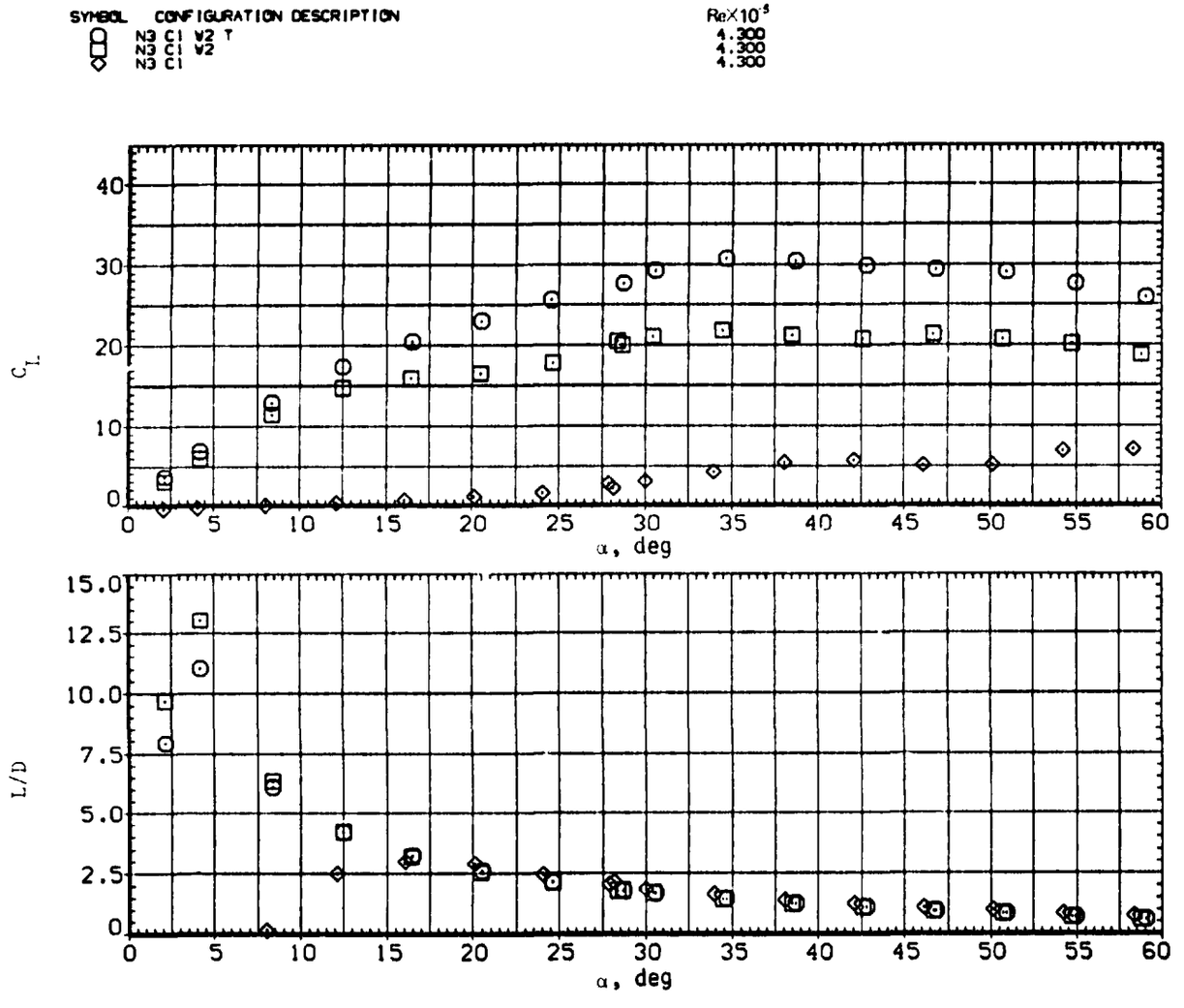

(d) C_L and L/D versus α.

Figure 29.– Concluded.

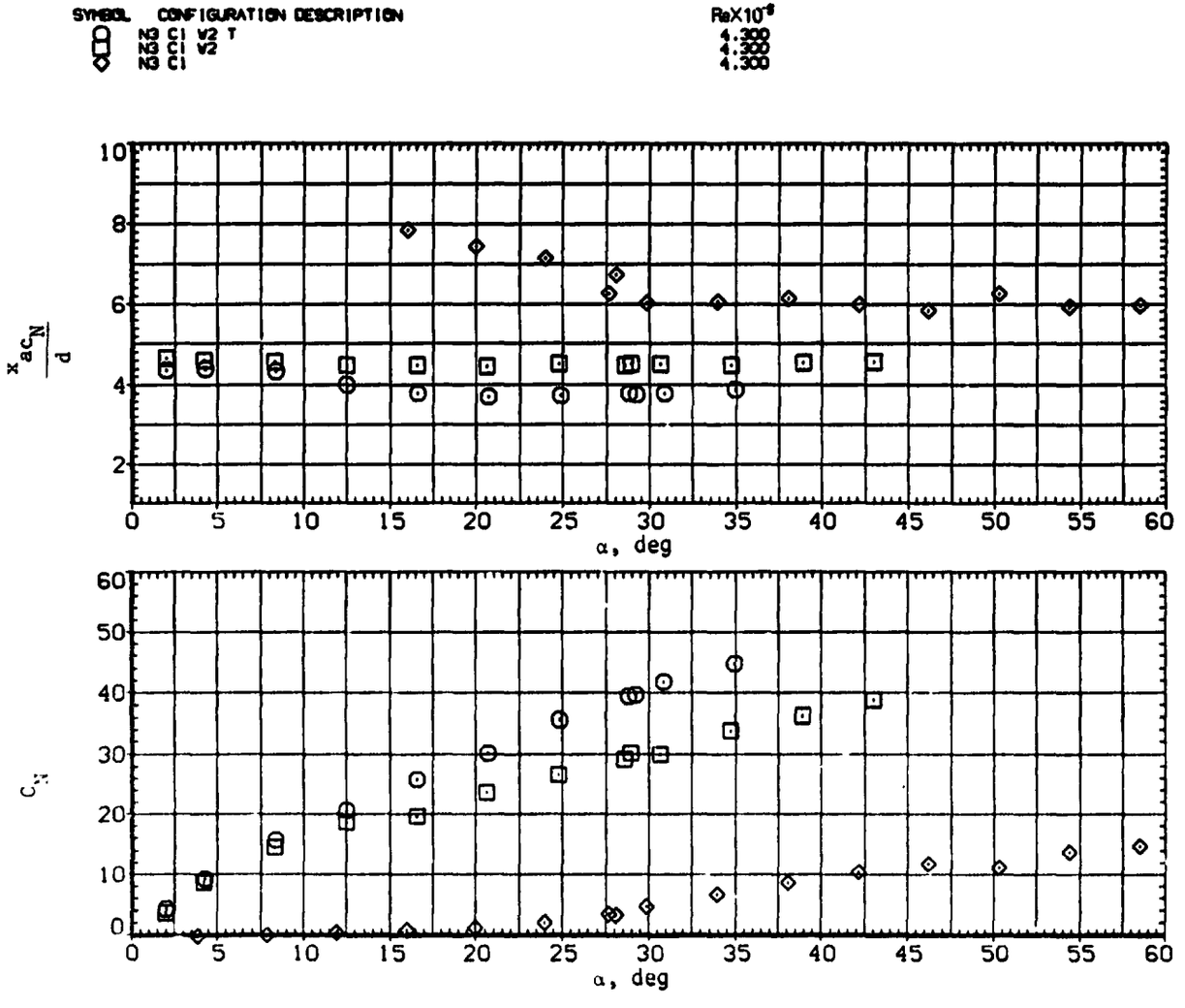

(a) x_{ac_N}/d and C_N versus α.

Figure 30. Effect of removing tail and wing from a circular body N_1 C_1 ($\ell_N/d = 5$); M = 0.9.

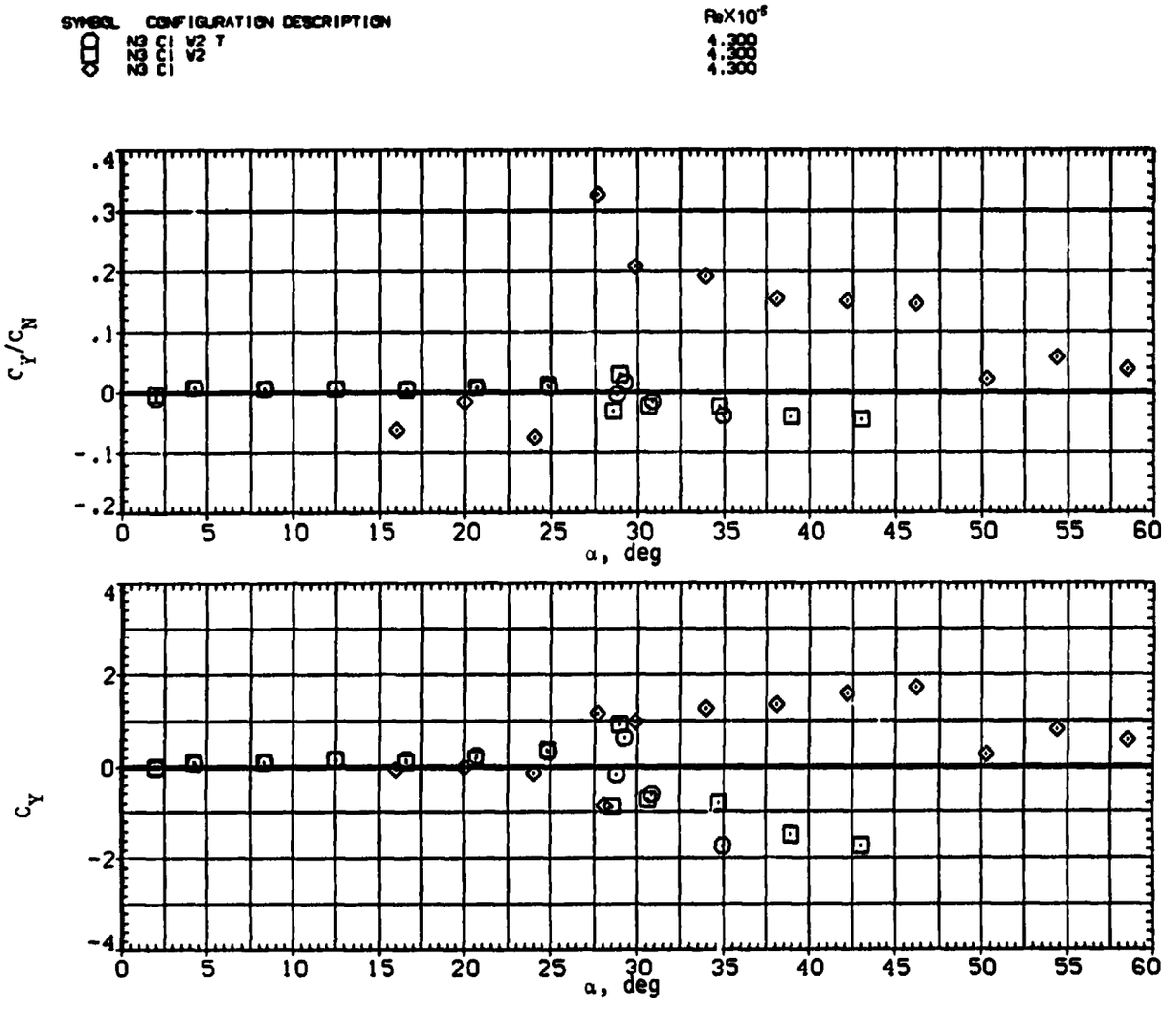

(b) C_Y/C_N and C_Y versus α.

Figure 30.– Continued.

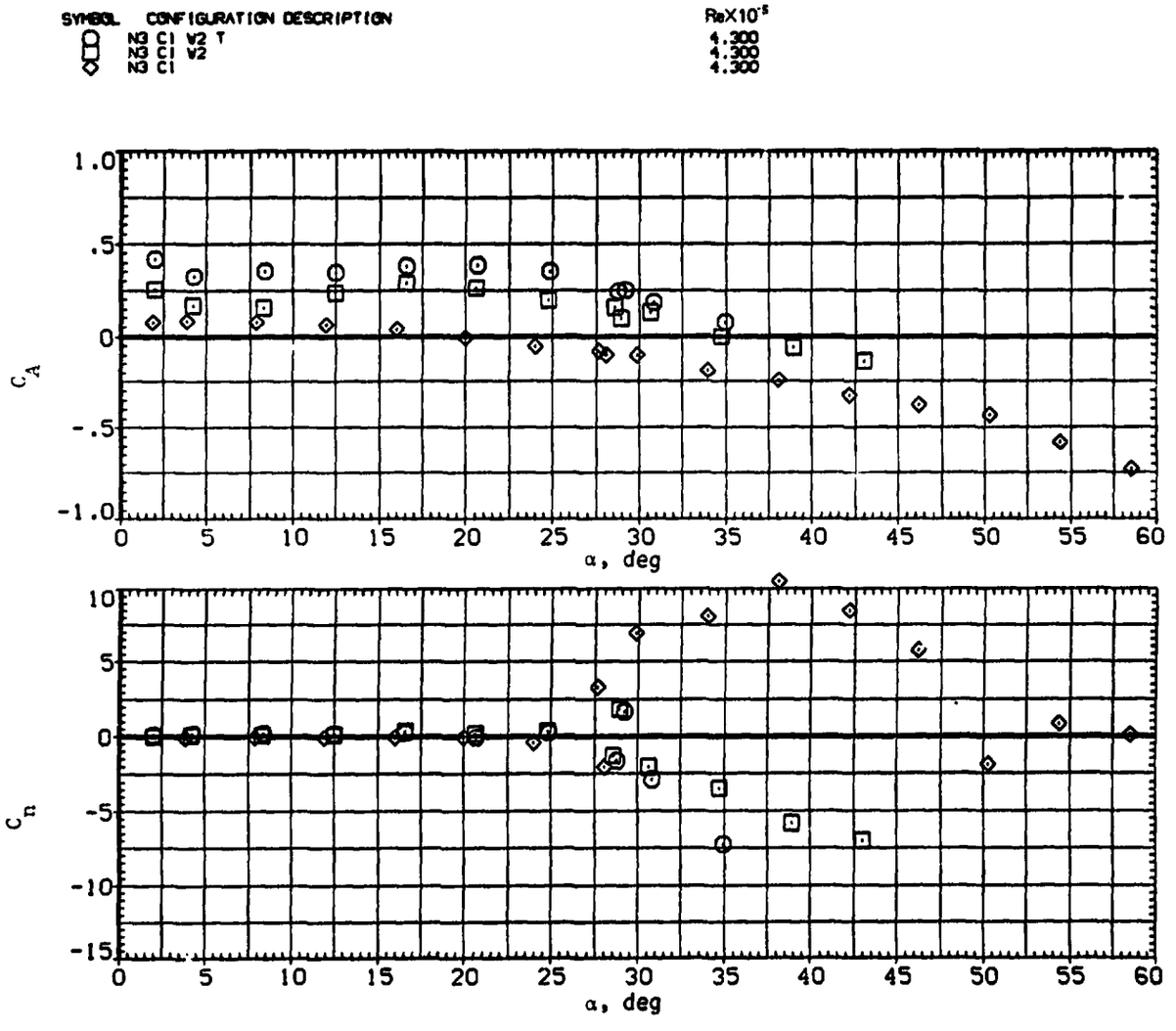

(c) C_A and C_n versus α.

Figure 30.– Continued.

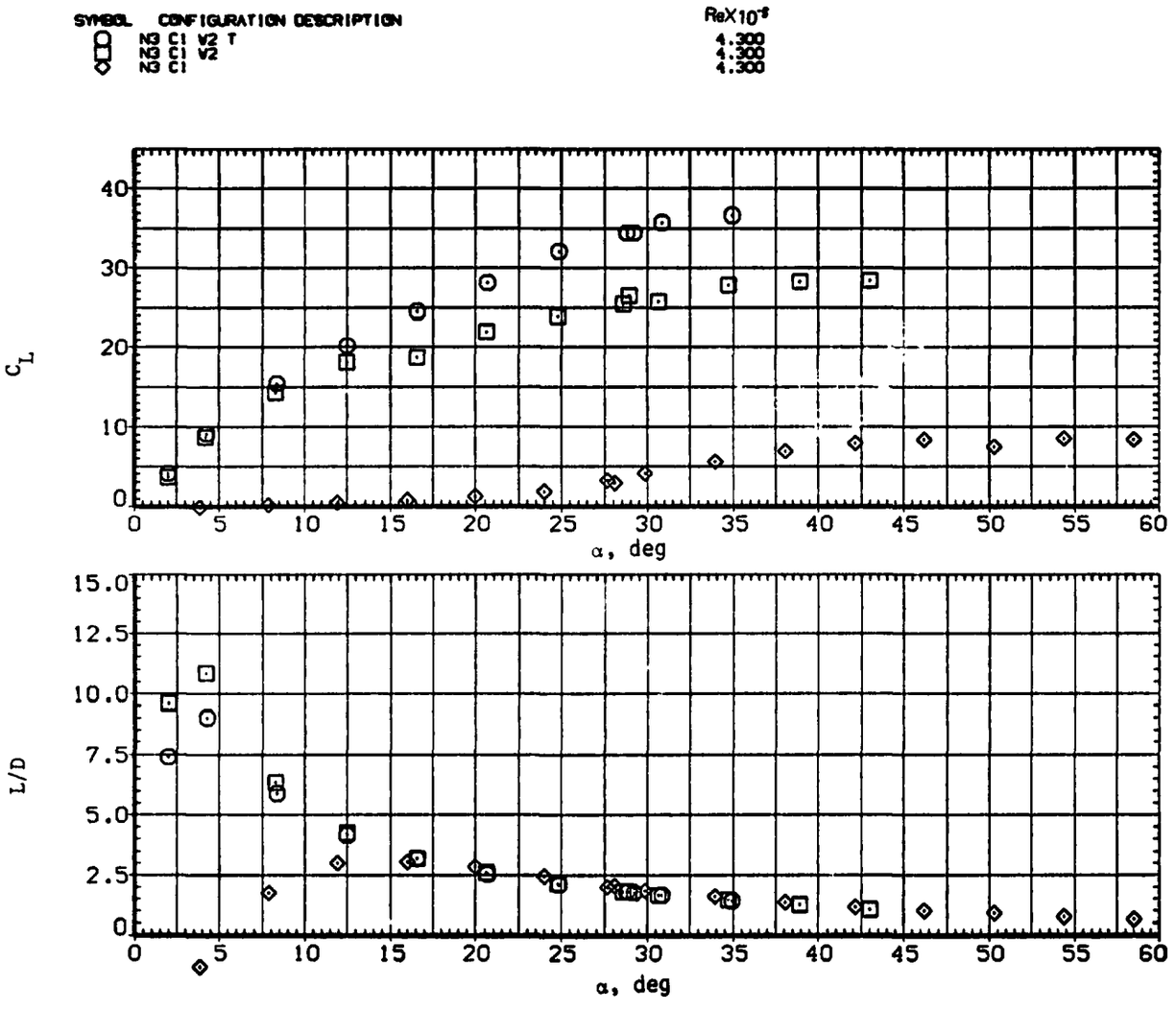

(d) C_L and L/D versus α.

Figure 30.– Concluded.

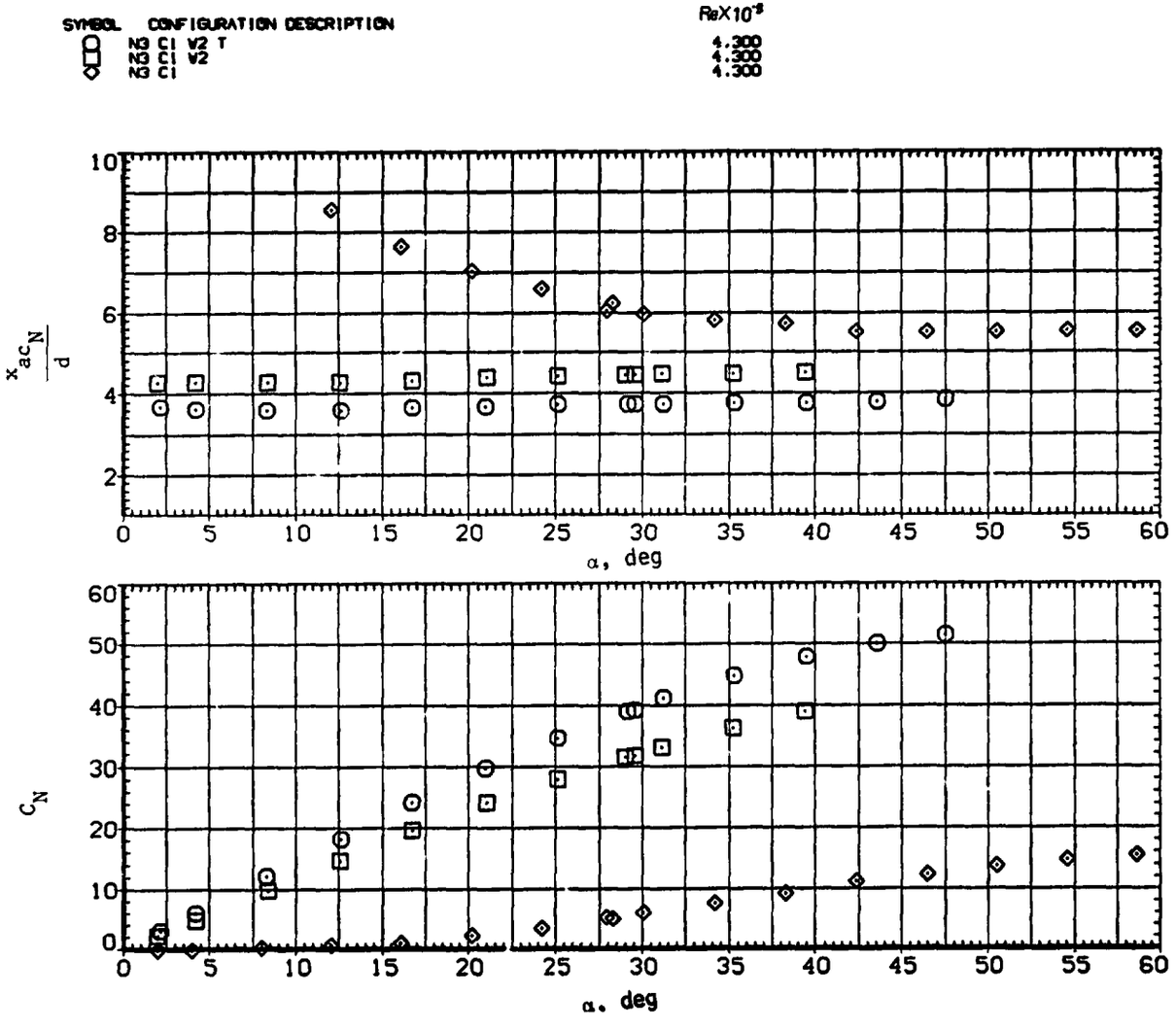

(a) x_{ac_N}/d and C_N versus α.

Figure 31.– Effect of removing tail and wing from a circular body N_3 C_1 ($\ell_N/d = 5$); M = 1.5.

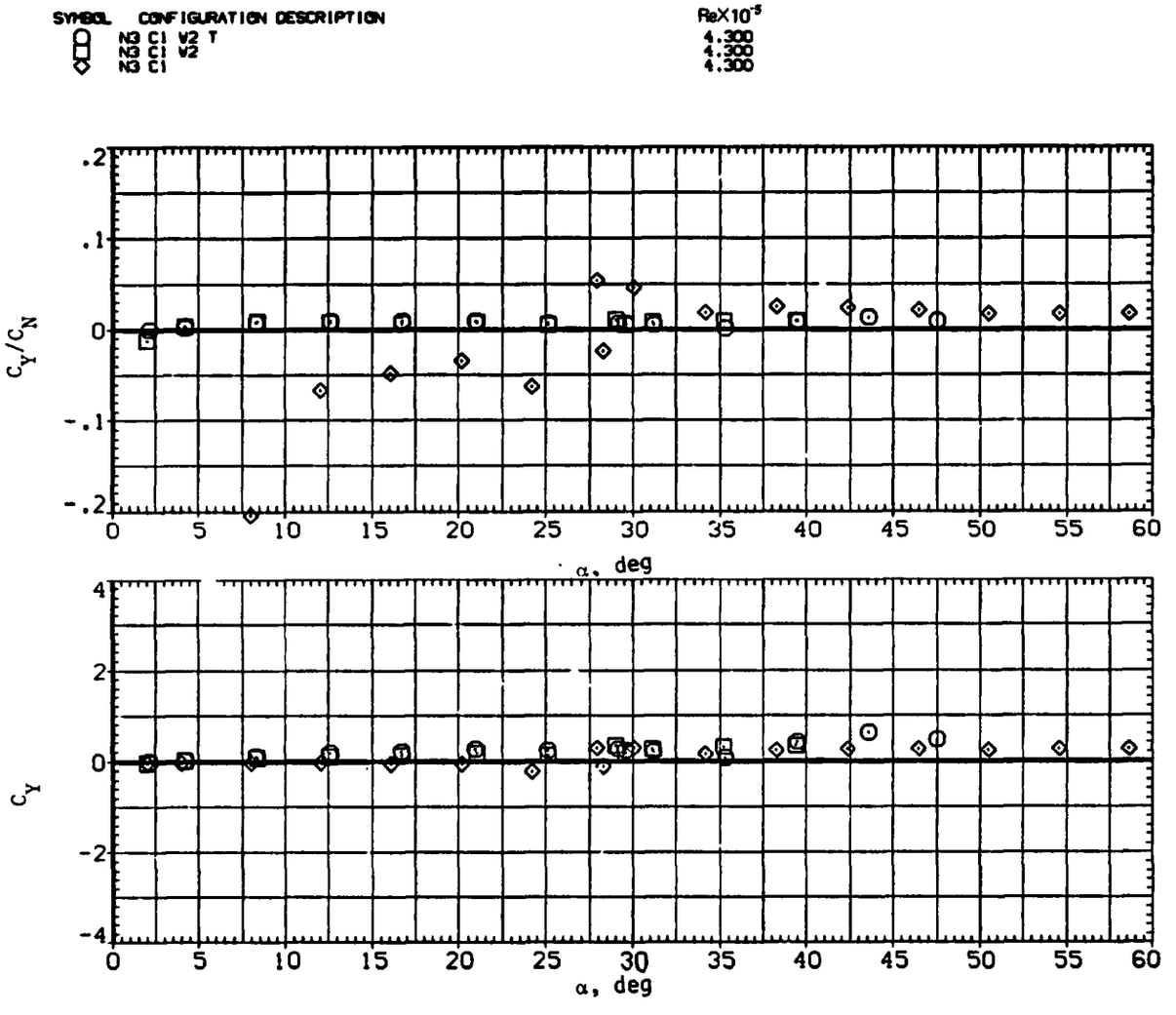

(b) C_Y/C_N and C_Y versus α.

Figure 31.– Continued.

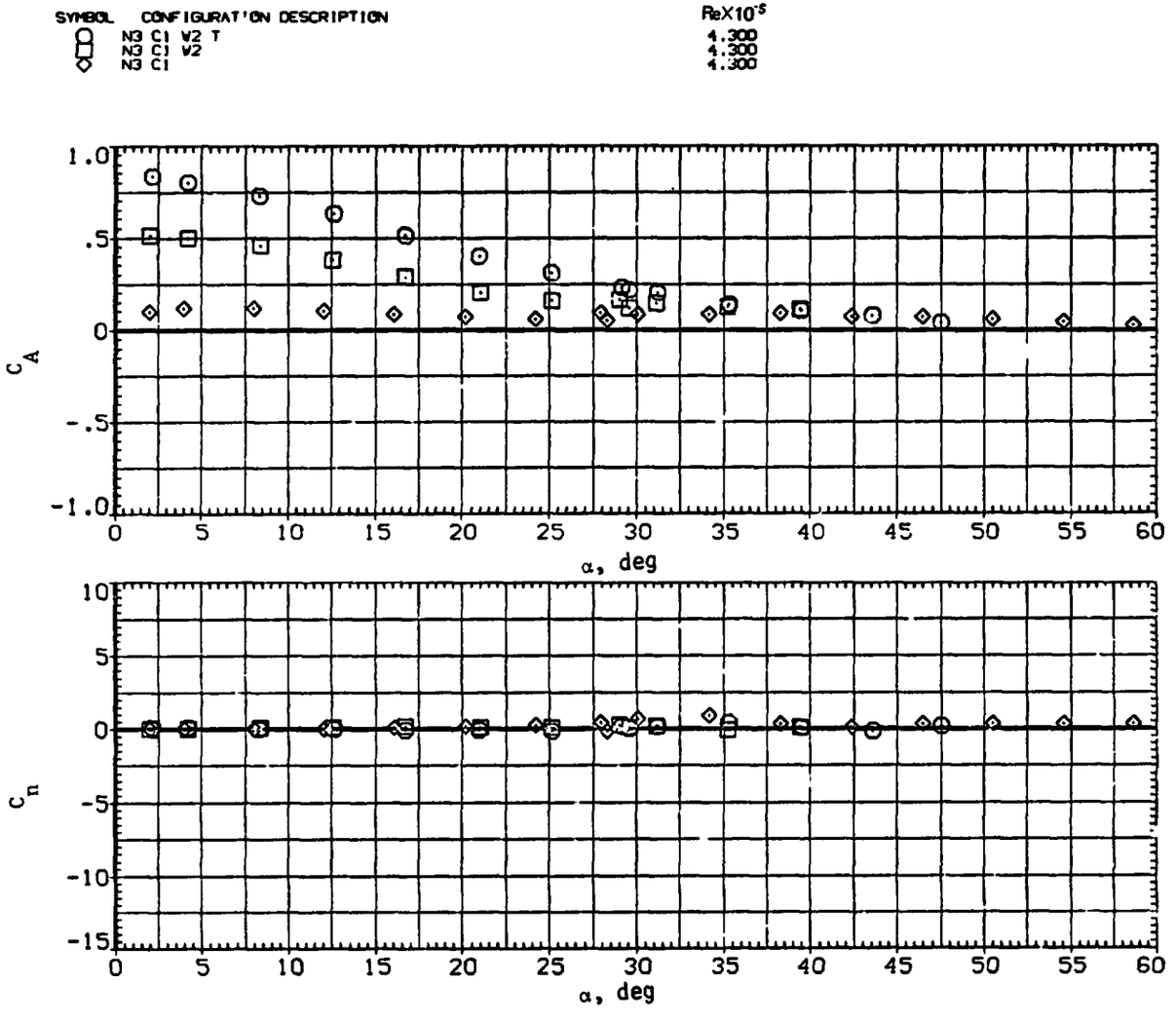

(c) C_A and C_n versus α.

Figure 31.– Continued.

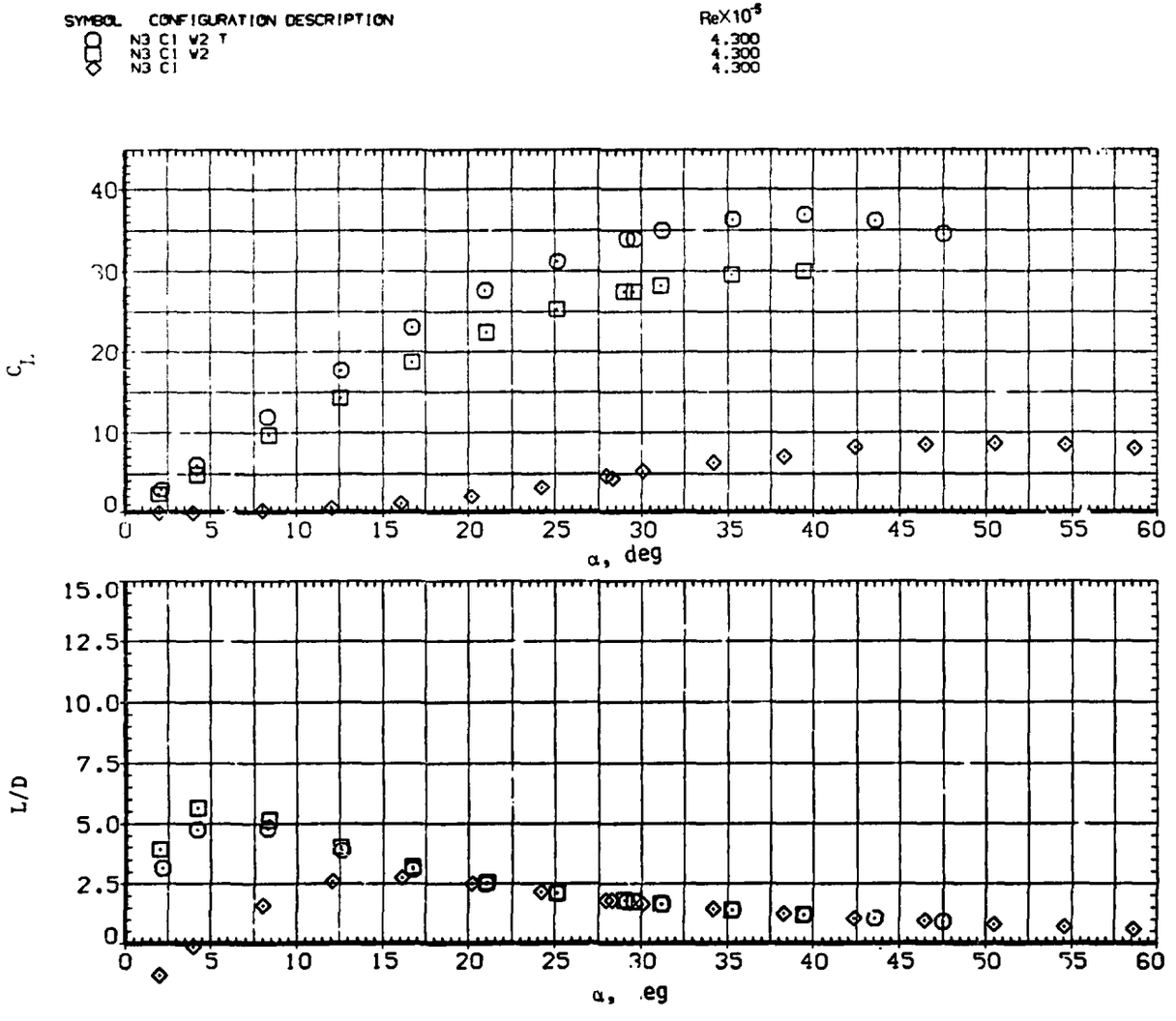

(d) C_L and L/D versus α.

Figure 31.– Concluded.

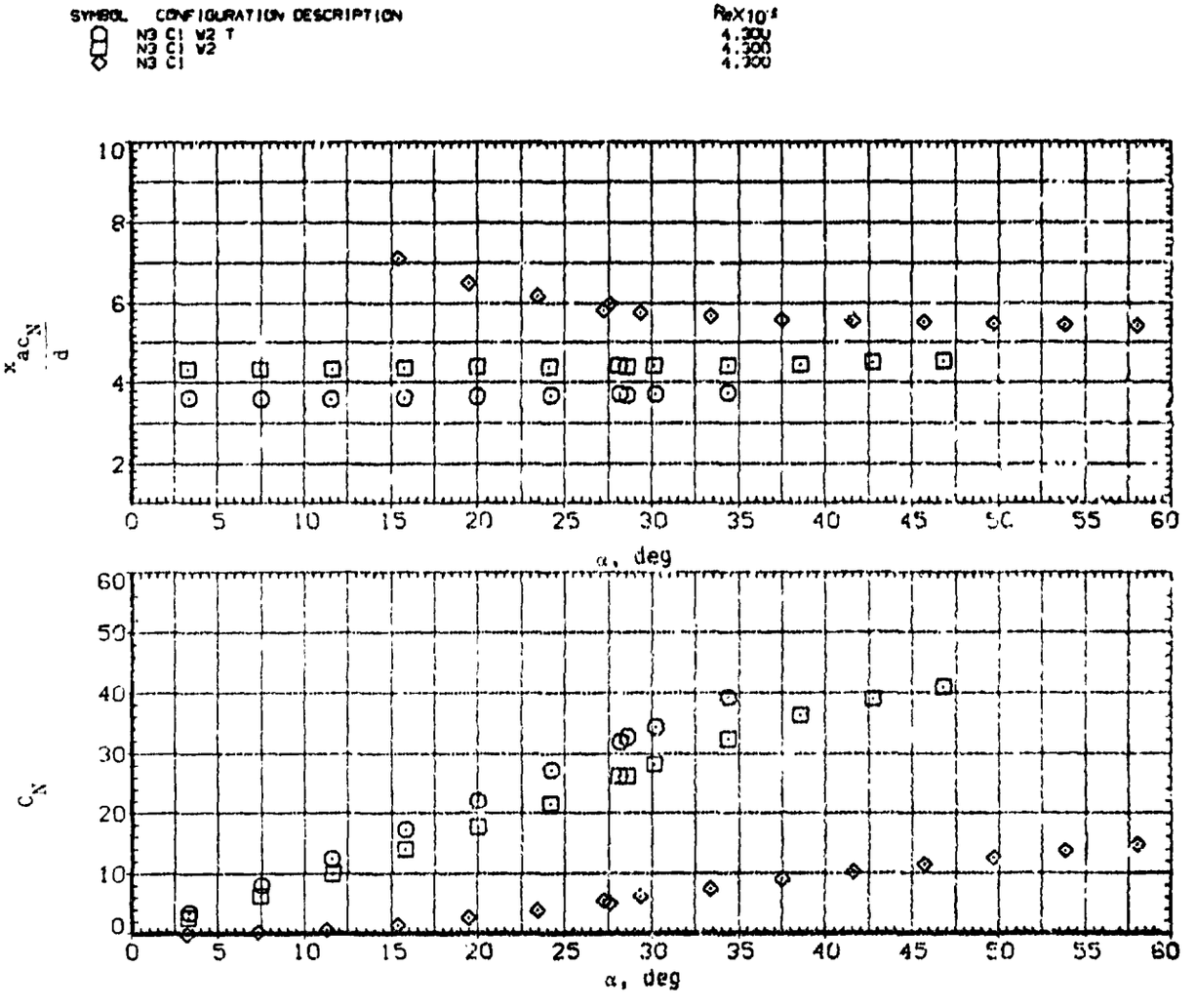

(a) x_{ac_N}/d and C_N versus α.

Figure 32.– Effect of removing tail and wing from a circular body N_3 C_1 ($\ell_N/d = 5$); M = 2.0.

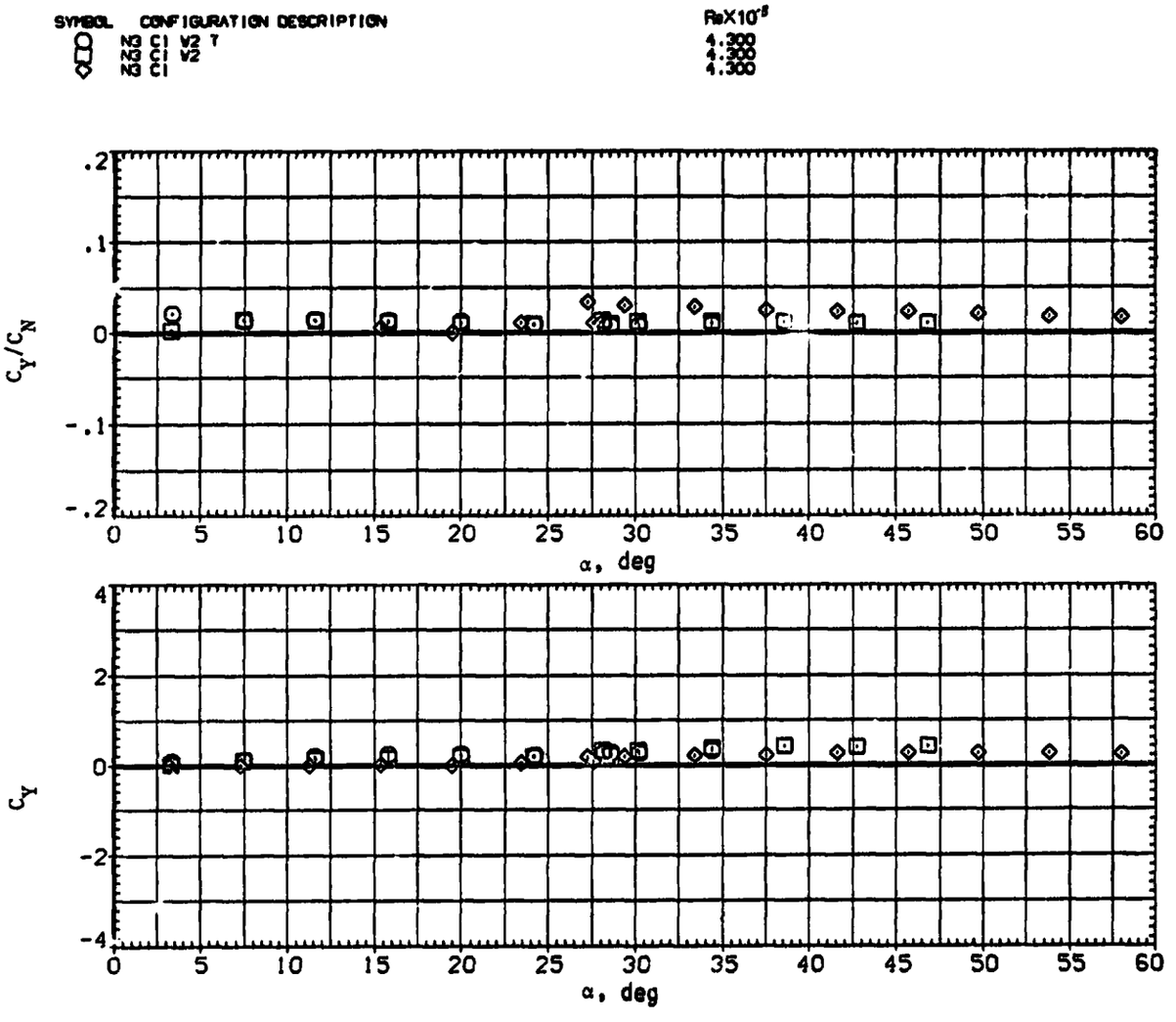

(b) C_Y/C_N and C_Y versus α.

Figure 32.– Continued.

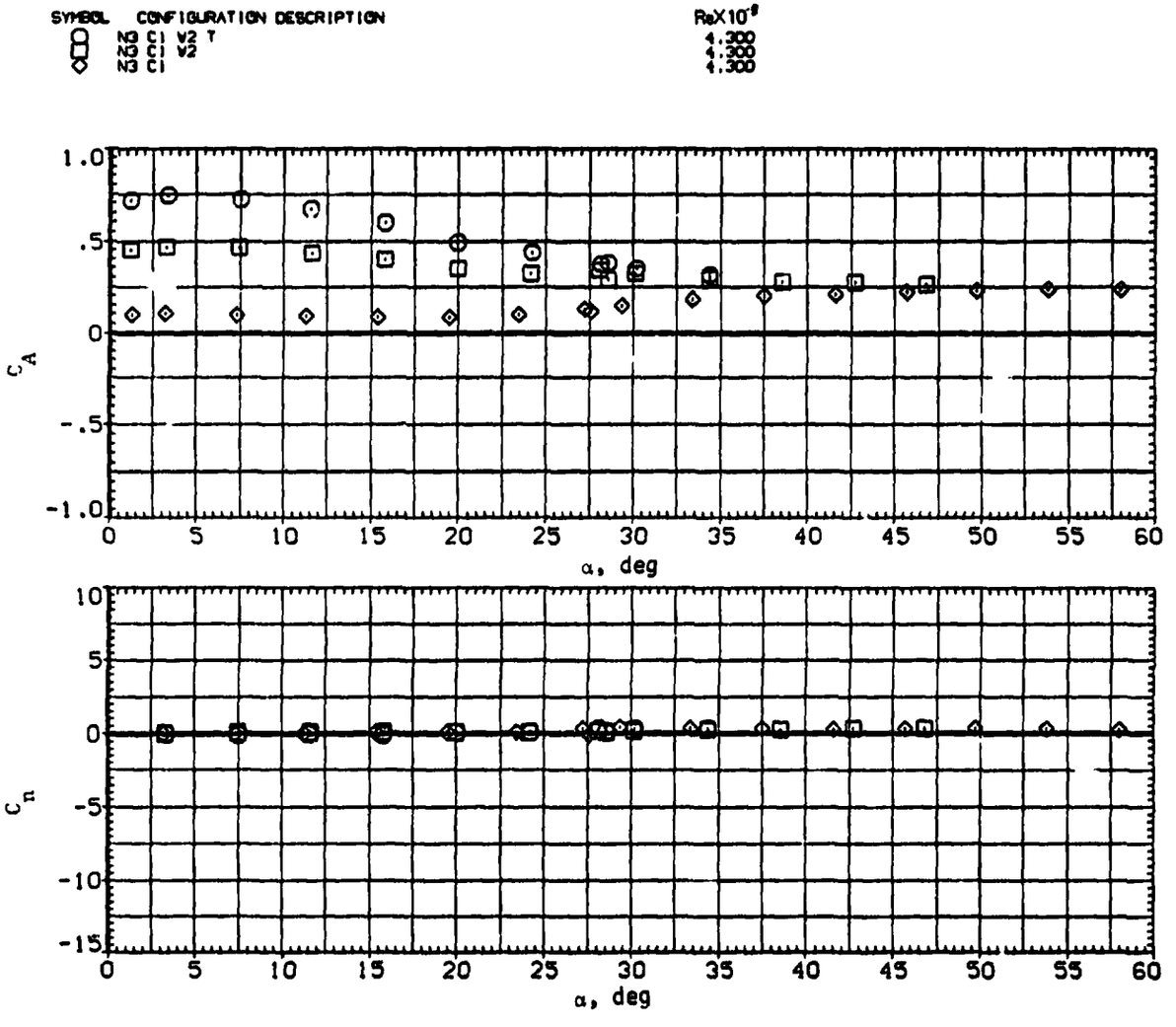

(c) C_A and C_n versus α.

Figure 32.– Continued.

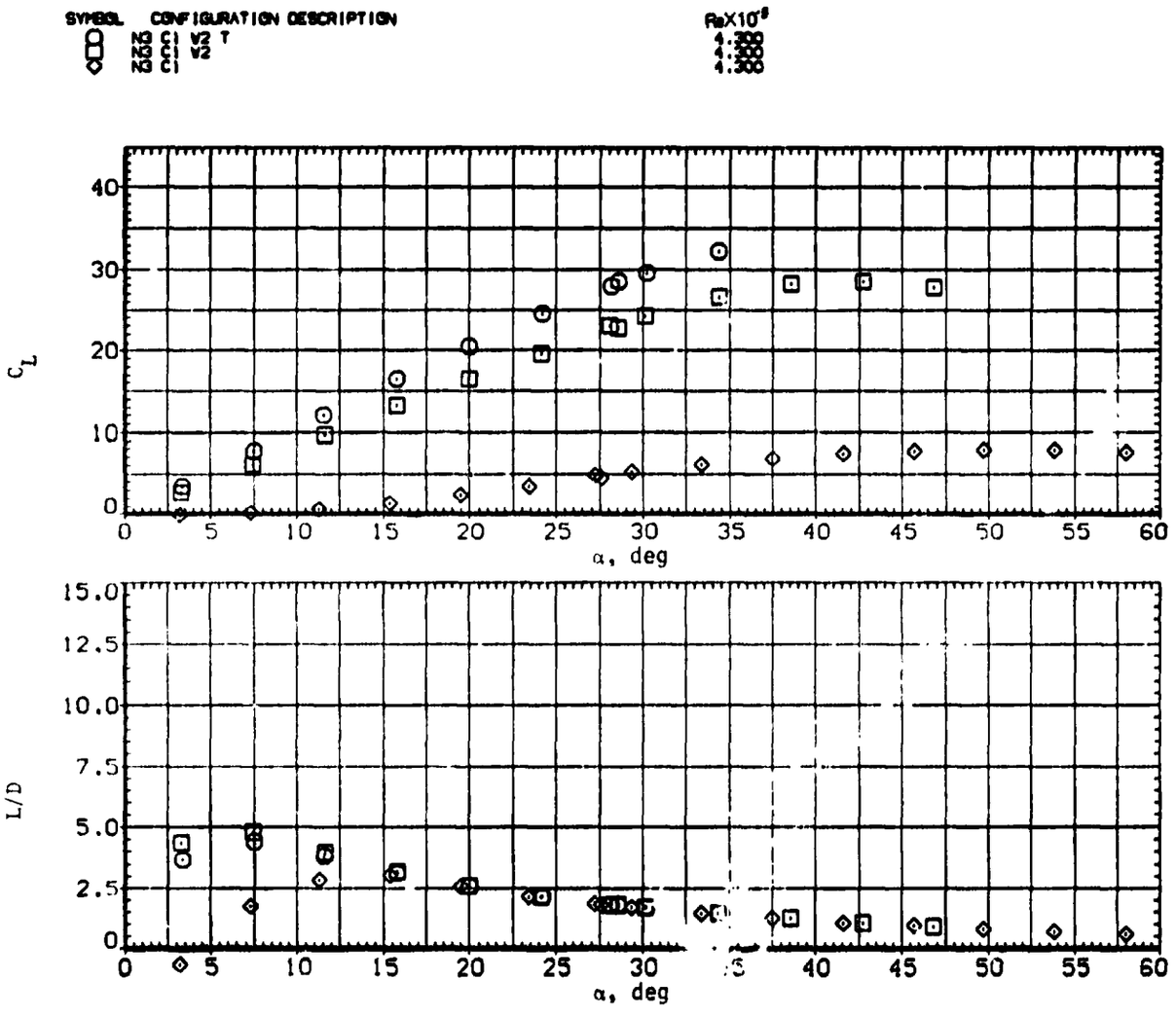

(d) C_L and L/D vers α.

Figure 32.– Concluded.

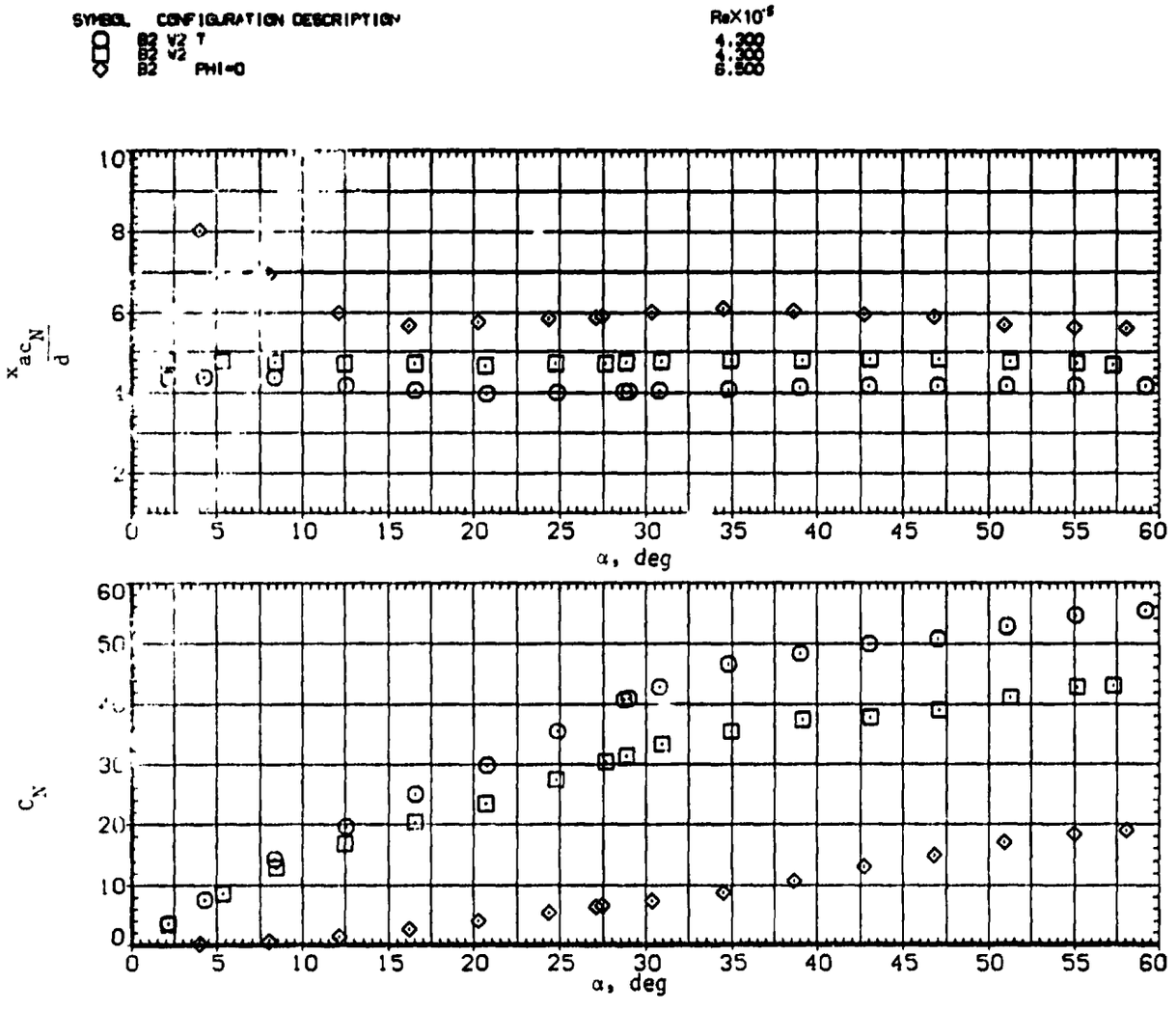

(a) x_{ac_N}/d and C_N versus α.

Figure 33. Effect of removing tail and wing from an elliptic body B_2, M = 0.6.

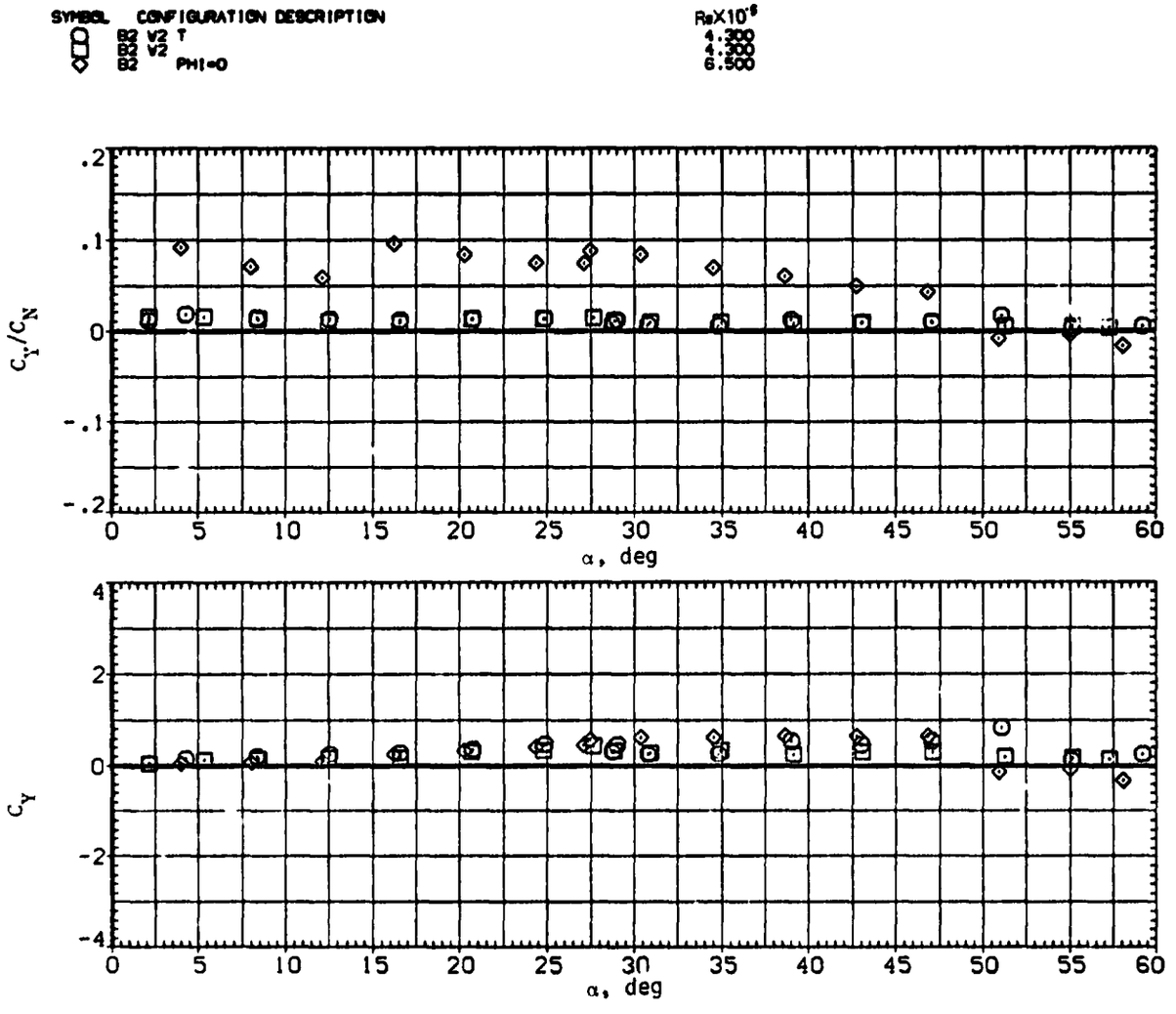

(b) C_Y/C_N and C_Y versus α.

Figure 33. – Continued.

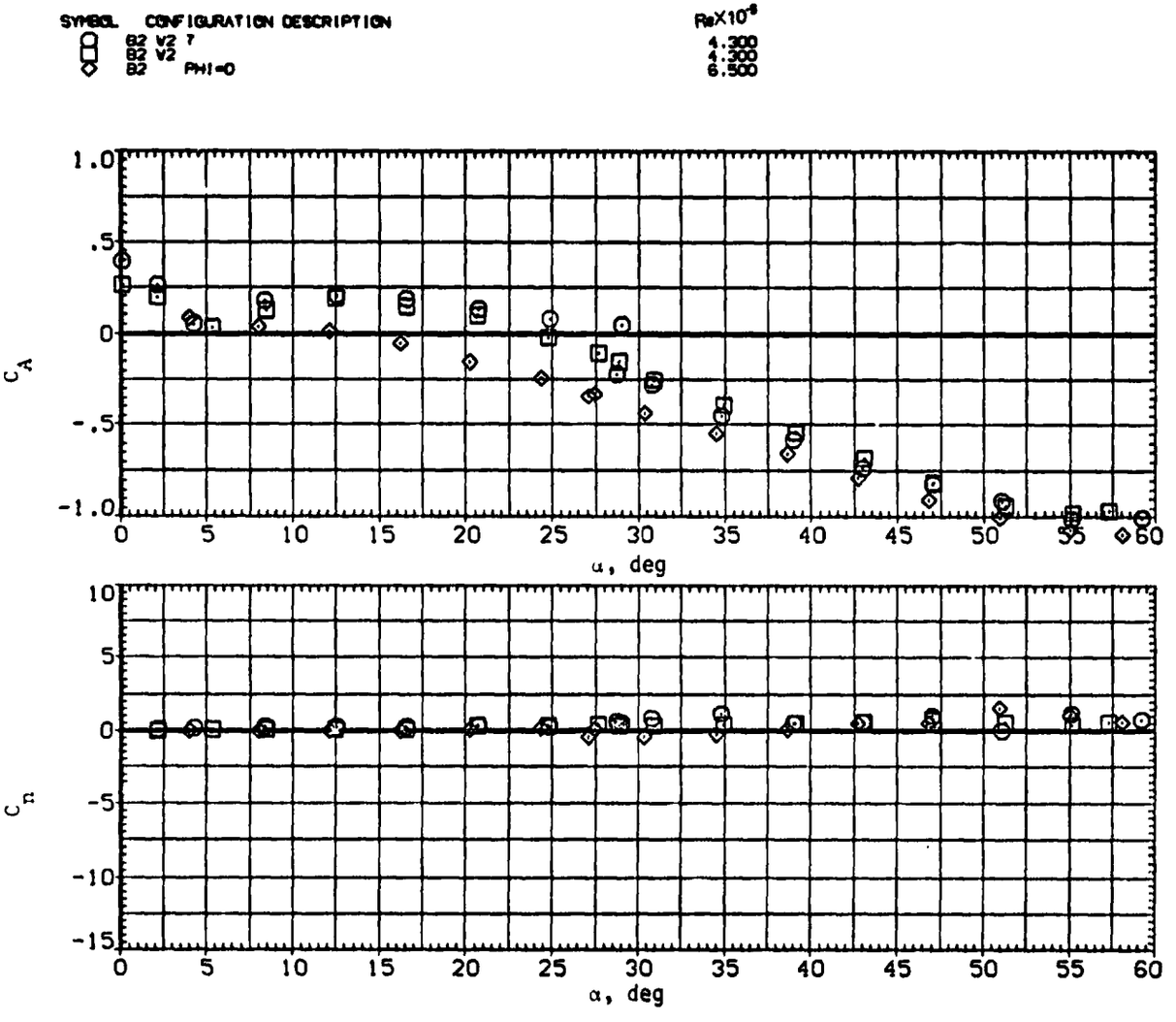

(c) C_A and C_n versus α.

Figure 33.– Continued.

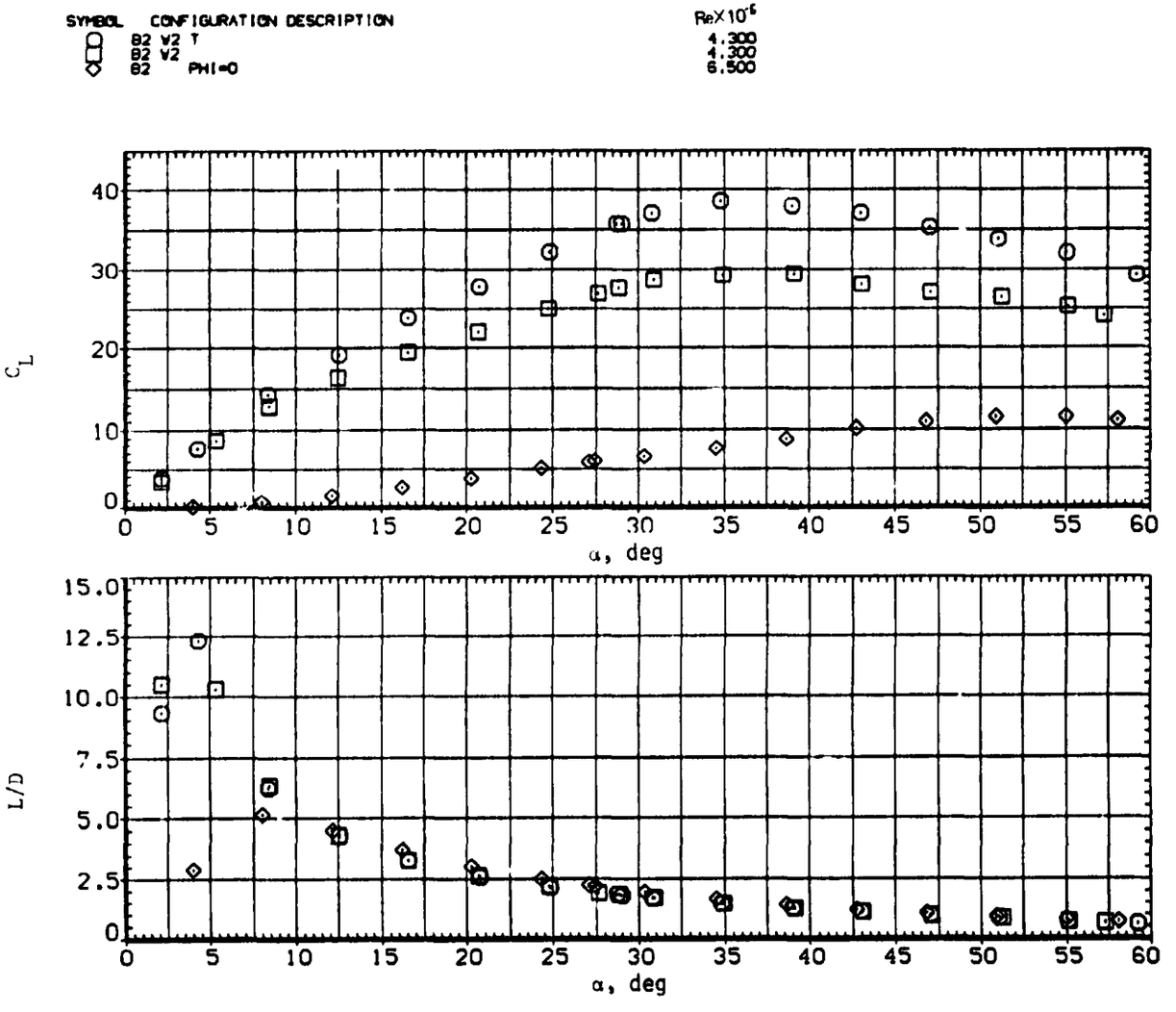

(d) C_L and L/D versus α.

Figure 33.– Concluded.

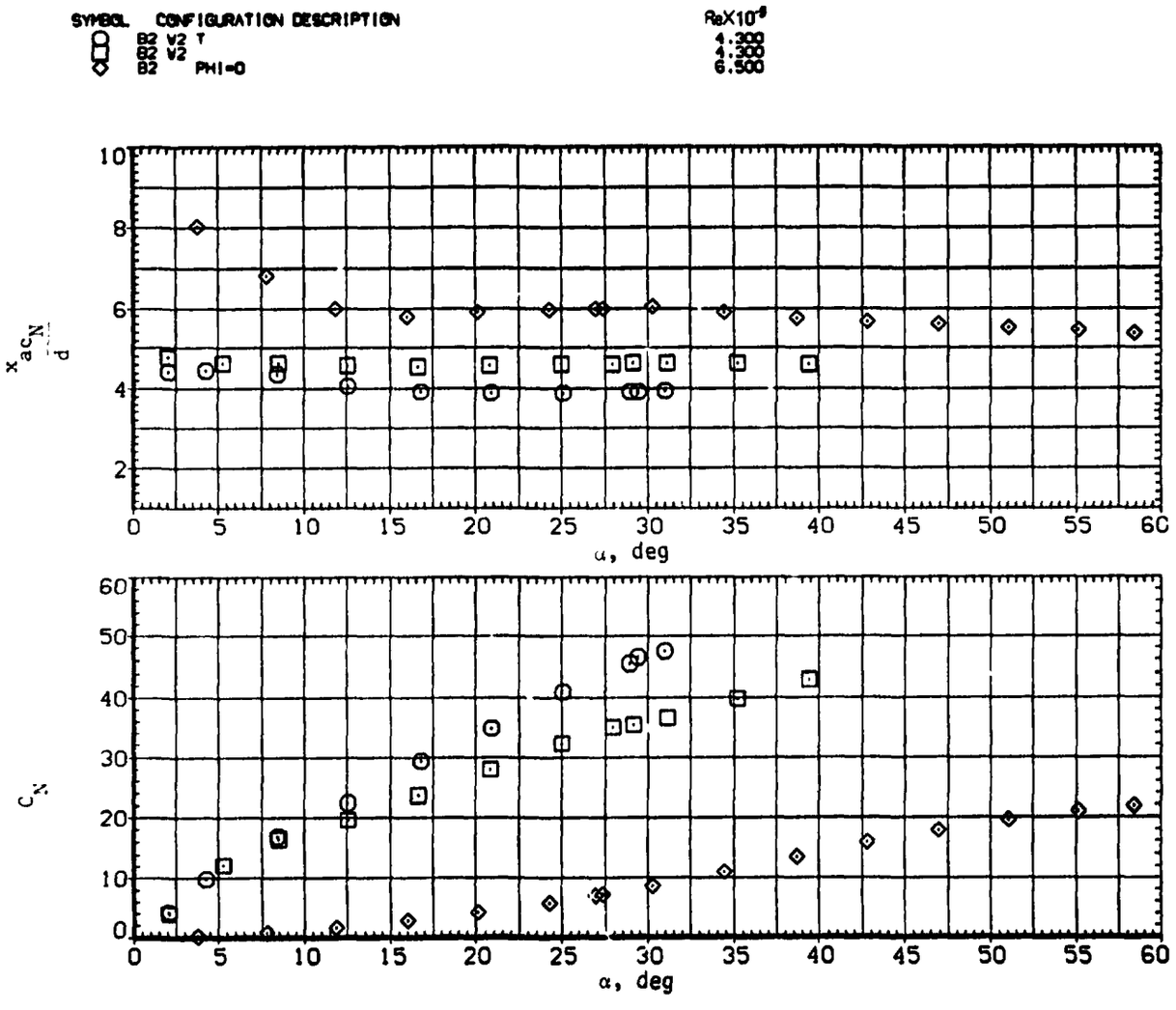

(a) x_{ac_N}/d and C_N versus α.

Figure 34.– Effect of removing tail and wing from an elliptic body B_2 ; M = 0.9.

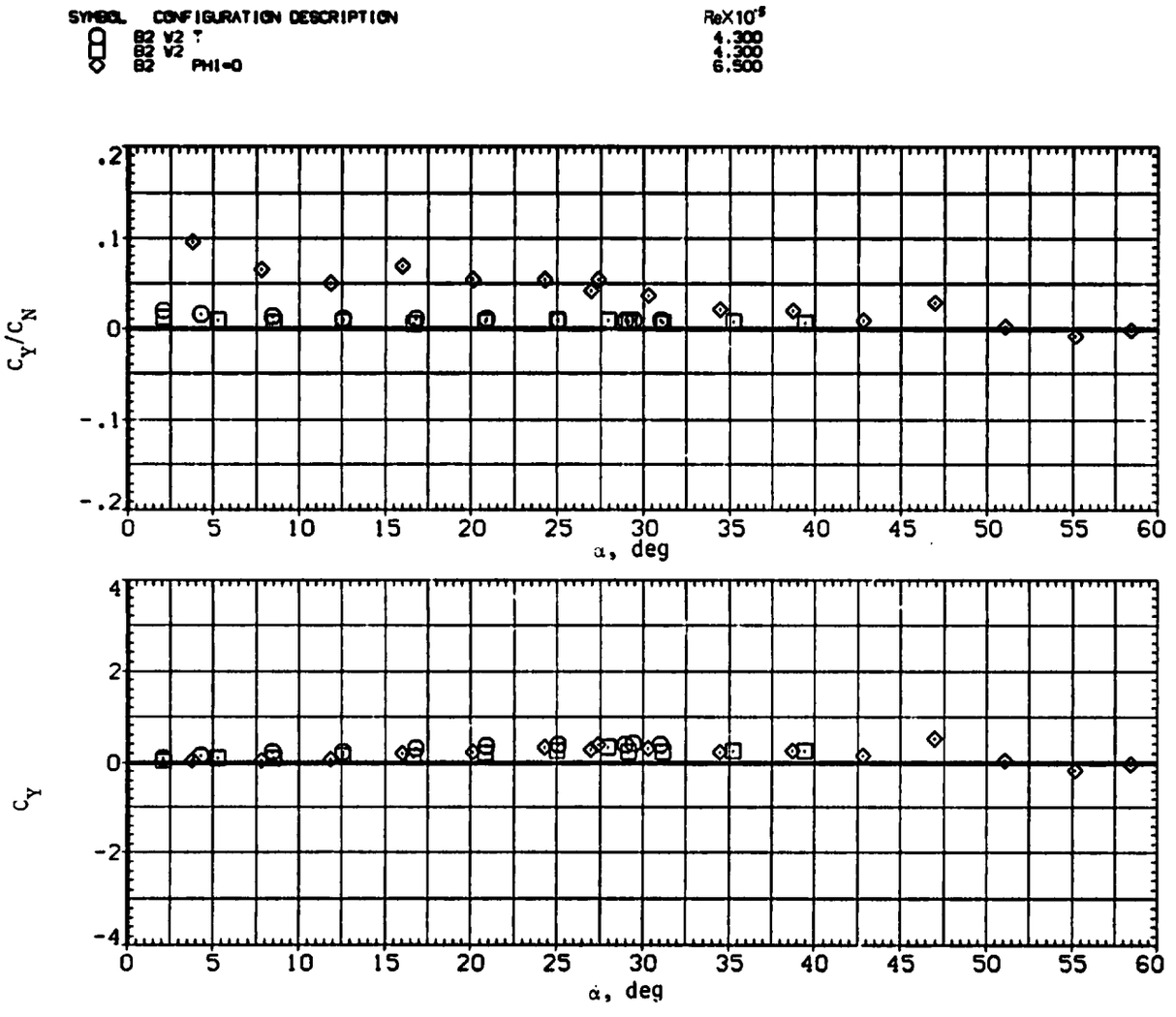

(b) C_Y/C_N and C_Y versus α.

Figure 34.– Continued.

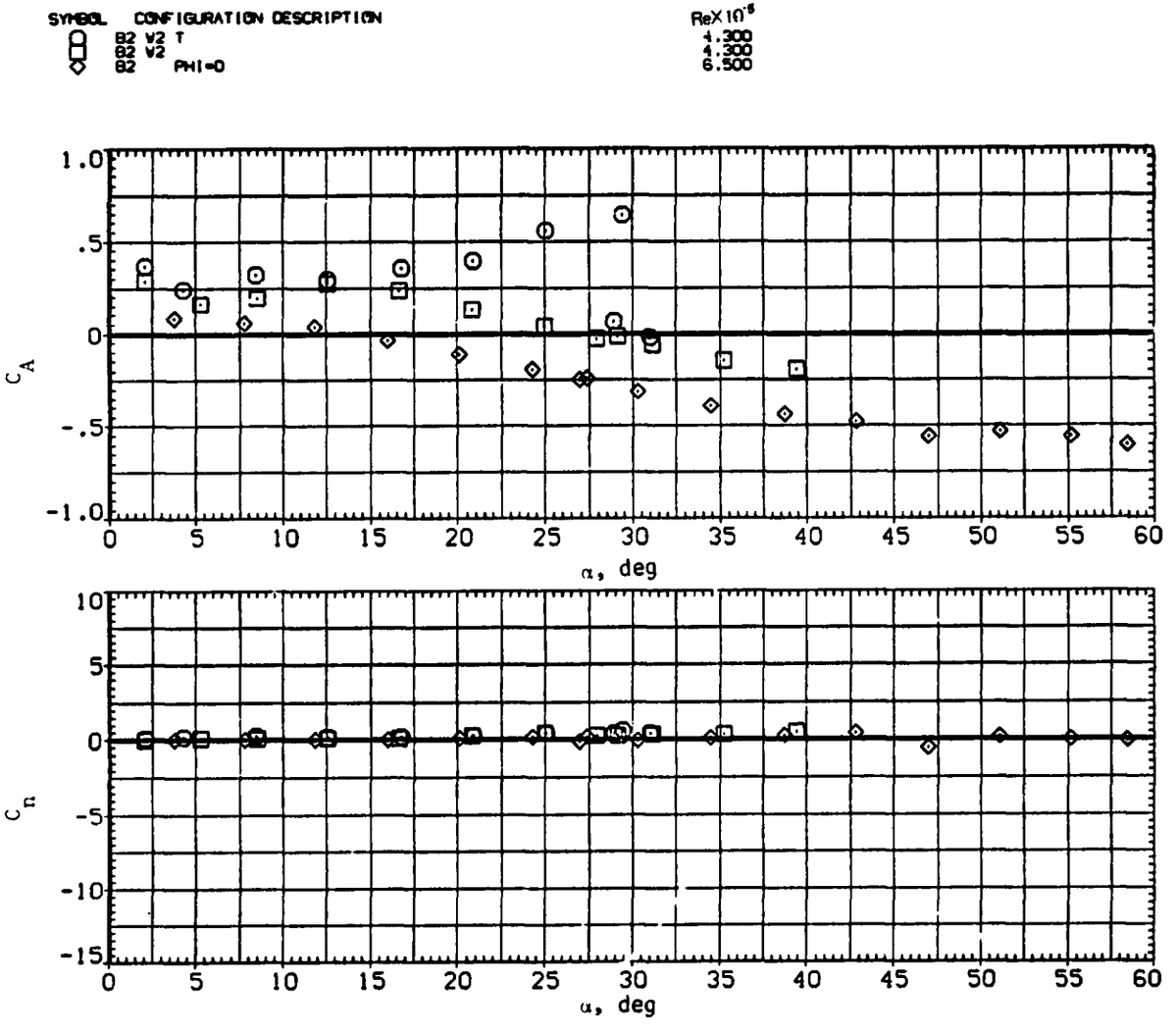

(c) C_A and C_n versus α.

Figure 34.– Continued.

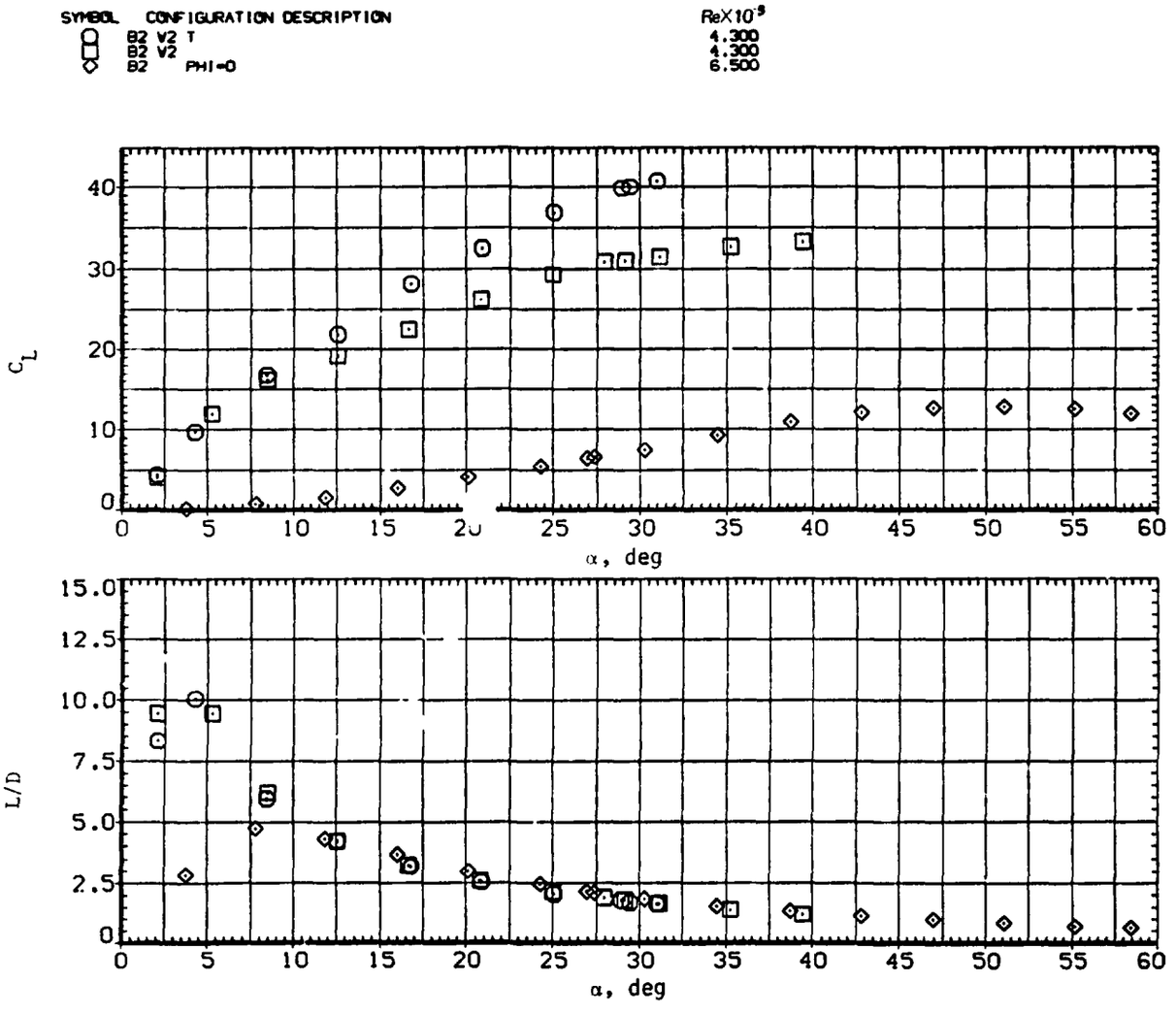

(d) C_L and L/D versus α.

Figure 34 – Concluded.

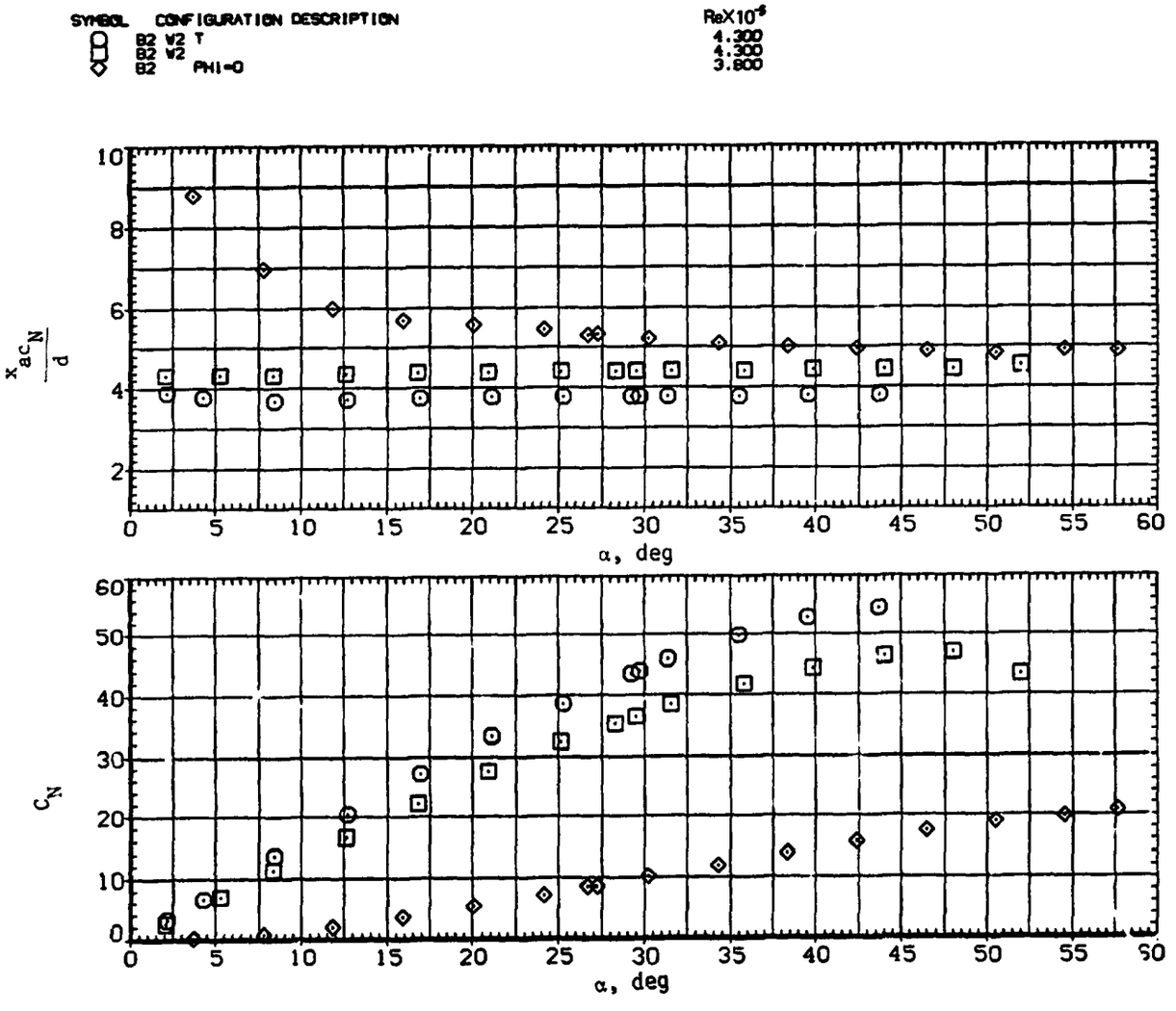

(a) x_{ac_N}/d and C_N versus α.

Figure 35.– Effect of removing tail and wing from an elliptic body B_2 ; M = 1.5.

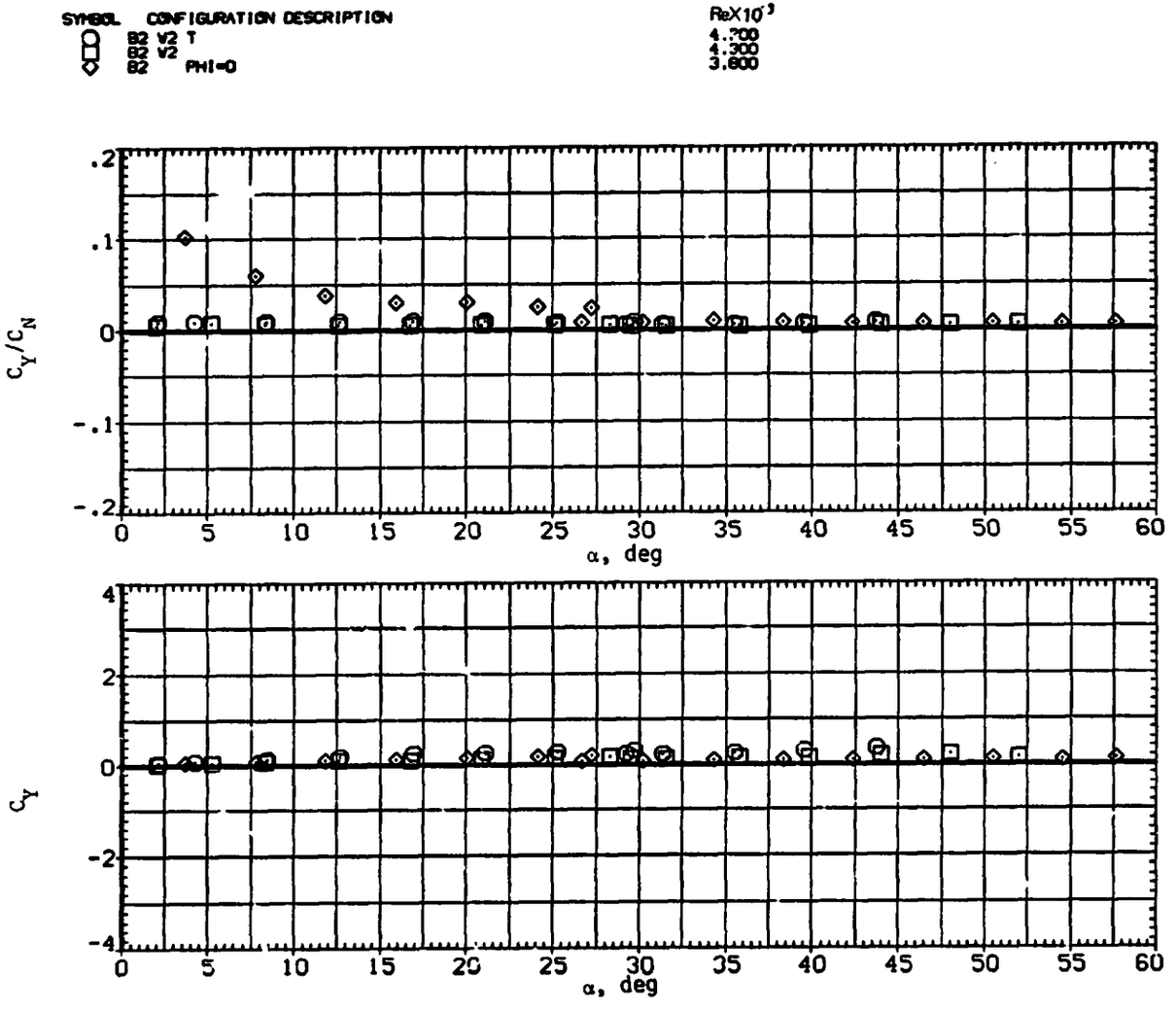

(b) C_Y/C_N and C_Y versus α.

Figure 35.– Continued.

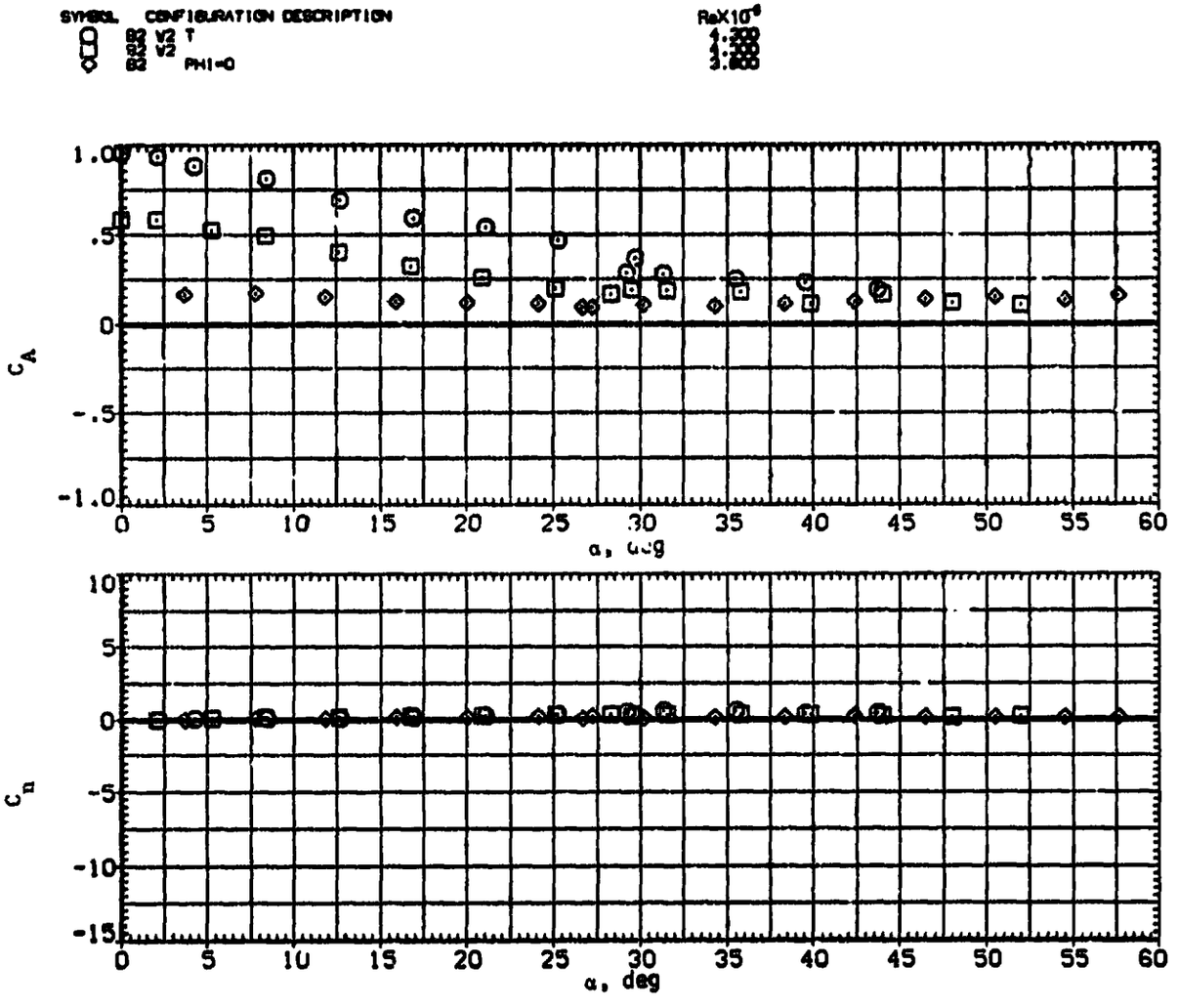

(c) C_A and C_n versus α.

Figure 35.– Continued.

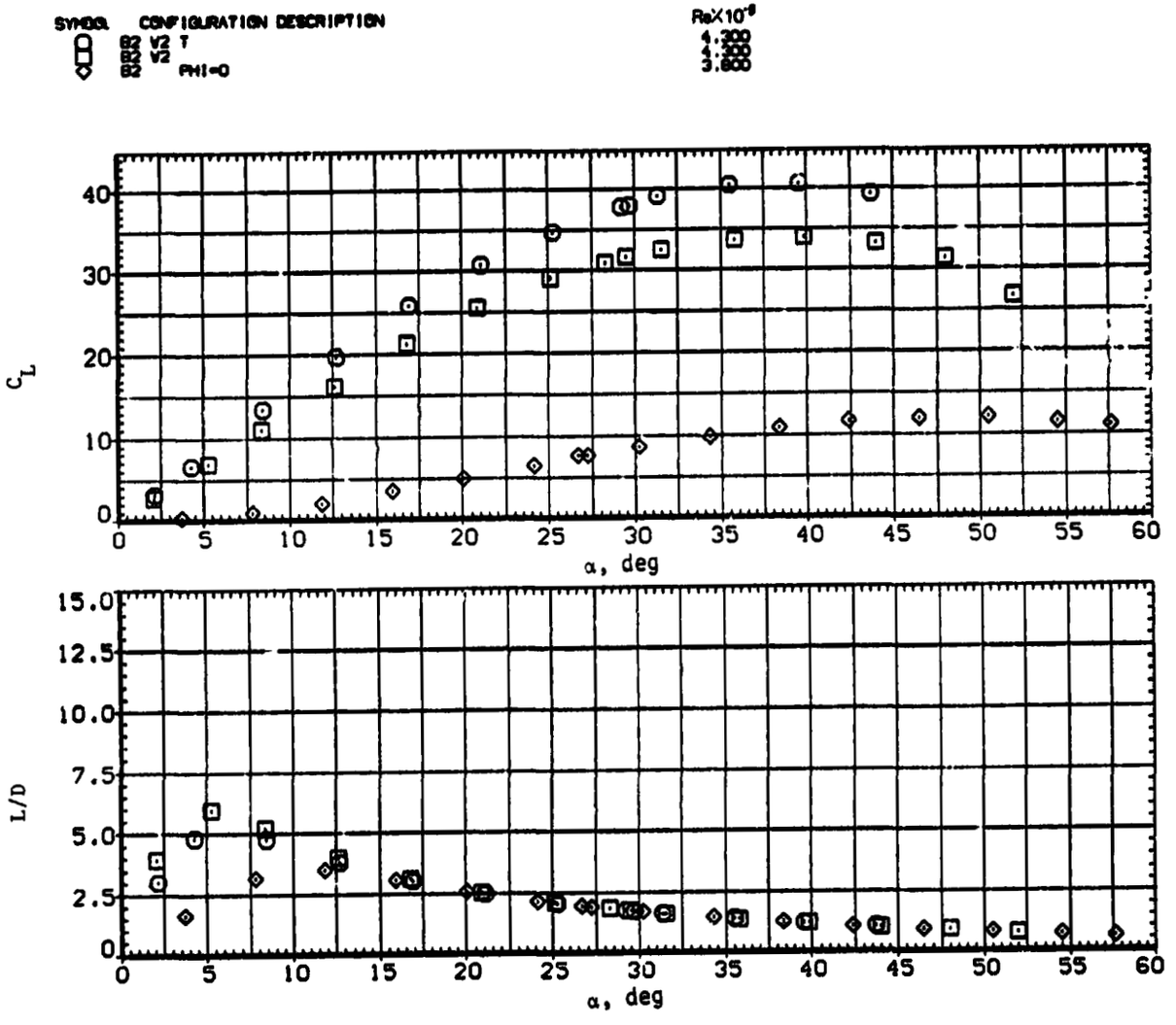

(d) C_L and L/D versus α.

Figure 35.– Concluded.

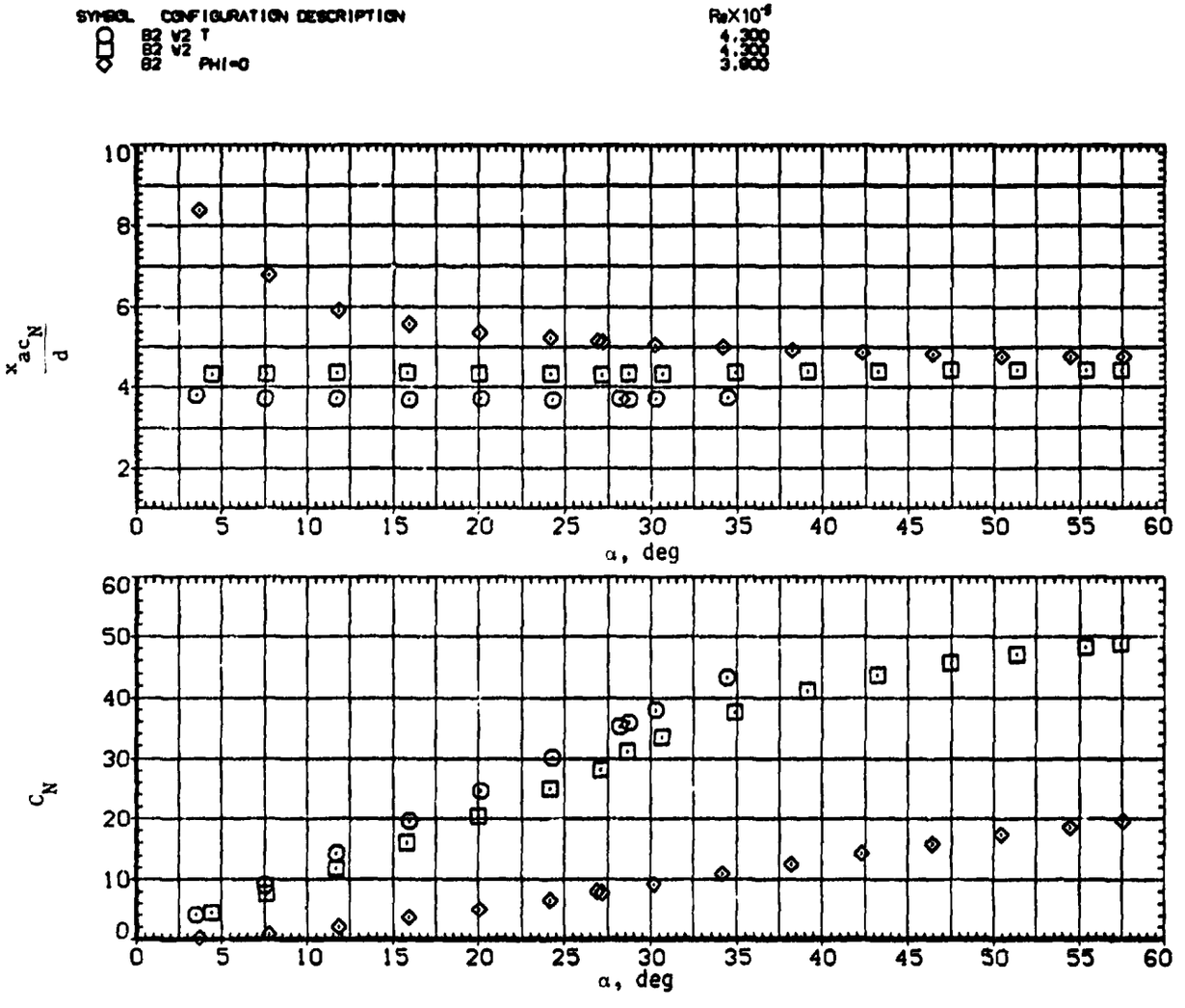

(a) x_{ac_N}/d and C_N versus α.

Figure 36. Effect of removing tail and wing from an elliptic body B_2 ; M = 2.0.

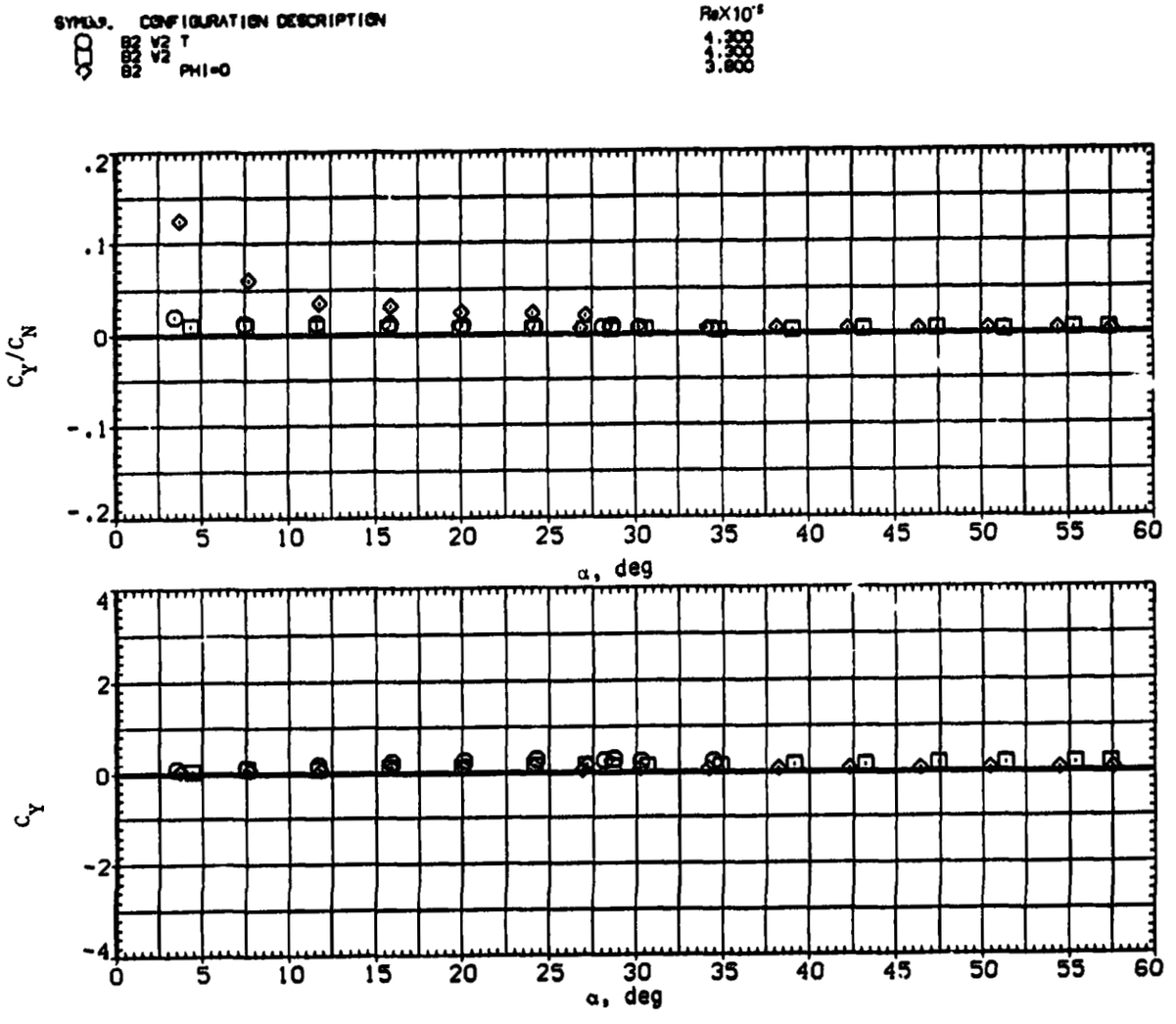

(b) C_Y/C_N and C_Y versus α.

Figure 36.– Continued.

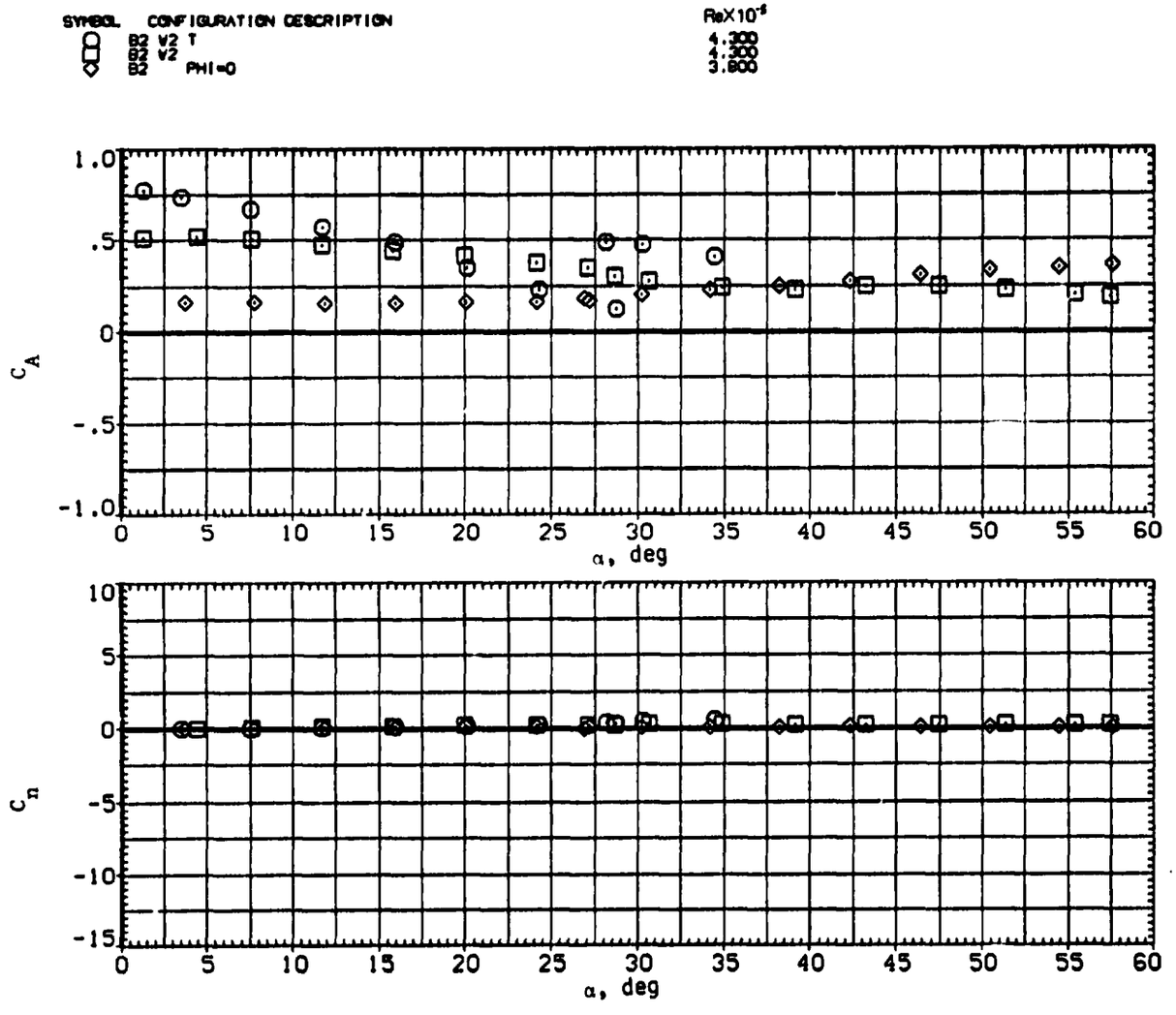

(c) C_A and C_n versus α.

Figure 36. – Continued.

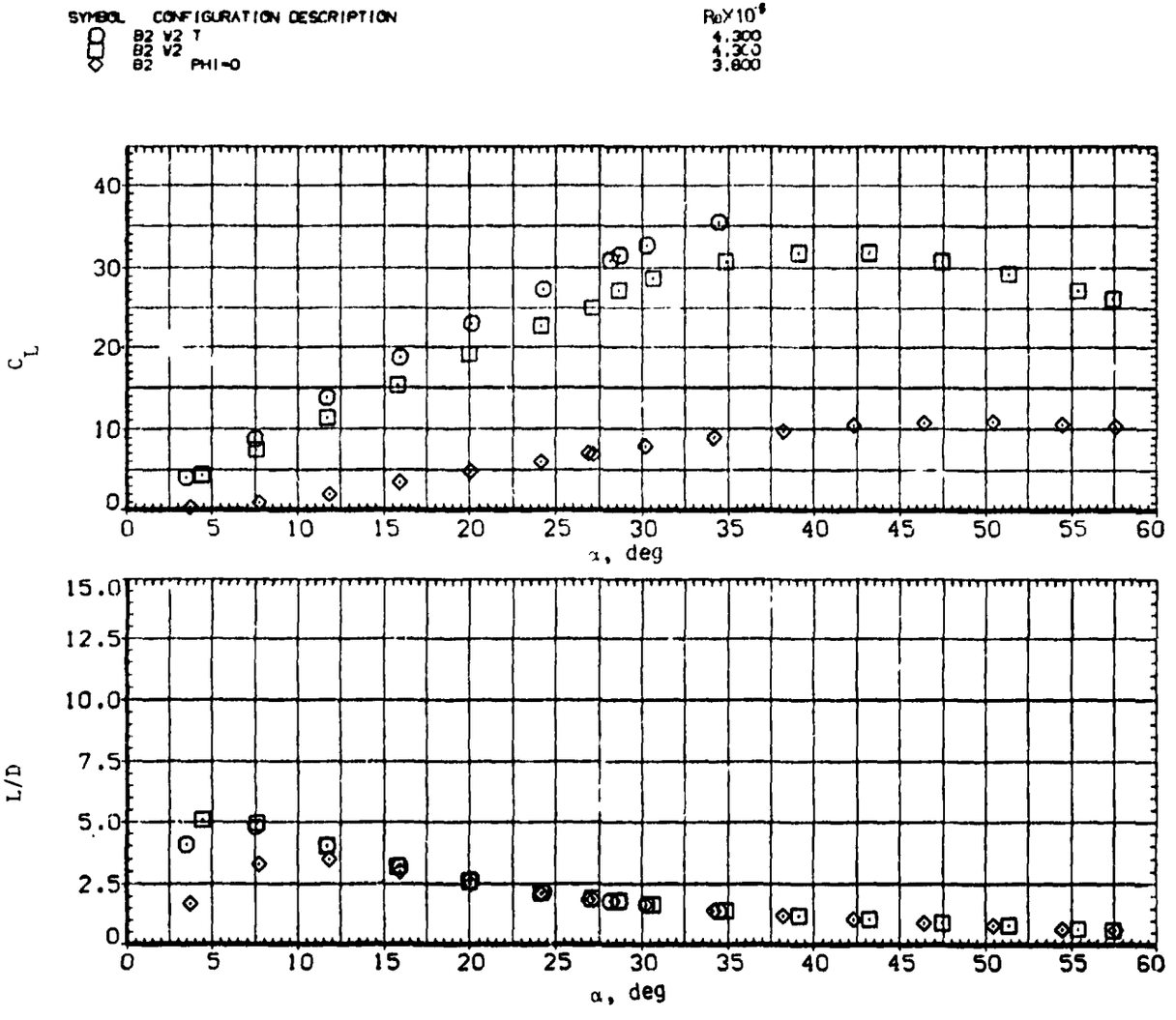

(d) C_L and L/D versus α.

Figure 36. - Concluded.